DEVELOPMENT OF FULL IN-FLIGHT ACOUSTIC DESIGN CRITERIA SCALING EFFECTS.

DEVELOPMENT OF FULL IN-FLIGHT ACOUSTIC DESIGN CRITERIA SCALING EFFECTS.

FINAL REPORT

June 27, 1969
Report No. 507
Copy No. 8

Prepared for the George C. Marshall Space Flight Center,
Huntsville, Alabama, under Contract No. NAS8-21461,
covering period June 29, 1968 to June 29, 1969.

Frederick Baganoff

BAGANOFF ASSOCIATES, INC.

6809 West Florissant

St. Louis, Missouri 63136

TABLE OF CONTENTS

INTRODUCTION

The methods reported are directed at developing engineering equations as a function of a great many geometric and flow variables for predicting the fluctuating pressure environments for future vehicles. This work is complicated by the large quantities of reduced fluctuating pressure data collected from numerous test programs that must be digested in order to develop these engineering equations. In this respect, the digital computer, with its tremendous storage and rapid decision-making capabilities, should be employed.

Before the curve fitting programs can be implemented, the characteristics of the reduced input data must be known. Largely to answer this question but also to answer questions of data handling, direct and indirect cross-correlation results are presented as experimental data. The experimental curves show a smooth transition, for instance, as a function of transducer separation and give promise that a combination of cross-correlation and cross power spectral density results can effectively serve as input to diagnostic programs. In this case, microphone data was reduced from the MSFC/Ames generalized protuberance tests.

In order to develop universal equations, the experimental data must first be non-dimensionalized. The question immediately put forth is whether to non-dimensionalize on a statistical basis or on geometric and

flow bases. Section (2.0) discusses a number of ways to normalize the cross-correlation and cross power spectral density functions.

The flow processes are known to be radically different in the attached flow, separated flow and oscillating shock regions. Trial analytical equations with familiar forms are advanced in Section (3.0) for the first two flow processes, as it applies to the 10 inch model test data. The experimental curves are uniform and lead one to suspect that these equations can be expanded to apply to a limited range of geometric and flow conditions.

Throughout this work it was found advantageous to consider the same microphone results, in both the time and frequency domain. For one, the characteristic dimension of time, which is present in the ordinate of the cross power spectral density function, is not present in the cross-correlation function. The relative advantages and disadvantages for the two results are discussed in Section (4.0) and the equation utilized for inverse Fourier transforming the cross power spectral density functions, is developed in Section (5.0).

The hybrid cross-correlation system computes cross-correlation and cross power spectral density outputs using the approximations also presented in Section (3.0). Periodic time functions were treated so that one can know beforehand the proper result for the Fourier coefficients.

Section (6.0) discusses the data analysis procedures as they apply to the curves presented. Further, the tape tracks for which the cross-correlation curves are presented are shown in the matrix grids.

The tabulations for the cross power spectral densities are presented in Data Report No. 505 and the tabulations for the transformed cross power spectral densities are presented in Data Report No. 506.

BAGANOFF ASSOCIATES, INC.

Report No. 507

Date June 27, 1969

OPTIONS FOR THE NORMALIZATION OF THE X-PSD AND THE CROSS-CORRELATION

Normalization of the cross-correlation function or the cross power spectral density can be based on either physical or statistical concepts. Since the cross power spectral density is the Fourier transform of the cross-correlation, any non-dimensionalization based on physical considerations which applies to the cross-correlation therefore applies to the X-PSD. This statement holds true, provided one accounts for the extra dimension of time introduced with the Fourier transform, in dividing the X-PSD by an appropriate characteristic time. In this case, one needs two physical quantities that characterize the physical process to complete the normalization of the two functions.

The present data were derived from pressure records and therefore, the cross-correlation function has the dimension of pressure squared. If one divides the cross-correlation, $R_{xy}(\tau)$, by the square of the free-stream dynamic pressure, q, one obtains a dimensionless quantity, $R_{xy}(\tau)/q^2$, which should behave like a pressure coefficient. In supersonic flow, all pressure coefficients exhibit the Mach Number dependence, $cp \sim (M-1)^{-2}$. Therefore, one should find $R_{xy}(\tau)/q^2 \sim (M-1)^{-2}$. Stated in another way, the dimensionless group, $(M-1)^2 R_{xy}(\tau)/q^2$, should show a very weak Mach Number dependence, except for $M \approx 1$ and situations where the flow undergoes a drastic change in the vicinity of a particular pressure transducer (due to separation, movement of a local shock wave, etc.), as the Mach Number is changed.

Another physical quantity that has been used for non-dimensionalizing the autocorrelation of a random pressure signal is the wall shear stress, τ_w , developed by the boundary layer at the location of the pressure transducer being considered. For the case of the cross-correlation function, two values of τ_w should be considered and the appropriate non-dimensionalization would become $R_{xy}(\tau)/ \tau_{w_x} \tau_{w_y}$. However, there is no reason to believe that this form of non-dimensionalization for $R_{xy}(\tau)$ is any less Mach Number dependent than the form, $(M-1)^2 R_{xy}(\tau)/q^2$; and since τ_w is difficult to calculate accurately, besides being rarely measured along with pressure data, there is no advantage in using the second form when reducing data for engineering purposes.

It would therefore be useful to plot $(M-1)^2 R_{xy}(\tau)/q^2$ versus τ when attempting to correlate supersonic data for different Mach Numbers or, if greater detail is desired in a plotted display, it would be very instructive to consider an isometric plot of $R_{xy}(\tau)/q^2$ in the space of τ and M. The utility of an isometric plot in the space of τ and M would be to show, for example, how the communication between two points changes, as the structure of the flow changes with the Mach Number. That is, if two points x and y are located in a region where the boundary layer is attached with y downstream from x, then $R_{xy}(\tau)$ should show correlation principally for positive τ, since most of the disturbance would propagate as a result of convection. However, if an increasing Mach Number causes the flow to become separated, with the possibility of reversing the direction of local convection, then correlation for negative τ could appear and this would be vividly

exhibited in such a plot. Likewise, an isometric plot in the space of τ and x would yield similar information concerning the spatial distribution at a fixed M.

A characteristic time is needed, in addition to a characteristic pressure, if one is to non-dimensionalize the X-PSD or, if non-dimensionalization of τ (or ω) is to be considered. The characteristic time frequently used with the power spectral density is the ratio δ/U , where δ is the boundary layer displacement thickness and U is the velocity at the outer edge of the boundary layer. Since the calculation of δ would be difficult for a complicated body or even difficult to define for a separated flow, the time δ/U is useful only for restricted application. In addition, if one scales the X-PSD with δ/U , this implies that the X-PSD scales with model size, just as δ scales with model size.

Another characteristic time frequently used is the time defined by h/U , where h is a dimension such as a step height. For a fixed ratio of h to model size, one would conclude, in this case, that the X-PSD scales directly with model size, which contradicts the conclusion drawn above (that it scales with δ) since δ and h do not scale the same with model size. Here one can see that the selection of a meaningful characteristic time can be difficult and must be done on a rational basis, since it is a very important quantity for scaling data with model size or to full scale vehicles. Although data could be obtained for only a limited range of model sizes, it would be very important that such a study be conducted so that a rational characteristic time could be selected.

Normalization based on statistical concepts leads to a somewhat different treatment of the data. This can best be seen with the aid of the following derivation. Consider two periodic functions, x(t) and y(t), with period 2T. For even functions of time, one can write

$$x(t) = \sum_{n=0}^{\infty} a_n(x) \cos \omega_n t$$
$$y(t) = \sum_{n=0}^{\infty} c_n(y) \cos(\omega_n t + \phi_n) \quad , \tag{1}$$

where the notation $a_n(x)$ and $c_n(y)$ is used to represent the constant coefficients in the series for x(t) and y(t) respectively. The Fourier transform of the signal x(t) is defined by the equation

$$X(\omega) = \int_{-\infty}^{\infty} x(t)\, e^{-i\omega t}\, dt \quad ,$$

and the Fourier transform of the cosine function is given in the following table:

x(t)	$\cos(\omega_n t + \phi_n)$
X(ω)	$2\pi e^{-i\phi_n} \delta(\omega - \omega_n)$

where $\delta(\omega - \omega_n)$ is the delta function located at ω_n The factor of two arises as a result of the fact that we are only considering positive frequencies; otherwise, one must locate the delta function at $\omega = \pm\omega_n$. Using the table, we can form the Fourier transform of the two signals x(t) and y(t) and obtain

$$X(\omega) = 2\pi \sum_{n=0}^{\infty} a_n(x)\, \delta(\omega - \omega_n)$$
$$Y(\omega) = 2\pi \sum_{n=0}^{\infty} c_n(y)\, e^{-i\phi_n}\, \delta(\omega - \omega_n)$$

Multiplying $X(\omega)$ by the complex conjugate $\overline{Y(\omega)}$, we have

$$X(\omega)\ \overline{Y(\omega)} = 4\pi^2 \sum_{n=0}^{\infty}\sum_{k=0}^{\infty} a_n(x)\ c_k(y)\ e^{i\phi k}\delta(\omega - \omega_n)\ \delta(\omega - \omega_k)$$

Since the product of two delta functions is non-zero only for $\omega_k = \omega_n$, the expression reduces to a single summation yielding

$$X(\omega)\ \overline{Y(\omega)} = 4\pi^2 \sum_{n=0}^{\infty} a_n(x)\ c_n(y)\ e^{i\phi n}\ \delta(\omega - \omega_n)$$

The cross power spectral density for the two signals $x(t)$ and $y(t)$ is defined to be

$$\Phi_{xy}(\omega) = \lim_{T \to \infty} \frac{X(\omega)\ \overline{Y(\omega)}}{T}$$

Because of cancellation below, we can lump all terms preceding the summation sign into a single constant K and write

$$\Phi_{xy}(\omega) = K \sum_{n=0}^{\infty} a_n(x)\ c_n(y)\ e^{i\phi n}\ \delta(\omega - \omega_n) \qquad (2)$$

The power spectra for $x(t)$ and $y(t)$ respectively are therefore given by

$$\Phi_{xx}(\omega) = K \sum_{n=0}^{\infty} a^2{}_n(x)\ \delta(\omega - \omega_n)$$

$$\Phi_{yy}(\omega) = K \sum_{n=0}^{\infty} c^2{}_n(y)\ \delta(\omega - \omega_n)$$

The total power contained in the signal $x(t)$ is given by the area under the curve for the power spectral density, $\Phi_{xx}(\omega)$, i.e.

$$\sigma_{xx}{}^2 = \int_{-\infty}^{\infty} \phi_{xx}(\omega)\ d\omega$$

Since the area under the delta function in ω space is defined to be $1/2\pi$, the above equations yield the results

$$\sigma_{xx}^2 = \frac{K}{2\pi} \sum_{n=0}^{\infty} a^2{}_n(x)$$

$$\sigma_{yy}^2 = \frac{K}{2\pi} \sum_{n=0}^{\infty} c^2{}_n(y) \qquad (3)$$

Because the X-PSD reduces to the PSD for the case $x(t) = y(t)$, it is natural to consider the quantity $\sqrt{\sigma_{xx}^2 \, \sigma_{yy}^2}$, i.e., the geometric mean of the two total powers, as the normalizing factor for the cross power spectral density, $\phi_{xy}(\omega)$. From the above expressions, we therefore obtain for the normalized X-PSD,

$$\tilde{\phi}_{xy}(\omega) = \phi_{xy}(\omega) \; / \; \sqrt{\sigma_{xx}^2 \, \sigma_{yy}^2} \quad ,$$

the relation

$$\tilde{\phi}_{xy}(\omega) = \frac{2\pi \sum_{n=0}^{\infty} a_n(x) \, c_n(y) \, e^{i\phi_n} \, \delta(\omega - \omega_n)}{\left[\left\{ \sum_{n=0}^{\infty} a^2{}_n(x) \right\} \left\{ \sum_{n=0}^{\infty} c^2{}_n(y) \right\} \right]^{1/2}} \quad , \qquad (4)$$

where the coefficient K has been cancelled as mentioned above.

Another candidate quantity for normalizing the cross power spectral density can be inferred as a natural extention to the relations given by Equation (3). That is, if we compute the total area under the curve, $\phi_{xy}(\omega)$, without regard to phase angle, we can introduce the total cross power

$$\sigma_{xy}^2 = \frac{K}{2\pi} \sum_{n=0}^{\infty} a_n(x)\, c_n(y) \qquad (5)$$

as a companion relation to σ_{xx}^2 and σ_{yy}^2 . Using the definition,

$$\tilde{\phi}_{xy}^*(\omega) = \phi_{xy}(\omega) \;/\; \sigma_{xy}^2(\omega) \quad ,$$

we obtain a second normalized cross power spectral density given by

$$\tilde{\phi}_{xy}^*(\omega) = \frac{2\pi \sum_{n=0}^{\infty} a_n(x)\, c_n(y)\, e^{i\phi_n}\, \delta(\omega - \omega_n)}{\sum_{n=0}^{\infty} a_n(x)\, c_n(y)} \qquad (6)$$

For the special case where the signals x(t) and y(t) are the same, the two normalized quantities, $\tilde{\phi}_{xy}(\omega)$ and $\tilde{\phi}_{xy}^*(\omega)$, become identical, i.e.

$$\tilde{\phi}_{xx}(\omega) \equiv \tilde{\phi}_{xx}^*(\omega) \quad ,$$

and they satisfy the unit area relation

$$\int_{-\infty}^{\infty} \tilde{\phi}_{xx}(\omega)d\omega = \int_{-\infty}^{\infty} \tilde{\phi}_{xx}^*(\omega)d\omega = 1$$

which is the desired definition of normalization for the power spectral density function.

An additional useful property of the two normalized quantities can be found by considering the special case where both x(t) and y(t) are single cosine waves

with frequency ω_k and phase difference ϕ_k . We then have from Equations (4) and (6), for the case n = k,

$$\tilde{\phi}_{xy}(\omega) = \tilde{\phi}_{xy}^*(\omega) = 2\pi\, e^{i\phi_k}\, \delta(\omega - \omega_k)$$

If we define $\tilde{\phi}_{xy}(\overline{\omega_k})$ to be the integrated quantity over the band, centered at ω_k, we then obtain

$$\tilde{\phi}_{xy}(\overline{\omega_k}) = \tilde{\phi}_{xy}^*(\overline{\omega_k}) = e^{i\phi_k}$$

which is equal to unity if $\phi_k = 0$ (no phase difference), equal to +i for $\phi_k = \pi/2$, and equal to -1 for $\phi_k = \pi$. Both normalized cross power spectral density functions defined here therefore exhibit the phase relation between x(t) and y(t) when they consist of a single and identical frequency.

The cross-correlation function, $R_{xy}(\tau)$, is obtained from the inverse Fourier transform of $\Phi_{xy}(\omega)$. Since the above expression for $\Phi_{xy}(\omega)$ consists of a sum of terms of the form $e^{-i\phi_n}\, \delta(\omega-\omega_n)$, the table shows that the inverse transform of each term is simply a cosine term and the expression for $R_{xy}(\tau)$ becomes

$$R_{xy}(\tau) = \frac{K}{2\pi} \sum_{n=0}^{\infty} a_n(x)\, c_n(y)\, \cos(\omega_n\tau - \phi_n)$$

For the case where x(t) and y(t) are the same function, the equation yields the expressions for the two autocorrelations, i.e.,

$$R_{xx}(\tau) = \frac{K}{2\pi} \sum_{n=0}^{\infty} a^2{}_n(x)\, \cos(\omega_n\tau)$$

$$R_{yy}(\tau) = \frac{K}{2\pi} \sum_{n=0}^{\infty} c^2{}_n(y)\, \cos(\omega_n\tau)$$

The total power contained in each signal is obtained by setting τ equal to zero in the respective autocorrelation function; thus we obtain

$$R_{xx}(o) = \frac{K}{2\pi} \sum_{n=0}^{\infty} a^2{}_n(x)$$

$$R_{yy}(o) = \frac{K}{2\pi} \sum_{n=0}^{\infty} c^2{}_n(y)$$

as expected. Using the geometric mean of the total powers as the normalizing factor,

$$\tilde{R}_{xy}(\tau) = R_{xy}(\tau) \; / \; \sqrt{R_{xx}(o)\; R_{yy}(o)}$$

the normalized cross-correlation becomes

$$\tilde{R}_{xy}(\tau) = \frac{\sum_{n=0}^{\infty} a_n(x)\; c_n(y)\; \cos(\omega_n \tau - \phi_n)}{[\{\sum_{n=0}^{\infty} a^2{}_n(x)\}\;\; \{\sum_{n=0}^{\infty} c^2{}_n(y)\}]^{1/2}} \qquad (7)$$

where the constant $K/2\pi$ has been cancelled.

It is quite obvious from the definition of $\tilde{R}_{xy}(\tau)$ that we recover the result

$$\tilde{R}_{xx}(o) = R_{yy}(o) = 1$$

However, in general we should not expect $R_{xy}(o)$ to be unity for $a_n(x) \neq c_n(y)$. If the cross-correlation function is properly normalized, we must have

$$| \tilde{R}_{xy}(\tau) | \leq 1$$

for all values of τ, as well as for the special case where $x(t)$ and $y(t)$ are the same. This can be shown with the aid of the following device. Let the vectors

$\overline{A}$ and $\overline{C}$ be defined by the components

$$A_n = a_n(x) \; / \; [\sum_{n=0}^{\infty} a^2{}_n(x)]^{1/2}$$

$$C_n = c_n(y) \; / \; [\sum_{n=0}^{\infty} c^2{}_n(y)]^{1/2}$$

Therefore, both $\overline{A}$ and $\overline{C}$ are unit vectors and we have

$$|\overline{A} \cdot \overline{C}| \; = \; |\sum_{n=0}^{\infty} A_n \, C_n| \leq 1$$

If we define the vector $\overline{C}'$ to be given by

$$C'_n = C_n \cos(\omega_n \tau - \phi_n) \quad ,$$

we see that the magnitude of $\overline{C}'$ is less than or equal to the magnitude of $\overline{C}$ because of the cosine term, i.e.,

$$| \overline{C}' | \; \leq \; | \overline{C} |$$

Therefore, we have

$$|\tilde{R}_{xy}(\tau)| = | \sum_{n=0}^{\infty} A_n \, C_n \cos(\omega_n \tau - \phi_n)| \leq | \sum_{n=0}^{\infty} A_n \, C_n| \leq 1$$

which shows that the magnitude of the normalized cross-correlation function is always less than or equal to unity.

One could also consider the dimensionless quantities

$$R_{xy}(\tau) \;/\; R_{xx}(o) \text{ and } R_{xy}(\tau) \;/\; R_{yy}(o)$$

which are ratios to the total power in the signals x(t) and y(t) respectively. However, the magnitude of each of these expressions is not necessarily less than unity for all values of τ. This can be seen quite easily from the relation

$$R_{xy}(\tau) \;/\; R_{xx}(o) = \tilde{R}_{xy}(\tau) \left[\frac{R_{yy}(o)}{R_{xx}(o)} \right]^{1/2}$$

which shows that it can be greater than unity if $R_{yy}(o) \;/\; R_{xx}(o) > 1$. Of course, this is also obvious physically. That is, if most of the power is contained in the signal y(t), the ratic $|R_{xy}(\tau)| / R_{xx}(o)$ consists of a relatively large number divided by a small number and the ratio can become large.

As is evident from the above discussion, the number of options available for normalization of the X-PSD and the autocorrelation functions is quite large. And in each case, the normalization can be introduced on the basis of a very rational argument. Obviously, the manner in which data is reduced depends on the kind of questions one is interested in answering. However, random data analysis is in an early state of development where many of the questions of interest to engineers are yet to be identified and formulated clearly. Therefore, it would be very desirable to display data in more than one form, where statistical concepts are stressed in one case and gas dynamic concepts are stressed in another, in order to maximize the interpretive value of a given set of data.

For example, from a gas dynamic point of view, one would view the quantity $R_{xy}(\tau)/q^2$ as a kind of a pressure coefficient; and it is well known that, for a fixed Mach number, pressure coefficients are rather insensitive to scale size, so that pressure coefficients obtained from wind-tunnel models can be applied almost directly to full scale vehicles. Here it would be of interest to learn whether the quantity $R_{xy}(\tau)/q$ behaves in the same manner, with regard to scaling with model size, or whether it behaves quite differently due to its statistical property.

As mentioned in the first part of this section, a characteristic time is needed if one is to non-dimensionalize the X-PSD. This quantity is difficult to establish for a complicated model and often it has been selected on an ad hoc basis. Since this quantity is directly involved in scaling the X-PSD with model size, it would be desirable to identify the correct characteristic time that should be used, from data for which model size is varied.

A question of vital importance to the understanding of data on random pressure fluctuations, concerns the distribution between generation, propagation and convection of random energy at each point, i.e., knowing what fraction of the total rms pressure fluctuation at a given point is due to local generation and what fraction is received from other points in a flow field can aid greatly in identifying and controlling the major sources of disturbances. The cross-correlation function is an ideal quantity for such a study and with suitable manipulation, this information could be readily obtainable.

RECOGNITION OF PATTERNS IN THE EXPERIMENTAL DATA

The groundwork can be prepared for discussing the experimental data by considering several special cases for which analytic expressions can be used to represent the plotted correlation functions. The expression derived in the above section for the normalized cross-correlation function, namely,

$$\tilde{R}_{xy}(\tau) = \sum_{n=0}^{\infty} A_n C_n \cos(\omega_n \tau - \phi_n) \qquad (1)$$

where

$$A_n = a_n(x) \; / \; [\sum_{n=0}^{\infty} a^2{}_n(x)]^{1/2}$$

$$C_n = c_n(y) \; / \; [\sum_{n=0}^{\infty} c^2{}_n(y)]^{1/2}$$

can be recognized as a finite difference analog to the integral relation between $\tilde{R}_{xy}(\tau)$ and $\Phi_{xy}(\omega)$. That is, $\tilde{R}_{xy}(\tau)$ is the inverse Fourier transform of $\Phi_{xy}(\omega)$

$$\tilde{R}_{xy}(\tau) = \frac{1}{2\pi} \int_{-\infty}^{\infty} \Phi_{xy}(\omega) \, e^{i\omega\tau} \, d\omega$$

Recognizing that $\Phi_{xy}(\omega)$ is a complex number, the equation becomes

$$\tilde{R}_{xy}(\tau) = \frac{1}{2\pi} \int_{-\infty}^{\infty} [\Phi^R_{xy}(\omega) + i\Phi^I_{xy}(\omega)] \, [\cos\omega\tau + i\sin\omega\tau] \, d\omega$$

Since $\tilde{R}_{xy}(\tau)$ must always be real, for a real process, we need only retain the non-zero part of the integral and write

$$\tilde{R}_{xy}(\tau) = \frac{1}{2\pi} \int_{-\infty}^{\infty} [\Phi^R_{xy}(\omega)\cos\omega\tau - \Phi^I_{xy}(\omega)\sin\omega\tau] \, d\omega$$

Written in a finite difference form, the integral becomes

$$\tilde{R}_{xy}(\tau) = \frac{\Delta\omega}{\pi} \sum_{n=0}^{\infty} [\Phi^{R}_{xy}(\omega_n)\cos\omega_n\tau - \Phi^{I}_{xy}(\omega_n)\sin\omega_n\tau] \qquad (2)$$

where $\Delta\omega$ is the width of the incremental frequency and ω_n is the center frequency at each incremental step. Comparing this last equation with the equation given above, we see that the coefficients A_nC_n and the phase angles ϕ_n are obtained from the real and imaginary parts of the complex numbers, $\phi_{xy}(\omega_n)$.

When considering the autocorrelation function, we have

$$\tilde{R}_{xx}(\tau) = \frac{\Delta\omega}{\pi} \sum_{n=0}^{\infty} \phi_{xx}(\omega_n) \cos \omega_n\tau \qquad (3)$$

since $\tilde{R}_{xx}(\tau)$ is both a real and an even function, and therefore, $\phi_{xx}(\omega)$ is also both real and even. Thus we see that for all autocorrelation functions, we have the simple result

$$A^2_n = \frac{\Delta\omega}{\pi} \Phi_{xx}(\omega_n) \qquad (4)$$

$$\phi_n = 0$$

When considering the cross-correlation function however, ϕ_n and $A_n C_n$ must be obtained from $\Phi^{R}_{xy}(\omega_n)$ and $\Phi^{I}_{xy}(\omega_n)$ for each individual case. Typical distributions for the quantities $A_n C_n$ and ϕ_n, can be found by considering some

representative functional forms for $\tilde{R}_{xy}(\tau)$. For example, Plot Numbers (14), (35) and (48), exhibit autocorrelations that can be represented by the form

$$\tilde{R}_{xx}(\tau) = e^{-\alpha|\tau|}$$

The Fourier transform of this function is

$$\phi_{xx}(\omega) = 2\alpha \; / \; (\alpha^2 + \omega^2)$$

and therefore we have for this case, from Equation (4),

$$A^2_n = \frac{2\alpha\Delta\omega/\pi}{(\alpha^2+\omega^2_n)}$$

$$\phi_n = 0 \quad ,$$

which shows that each frequency component of the signal x(t) must vary like $A_n \sim \omega_n^{-1}$ and no phase difference exists between the respective components. A slightly more complicated autocorrelation function,

$$\tilde{R}_{xx}(\tau) = e^{-\alpha|\tau|} \cos\beta\tau \; ,$$

which would represent Plots (8), (27), (42), (64) and (93), yields the result

$$A^2_n = \frac{\alpha\Delta\omega}{\pi} \left\{ \frac{1}{\alpha^2+(\beta-\omega_n)^2} + \frac{1}{\alpha^2+(\beta+\omega_n)^2} \right\}$$

$$\phi_n = 0$$

showing a similar decay for large frequencies.

Several of the autocorrelation plots, such as Plot numbers (1), (18), (23), (30), (70) and (75), appear to be the sum of two exponentials such as

$$\tilde{R}_{xx}(\tau) = (1-\kappa)\, e^{-\alpha|\tau|} + \kappa\, e^{-\gamma|\tau|}$$

where the time scale of the first term is much smaller than the time scale of the second term. For example, Plot (23) seems to be an extreme case, so the combination, $\kappa = 1/4$, $\gamma = \alpha/10$, would not be an unreasonable approximation. Using these values, we find

$$\Phi_{xx}(\omega) = \frac{3\alpha/2}{\alpha^2+\omega^2} + \frac{5\alpha}{\alpha^2+(10\omega)^2}$$

showing that the part of $\tilde{R}_{xx}(\tau)$, corresponding to a broad correlation, appears as a spike in the frequency domain. This can be seen most easily with the following plot of the individual parts

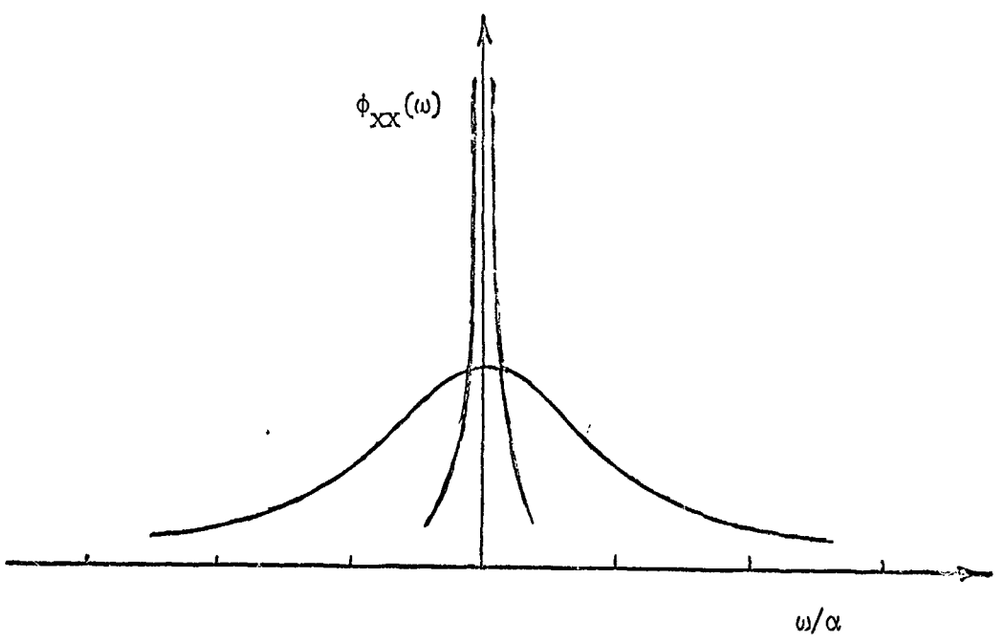

Since the sharp spike in the plot of $\Phi_{xx}(\omega)$ corresponds to the more important information, in terms of broadness of correlation, we see that the curve would have to be established very accurately near the origin, i.e. for $\omega \to 0$. But this is precisely the area where it is difficult to resolve a sharp spike when working with experimental data. Therefore, in order to reduce errors associated with data reduction in such a case, one should compute $R_{xy}(\tau)$ directly from the raw data, rather than from the inverse Fourier transform of $\Phi_{xy}(\omega)$.

Several of the plots of the cross-correlation function resemble a one-sided exponential, for example Plot number (28). Our analytic representation becomes

$$\tilde{R}_{xy}(\tau) = \begin{cases} e^{-\alpha\tau} & \tau > 0 \\ 0 & \tau < 0 \end{cases}$$

the corresponding X-PSD is

$$\Phi_{xy}(\omega) = \frac{\alpha+i\omega}{\alpha^2+\omega^2}$$

and using Equation (2) for $\tilde{R}_{xy}(\omega)$, we have

$$\tilde{R}_{xy}(\omega) = \frac{\Delta\omega}{\pi} \sum_{n=0}^{\infty} \frac{\alpha \cos\omega_n\tau - \omega_n \sin\omega_n\tau}{\alpha^2 + \omega_n^2}$$

And on comparing with Equation (1), we find

$$A_n C_n = \frac{\Delta\omega/\pi}{(\alpha^2+\omega_n^2)^{1/2}}$$

$$\phi_n = -\tan^{-1}\frac{\omega_n}{\alpha}$$

showing that ϕ_n is non-zero for cross-correlations.

A more realistic functional representation for many of the plotted cross-correlation functions is of the form

$$\tilde{R}_{xy}(\tau) = e^{-\alpha|\tau-\tau_0|}\cos\beta(\tau-\tau_0)$$

See for example, Plots (2), (3), (5), (9), (10), (15), (19), etc. Following the same procedure as above, we have

$$\Phi_{xy}(\omega) = \alpha e^{-i\omega\tau_0}\left\{\frac{1}{\alpha^2+(\beta-\omega)^2} + \frac{1}{\alpha^2+(\beta+\omega)^2}\right\}$$

$$A_n C_n = \frac{\alpha\Delta\omega}{\pi}\left[\frac{}{\alpha^2+(\beta-\omega_n)^2} + \frac{}{\alpha^2+(\beta+\omega_n)^2}\right]^{-1}$$

$$\phi_n = \tau_0\omega_n$$

This last result exhibits the relation between the peak of the curve, $\tilde{R}_{xy}(\tau)$, given by τ_0, and the phase angle ϕ_n, as one would expect for an even cross-correlation function displaced a distance, τ_0 , from the origin.

The above collection of examples shows that the frequency dependence of the coefficients A_n and C_n, corresponding to the various experimental plots should be expected to be rather weak, since all of the examples varied like ω_n^{-1}. That is, many frequencies are present in the pressure signals x(t) and y(t) and therefore statistical properties are to be expected when analyzing the data.

One of the more prominent features of much of the cross-correlation data, as one compares plots for a succession of station pairs, is the presence of one or two maxima, which seem to be the result signal convection with some mean fluid speed. This can be seen in the sequence of Plots (49) through (54), where each combination of stations 10 - 10 to 10 - 5 is represented. As the separation distance is increased, one first sees a single peak for positive τ and then the development of a second peak for negative τ, with both peaks receding from the origin as the separation distance increases. If we focus our attention on Plot (52), we see the process in an advanced state of development with two distinct peaks located at the points τ = 210 microseconds and τ = 110 microseconds respectively. From a physical point of view, the occurrence of positive correlation at the two points indicates that information is being convected in both directions between the two stations 10 and 7. In a normal turbulent boundary layer with station 10 upstream from station 7, one would not expect the upstream propagation to be significant compared with the downstream convection of infor-

mation. Therefore, a positive cross-correlation should only appear for positive τ . However, in the present case, stations 10 and 7 probably encompass the separation point in the boundary layer and therefore the recirculating flow provides a two-way path for the convection of information between the two points; i.e., near the model surface the flow is from 7 to 10 and further from the surface, the flow is from 10 to 7.

The occurrence of two distinct maxima in a cross-correlation function can be explained with the aid of the following simple physical model. Let the pressure signal x(t), at the point x in a fluid, be composed of a locally generated signal, f(t), and a transmitted signal, g(t), which is delayed an amount, τ_x, and attenuated by a factor of ε.

$$x(t) = f(t) + \varepsilon g(t - \tau_x)$$

Likewise, let the pressure signal y(t) be the opposite combination, with g(t) being the locally generated signal at the point y in a fluid, and f(t) the transmitted signal, which is delayed an amount, τ_y, and attenuated by the factor ε.

$$y(t) = g(t) + \varepsilon f(t - \tau_y)$$

The cross-correlation, $R_{xy}(\tau)$, of the two pressure signals, x(t) and y(t), is obtained by forming the mean of the equation

$$x(t)y(t) = [f(t)+\varepsilon g(t-\tau_x)]\ [g(t+\tau) + \varepsilon f(t+\tau-\tau_y)]$$

If we assume that the signals f(t) and g(t) are generated independently of one another, i.e., statistically independent, and furthermore that the two signals are stationary, we then have

$$R_{xy}(\tau) = \epsilon R_{gg}(\tau+\tau_x) + \epsilon R_{ff}(\tau-\tau_y)$$

Since $R_{gg}(\tau)$ and $R_{ff}(\tau)$ are autocorrelation functions, they are real, symmetric and positive, and they peak at the origin. Therefore, the first term has a maximum at the point $\tau = -\tau_x$ and the second term has a maximum at $\tau = \tau_y$. Comparing this result with Plot number (52), we see that we can interpret the peak occurring at positive τ as a result of the convection of the signal from stations 10 to 7 in the outer flow, while the peak occurring at negative τ is the result of the convection of the signal from stations 7 to 10 in the recirculating flow near the model surface.

The above relation for $R_{xy}(\tau)$ was obtained using the assumption that f(t) and g(t) are the only signals that are produced and that they are statistically independent, i.e., $R_{fg}(\tau) = 0$. In an actual flow process, this assumption is not entirely correct, since certain portions of the correlated pressure signals may be the result of global fluctuations in the fluid, or fluctuations generated between the two points x and y, which add a common signal to both x(t) and y(t). The possibility of a common signal being present in x(t) and y(t) would certainly be greater as the separation distance between points x and y increases. Thus, it would be reasonable to

to expect $R_{xy}(\tau)$ to assume negative values as the separation distance increases, due to the non-zero value of $R_{fg}(\tau)$ in the above mathematical model.

A development in this direction definitely appears in the sequence following Plot (52), i.e., Plot (53) through (56). This observation appears to hold for all of the stations located in or near the separated region, while for stations well ahead of the separation points, approximately station 9, the picture is quite different. The sequence of Plots (30) through (34) is an example where one of the correlated signals is obtained from a point well ahead of the separation point. The most distinctive features of the sequence is the extreme broadness of the correlations and the nature of the trend between plots. Plot number (32), which is a cross-correlation between the pressure signals at stations 13 and 10, shows evidence of signal propagation in only the upstream direction because of the smallness of the correlation for positive τ . This could very likely be the case, for both stations are upstream of the separation point and most of the noise is generated in the separated region of the flow field (the rms pressure fluctuation in the separated region is generally four or five times greater than the value in a turbulent boundary layer). Since the flow is subsonic in the portion of the boundary layer near the wall, it is quite possible stations 13 and 10 are in the path of waves propagating upstream from the separation point, which would explain the strong correlation for negative τ

in Plot (32). If we conclude that a main portion of the signal amplitude being correlated is the result of propagation upstream, rather than generation within the turbulent boundary layer, then only those frequencies will be present that can be transmitted along this boundary layer.

Since certain frequencies would be favored in propagating along a boundary layer, e.g., the Tollmien Schlichting waves in a laminar boundary layer, one would expect the signals $x(t)$ and $y(t)$ to exhibit a relatively limited range of frequencies; and therefore the corresponding cross power spectrum, $\Phi_{xy}(\omega)$, would show a rapid decay in magnitude as ω increases. Referring to the examples cited above, we see that this situation requires that the cross-correlation function, $R_{xy}(\tau)$, exhibit a broad correlation. But this is exactly what is observed in Plots (30) and (31), which show correlation intervals much greater than the plots for data obtained in the separated region. Therefore, the sequence of Plots (30) through (32), which exhibit data obtained from points upstream of the separation point, have a common thread of consistency.

CROSS POWER SPECTRUM VERSUS CROSS-CORRELATION RESULTS

The answer to the question of which result is more useful, ultimately lies in its engineering application. The hybrid system has the capability to compute both statistical results independently of the other. This Report compares curves of cross-correlations with the transformed cross power spectra, to help answer questions regarding data handling.

Many times a researcher makes use of a result form that is readily obtainable from a computer, rather than the kind that directly conveys answers to the questions being asked. A case in point, is the use of narrow band cross power spectra to relay convection velocity information. The difficulty in this approach is depicted in the drawing, which shows that the complex vector, made up of the real and imaginary parts as a function of ω, produces a line in three-dimensional space.

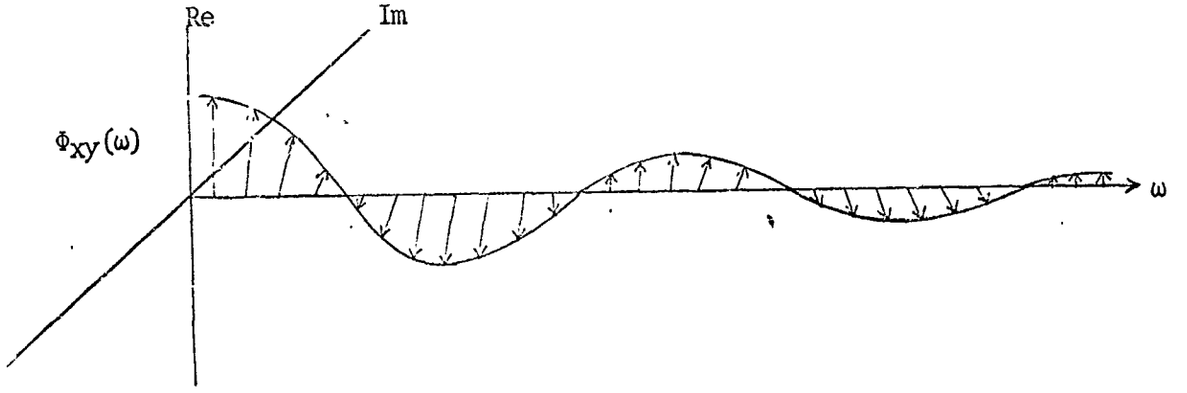

The number of times that the complex vector has rotated about the ω-axis, in going from $\omega = 0$ to $\omega = \omega_1$, must be known for narrow band velocity calculations.

Theory states that the trajectory of the complex vector produces a simply connected line. It may be expected that as very small steps in ω are taken, which is equivalent to using very narrow filter bands, the phase angle, $\theta(\omega)$, can be followed. The penalty that is usually paid is that the BT product is permitted to substantially decrease. This condition of a weak statistical estimate is most assuredly the worst condition of the two.

In solving the inverse Fourier transform for $R_{xy}(\tau)$, as follows,

$$R_{xy}(\tau) = \int_{-\infty}^{\infty} \Phi_{xy}(\omega)\ e^{i\omega\tau}\ d\omega$$

the complex value of $\Phi_{xy}(\omega)$ at each ω is all that is required. The number of times that the complex vector has rotated about the ω-axis in arriving at a particular ω, does not enter into the equation. The computation of $R_{xy}(\tau)$, which involves averaging over ω, produces several advantages, plus removing the difficulty of calculating the narrow band convection velocity in the frequency domain.

For real functions such as fluctuating pressure signals, the cross power spectrum $\Phi_{xy}(\omega)$, must be Hermitian. This fact implies that the real part is even and that the imaginary part is odd. The imaginary part, being odd, dictates that as ω approaches 0, the phase angle $\theta(\omega)$, must also go to 0. The generally advanced concept, that radiation is taking place in the physical process at the low frequencies, may not be the case.

The cross-correlation function is a real quantity and is therefore easier to interpret in terms of the physical process; whereas the cross power spectrum is a complex quantity and therefore is more difficult to interpret. The probability that two different processes exist in the flow for two different velocities is much greater than that they have different frequency components. The cross-correlation function which shows the tau or velocity decompostion, is much more assessable by just looking at three-dimensional plots.

The present experimental data indicates that a seventh or eighth order transfer function would satisfactorily describe each of the flow processes. In the separated flow region, the curves are double humped, with one peak occurring for positive tau and the other for negative tau. This could make good sense in the recirculation region, where there is both downstream and upstream flow. The sharpness of the two peaks indicates that the frequency components are confined to relatively narrow bandwidths, or that the gas structure is confined to small particles.

The slow decay of the single cross-correlation peak for the attached flow, is also readily discernible. The large cross-correlation values seem to indicate that large gas structures exist in the boundary layer.

Experimental data has shown that the cross power spectrum has completed several revolutions and has substantially decayed in amplitude for large ω. If the frequency spectrum between 12 and 20,000 Hz is broken up into one-third octave

filter bands, and if the phase uniformly changes with the logarithm of the frequency, then the phase change between the filter center frequencies should be approximately 22°. Keeping track of the approximately 33 steps in $\theta(\omega)$ is tedious and becomes even more difficult if the BT product is allowed to decrease. Once again, the averaging over frequency, to arrive at a tau or velocity decomposition, overcomes the above problem and the problem of the short vector lengths.

In general, the turbulent flow upstream of two pressure transducers, is complicated and may be both dispursive and diffusive in nature. The average velocity, which is all that can be measured between two points, does not give enough information about the process. Computer programs that take into account three or more spatial cross-correlation points can, for instance, give the fluid's acceleration.

The cross power spectral density matrix, for a randomly varying pressure field, $[\Phi_{pp}(i\omega)]$, has distinct advantages over its counterpart cross-correlation matrix, as an input for structural response calculations.

EQUATION FOR FOURIER TRANSFORMING CROSS POWER SPECTRAL DENSITIES

The purpose of this section is to derive an equation for the inverse Fourier transformation of one-third octave cross power spectrums. This development is along the lines suggested by Mr. Luke Schutzenhofer of NASA, to obtain experimental transformed cross power spectra, to compare with directly derived cross-correlations.

The experimental results show that the approach taken worked successfully. The numerical problem associated with the function $\sin x/x$ for small x was eliminated by replacing it with its proper limit. The transformed cross power spectra were found to not oscillate and to decay regularly due to the fact that the cross power spectra diminished to very small amplitudes for large τ. Experimentally, it is shown that the one-third octave bandwidths are sufficiently narrow for the accurate transformation from the frequency to the time domain. This result can probably be made to apply in the other direction through inductive reasoning

The equation used for the inverse Fourier transform will be derived, and an equation that holds promise of being simpler will be discussed at the end of this section. The cross power spectral density function is a complex quantity and may be expressed in general as

$$\Phi_{xy}(f) = M(f_c)\, e^{i\theta(f_c)} \qquad \cdot \quad (1)$$

The one-third octave, cross power spectra produced by the computer are composed of a modulus $M(f_c)$ and a phase angle $\theta(f_c)$ at each filter center frequency. The above continuous function may be modified to apply to the discrete case by using a truncated Taylor series expansion.

$$\Phi_{xy}(f) = \Phi_{xy}(f_c) + \Phi'_{xy}(f_c)\,\Delta f \qquad (2)$$

If Equation (1) is differentiated and substituted into Equation (2), the cross power spectra becomes

$$\Phi_{xy}(f) = [M(f_c) + \alpha\Delta f]\, e^{i\theta(f_c)} + i\beta\Phi_{xy}(f_c)\,\Delta f \qquad (3)$$

where $\alpha = M'(f_c)$ and $\beta = \theta'(f_c)$. The addition of a third term to the above equation, which is small, produces

$$\Phi_{xy}(f) = [M(f_c) + \alpha\Delta f]\, e^{i\theta(f_c)} + i\beta\Phi_{xy}(f_c)\Delta f + \alpha\Delta f e^{i\theta(f_c)} i\beta\Delta f \qquad (4)$$

This equation may be collected to give

$$\Phi_{xy}(f) = [M(f_c) + \alpha\Delta f]\, e^{i\theta(f_c)} + [M(f_c) + \alpha\Delta f]\, e^{i\theta(f_c)}\, i\beta\Delta f$$

$$= [M(f_c) + \alpha\Delta f]\, e^{i\theta(f_c)}\, [1 + i\beta\Delta f] \qquad (5)$$

If $\beta\Delta f$ is small relative to unity, the following form is obtained and thus was used in the digital program.

$$\Phi_{xy}(f) = [M(f_c) + \alpha\Delta f]\, e^{i[\theta(f_c) + \beta\Delta f]} \qquad (6)$$

The inverse Fourier transformation program prints out β, and simple calculations showed that the experimental product finally reaches unity for the 20,000 Hz center frequency filter. In conclusion, $\beta\Delta f$ was substantially less than one radian or 60 (degrees).

Analytical cross power spectra could be generated and a parametric study performed of Δf versus β.

Compute the Inverse Fourier Transform for:

$$G_{xy}(f) = \{M(f_c)+\alpha(f-f_c)\}\, e^{i\{\theta(f_c)+\beta(f-f_c)\}} \qquad (7)$$

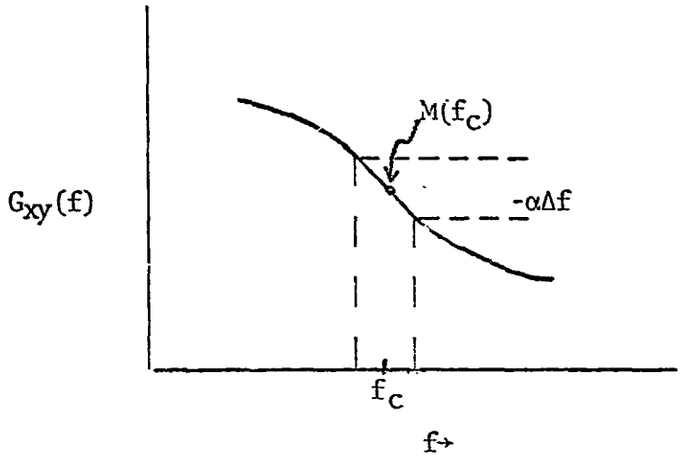

Let $f = f_c$, the modulus becomes:

$$M(f_c)+(-\alpha)(f_c-f_c) = M(f_c)$$

Let $f = f_c-\Delta f/2$, the modulus becomes:

$$M(f_c)+(-\alpha)(f_c-\Delta f/2-f_c) = M(f_c)+\alpha\Delta f/2$$

$$R_{xy}(\tau) = \int_{f_c-\Delta f/2}^{f_c+\Delta f/2} \{M(f_c)+\alpha(f-f_c)\}\, e^{i\{\theta(f_c)+\beta(f-f_c)\}}\, e^{i2\pi\tau f}\, df \qquad (8)$$

Integrating by parts, the narrow-band cross-correlation reduces to:

$$R_{xy}(\tau) = e^{i\theta(f_c)} \left[\left(\frac{M(f_c)}{i(\beta+2\pi\tau)} e^{i\{\beta(f-f_c)+2\pi\tau f\}}\right) \right. \tag{9}$$

$$+ \left(\frac{\alpha(f-f_c)}{i(\beta+2\pi\tau)} e^{i\{\beta(f-f_c)+2\pi\tau f\}}\right)$$

$$\left. + \left(\frac{\alpha}{(\beta+2\pi\tau)^2} e^{i\{\beta(f-f_c)+2\pi\tau f\}}\right) \right]_{f_c-\Delta f/2}^{f_c+\Delta f/2}$$

$$R_{xy}(\tau) = e^{i\{\theta(f_c)+2\pi\tau f_c\}} \Delta f \{ M(f_c) \left(\frac{e^{i\{\beta+2\pi\tau\}\Delta f/2} - e^{-i\{\beta+2\pi\tau\}\Delta f/2}}{2i(\beta+2\pi\tau)\Delta f/2}\right) \tag{10}$$

$$+ \frac{\alpha\Delta f}{i} \left(\frac{e^{i\{\beta+2\pi\tau\}\Delta f/2} + e^{-i\{\beta+2\pi\tau\}\Delta f/2}}{2(\beta+2\pi\tau)\Delta f/2}\right)$$

$$+ \frac{i\alpha}{(\beta+2\pi\tau)} \left(\frac{e^{i\{\beta+2\pi\tau\}\Delta f/2} - e^{-i\{\beta+2\pi\tau\}\Delta f/2}}{2i(\beta+2\pi\tau)\Delta f/2}\right) \}$$

$$R_{xy}(\tau) = \Delta f \{ M(f_c) \frac{\sin(\beta+2\pi\tau)\Delta f/2}{(\beta+2\pi\tau)\Delta f/2} \cos\{\theta(f_c)+2\pi\tau f_c\} \tag{11}$$

$$+ \frac{\alpha\Delta f}{2} \frac{\cos(\beta+2\pi\tau)\Delta f/2}{(\beta+2\pi\tau)\Delta f/2} \sin\{\theta(f_c)+2\pi\tau f_c\}$$

$$- \frac{\alpha}{(\beta+2\pi\tau)} \frac{\sin(\beta+2\pi\tau)\Delta f/2}{(\beta+2\pi\tau)\Delta f/2} \sin\{\theta(f_c)+2\pi\tau f_c\} \}$$

The broadband cross-correlation can be obtained as the sum of these bands.

$$R_{xy}(\tau)/\Delta f = \sum_{c=1}^{P} \{M(f_c)\frac{\sin(\beta+2\pi\tau)\Delta f/2}{(\beta+2\pi\tau)\Delta f/2} \cos\{\theta(f_c)+2\pi\tau f_c\} \quad (12)$$

$$+ [\frac{\alpha\Delta f \cos(\beta+2\pi\tau)\Delta f/2}{2(\beta+2\pi\tau)\Delta f/2} - \frac{\alpha \sin(\beta+2\pi\tau)\Delta f/2}{(\beta+2\pi\tau)^2\Delta f/2}]$$

$$\cdot \sin\{\theta(f_c)+2\pi\tau f_c\}$$

Equation (1) above may be expanded to the following generalized form:

$$R_{xy}(\tau) = \sum_{c=1}^{P} \{C_{xy} \cos(2\pi f_c\tau) + C_{xy}(\text{error}) \cos(2\pi f_c\tau) \quad (13)$$

$$- Q_{xy} \sin(2\pi f_c\tau) + Q_{xy}(\text{error}) \sin(2\pi f_c\tau)\}$$

where

$$C_{xy} = [M(f_c) \frac{\sin(\beta+2\pi\tau)\Delta f/2}{(\beta+2\pi\tau)\Delta f/2}] \cos\theta(f_c)$$

$$Q_{xy} = [M(f_c) \frac{\sin(\beta+2\pi\tau)\Delta f/2}{(\beta+2\pi\tau)\Delta f/2}] \sin\theta(f_c)$$

$$C_{xy}(\text{error}) = [\frac{\alpha\Delta f \cos(\beta+2\pi\tau)\Delta f/2}{2(\beta+2\pi\tau)\Delta f/2} - \frac{\alpha \sin(\beta+2\pi\tau)\Delta f/2}{(\beta+2\pi\tau)^2\Delta f/2}] \sin\theta(f_c)$$

$$Q_{xy}(\text{error}) = [\frac{\alpha\Delta f \cos(\beta+2\pi\tau)\Delta f/2}{2(\beta+2\pi\tau)\Delta f/2} \quad \frac{\alpha \sin(\beta+2\pi\tau)\Delta f/2}{(\beta+2\pi\tau)^2\Delta f/2}] \cos\theta(f_c).$$

Equation (12) was programmed, but the following equation may produce an even more accurate transformation. The cross-correlation system produces one-third octave spectrums consisting of a complex quantity $\overline{S}_k$ in discrete frequency steps $f_k = f_o(1 + k\sqrt{2}/6)$ and $\Delta f = \sqrt{2}/6\ f_o$. The value $\overline{S}_k$ is a constant at the center of the k th filter band, and the slope information $\overline{S}_k'$ can be computed from the adjacent band values. The truncated Taylor series for $\overline{S}$ becomes

$$\overline{S} = \overline{S}_k + \overline{S}_k' \Delta f \tag{14}$$

By substituting $\overline{S}$ into the inverse Fourier integral, the cross-correlation becomes

$$\begin{aligned} R_{xy}(\tau) &= \overline{S}_k \int_{f_k - \Delta f/2}^{f_k + \Delta f/2} e^{i2\pi f\tau}\, df + \overline{S}_k' \int_{f_k-\Delta f/2}^{f_k+\Delta f/2} (f-f_k)\, e^{i2\pi f\tau}\, df \\ &= \overline{S}_k \int_{f_k-\Delta f/2}^{f_k+\Delta f/2} e^{i2\pi f\tau}\, df + \overline{S}_k' \int_{f_k-\Delta f/2}^{f_k+\Delta f/2} f e^{i2\pi f\tau}\, df \\ &\quad - \overline{S}_k' \int_{f_k-\Delta f/2}^{f_k+\Delta f/2} e^{i2\pi f\tau}\, df \end{aligned} \tag{15}$$

Both the first and last integrals in Equation (15) produce algebraic functions of the form sin x/x, and the function for the second integral is obtained by differentiating the first algebraic function.

DATA PROCESSING METHODS

This Report contains 121 inverse transformed, cross power spectra, of which 61 are compared with directly computed cross-correlations. The following four digital programs had to be written to work in conjunction with the hybrid cross-correlation system to make these data comparisons possible. It will be a relatively easy matter to refine the programs and subsequently to run hundreds of additional comparisons.

1) Cross power program with instrumentation corrections for CP-100 and FR-1200 recorders.

2) Automatic plotting program for the directly reduced cross-correlations.

3) Program for numerically performing the inverse Fourier transform on one-third octave cross power data.

4) Plotting program for indirectly computed cross-correlations.

In another section, the significance of the curves, as related to the aerodynamics, is discussed. The comparisons of the shapes of the curves are surprisingly good, although the amplitude scales are different. Steps are being taken to correct the digital programs by applying the proper scalers for future analysis.

In the process of normalizing the direct and indirect cross-correlations, different scalers were used. The direct cross-correlations were normalized by the square root of the product of the mean square values, while the indirect cross-correlations were normalized by the sum of the narrow band cross power spectra moduli. The numerical program was originally written to transform analytical cross power spectra and the capability to compute the mean square values has not been incorporated as yet. Mathematical expressions for these two forms of normalization are shown respectively in Equations (4) and (6) of Section (2.0).

One can show that the two scalers reduce to the same number, when the Fourier coefficients associated with the two scalers are the same. Experimentally, this condition can be verified by observing Plot number (15), where the two curves are of equal amplitude because of the small transducer separation. Plot number (16), for a slightly larger separation, dramatically shows that the frequency composition of the downstream transducer signal has changed significantly. These two forms of normalization, based on statistics, produce striking results when compared.

A sub-routine in the digital program determines the $\Delta\tau$ increments for the numerical transform. It does this by noting the frequency at which the modulus has the largest peak. The program then computes $\Delta\tau = .005$ of the period. The experimental data show that at times the modulus

peaks are at a very low frequency and correspondingly, the $\Delta\tau$ increments are fairly large. This slight difficulty will also be refined for future work.

The indirect autocorrelations are presented, while the direct counterparts are not presented, because they were not reduced in previous work. Plot numbers (1) and (8) are representative of the autocorrelation curves and the matrix grids may be consulted to identify the remaining ones. The $R_{XX}(\tau)$ values can be seen to be one-half of their proper amplitude, while the $\tau = 0$ value is one-fourth of its amplitude. Inadvertently, a one-half constant was introduced into the numerical program, along with the normalization scaler. In the course of plotting the data, an additional one-half factor was applied for the $\tau = 0$ value. From Plot number (70) on, this later error was corrected. For Plot numbers (42) through (46), the cross power spectral analyses were repeated, because the operator questioned the set-up. The experimental data show that the cross-correlations superimpose perfectly, while the autocorrelations differ.

Ames/MSFC GENERAL PROTUBERANCE STUDY
TAPE TRACK COMBINATIONS
Wind Tunnel 9 x 7
CP-100

Report No. 507
Date 6-27-69

Conf. No. 27

	11	8	7	6	5	4	3	2	1
11									
8									
7									
6									
5									
4									
3									
2									
1									

Run Nos.

243-1

Symbols

Good Data ✻

Marginal Data @

Inoper. Chan. #

Number of Runs 17

FR-1200

Reference Tape Tracks

	13	12	11	10	9	8	7	6	5	4	3	2	1
13													
12													
11													
10													
9													
8						✻	#	✻	✻	✻	✻	✻	✻
7													
6								✻	✻	✻	✻	✻	✻
5													
4										✻	✻	✻	✻
3													
2													
1													

Ames/MSFC GENERAL PROTUBERANCE STUDY
TAPE TRACK COMBINATIONS
Wind Tunnel 9 x 7
CP-100

Report No. 507
Date 6-27-69

Conf. No. 27

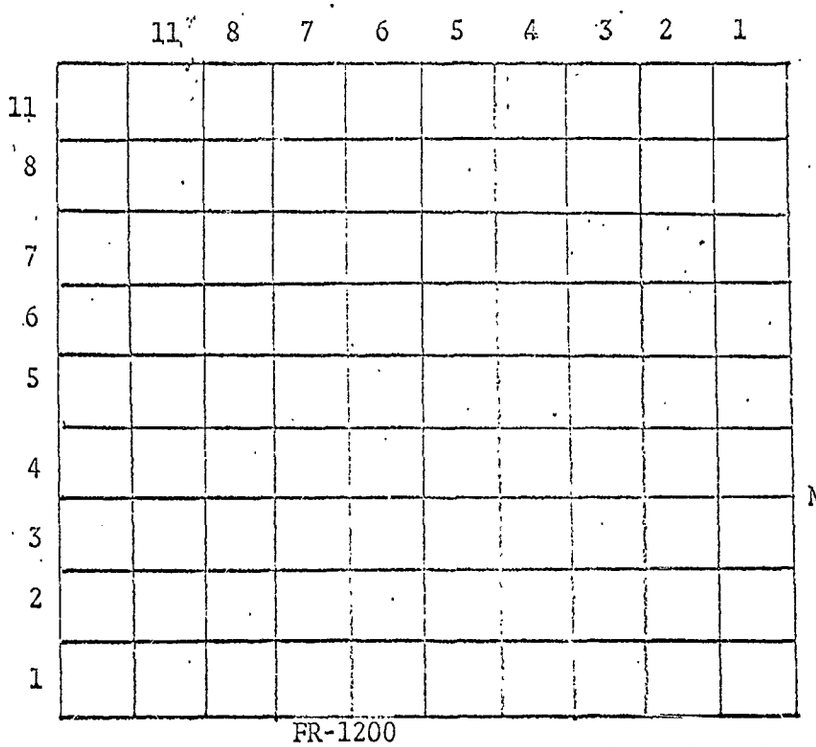

Run Nos.

249-1

Symbols

Good Data *

Marginal Data @

Inoper. Chan. #

Number of Runs 12

FR-1200

Reference Tape Tracks

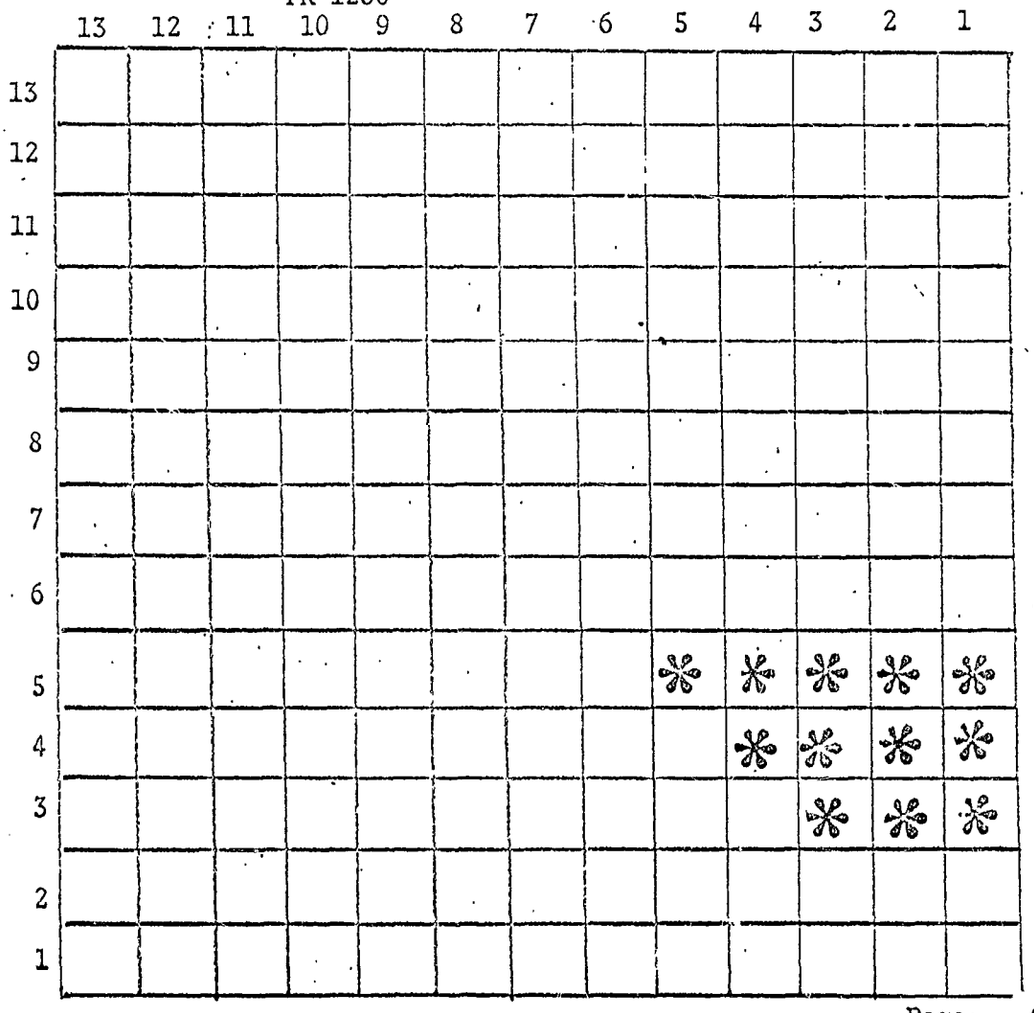

Ames/MSFC GENERAL PROTUBERANCE STUDY
TAPE TRACK COMBINATIONS
Wind Tunnel 9 x 7
CP-100

Report No. 507
Date 6-27-69

Conf. No. 17

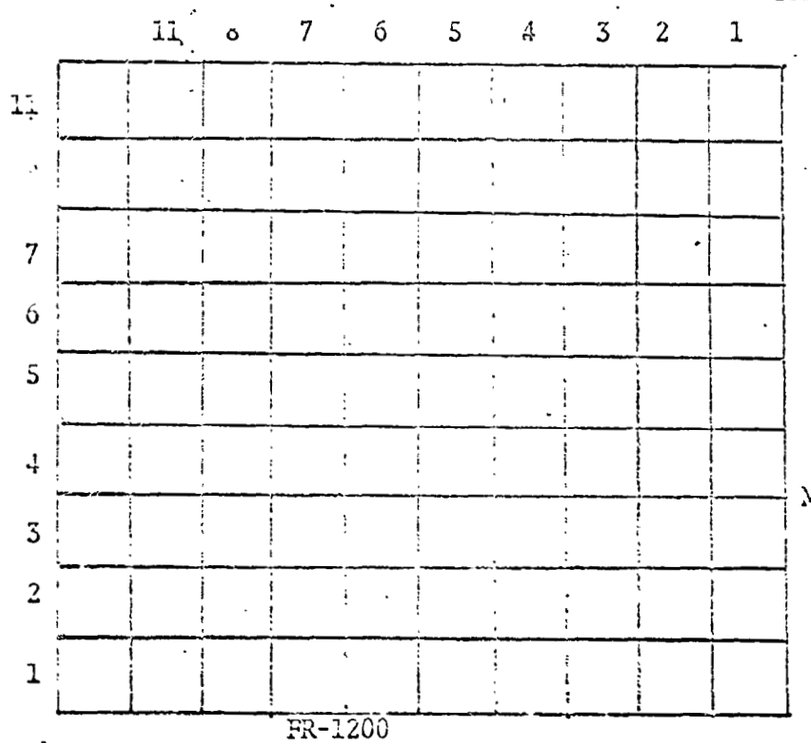

Run Nos.

162-1

Symbols

Good Data

Marginal Data

Inoper. Chan.

Number of Runs 35

FR-1200

Reference Tape Tracks

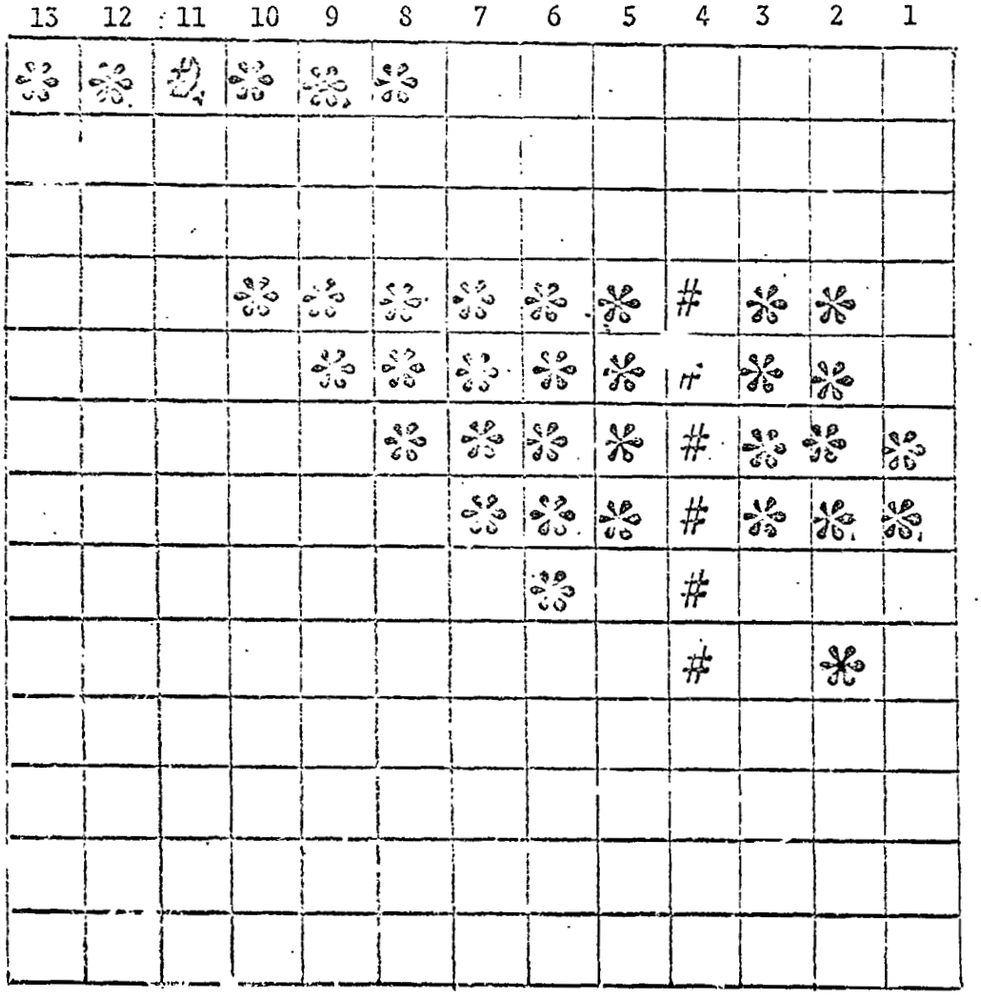

Ames/MSFC GENERAL PROTUBERANCE STUDY
TAPE TRACK COMBINATIONS
Wind Tunnel 9 x 7
CP-100

Report No. 507
Date 6-27-69

Conf. No. 17

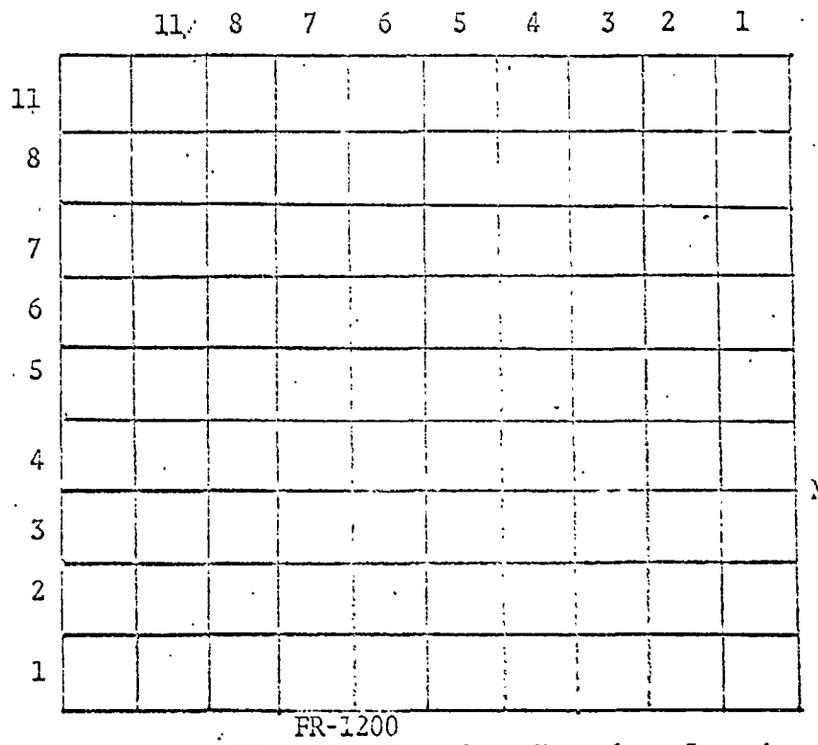

Run Nos.

167-1

Symbols

Good Data

Marginal Data

Inoper. Chan.

Number of Runs 30

FR-1200

Reference Tape Tracks

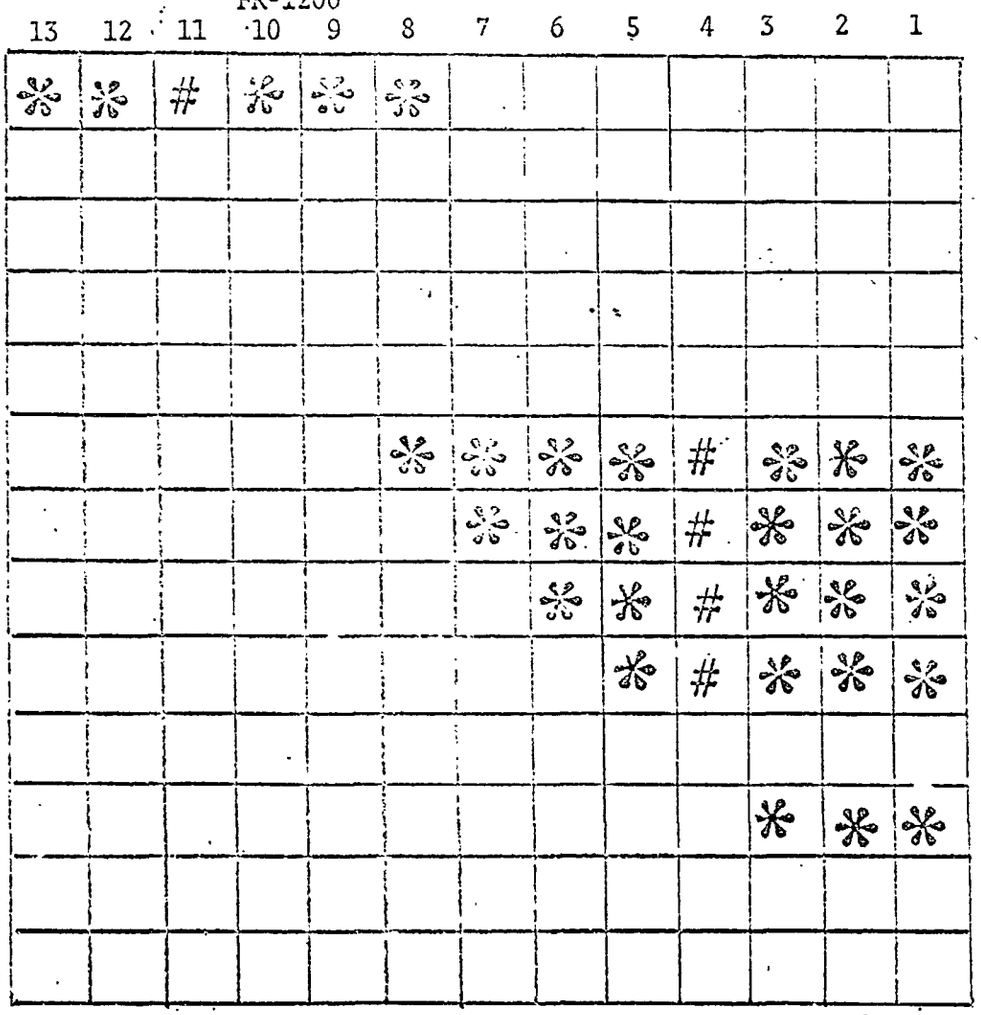

Ames/MSFC GENERAL PROTUBERANCE STUDY
TAPE TRACK COMBINATIONS
Wind Tunnel 9 x 7
CP-100

Report No. 507
Date 6-27-69

Conf. No. 7

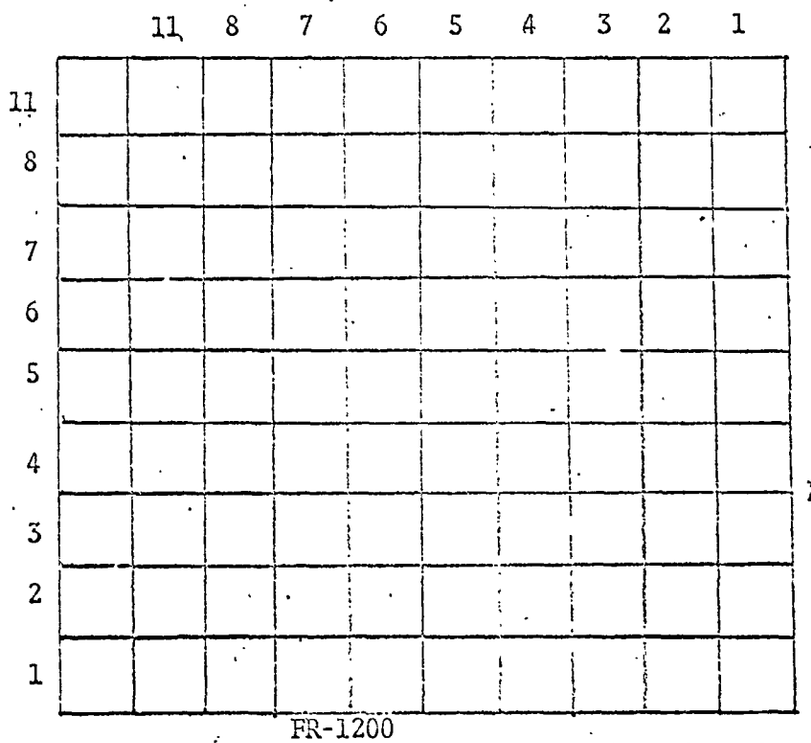

Run Nos.

280

Symbols

Good Data

Marginal Data

Inoper. Chan.

Number of Runs 9

FR-1200

Reference Tape Tracks

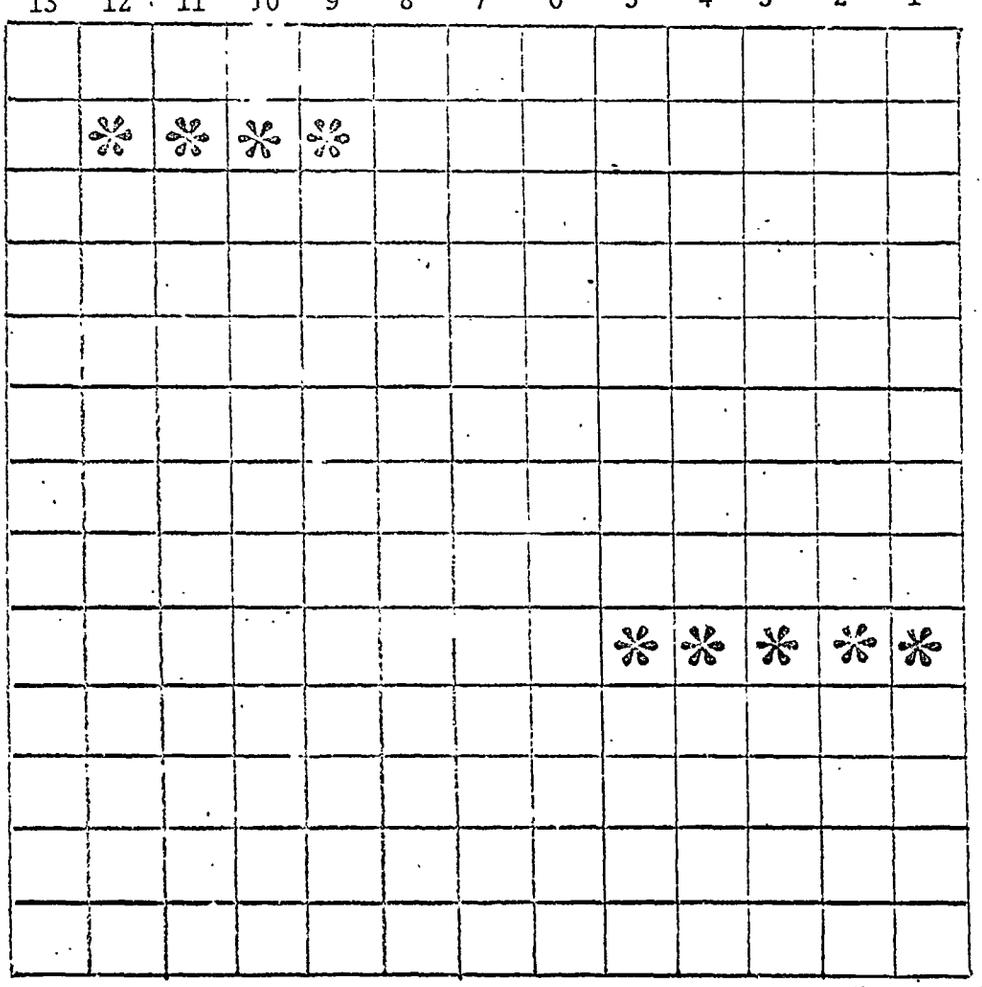

Ames/MSFC GENERAL PROTUBERANCE STUDY
TAPE TRACK COMBINATIONS
Wind Tunnel 9 x 7
CP-100

Report No. 507
Date 6-27-69

Conf. No. 7

	11	8	7	6	5	4	3	2	1
11									
8									
7									
6									
5									
4									
3									
2									
1									

Run Nos.

281

Symbols

Good Data *

Marginal Data @

Inoper. Chan. #

Number of Runs 7

FR-1200

Reference Tape Tracks

	13	12	11	10	9	8	7	6	5	4	3	2	1
13													
12													
11			*	*									
10													
9													
8													
7													
6													
5									*	*	*	*	*
4													
3													
2													
1													

Ames/MSFC GENERAL PROTUBERANCE STUDY
TAPE TRACK COMBINATIONS
Wind Tunnel 9 x 7
CP-100

Report No. 507
Date 6-27-69

Conf. No. 17

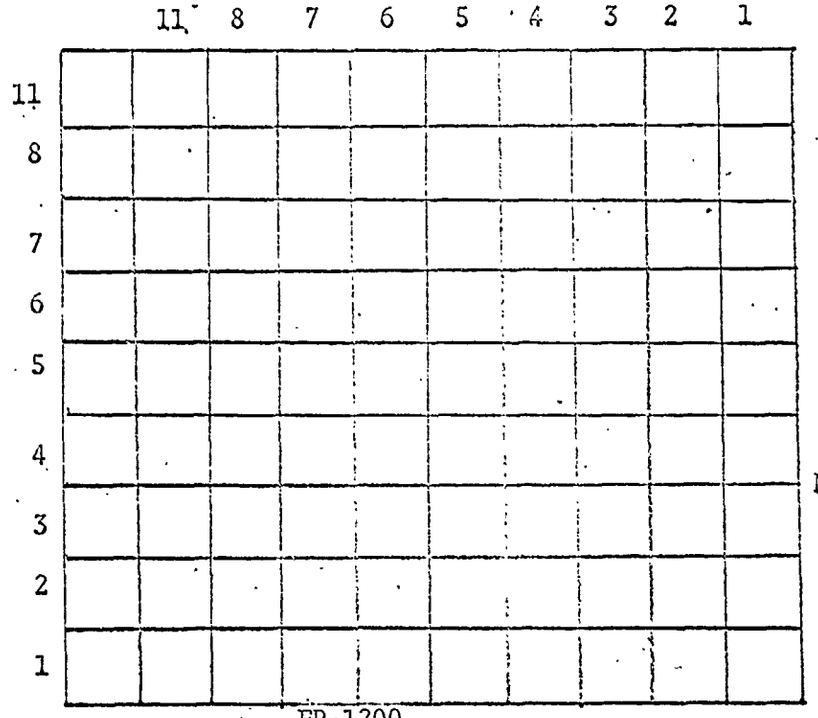

Run Nos.

295

Symbols

Good Data *

Marginal Data @

Inoper. Chan. #

Number of Runs 6

FR-1200

Reference Tape Tracks

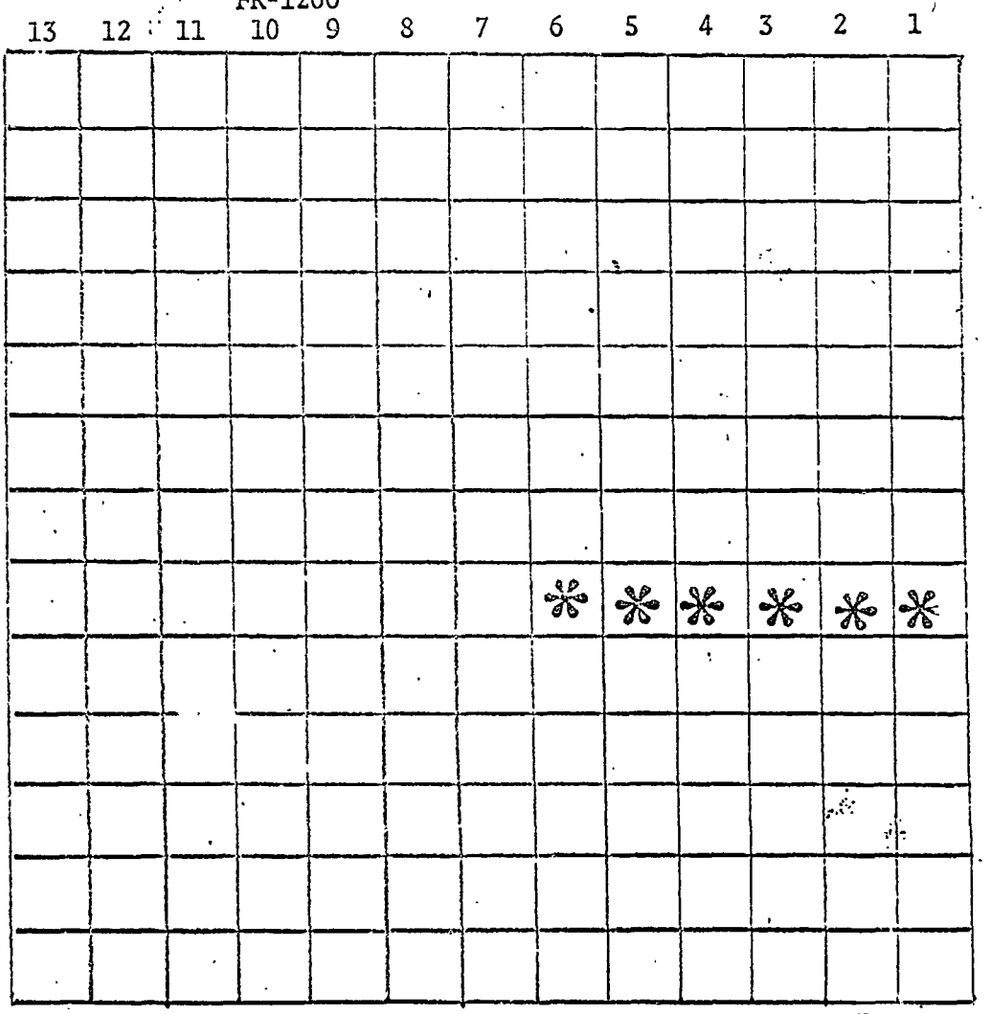

BAGANOFF ASSOCIATES

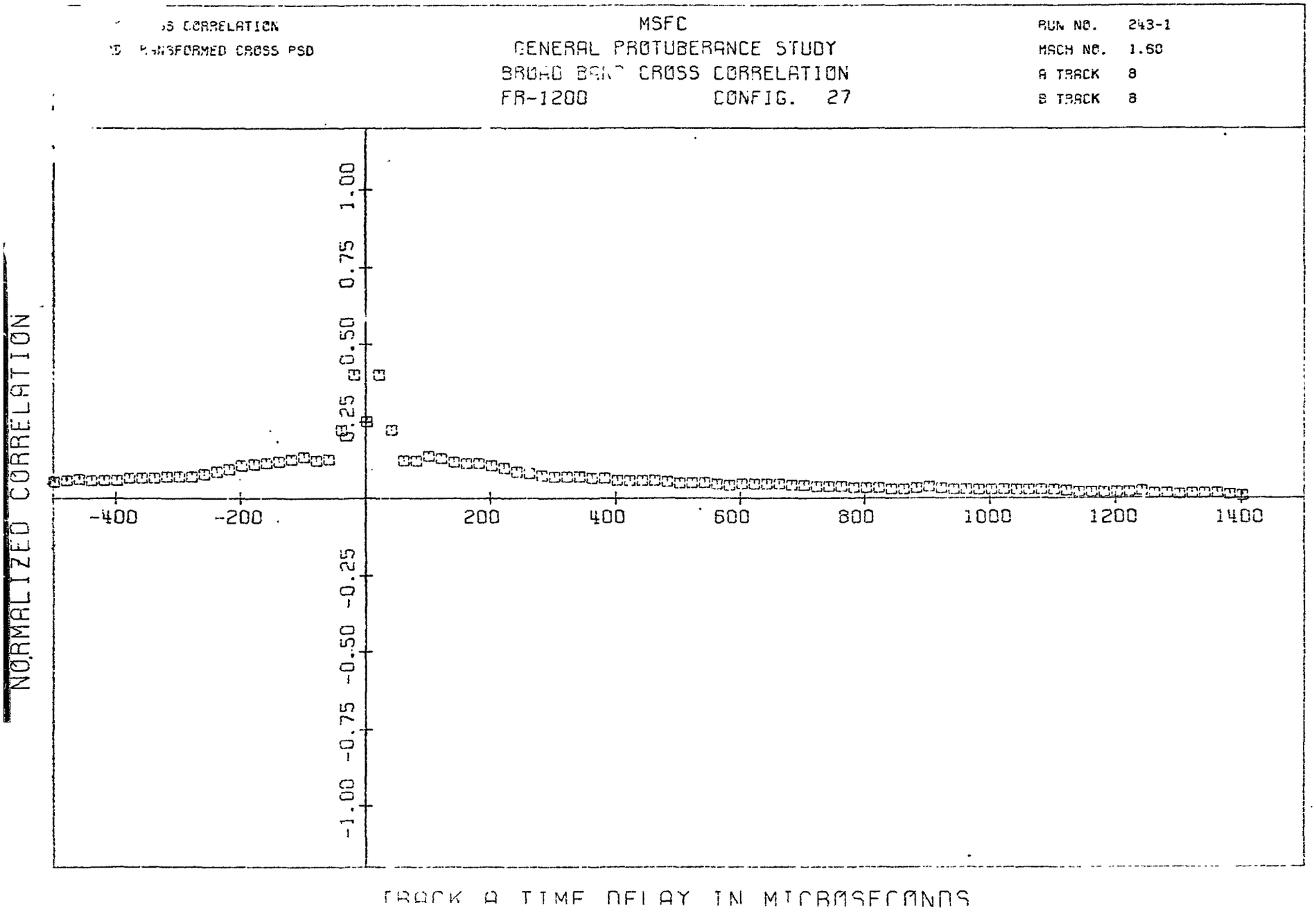

PLOT (1)

BACANOFF ASSOCIATES

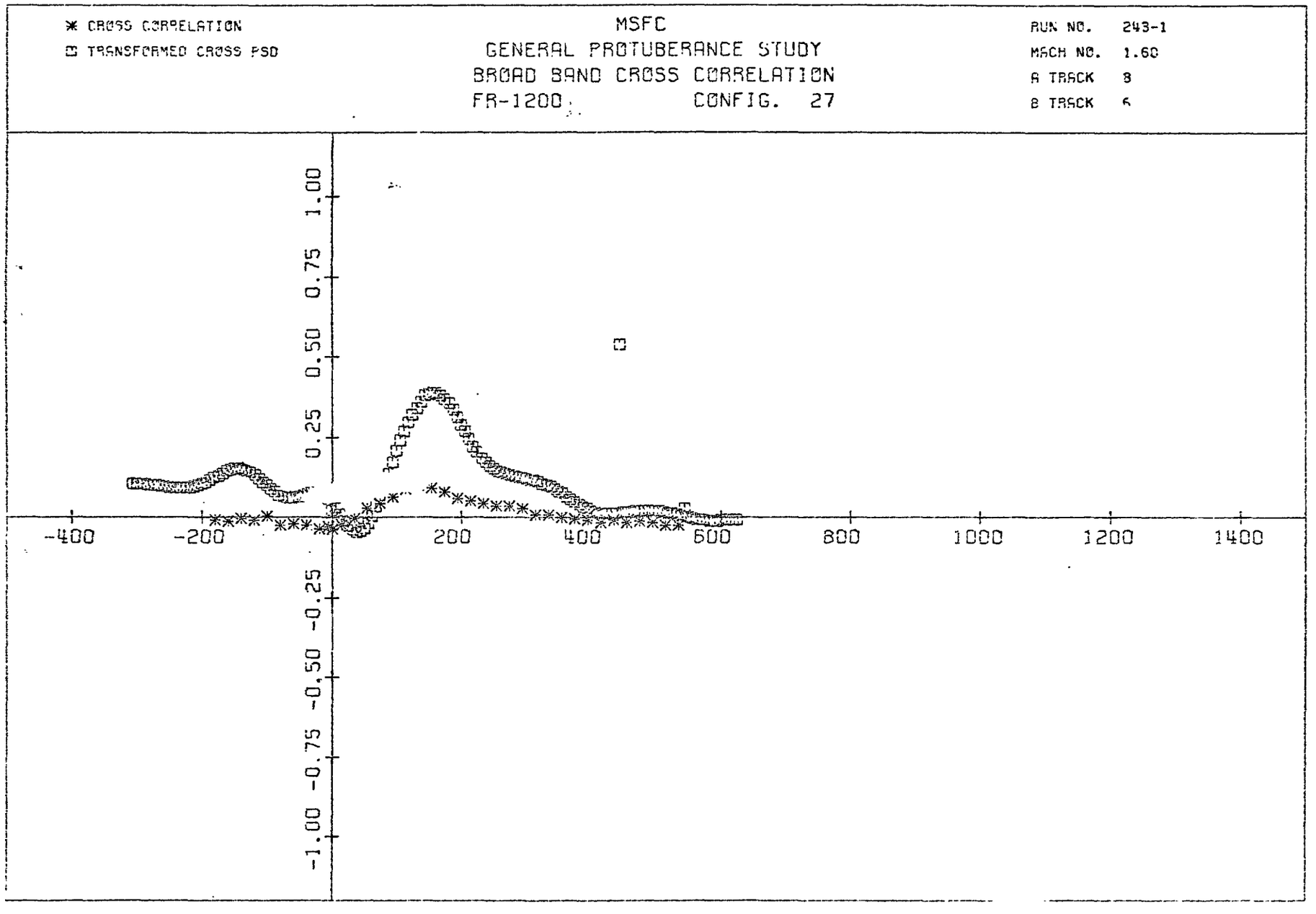

PLOT (2)

BAGANOFF ASSOCIATES

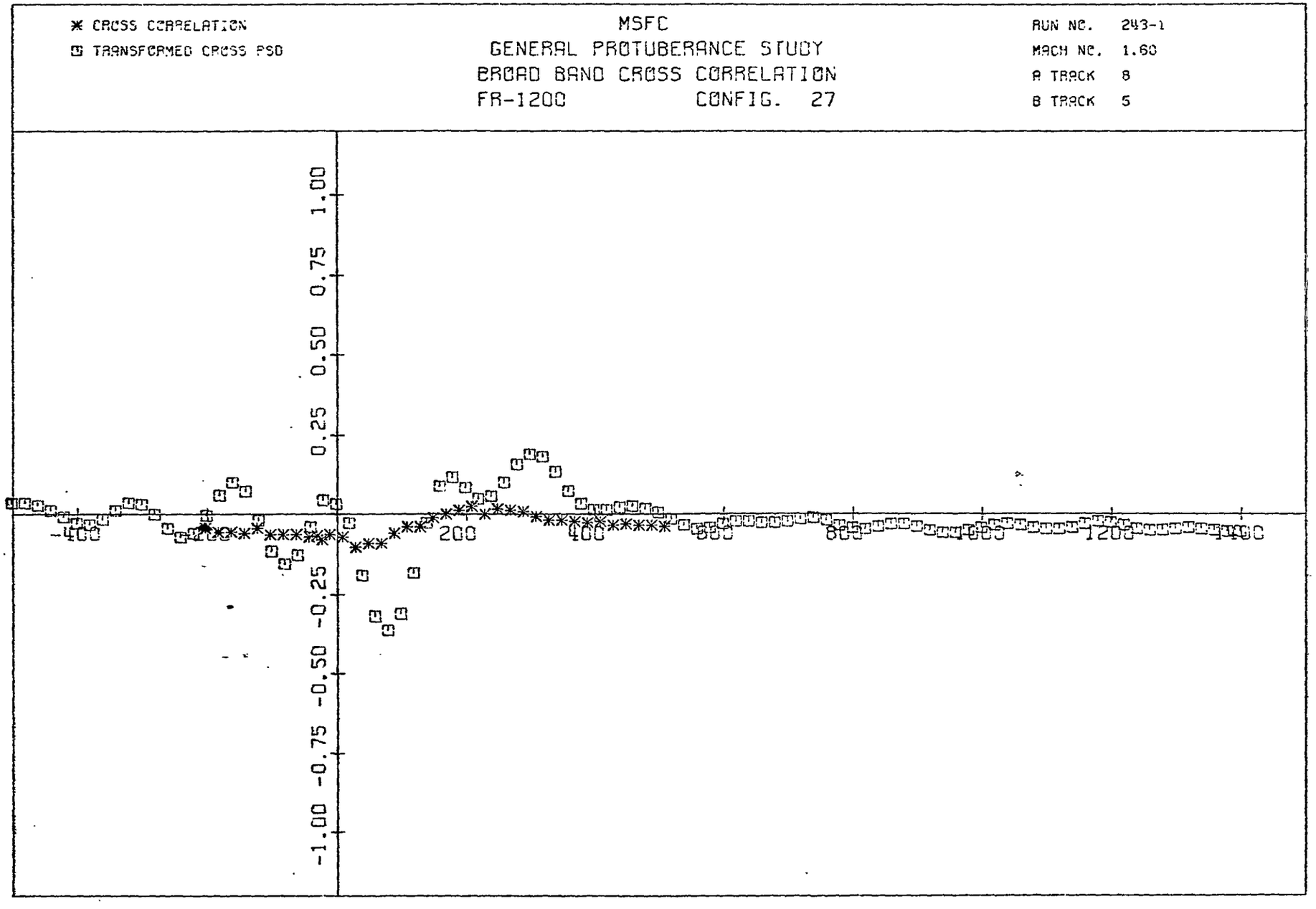

PLOT (3)

BAGANOFF ASSOCIATES

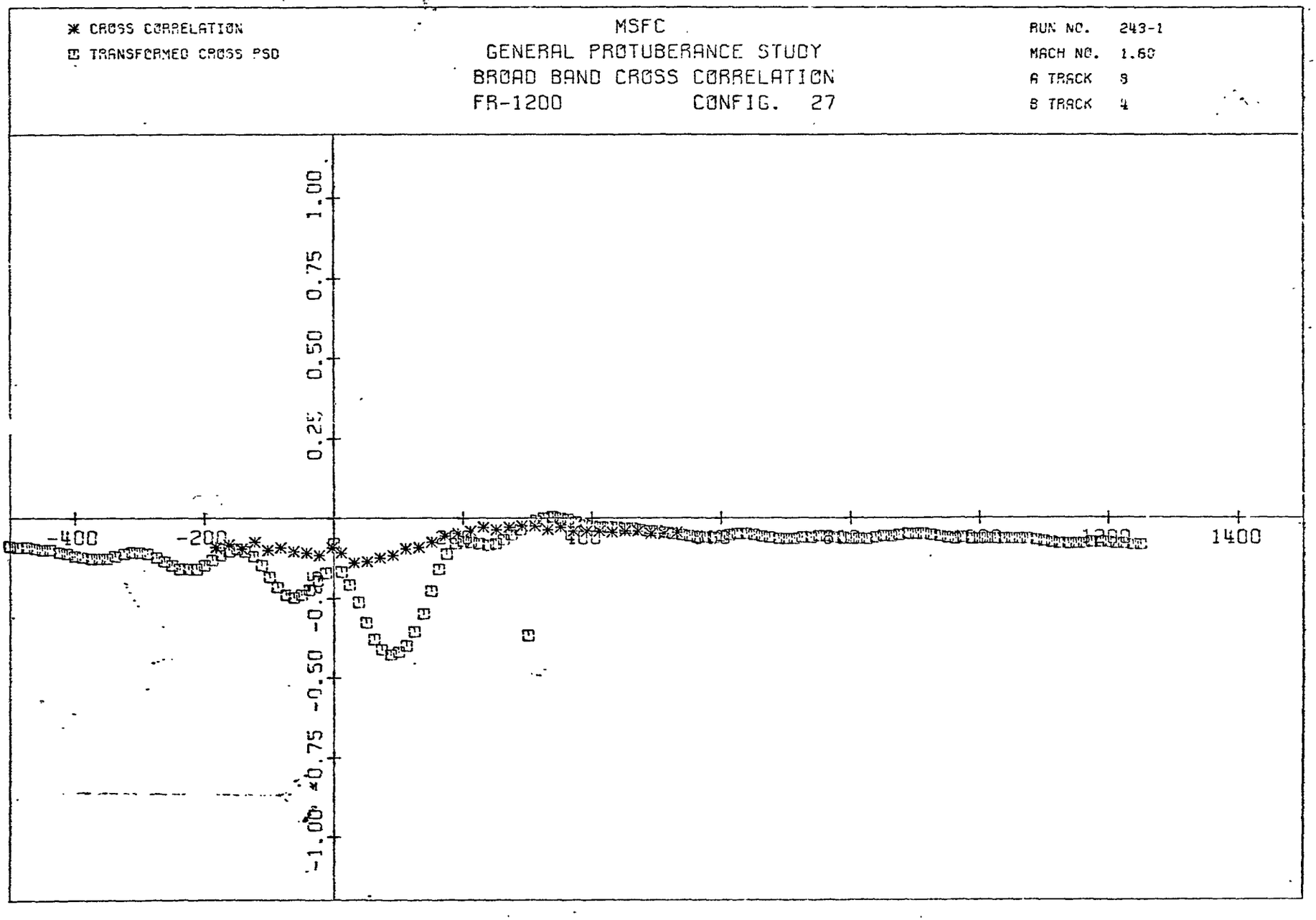

BAGANOFF ASSOCIATES

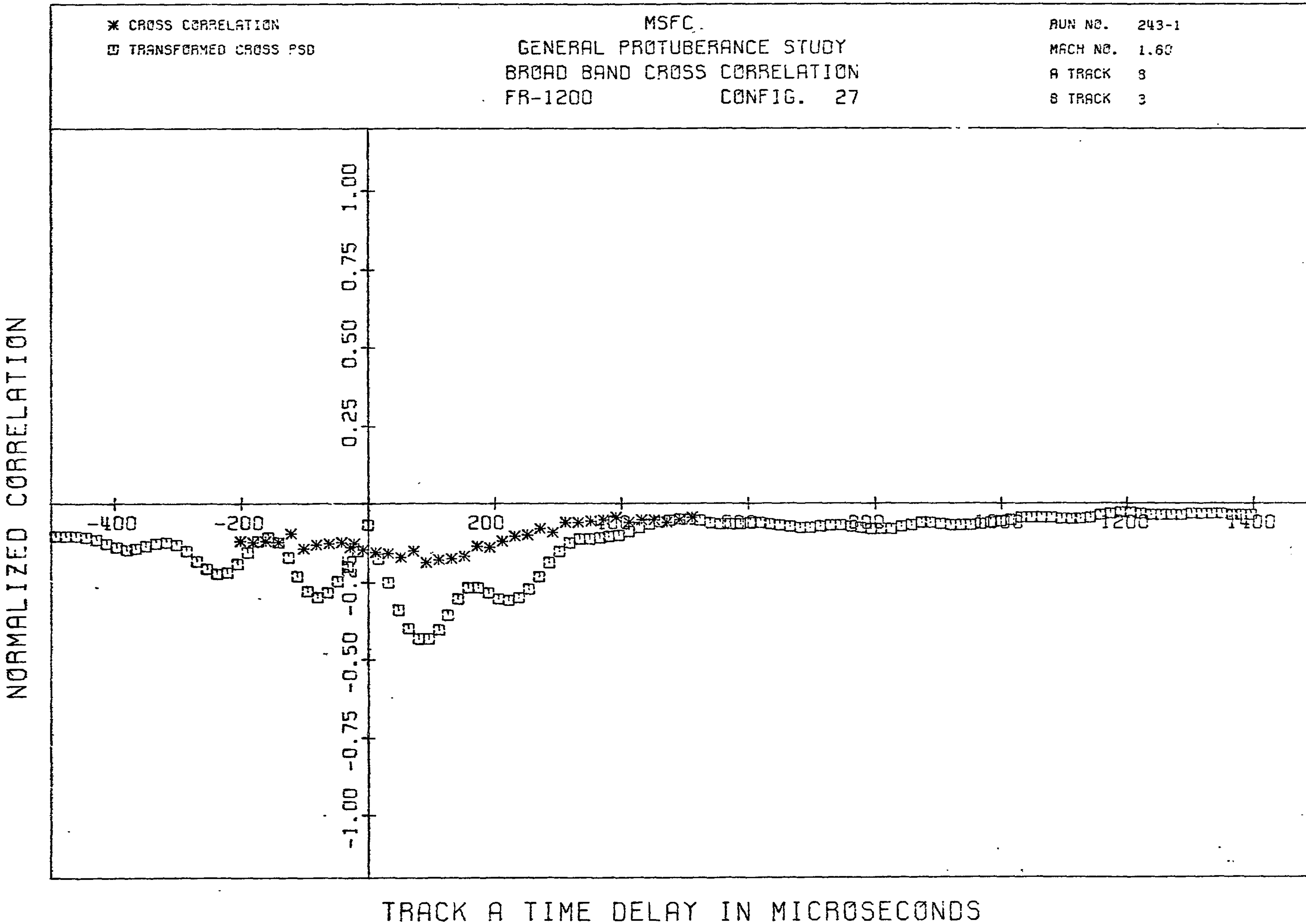

PLOT (5)

BAGANOFF ASSOCIATES

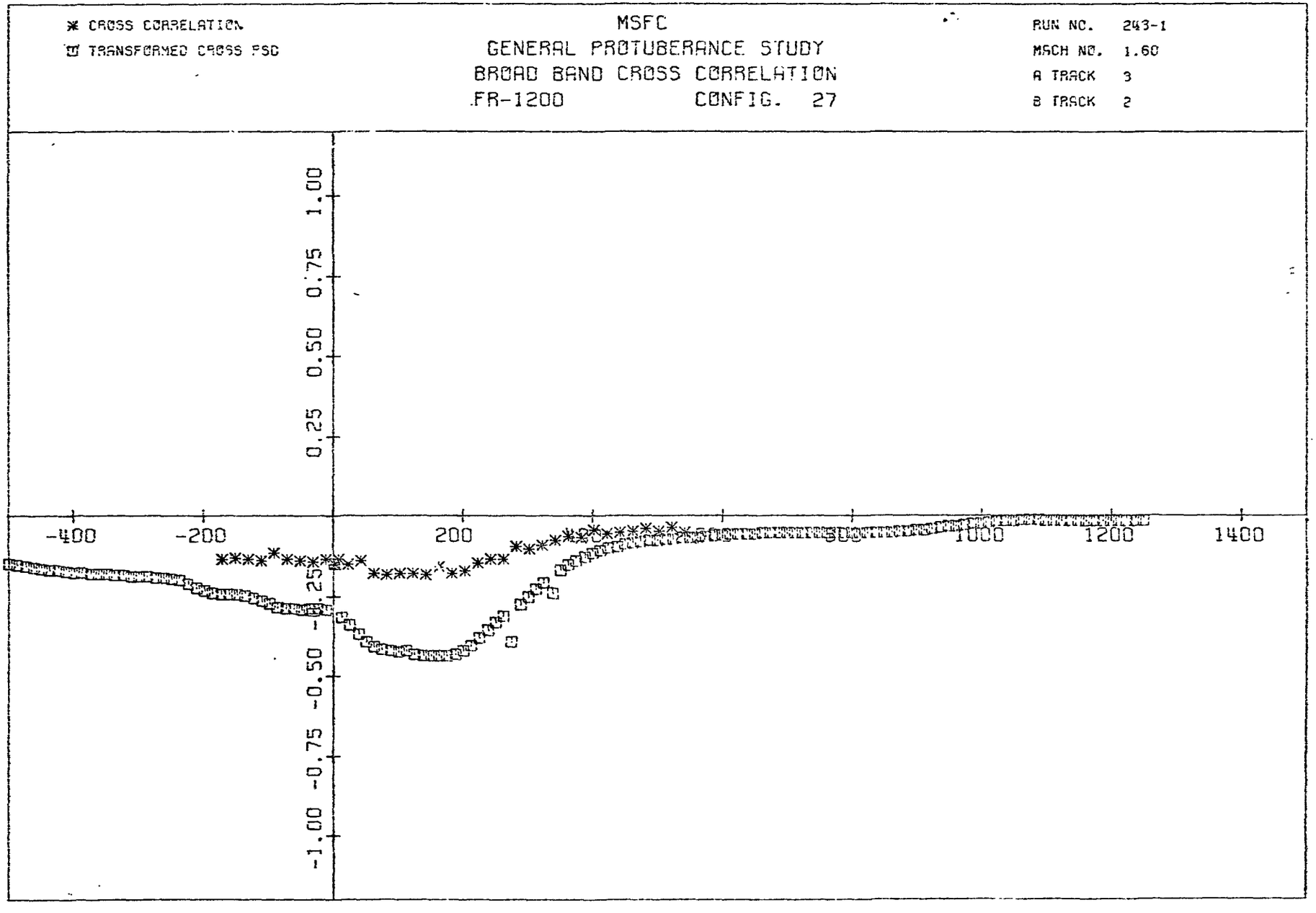

PLOT (9)

BAGANOFF ASSOCIATES

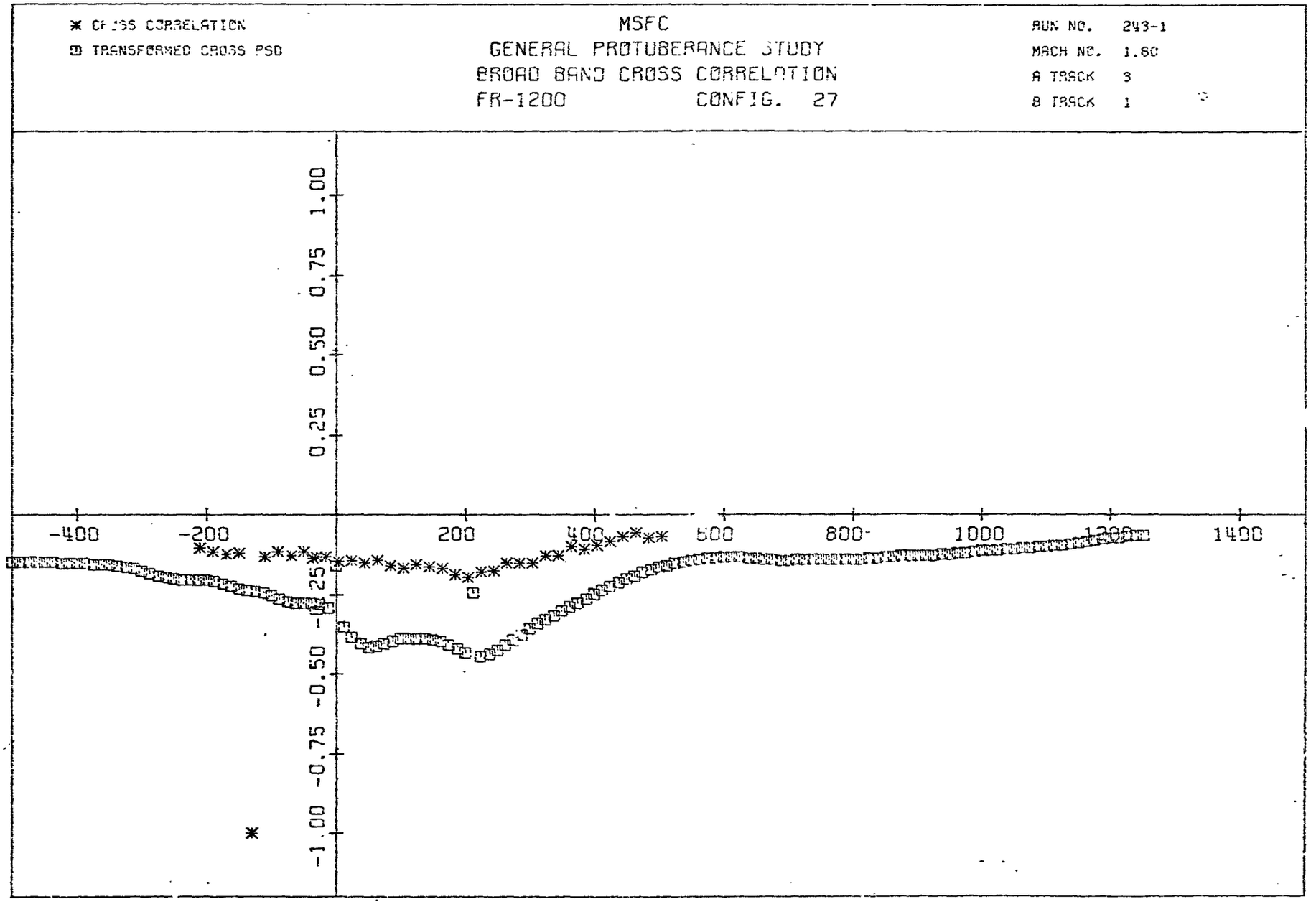

BAGANOFF ASSOCIATES

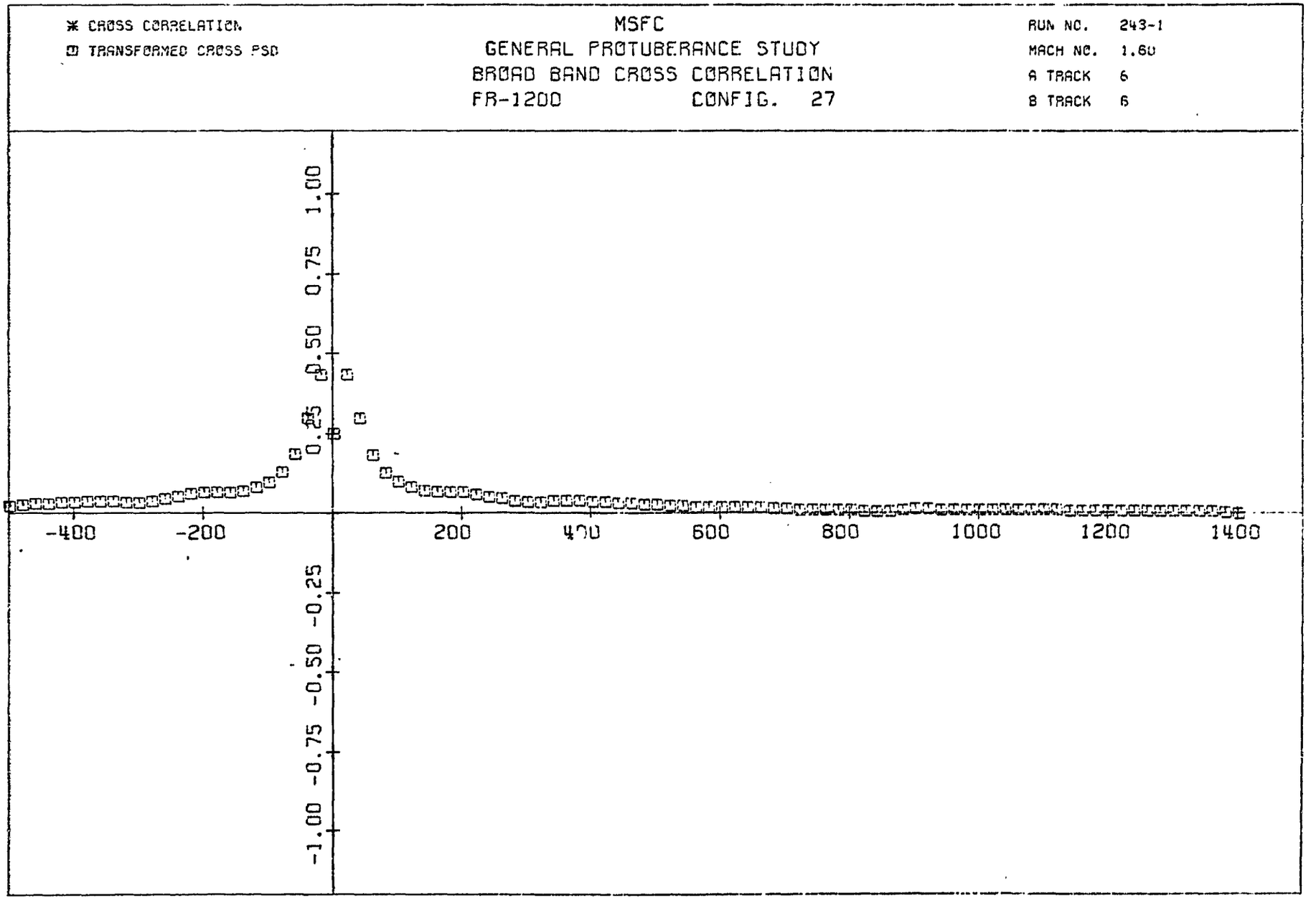

TRACK A TIME DELAY IN MICROSECONDS

BAGANOFF ASSOCIATES

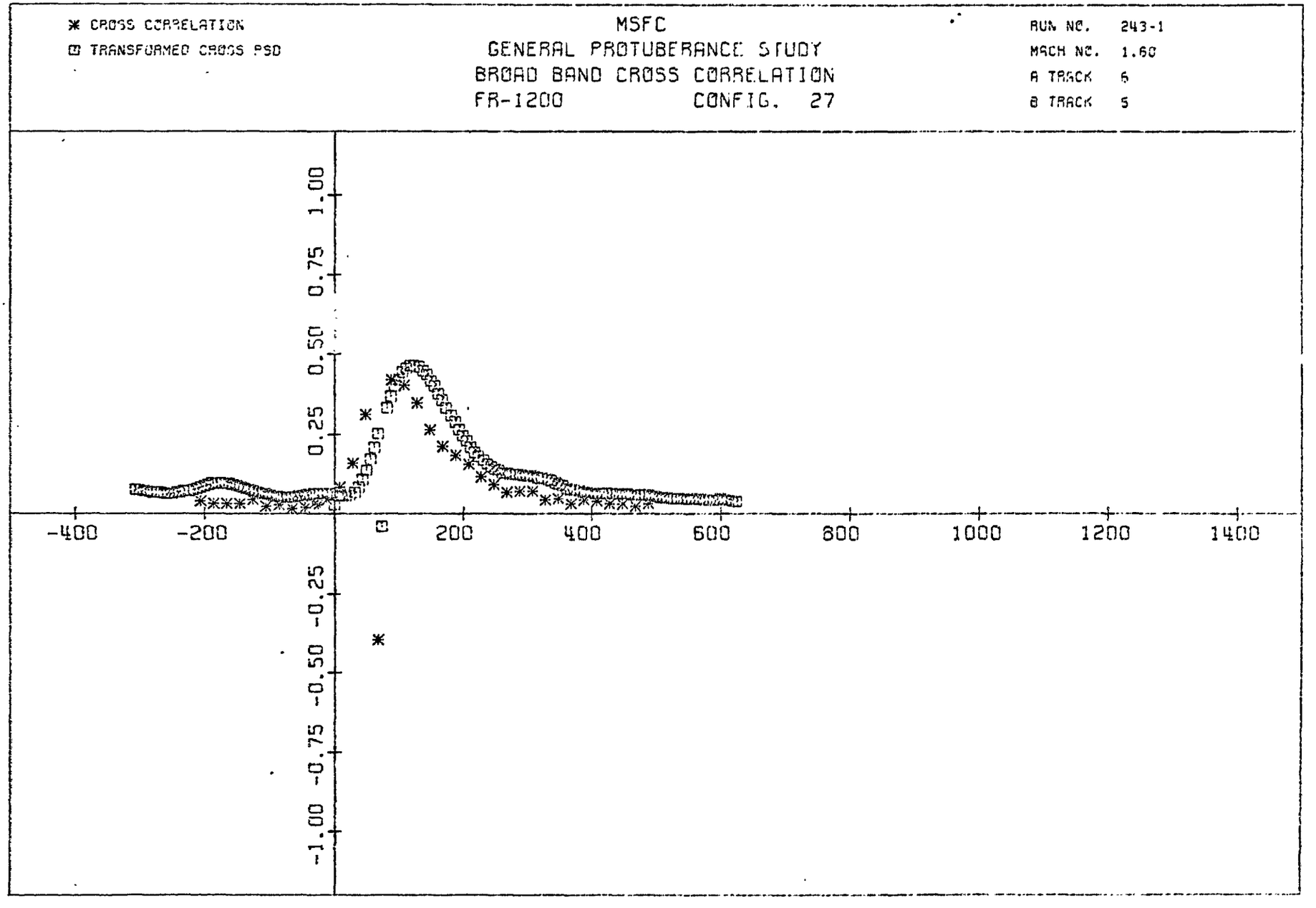

PLOT (9)

TRACK A TIME DELAY IN MICROSECONDS

BAGANOFF ASSOCIATES

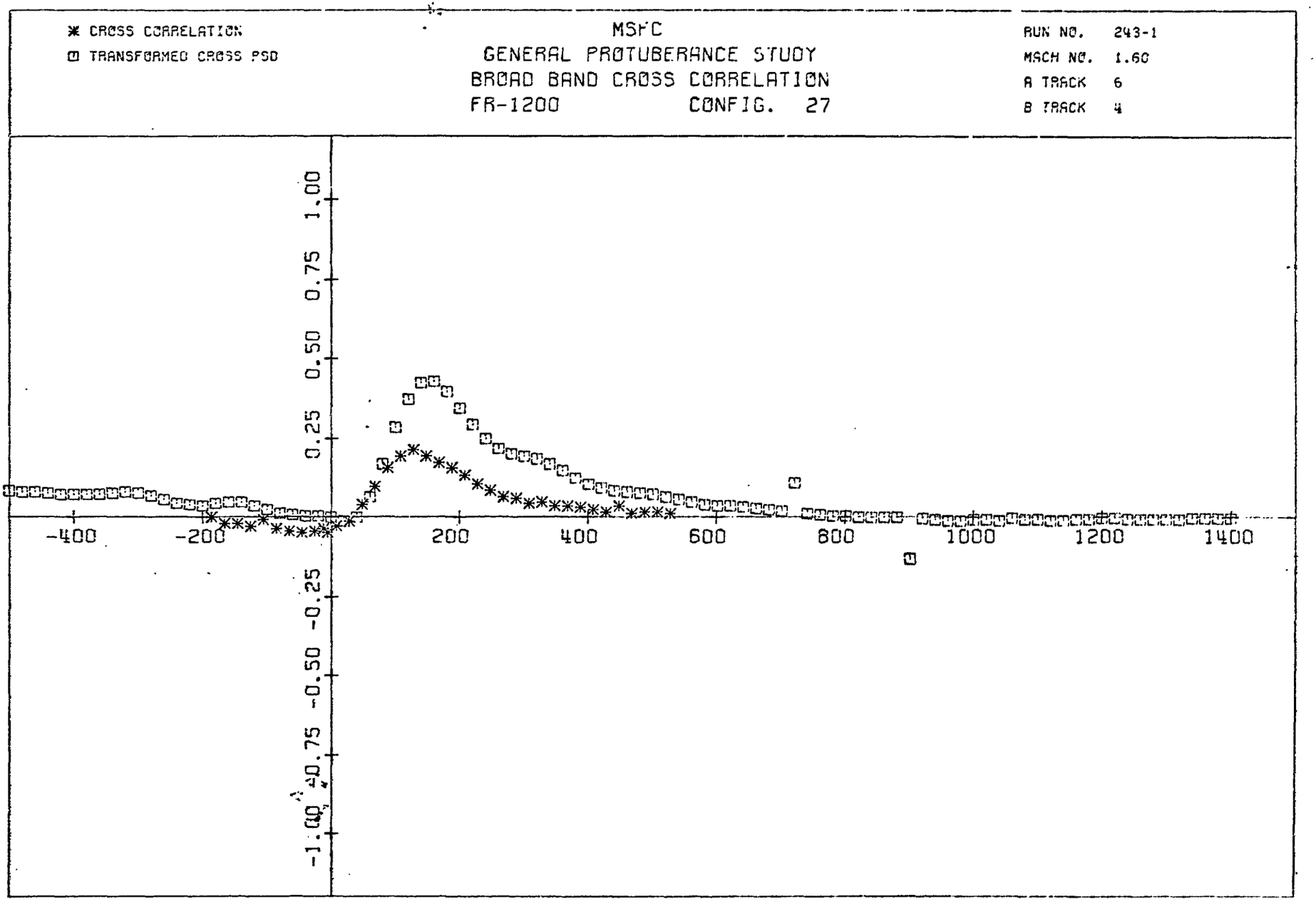

PLOT (10)

BAGANOFF ASSOCIATES

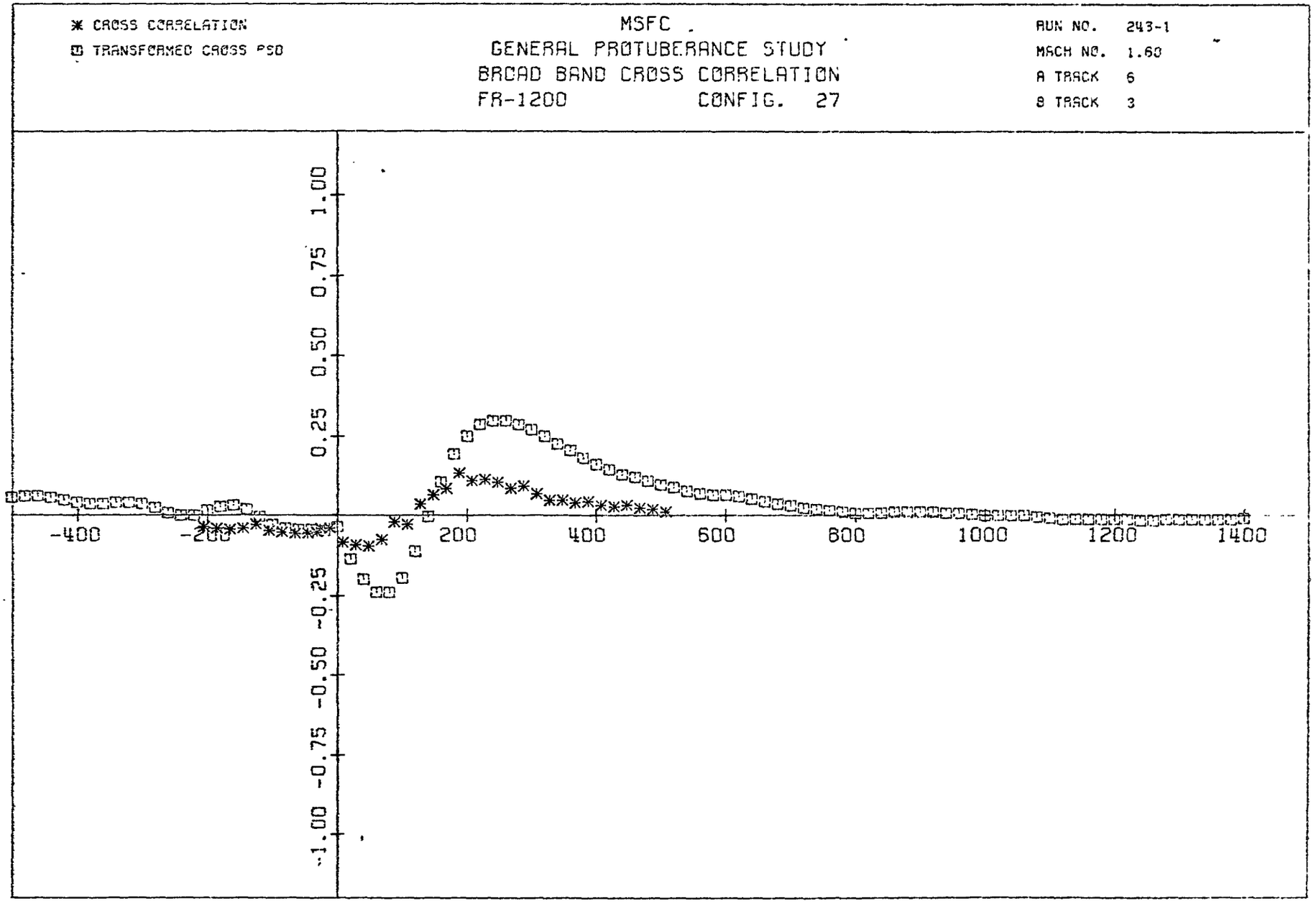

PLOT (11)

TRACK A TIME DELAY IN MICROSECONDS

BAGANOFF ASSOCIATES

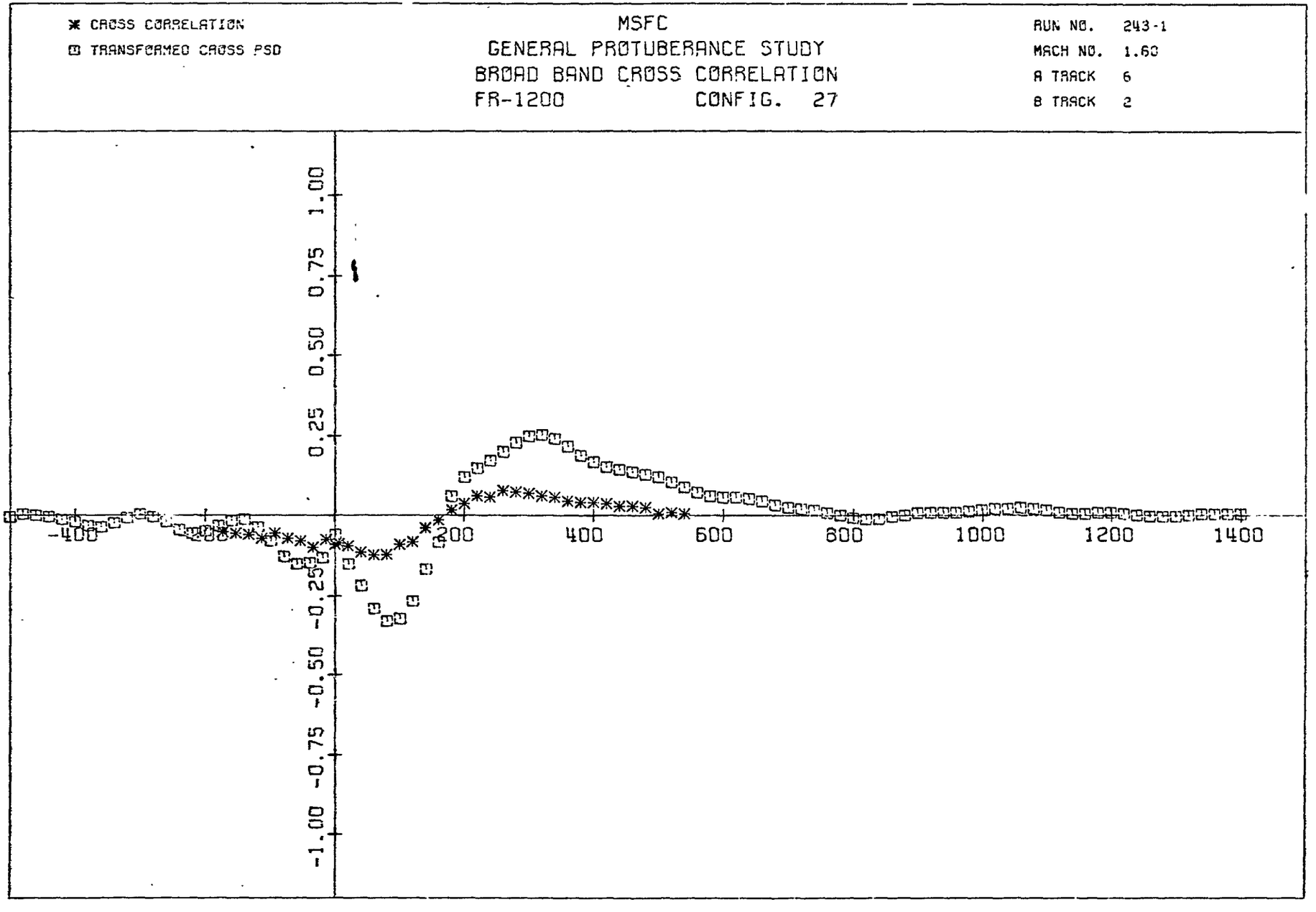

PLOT (12)

TRACK A TIME DELAY IN MICROSECONDS

BAGANOFF ASSOCIATES

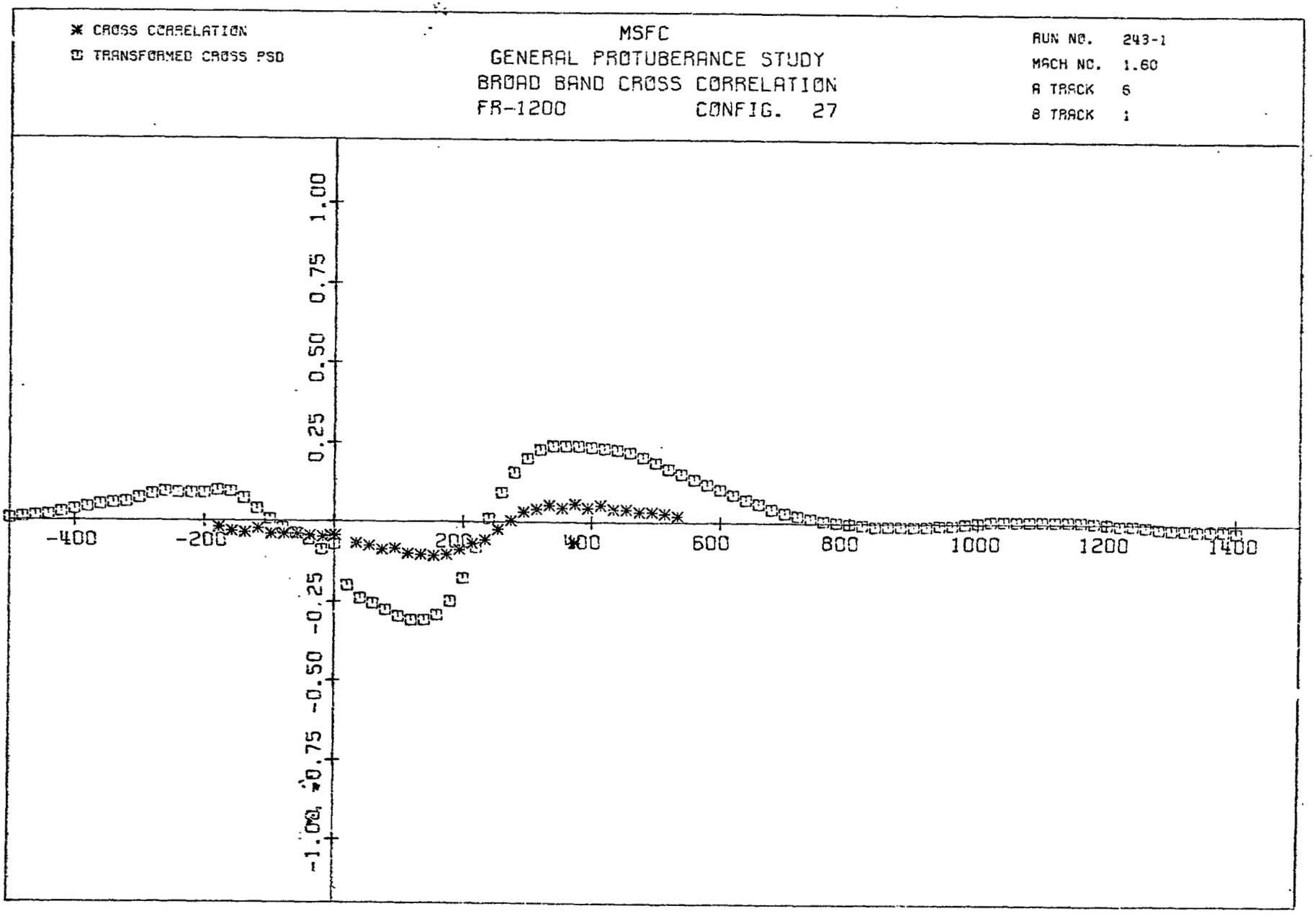

PLOT (13)

TRACK A TIME DELAY IN MICROSECONDS

BAGANOFF ASSOCIATES

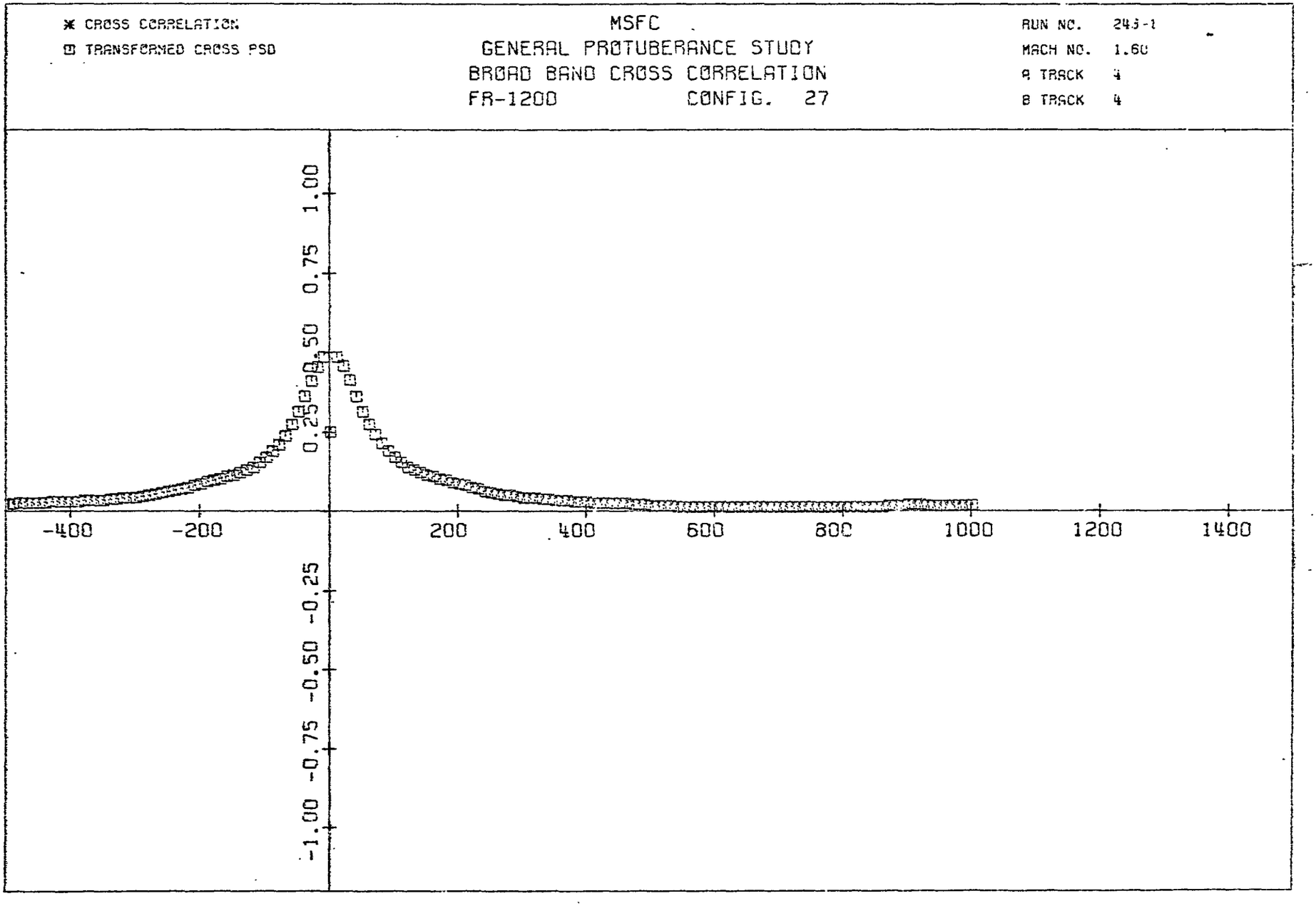

BAGANOFF ASSOCIATES

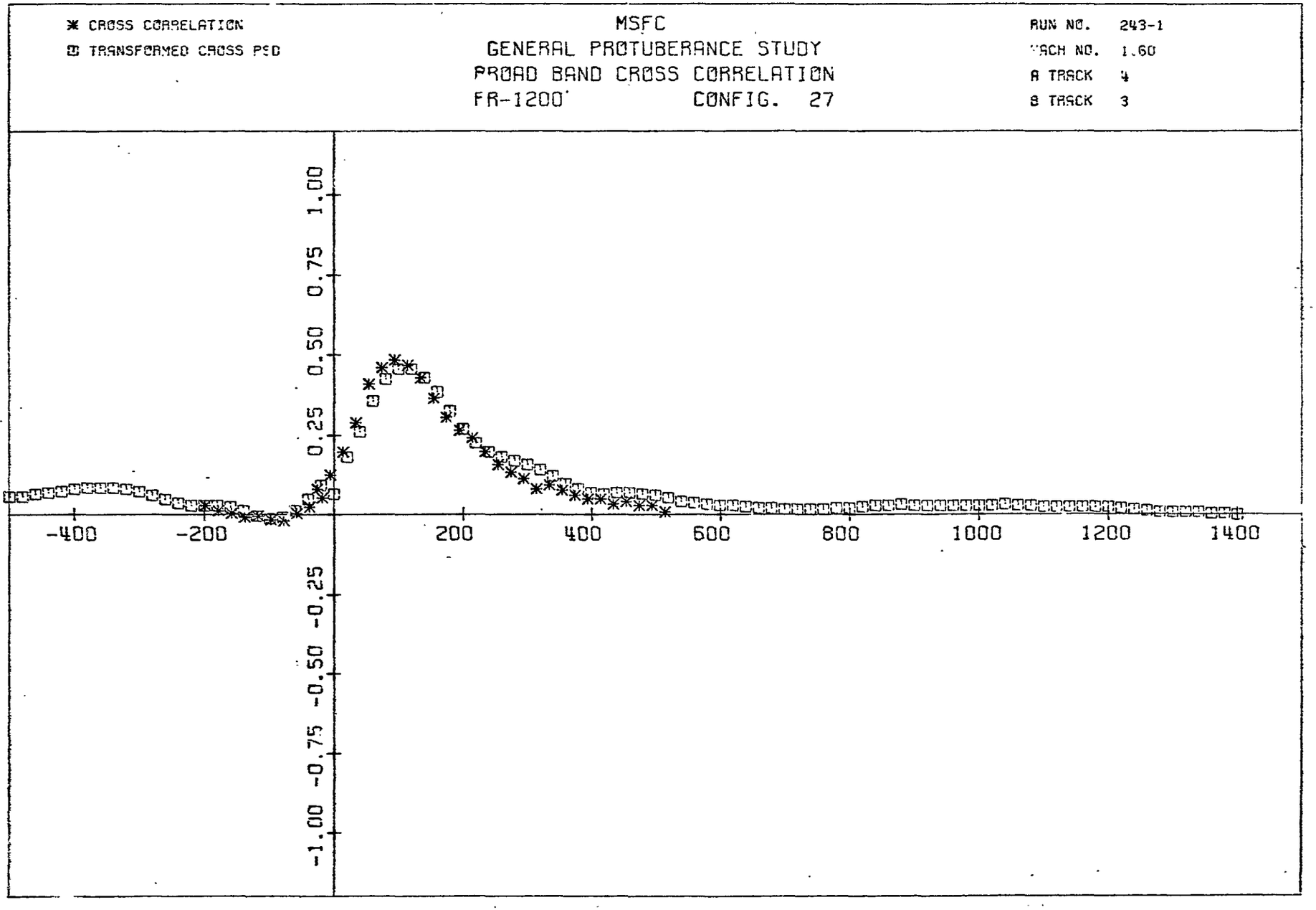

PLOT (15)

BAGANOFF ASSOCIATES

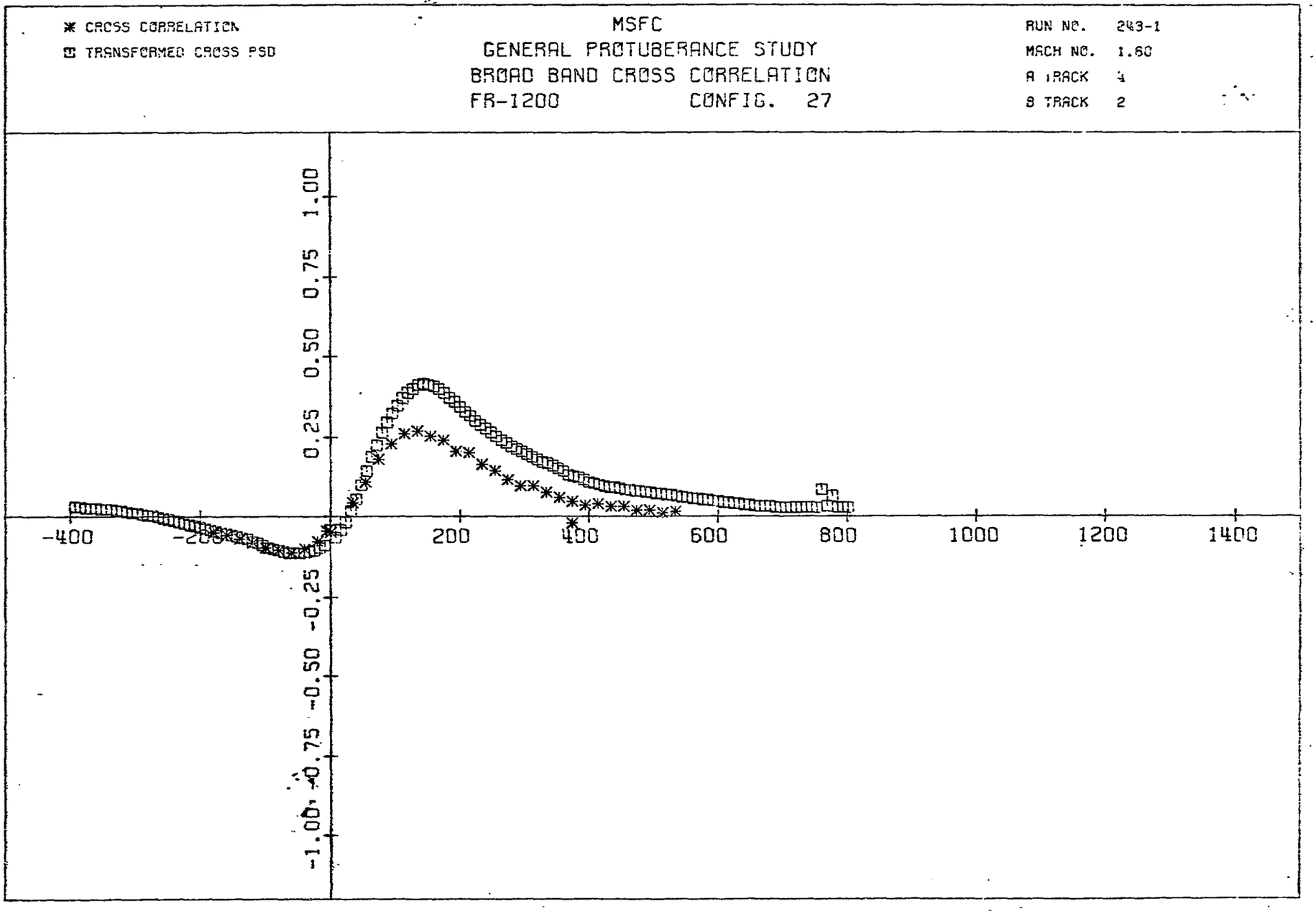

PLOT (16)

TRACK A TIME DELAY IN MICROSECONDS

BAGANOFF ASSOCIATES

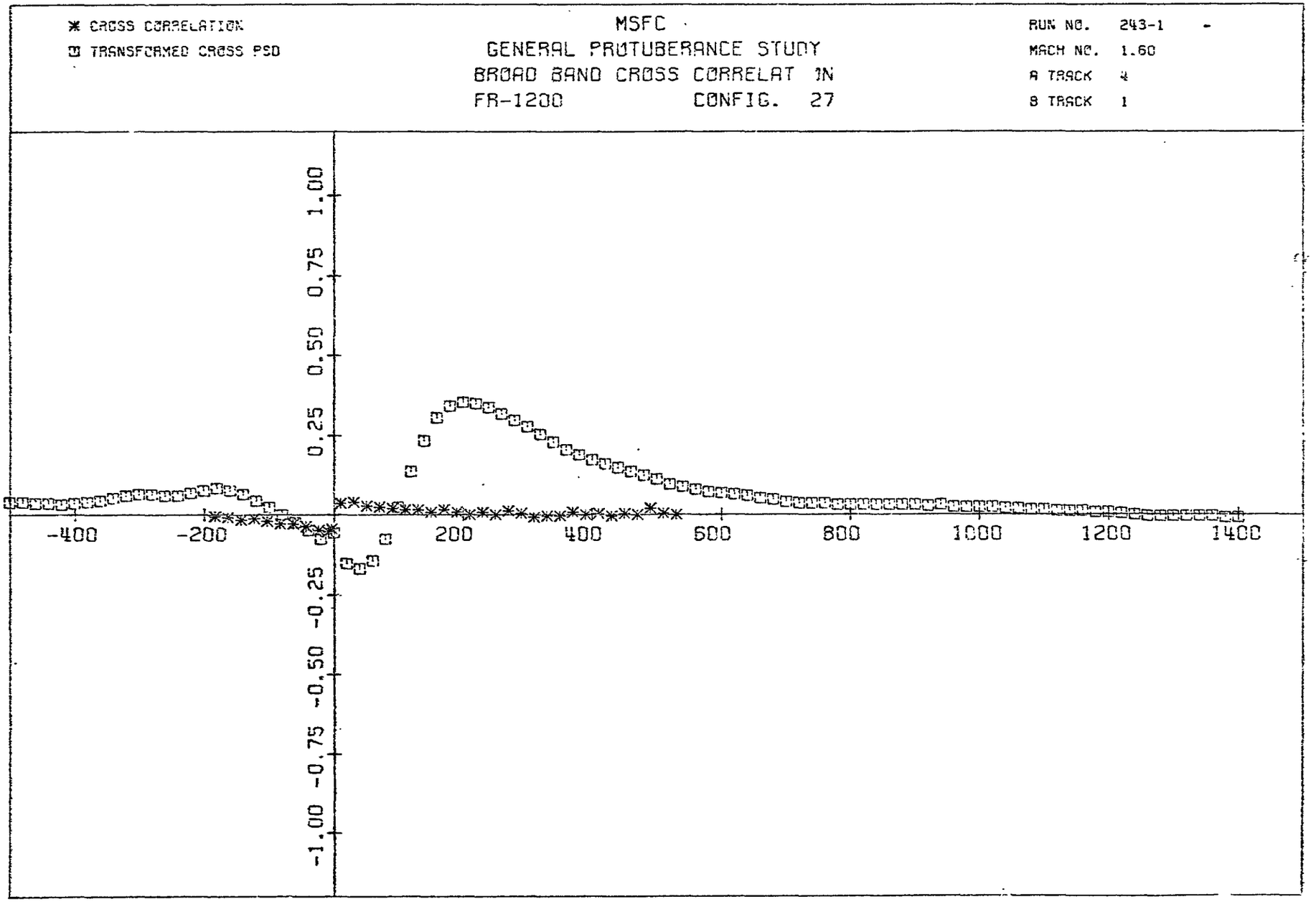

PLOT (17)

BAGANOFF ASSOCIATES

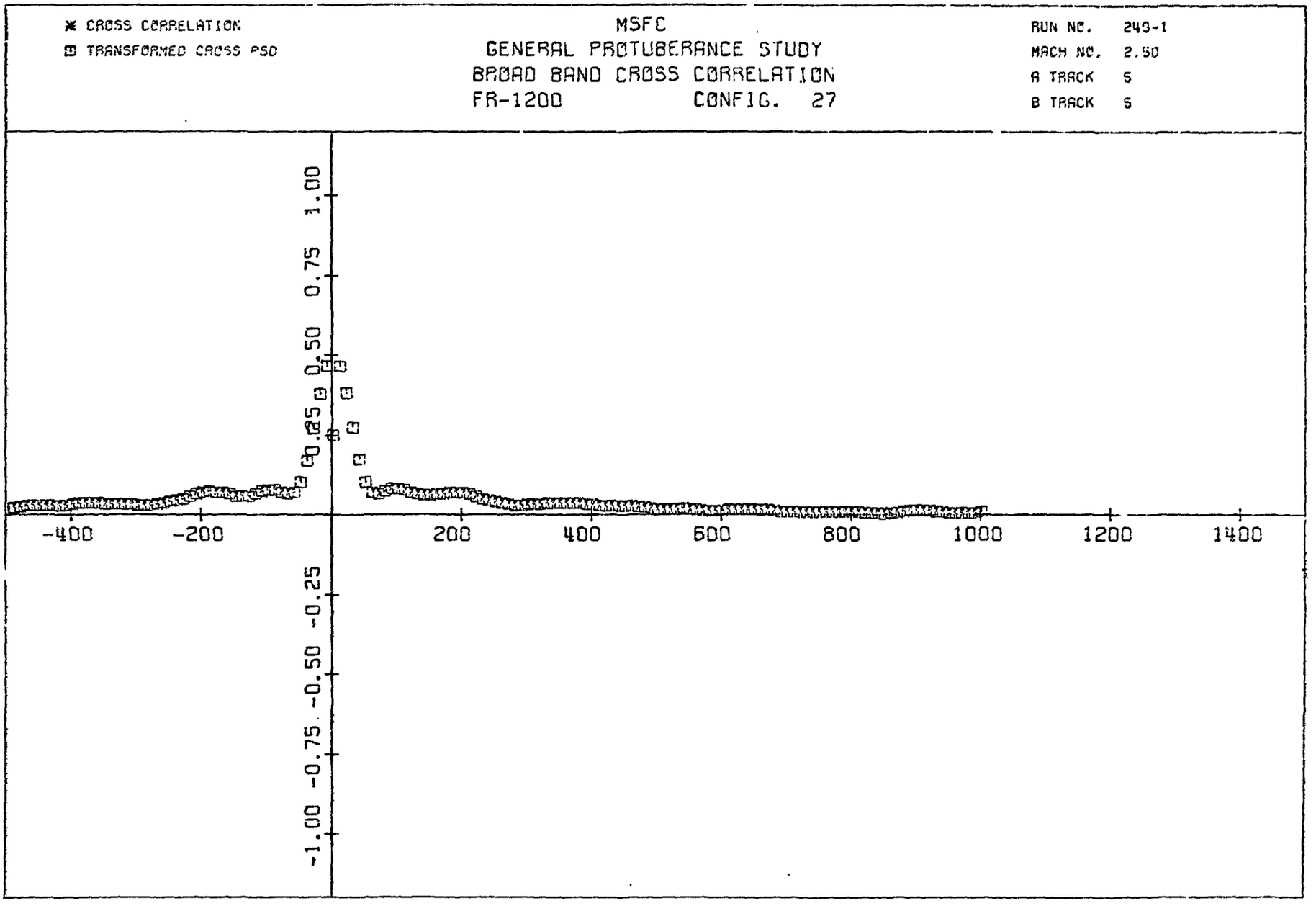

PLOT 1181

BAGANOFF ASSOCIATES

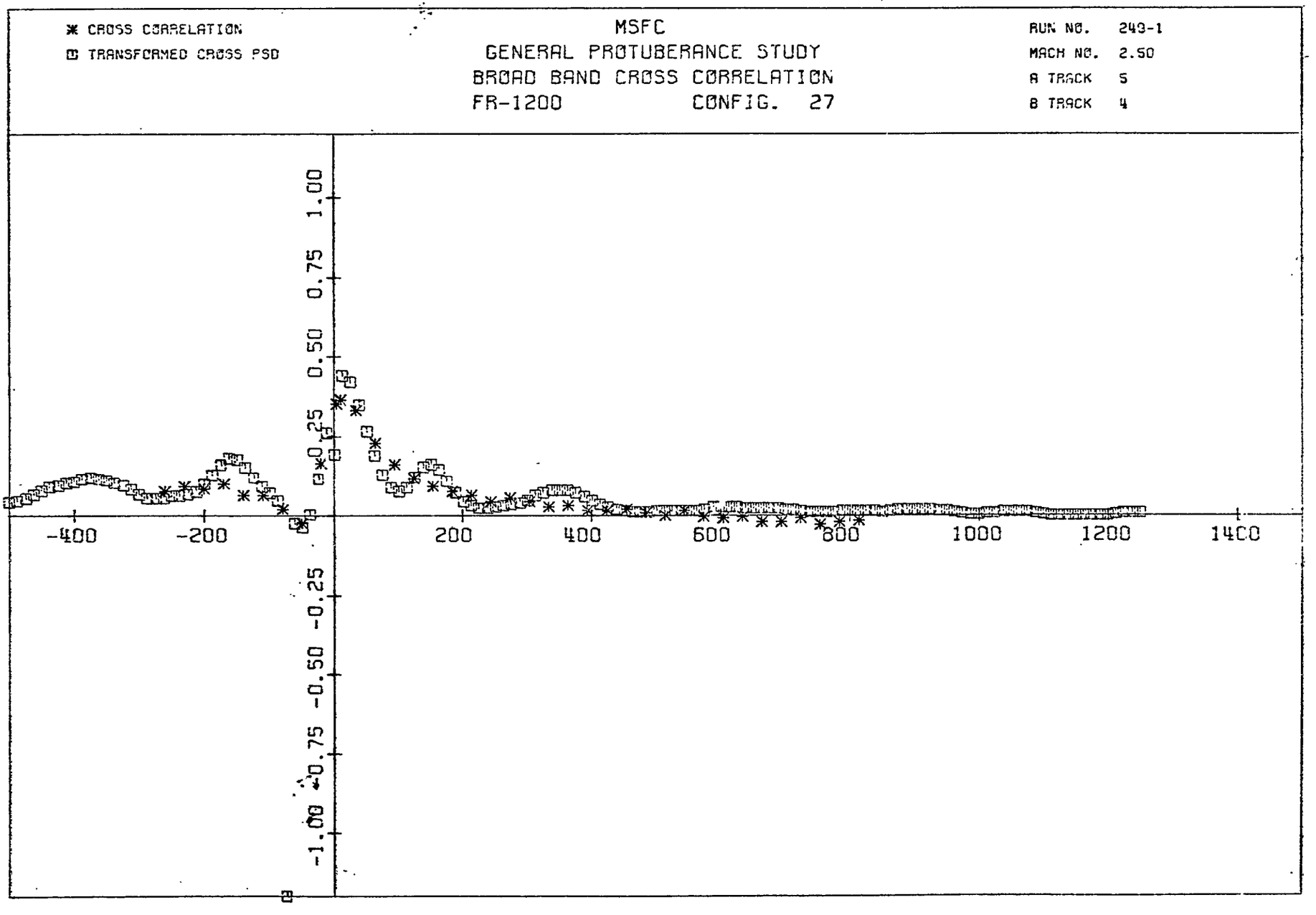

BAGANOFF ASSOCIATES

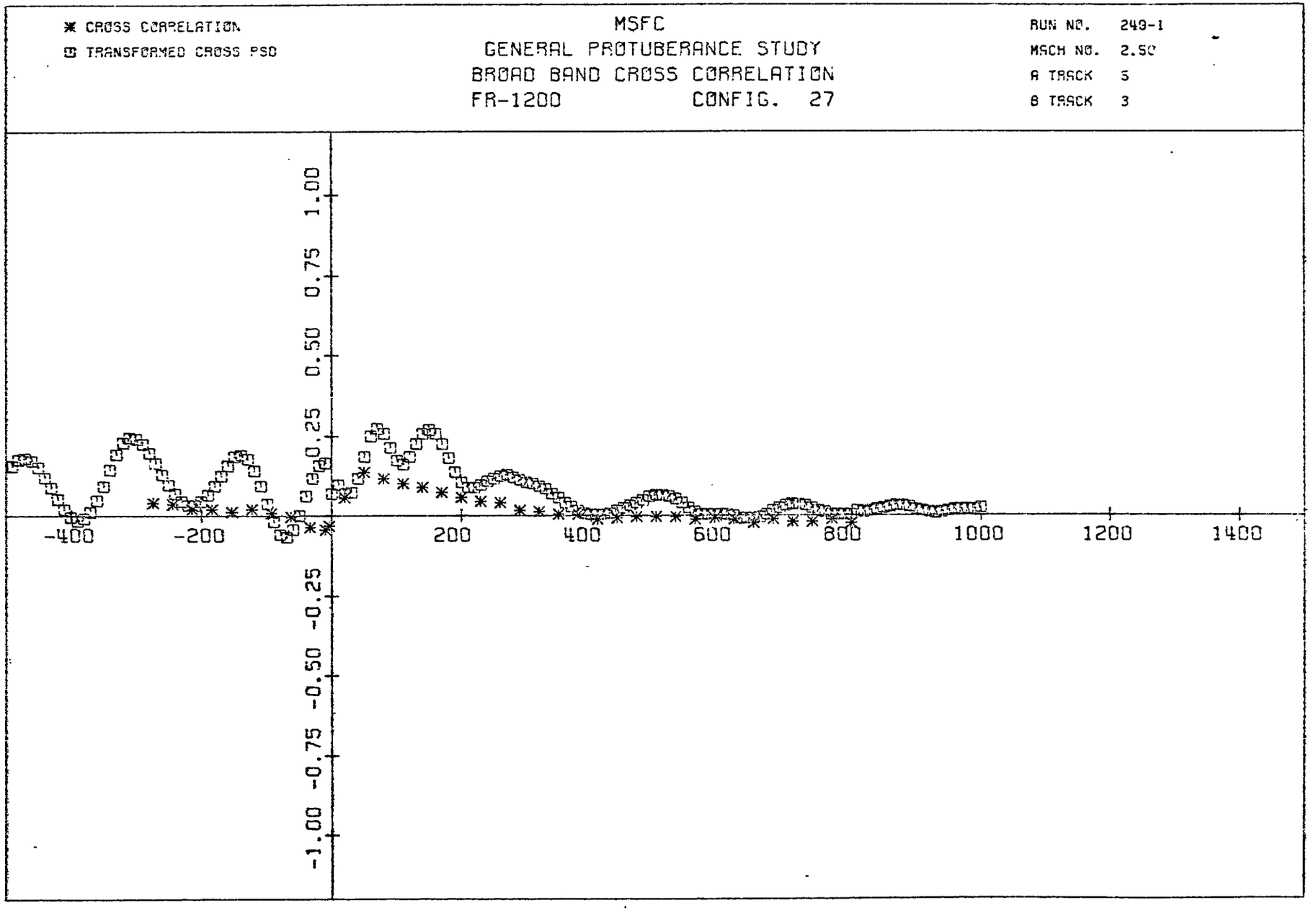

NORMALIZED CORRELATION

PLOT (20)

TRACK A TIME DELAY IN MICROSECONDS

BAGANOFF ASSOCIATES

PLOT (21)

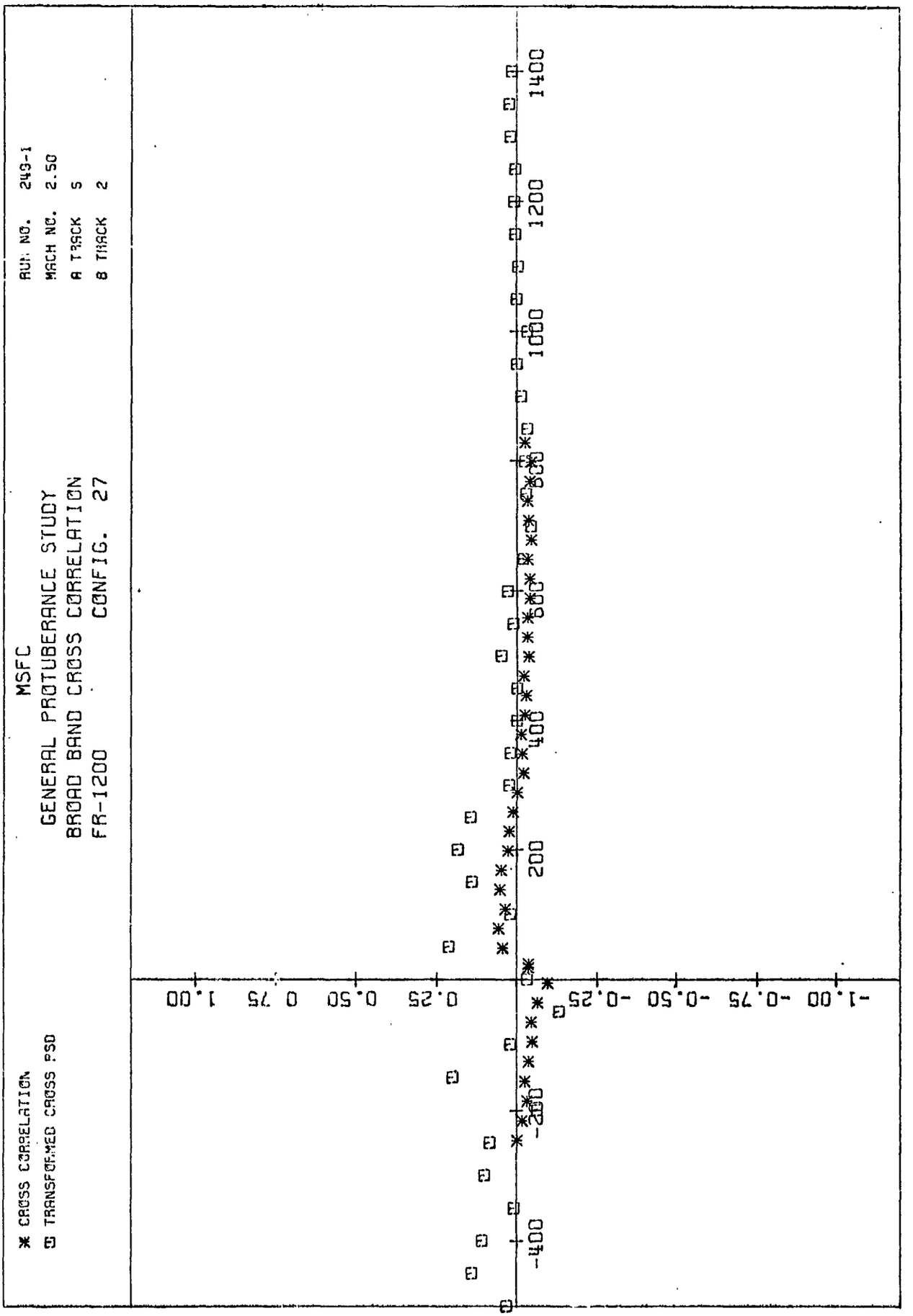

BAGANOFF ASSOCIATES

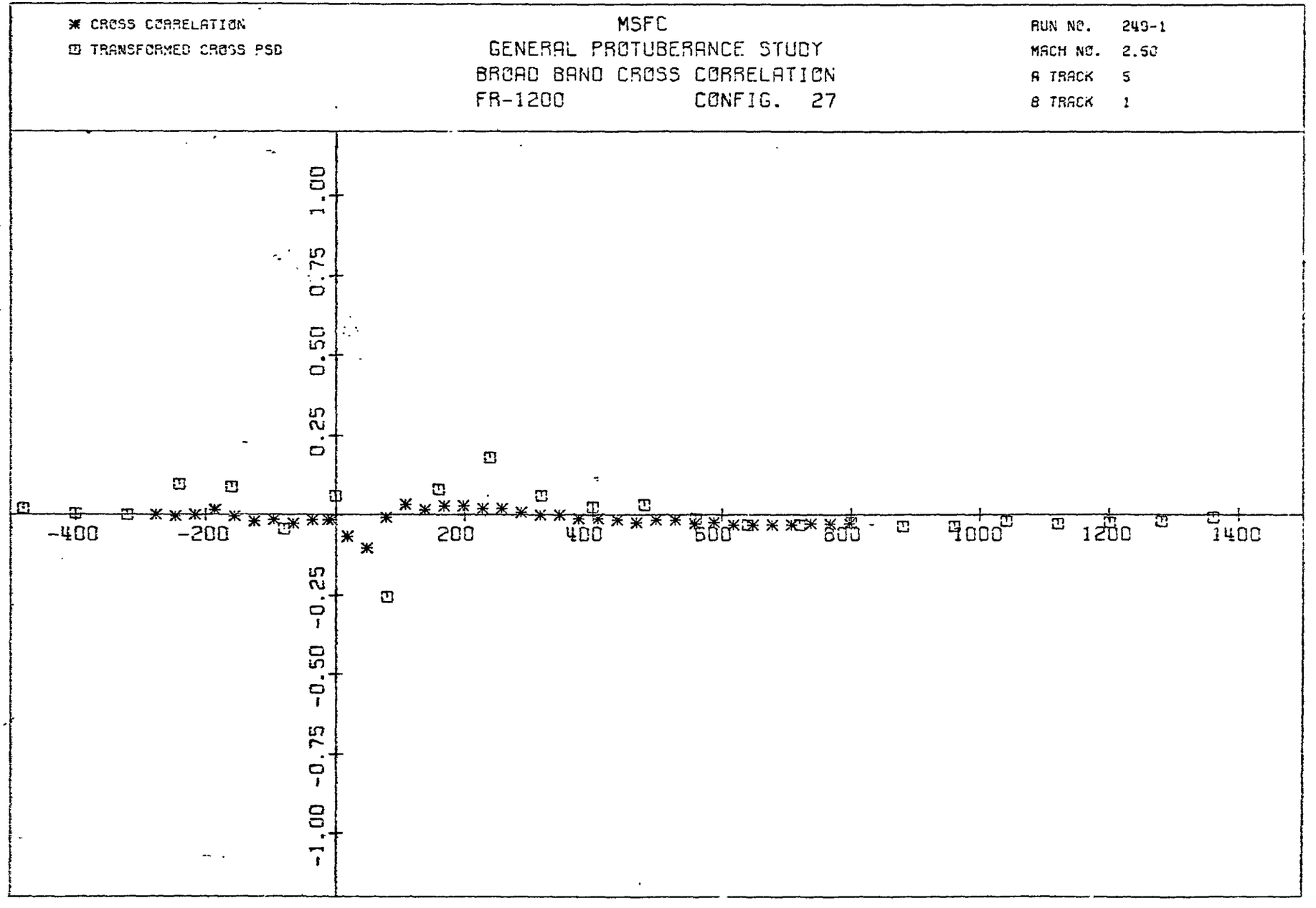

PLOT (22)

BAGANOFF ASSOCIATES

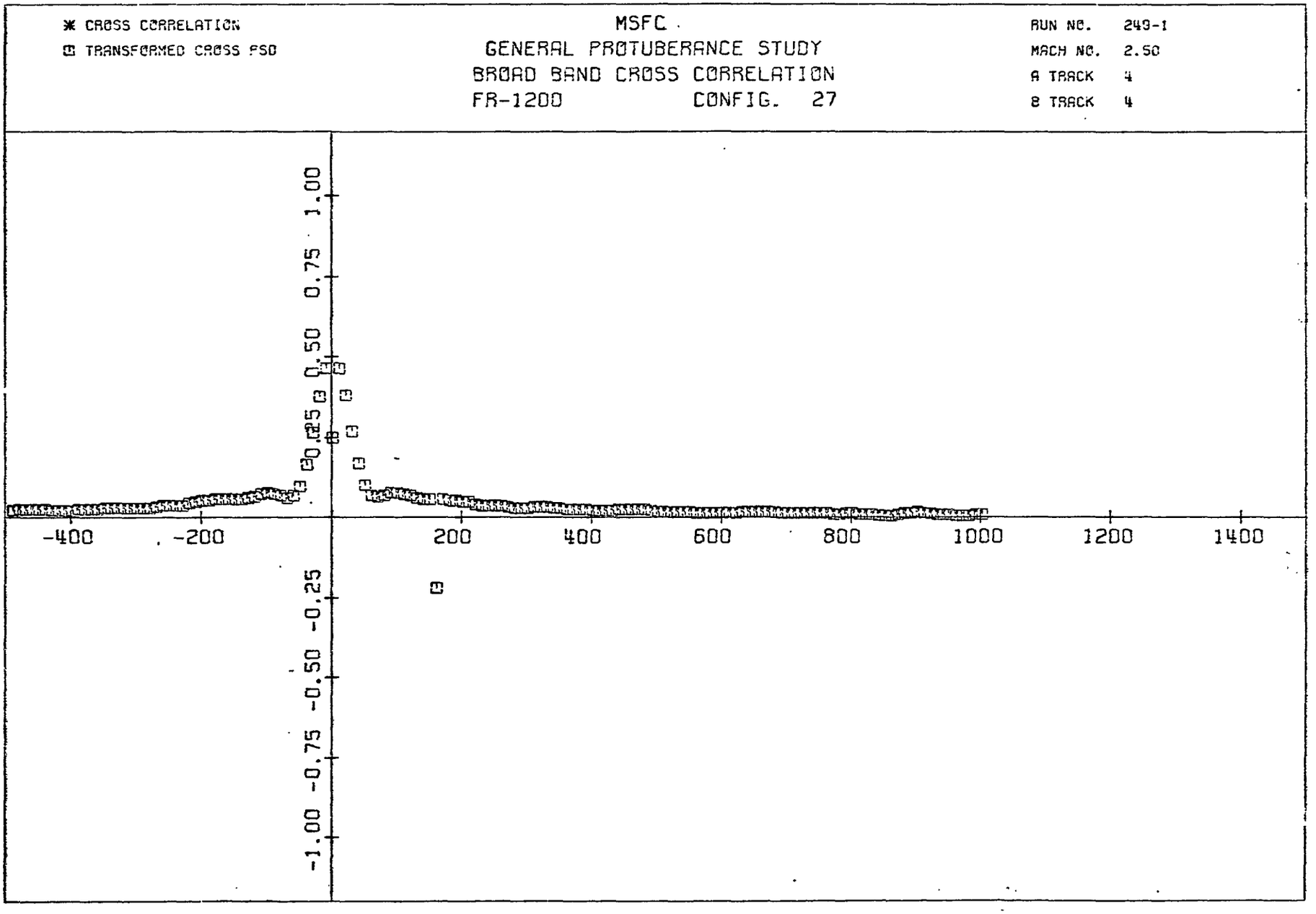

NORMALIZED CORRELATION

TRACK A TIME DELAY IN MICROSECONDS

FIG. 123

BAGANOFF ASSOCIATES

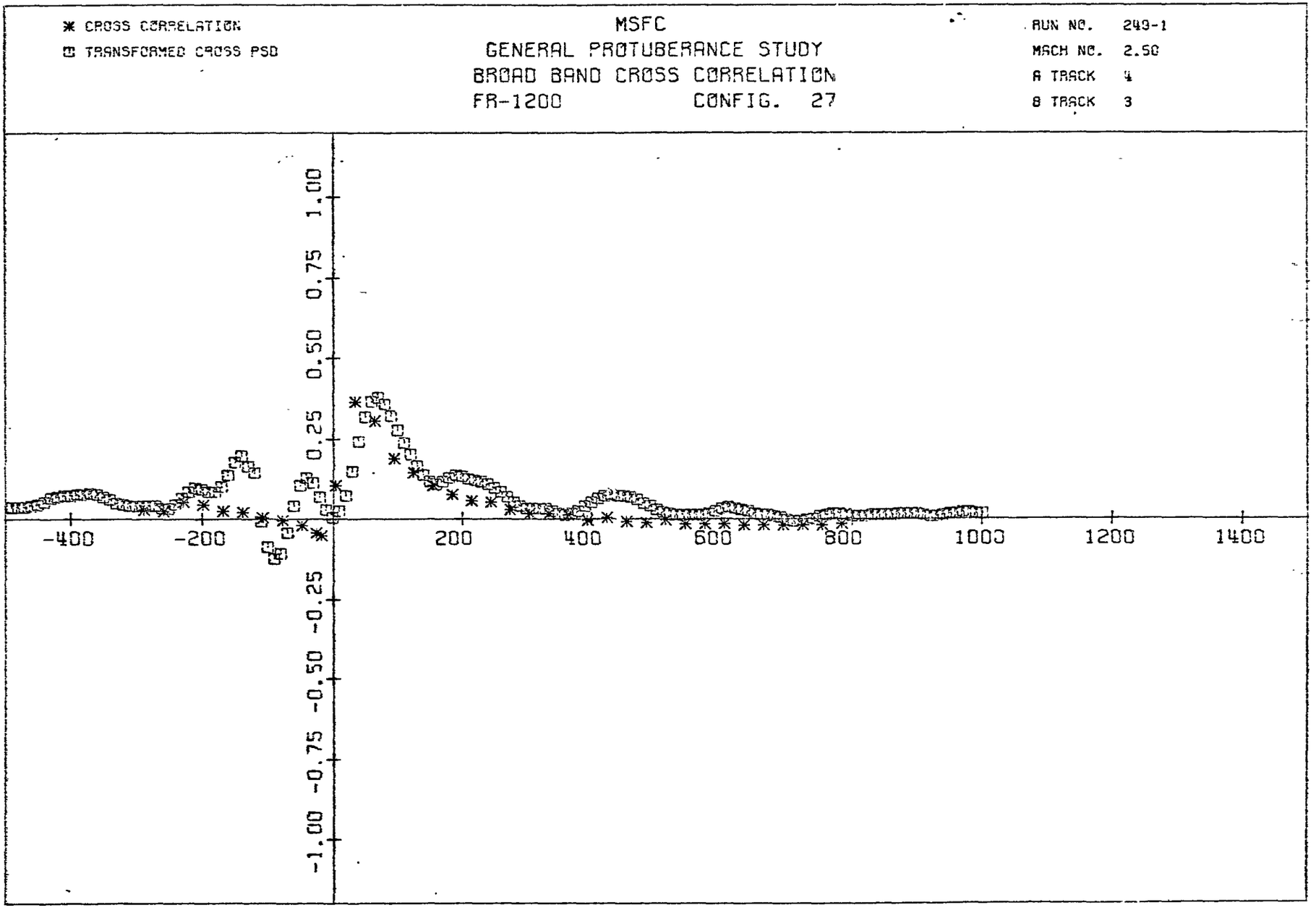

NORMALIZED CORRELATION

PLOT (24)

TRACK A TIME DELAY IN MICROSECONDS

BAGANOFF ASSOCIATES

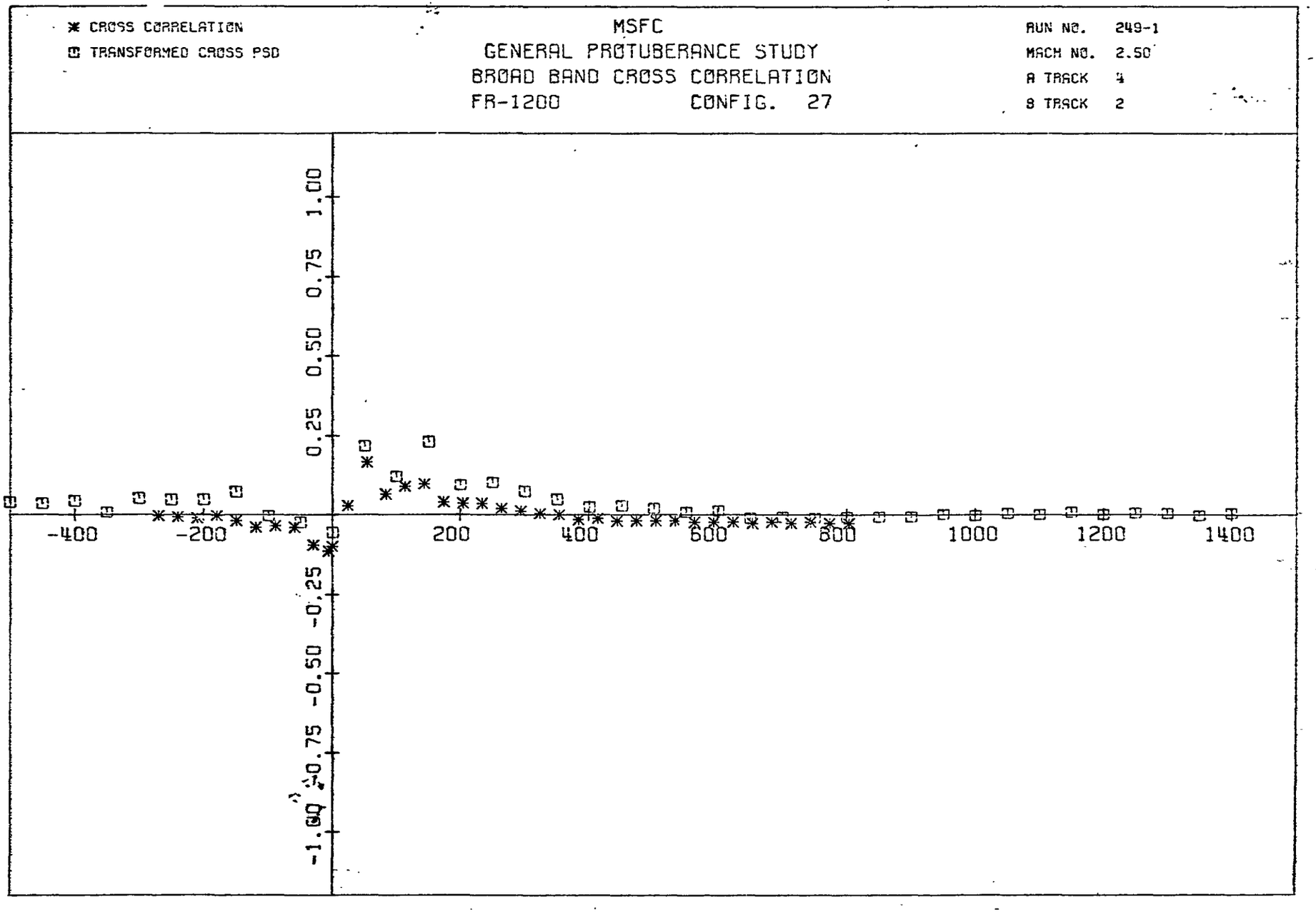

PLOT (26)

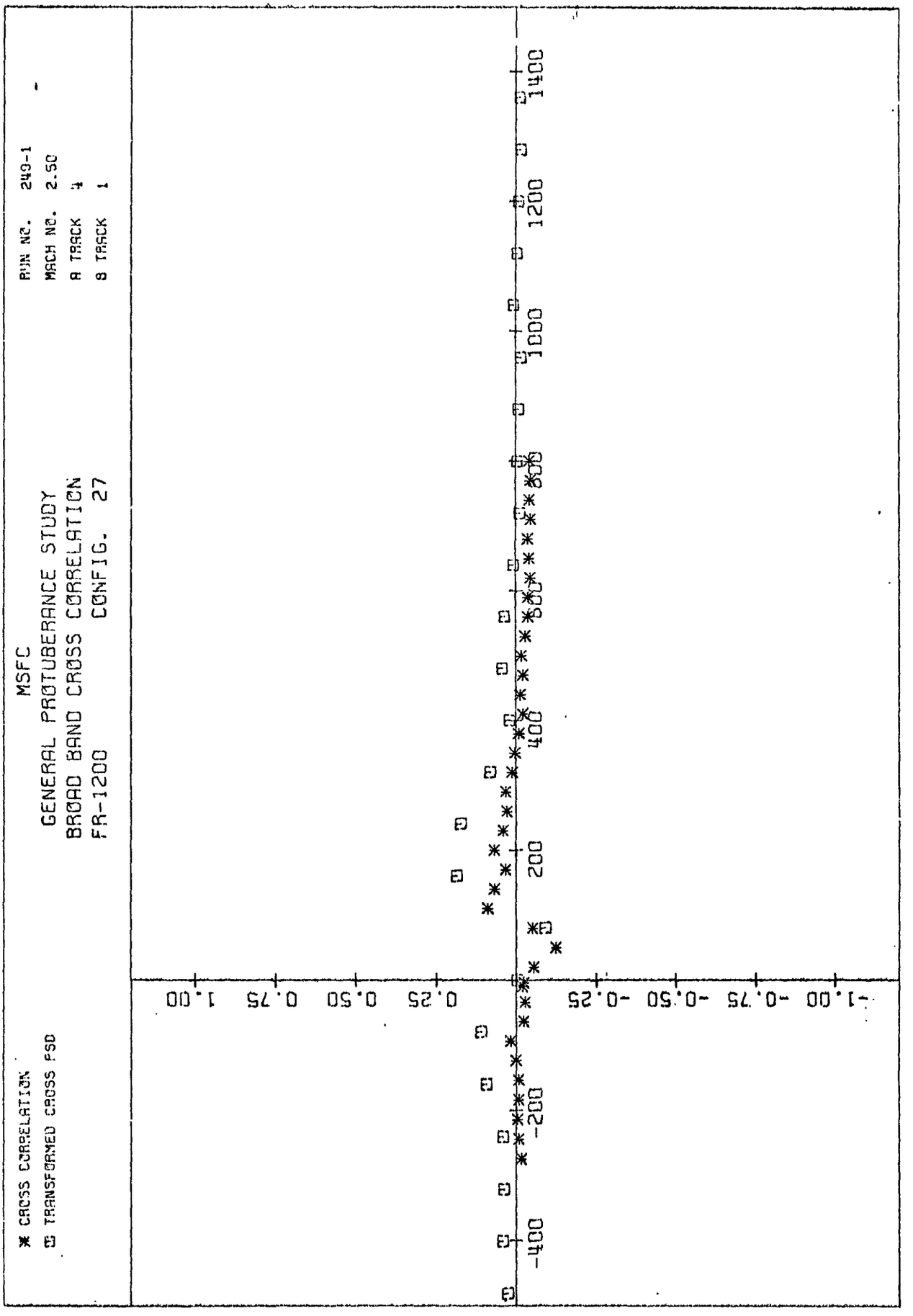
MSFC
GENERAL PROTUBERANCE STUDY
BROAD BAND CROSS CORRELATION
FR-1200 CONFIG. 27
RUN NO. 249-1
MACH NO. 2.50
A TRACK 4
B TRACK 1
* CROSS CORRELATION
B TRANSFORMED CROSS PSD
NORMALIZED CORRELATION
TRACK A TIME DELAY IN MICROSECONDS
1400
1200
1000
800
600
400
200
-200
-400
1.00
0.75
0.50
0.25
-0.25
-0.50
-0.75
-1.00

BAGANOFF ASSOCIATES

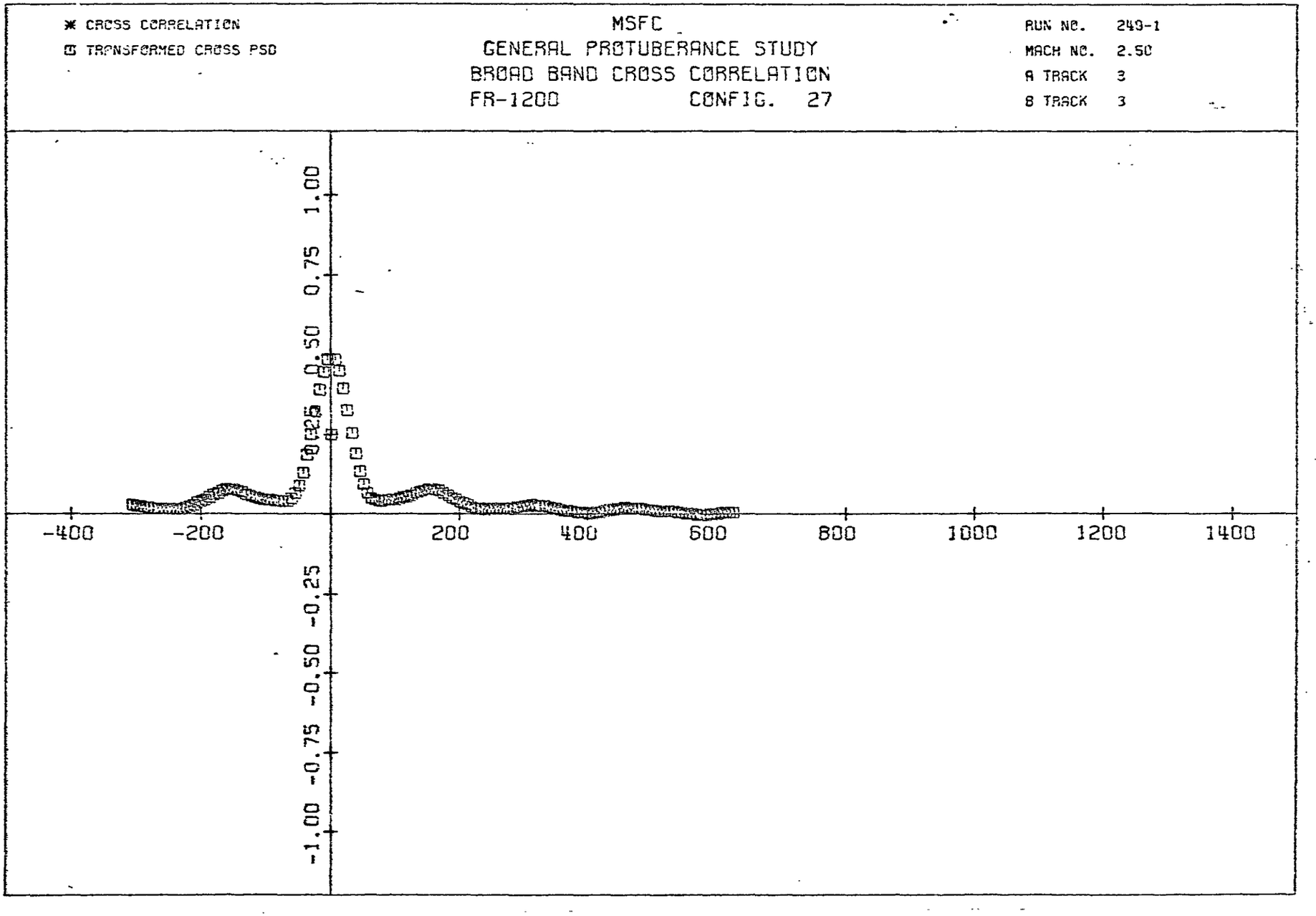

NORMALIZED CORRELATION

PLOT (27)

TRACK A TIME DELAY IN MICROSECONDS

BAGANOFF ASSOCIATES

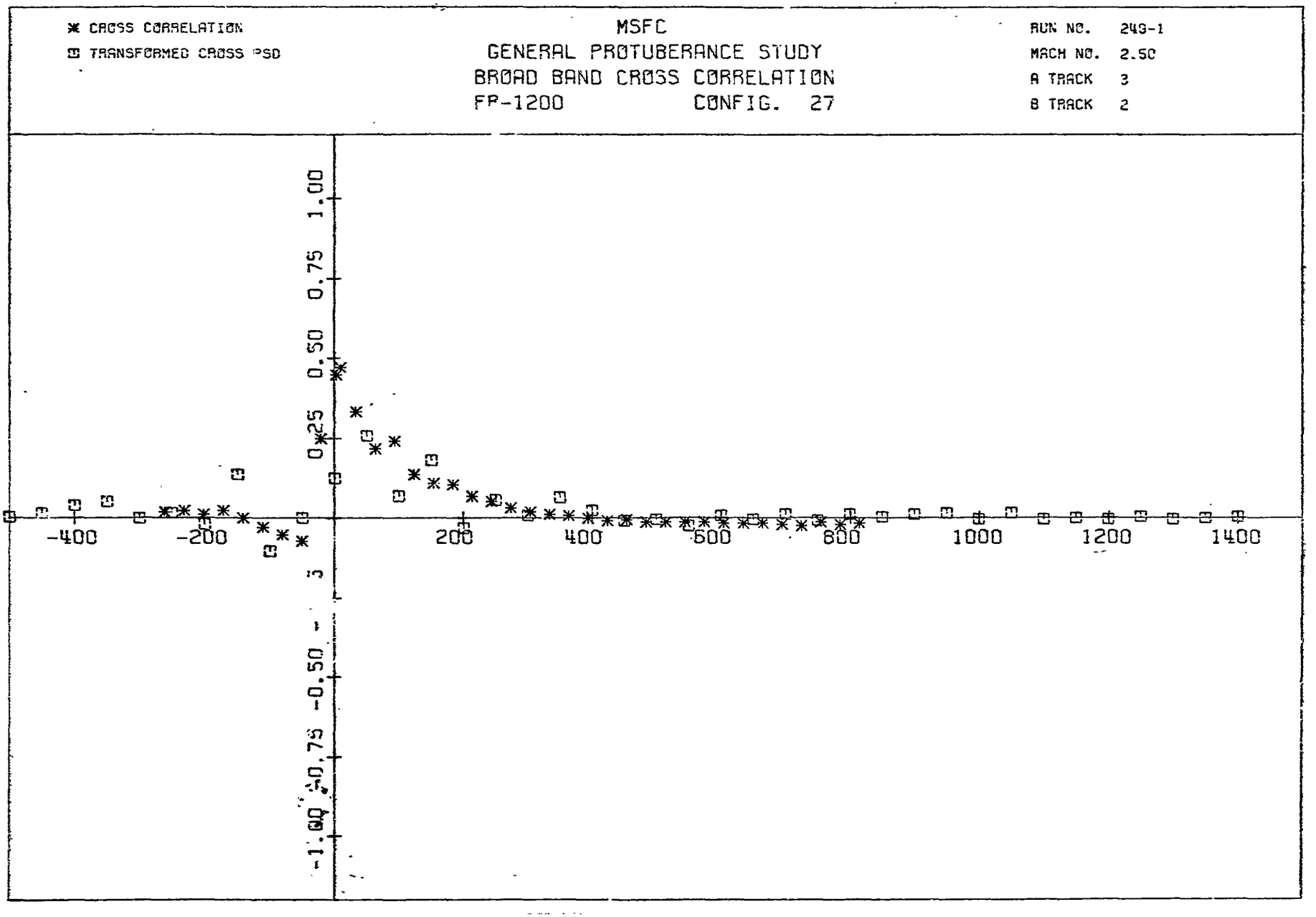

PLOT (28)

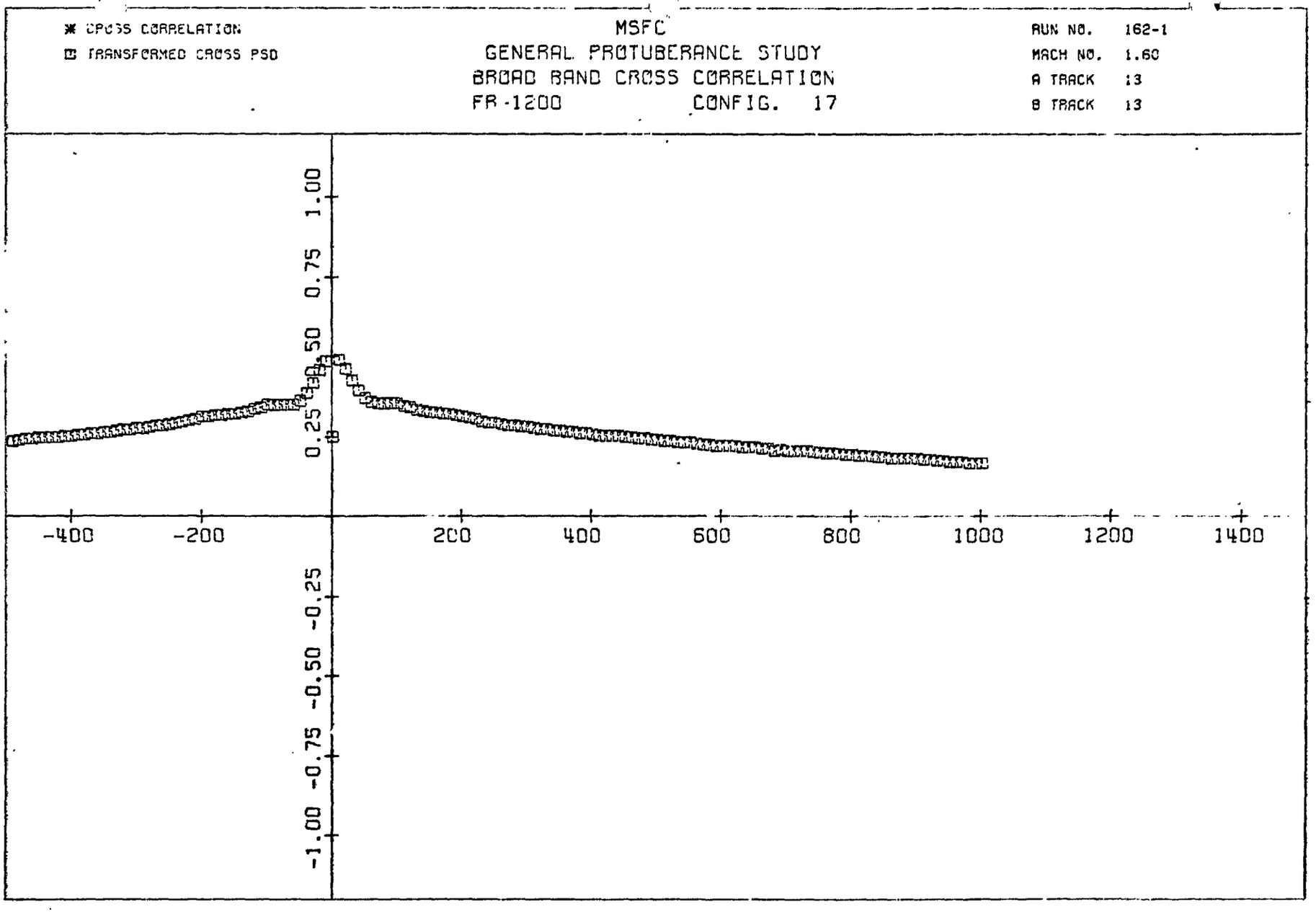
* CROSS CORRELATION
⊡ TRANSFORMED CROSS PSD
MSFC
GENERAL PROTUBERANCE STUDY
BROAD BAND CROSS CORRELATION
FR-1200 CONFIG. 17
RUN NO. 162-1
MACH NO. 1.60
A TRACK 13
B TRACK 13
1.00
0.75
0.50
0.25
-0.25
-0.50
-0.75
-1.00
-400
-200
200
400
600
800
1000
1200
1400
NORMALIZED CORRELATION
TRACK A TIME DELAY IN MICROSECONDS
PLOT (30)

PLOT (31)

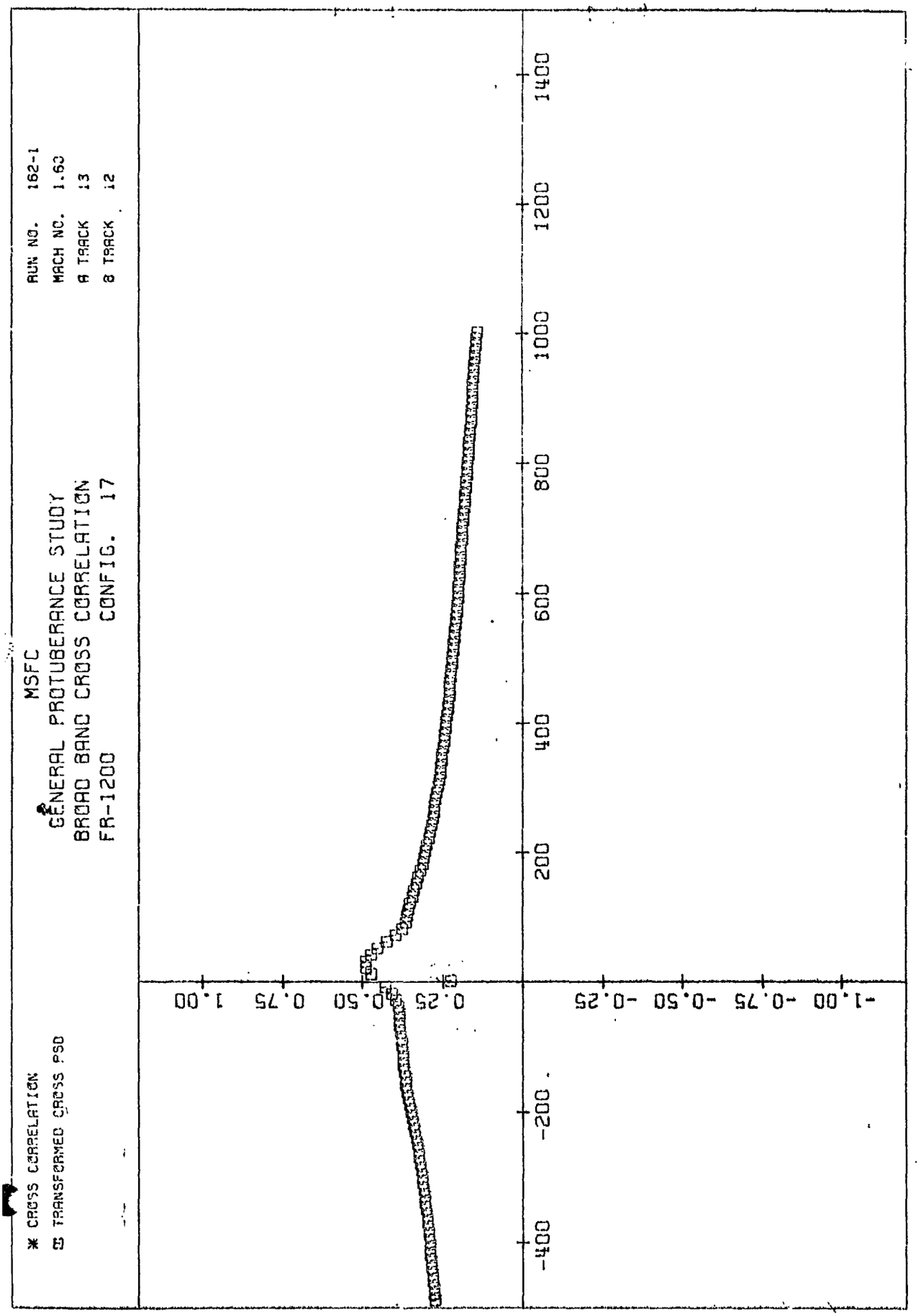
* CROSS CORRELATION
⊡ TRANSFORMED CROSS PSD
MSFC
GENERAL PROTUBERANCE STUDY
BROAD BAND CROSS CORRELATION
FR-1200 CONFIG. 17
RUN NO. 162-1
MACH NO. 1.60
A TRACK 13
B TRACK 12
1.00
0.75
0.50
0.25
-1.00
-0.75
-0.50
-0.25
-400
-200
200
400
600
800
1000
1200
1400
NORMALIZED CORRELATION
TRACK A TIME DELAY IN MICROSECONDS

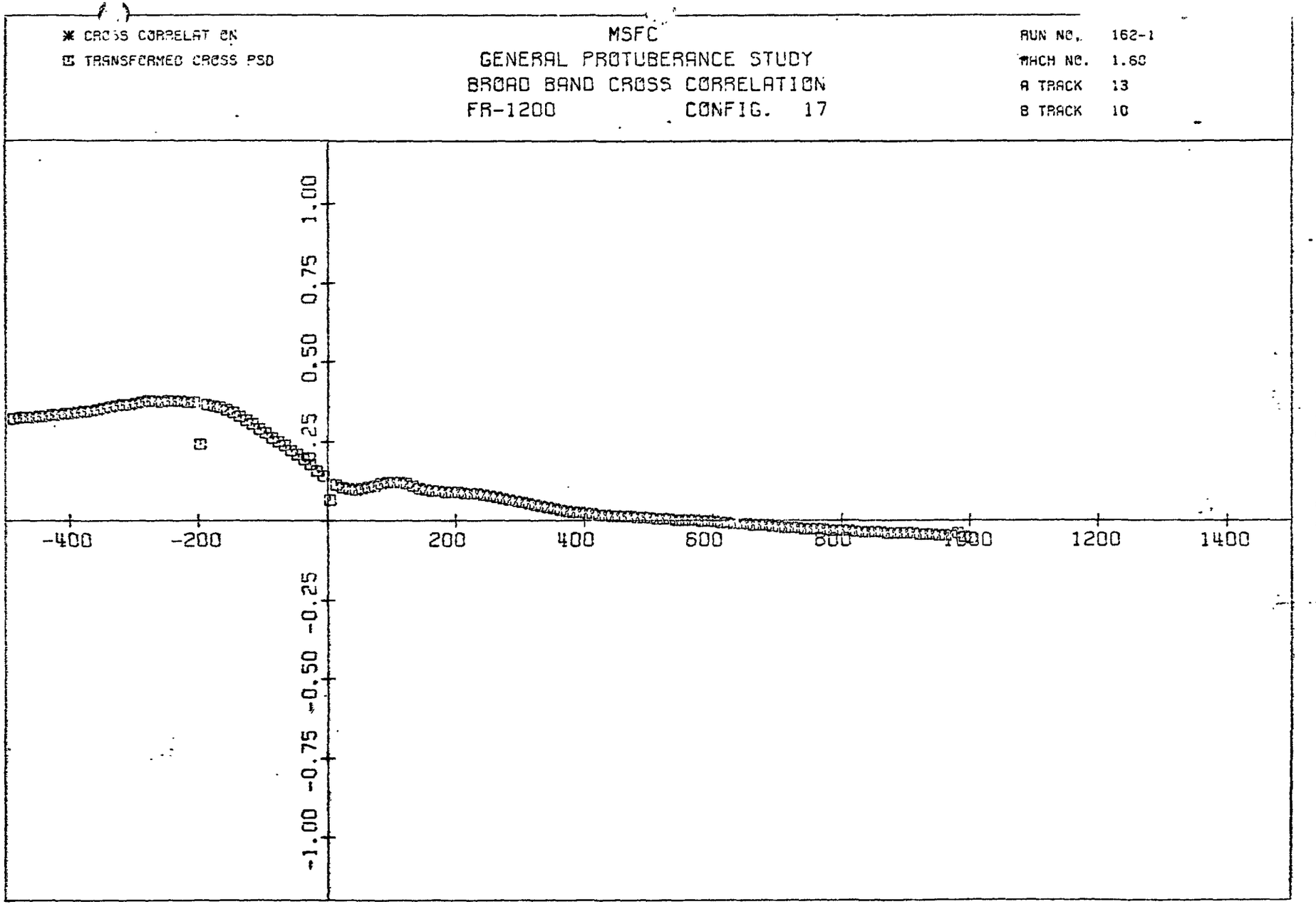
* CROSS CORRELAT ON
B TRANSFORMED CROSS PSD
MSFC
GENERAL PROTUBERANCE STUDY
BROAD BAND CROSS CORRELATION
FR-1200 CONFIG. 17
RUN NO. 162-1
MACH NO. 1.60
A TRACK 13
B TRACK 10
1.00
0.75
0.50
0.25
-0.25
-0.50
-0.75
-1.00
-400
-200
200
400
600
800
1000
1200
1400
B
B
NORMALIZED CORRELATION
TRACK A TIME DELAY IN MICROSECONDS

PLOT (32)

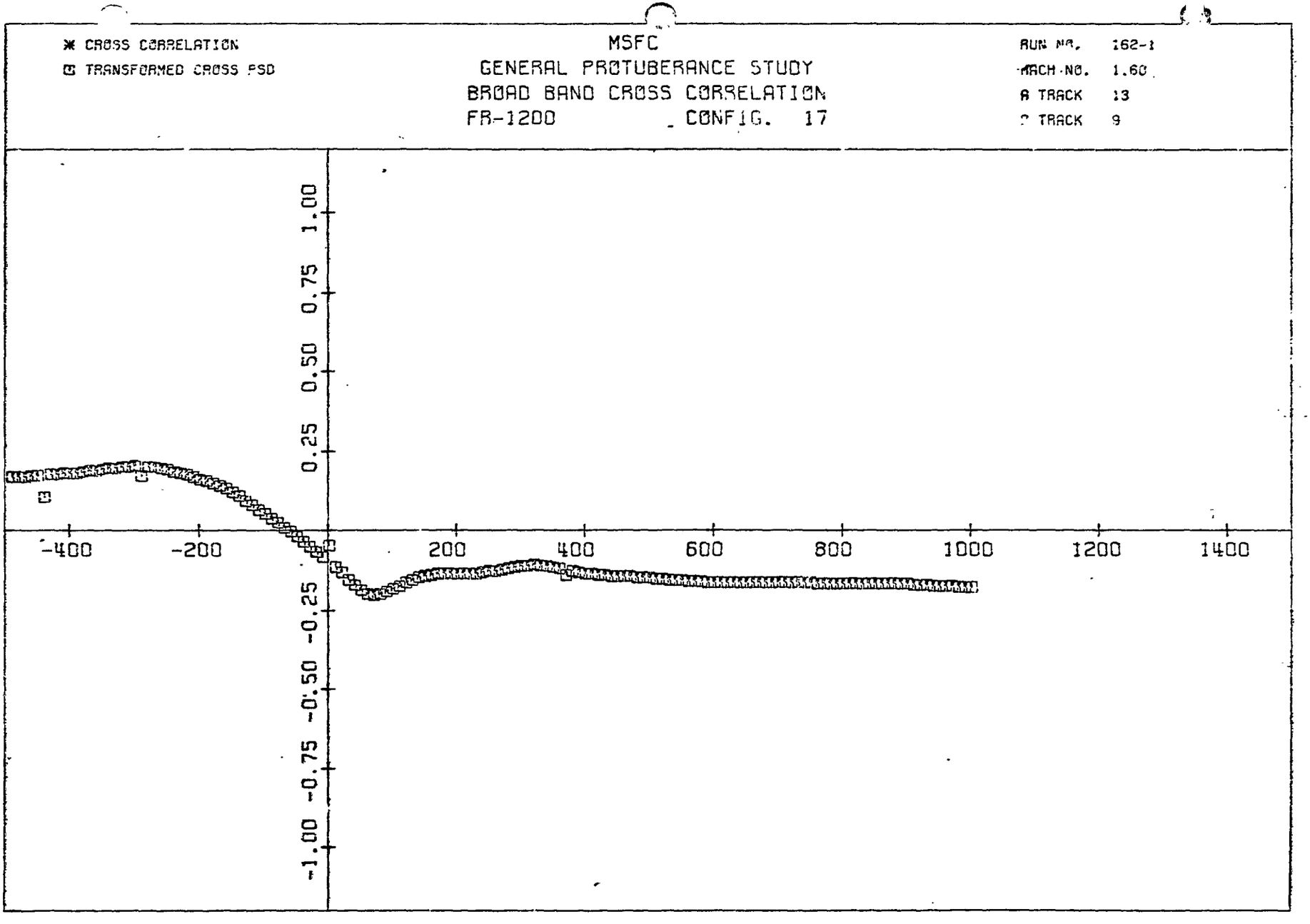
* CROSS CORRELATION
□ TRANSFORMED CROSS PSD
MSFC
GENERAL PROTUBERANCE STUDY
BROAD BAND CROSS CORRELATION
FR-1200 CONFIG. 17
RUN NO. 162-1
MACH NO. 1.60
A TRACK 13
B TRACK 9
NORMALIZED CORRELATION
1.00
0.75
0.50
0.25
-0.25
-0.50
-0.75
-1.00
-400
-200
200
400
600
800
1000
1200
1400
TRACK A TIME DELAY IN MICROSECONDS

PLOT 133

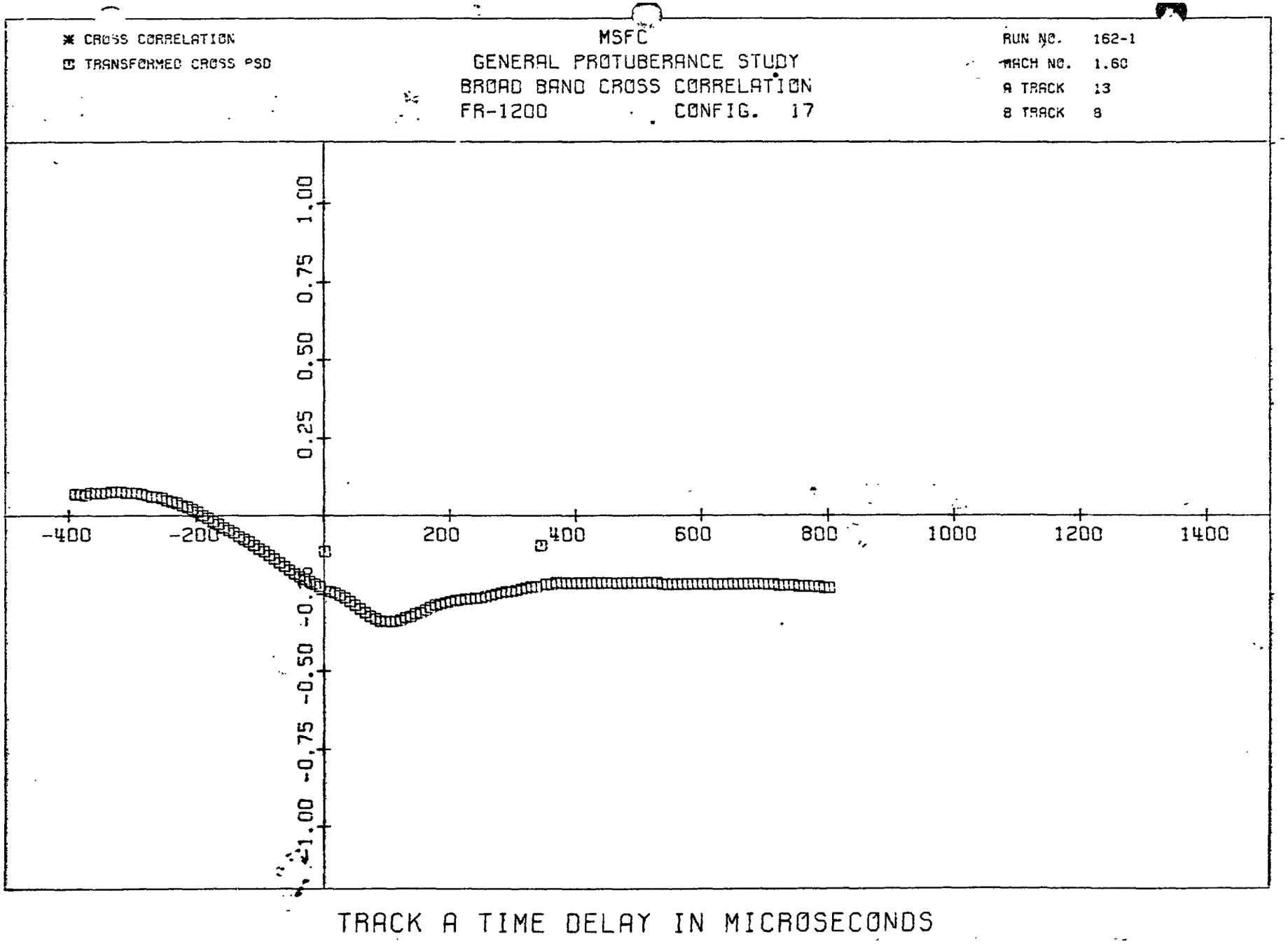
* CROSS CORRELATION
□ TRANSFORMED CROSS PSD
MSFC
GENERAL PROTUBERANCE STUDY
BROAD BAND CROSS CORRELATION
FR-1200 CONFIG. 17
RUN NO. 162-1
MACH NO. 1.60
A TRACK 13
B TRACK 8
NORMALIZED CORRELATION
1.00
0.75
0.50
0.25
-0.
-0.50
-0.75
-1.00
-400
-200
200
400
600
800
1000
1200
1400
TRACK A TIME DELAY IN MICROSECONDS
PLOT (34)

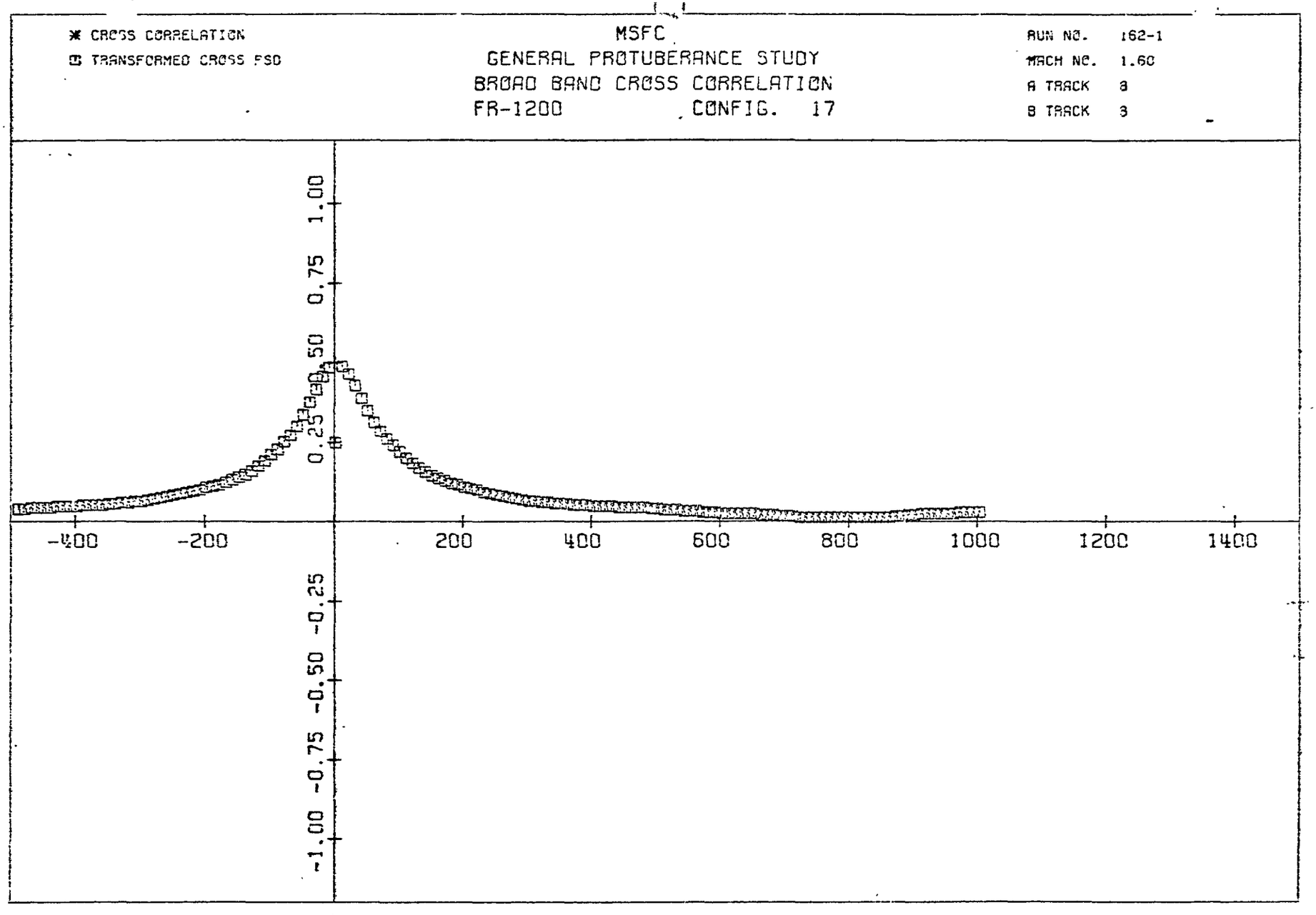
* CROSS CORRELATION
□ TRANSFORMED CROSS PSD
MSFC
GENERAL PROTUBERANCE STUDY
BROAD BAND CROSS CORRELATION
FR-1200 CONFIG. 17
RUN NO. 162-1
MACH NO. 1.60
A TRACK 8
B TRACK 3
1.00
0.75
0.50
0.25
-0.25
-0.50
-0.75
-1.00
-400
-200
200
400
600
800
1000
1200
1400
NORMALIZED CORRELATION
TRACK A TIME DELAY IN MICROSECONDS

PLOT (35)

BAGANOFF ASSOCIATES

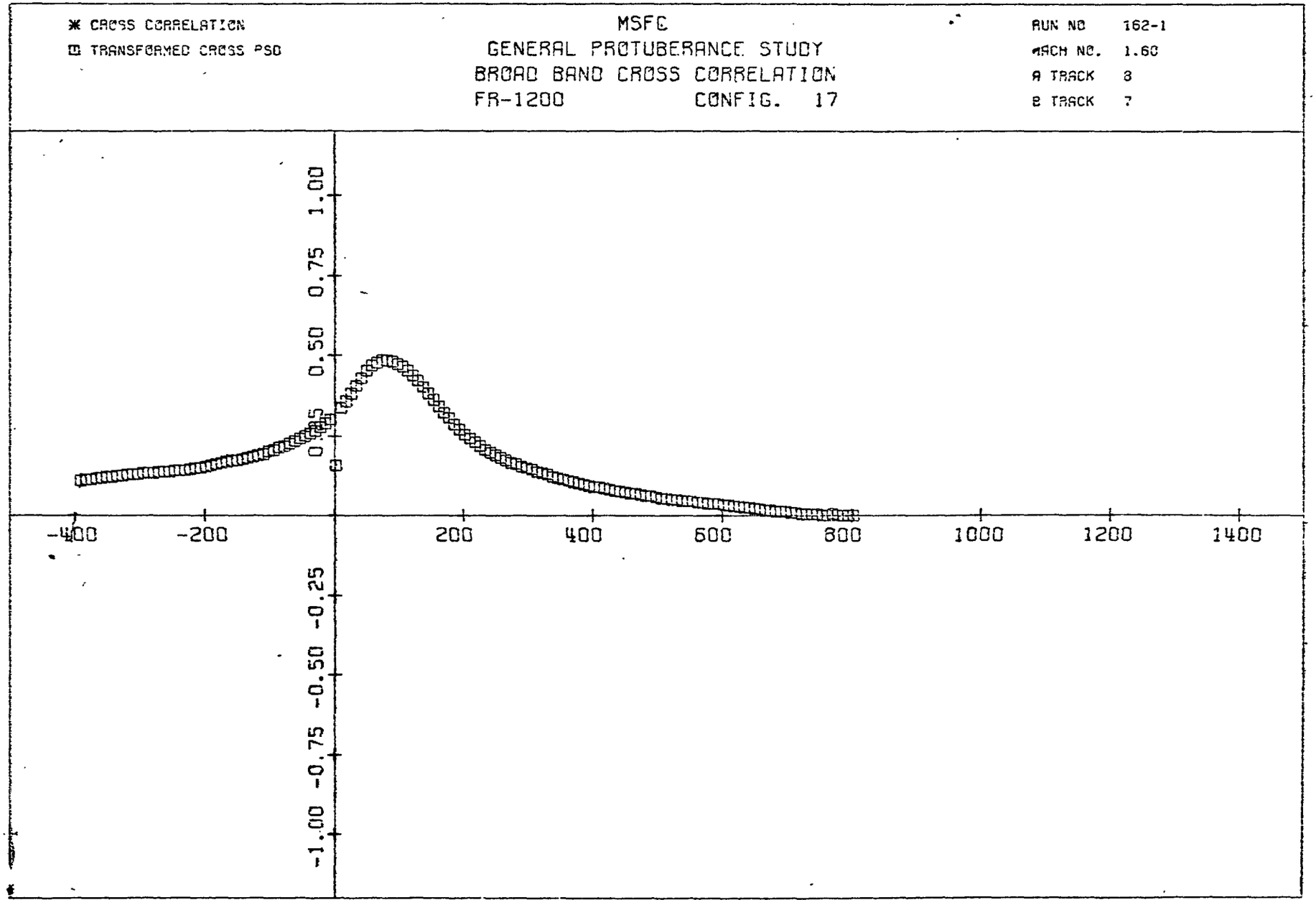

NORMALIZED CORRELATION

PLOT (36)

TRACK A TIME DELAY IN MICROSECONDS

BAGANOFF ASSOCIATES

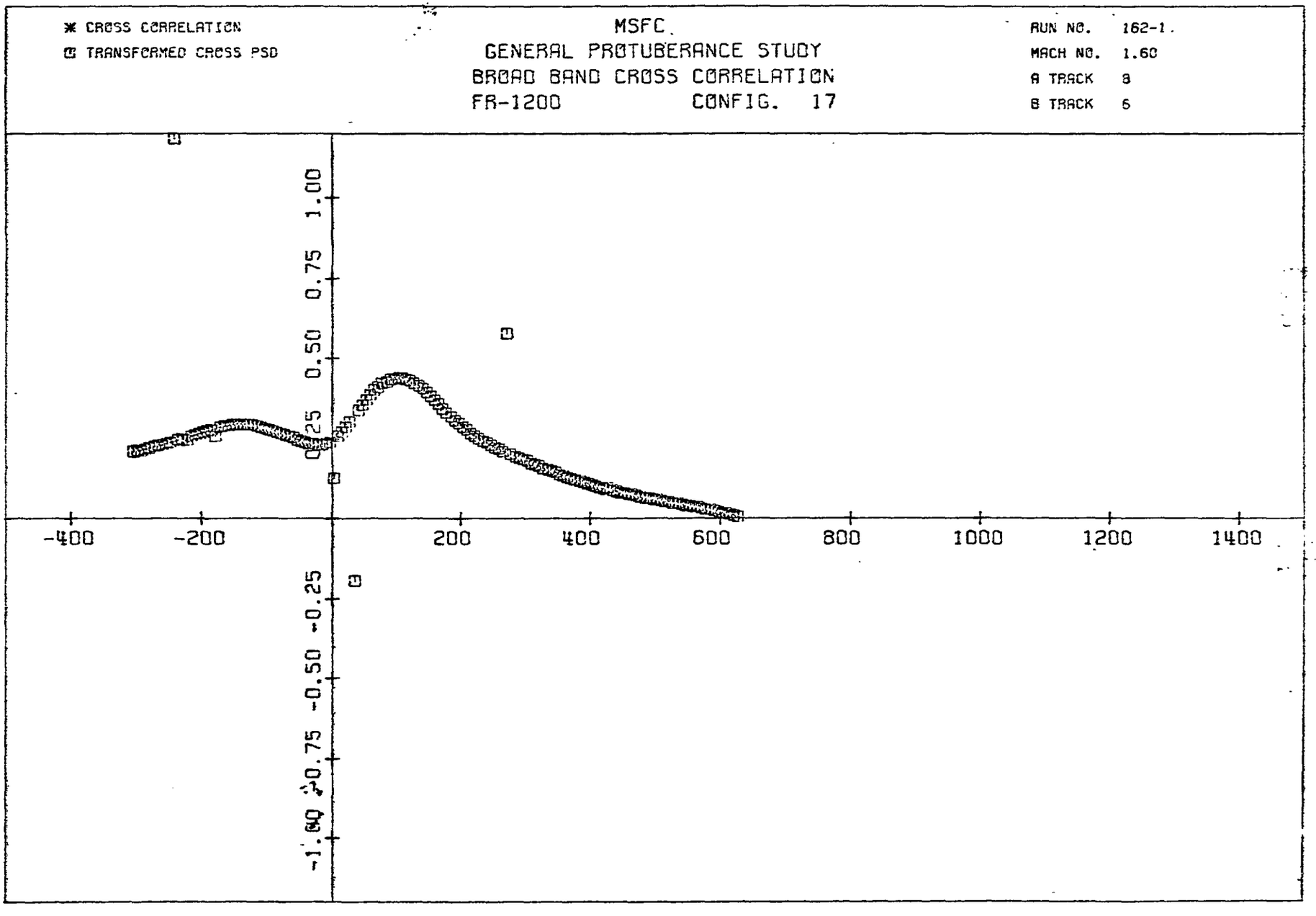

FIGURE (31)

BAGANOFF ASSOCIATES

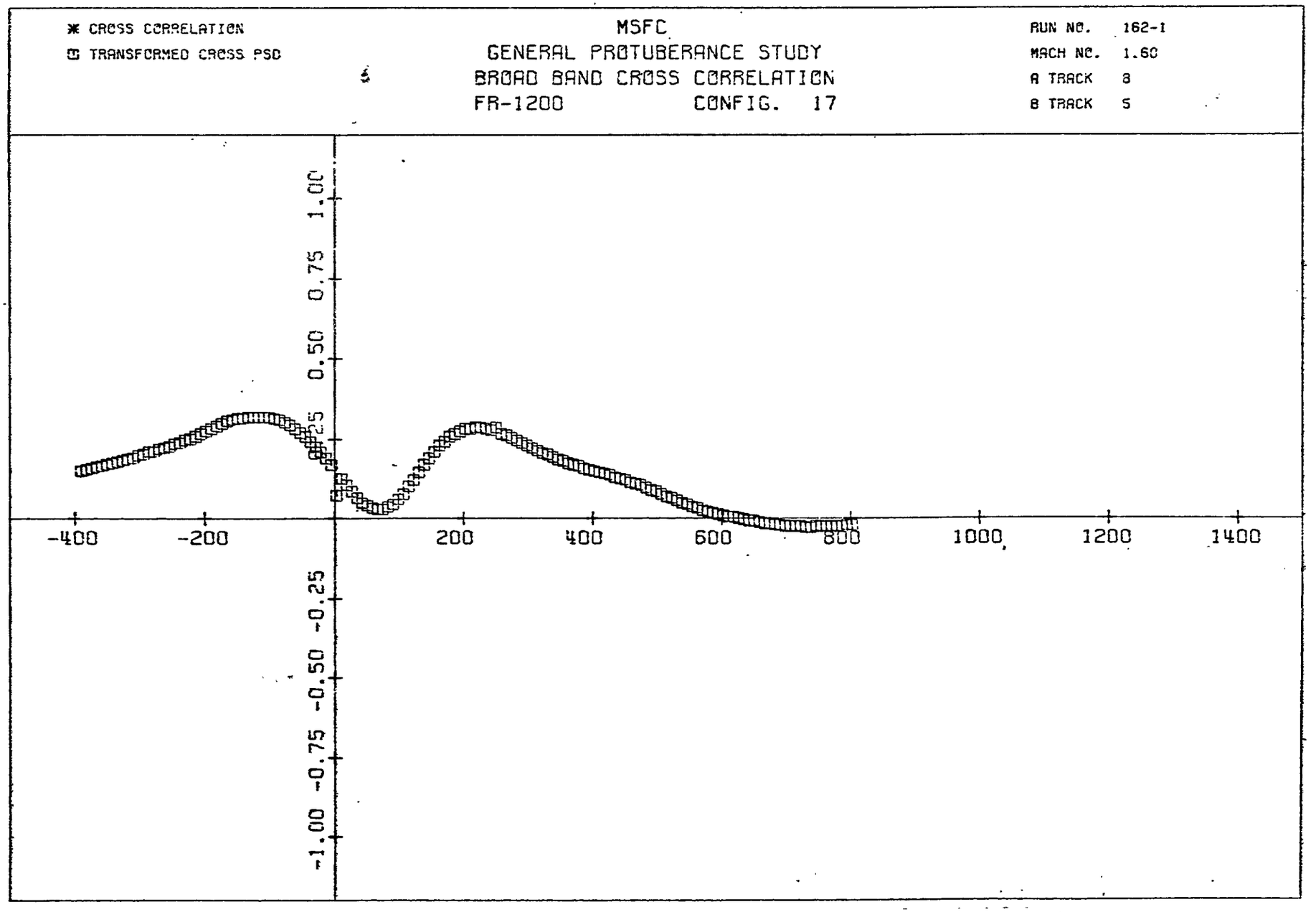

NORMALIZED CORRELATION

PLOT (38)

TRACK A TIME DELAY IN MICROSECONDS

BAGANOFF ASSOCIATES

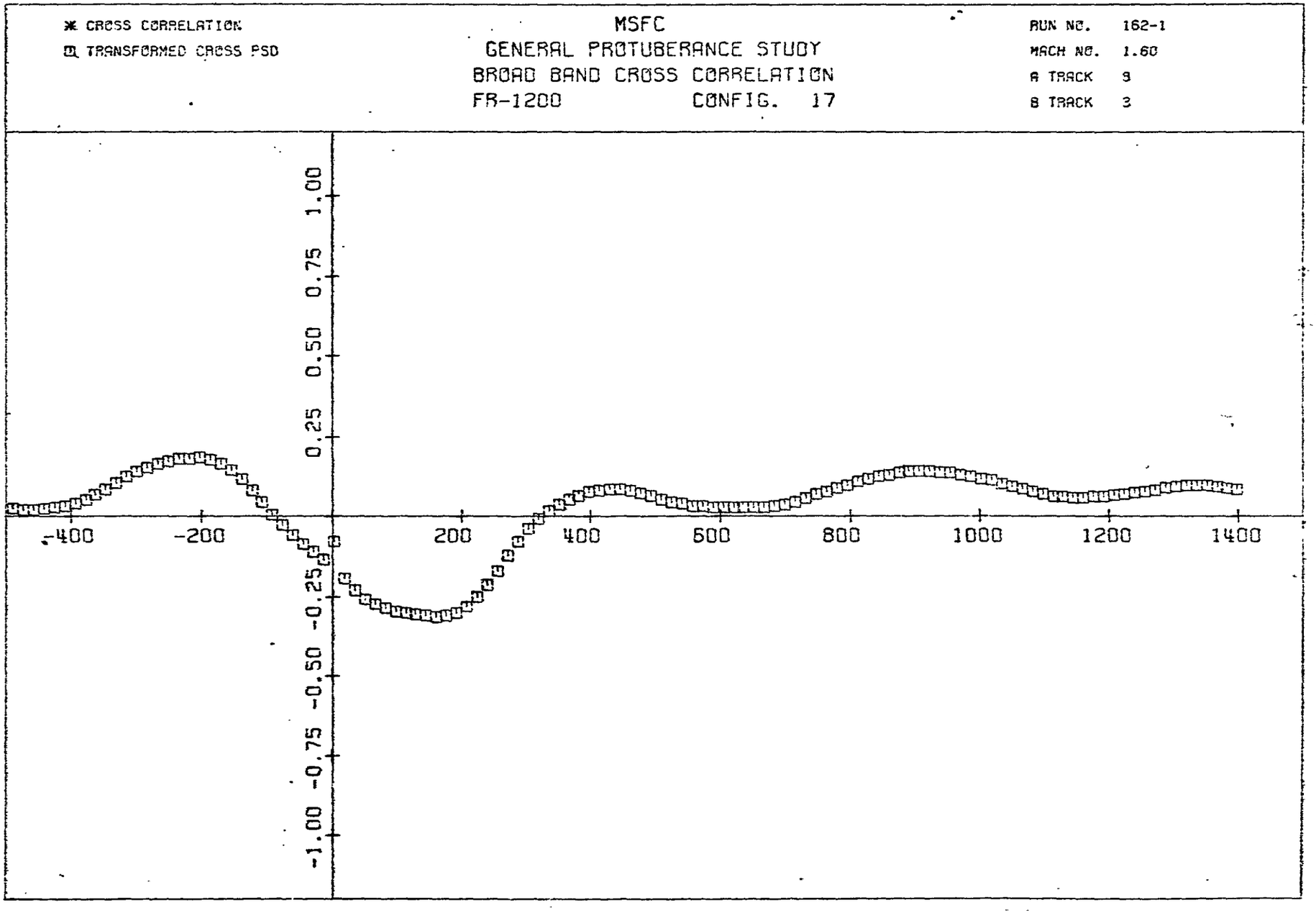

PLOT (39)

BRANOFF ASSOCIATES

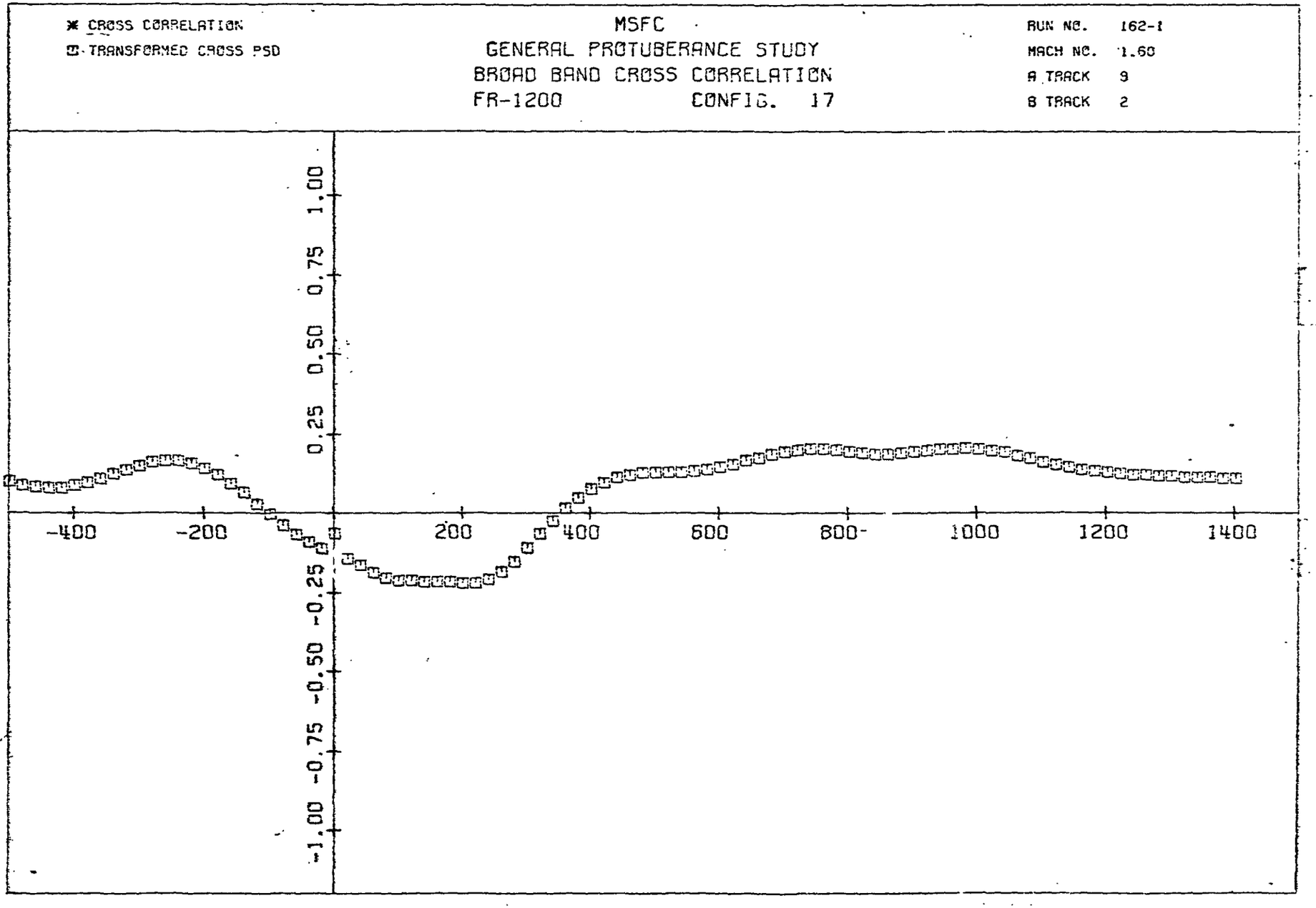

BAGANOFF ASSOCIATES

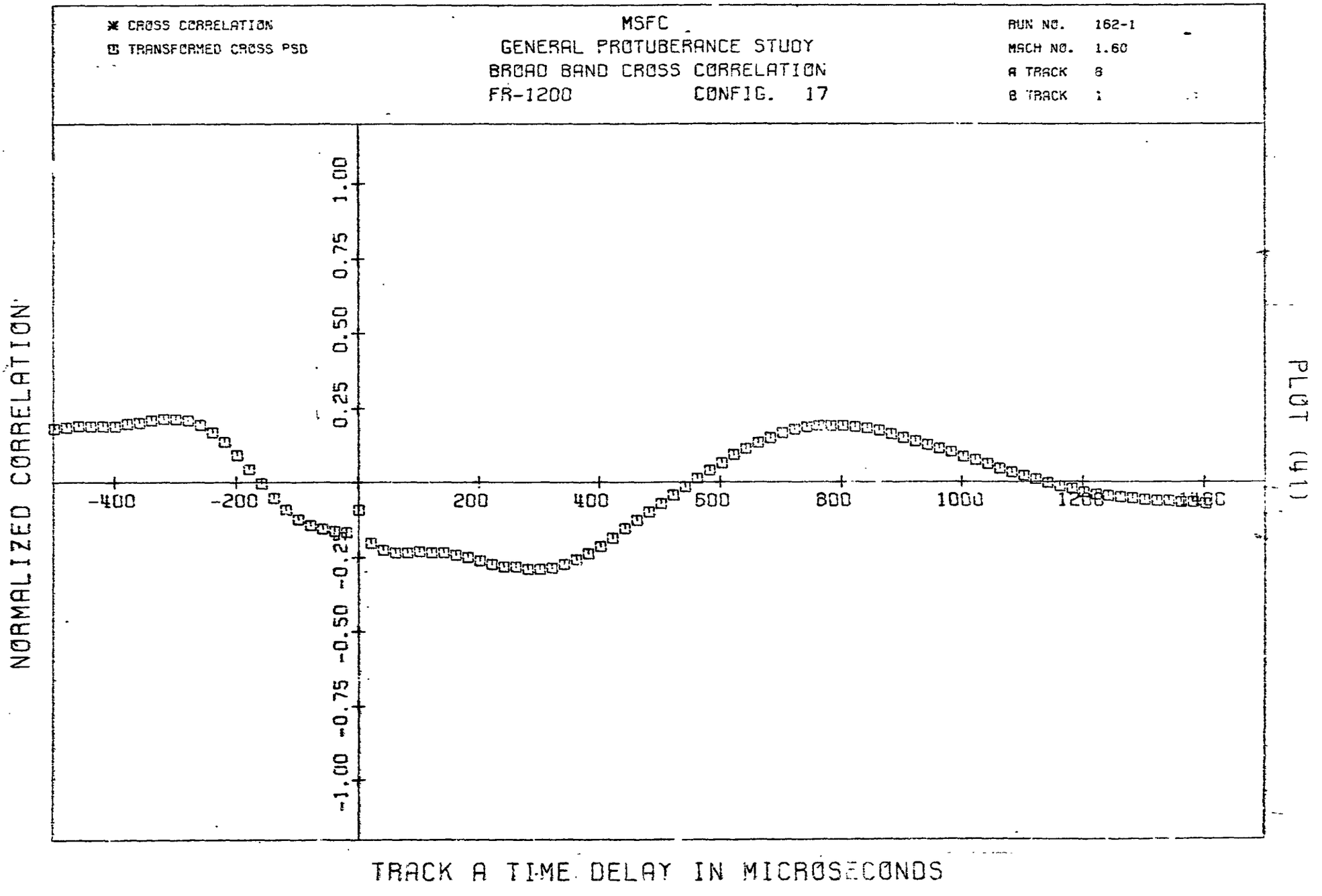

BAGANOFF ASSOCIATES

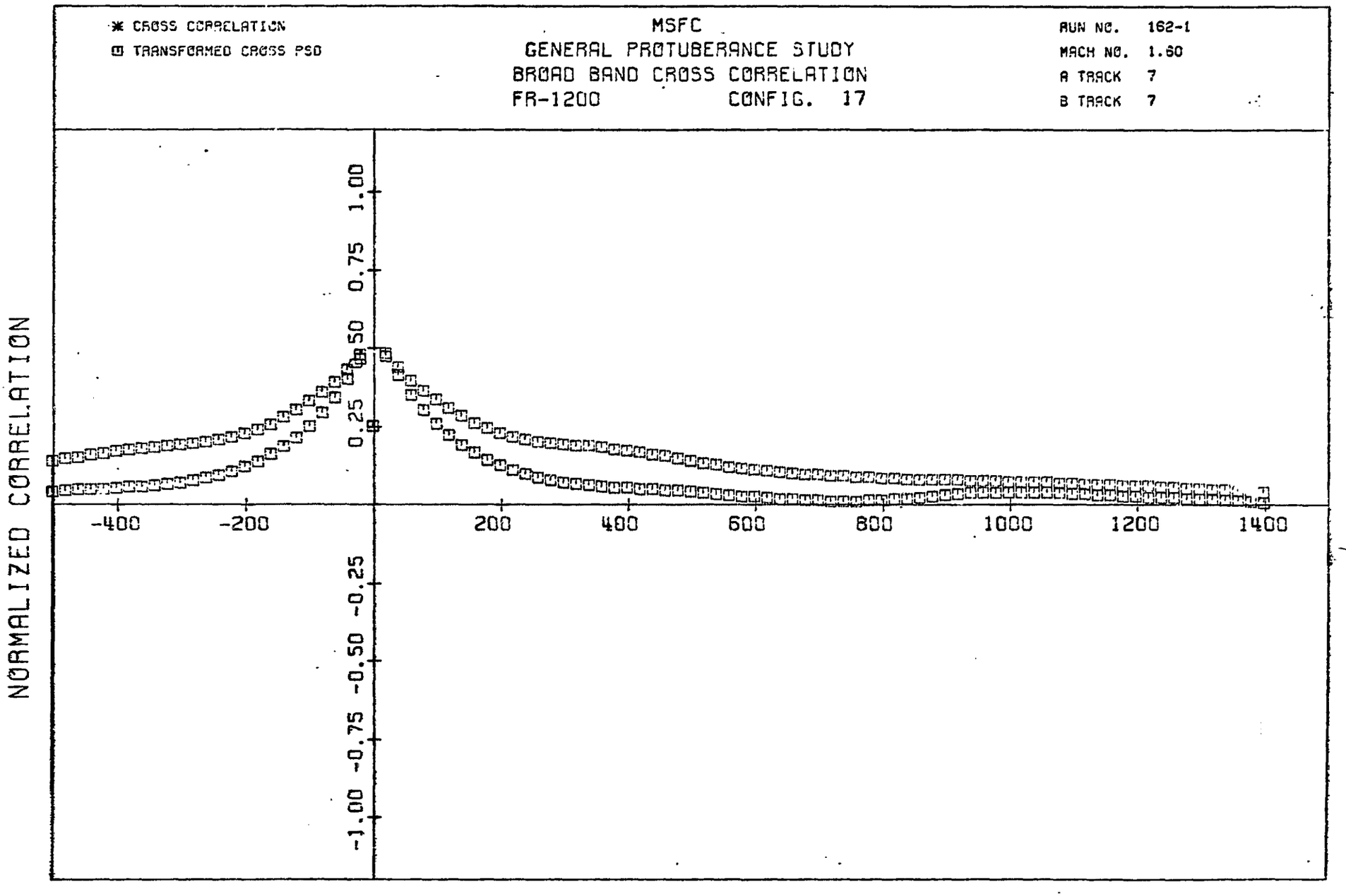

PLOT (88) 47

BAGANOFF ASSOCIATES

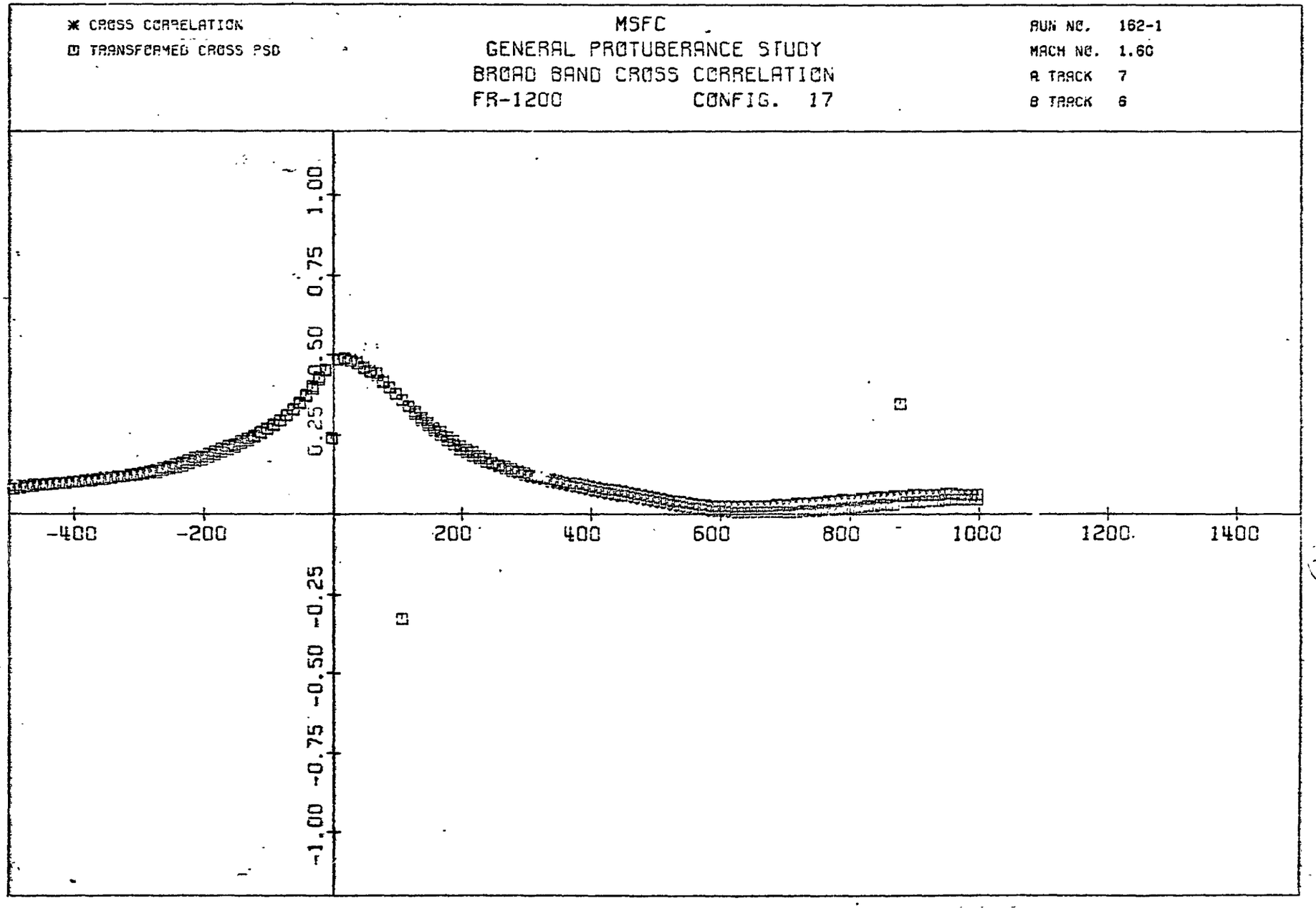

PLOT (B3) 4/3

BAGANOFF ASSOCIATES

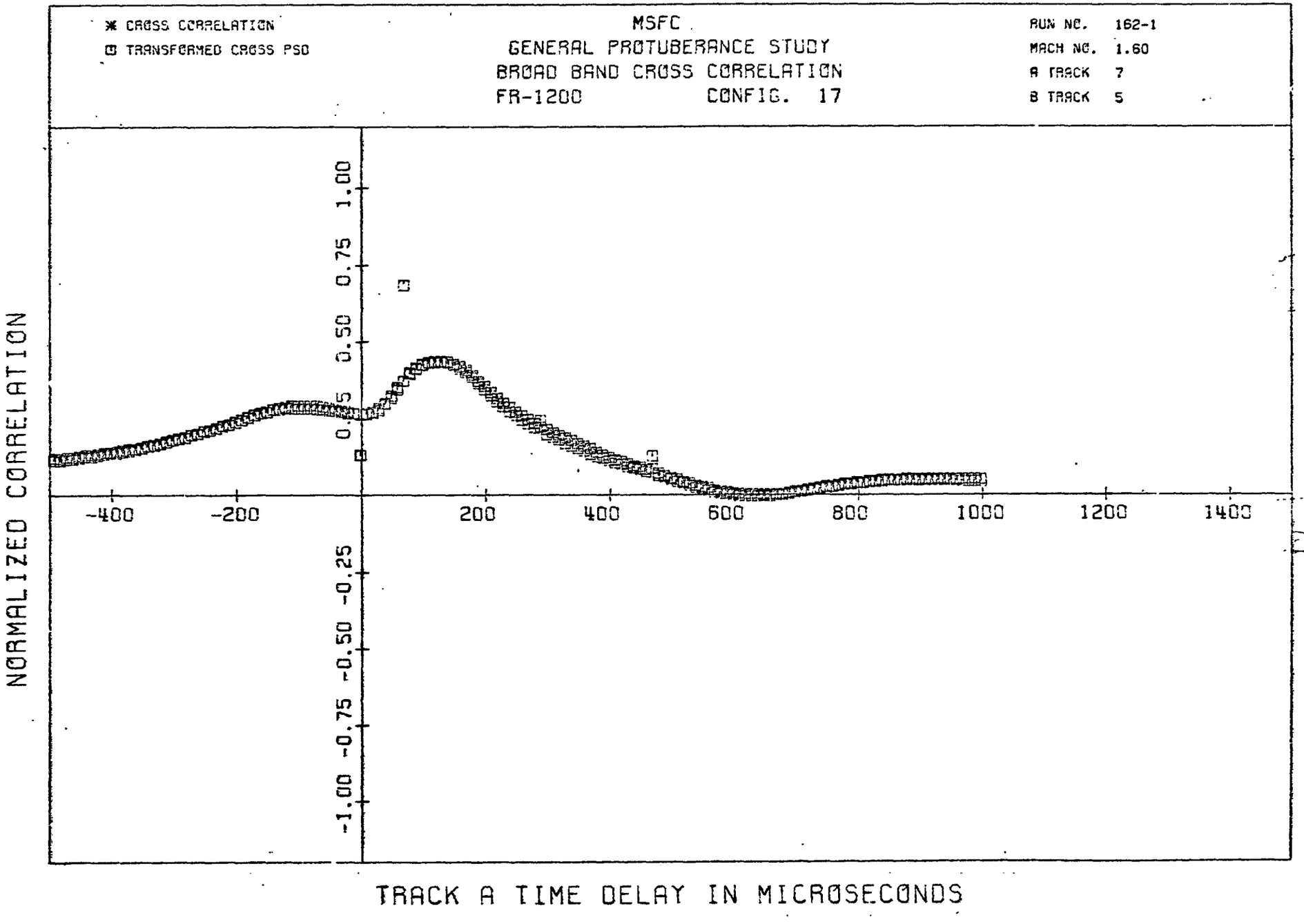

BAGANOFF ASSOCIATES

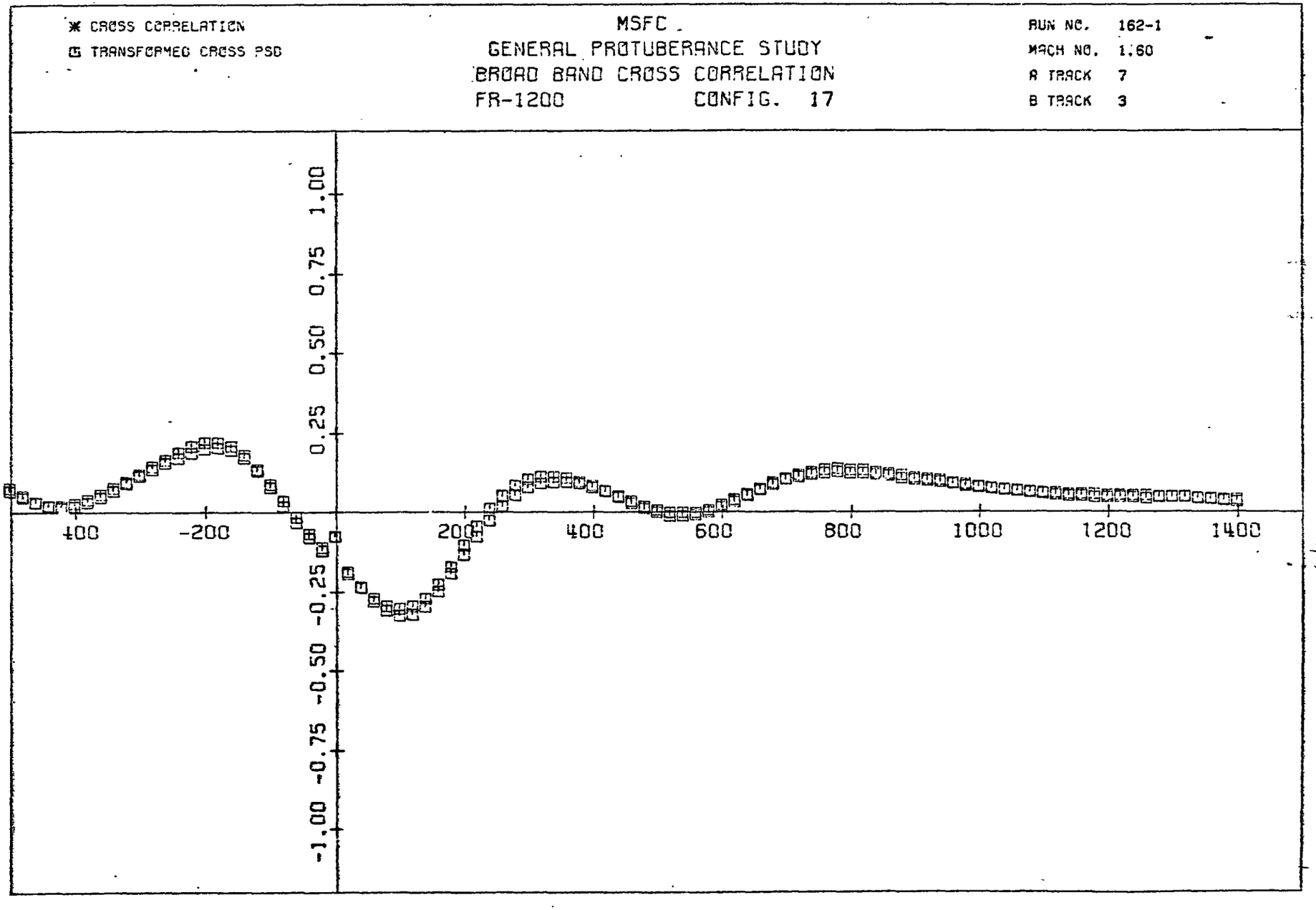

PLOT (B3)

TIME DELAY IN MICROSECONDS

BAGANOFF ASSOCIATES

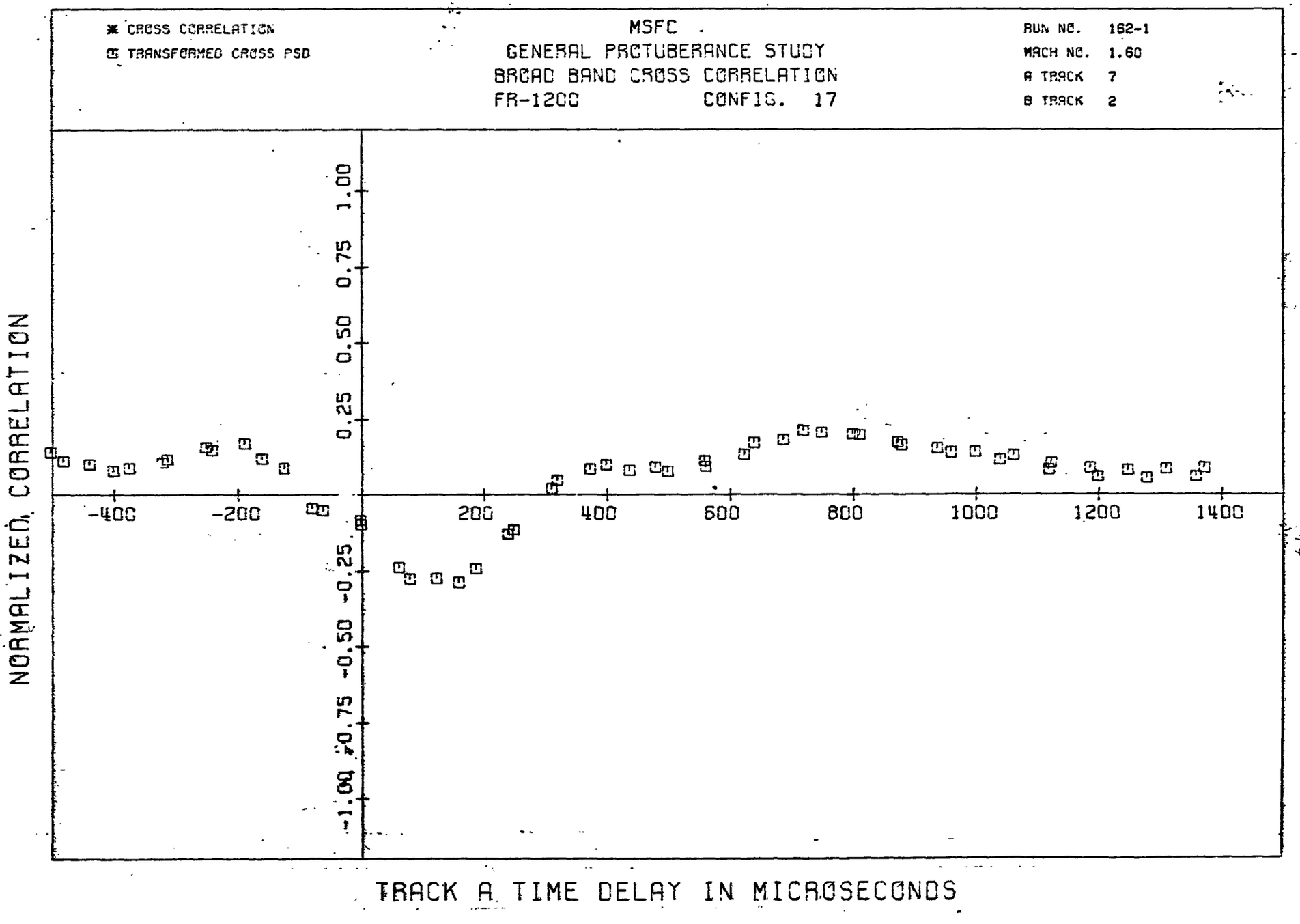

PLOT (88) 44

BAGANOFF ASSOCIATES

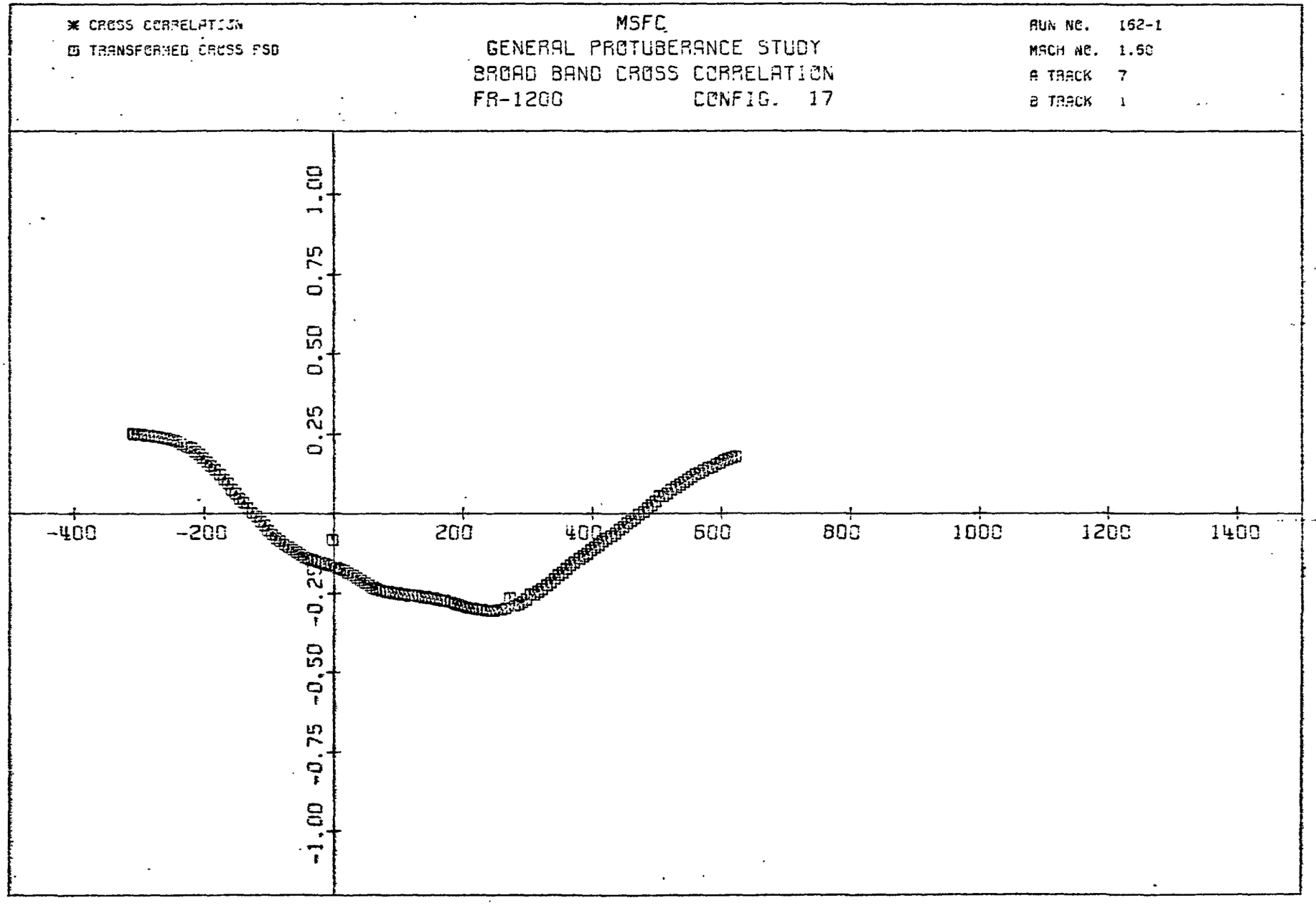

BAGANOFF ASSOCIATES

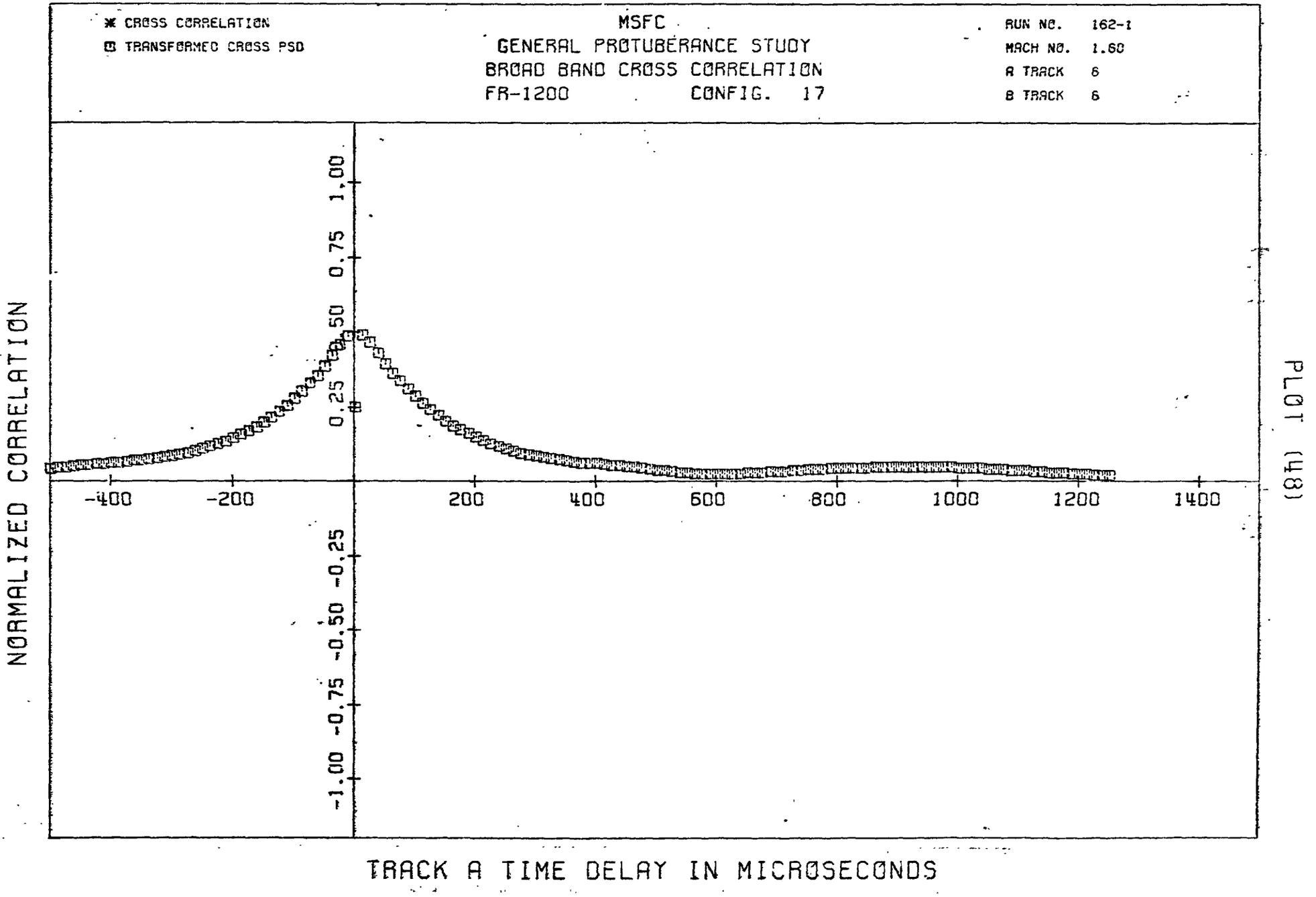

BAGANOFF ASSOCIATES

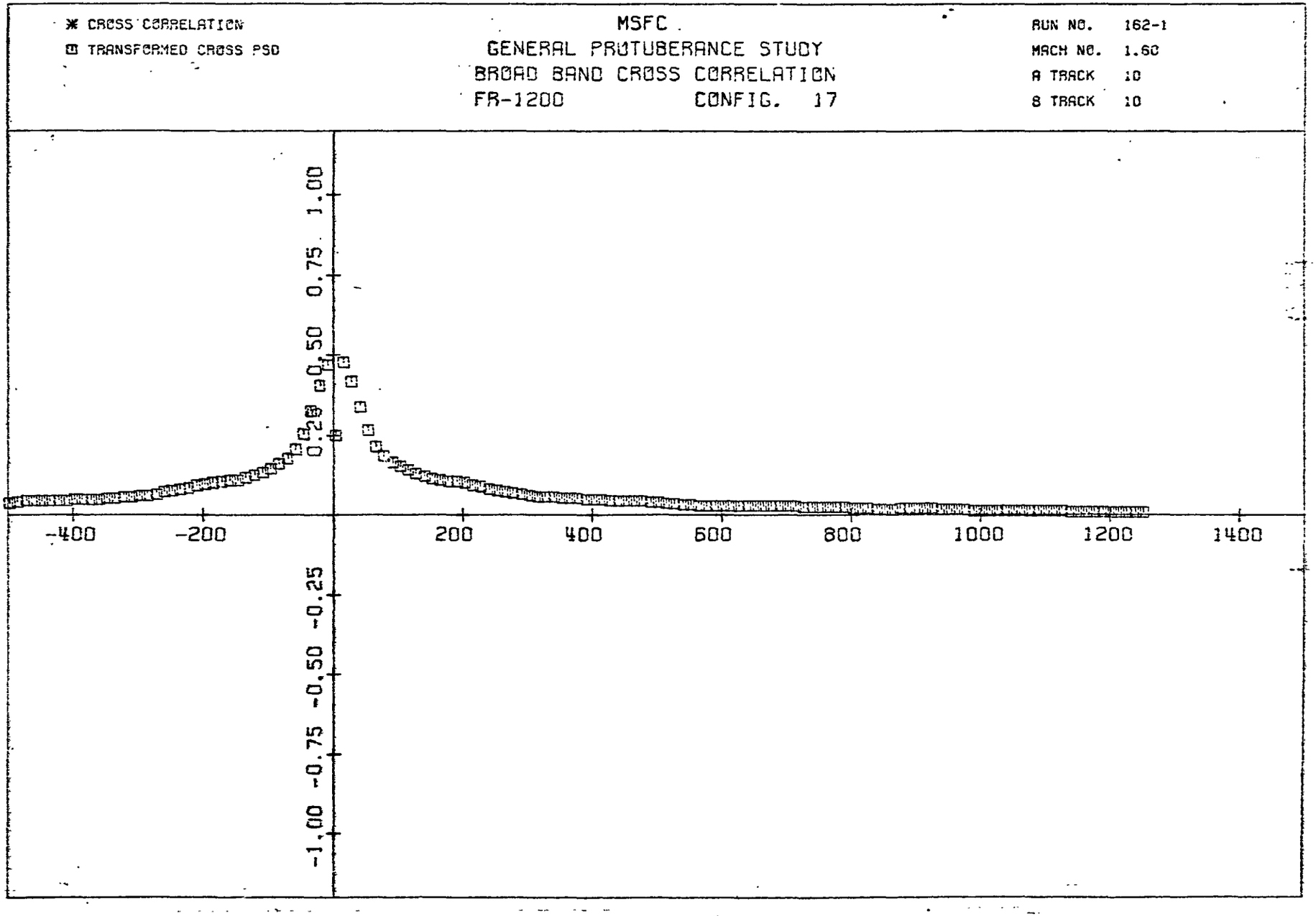

BAGHNOFF ASSOCIATES

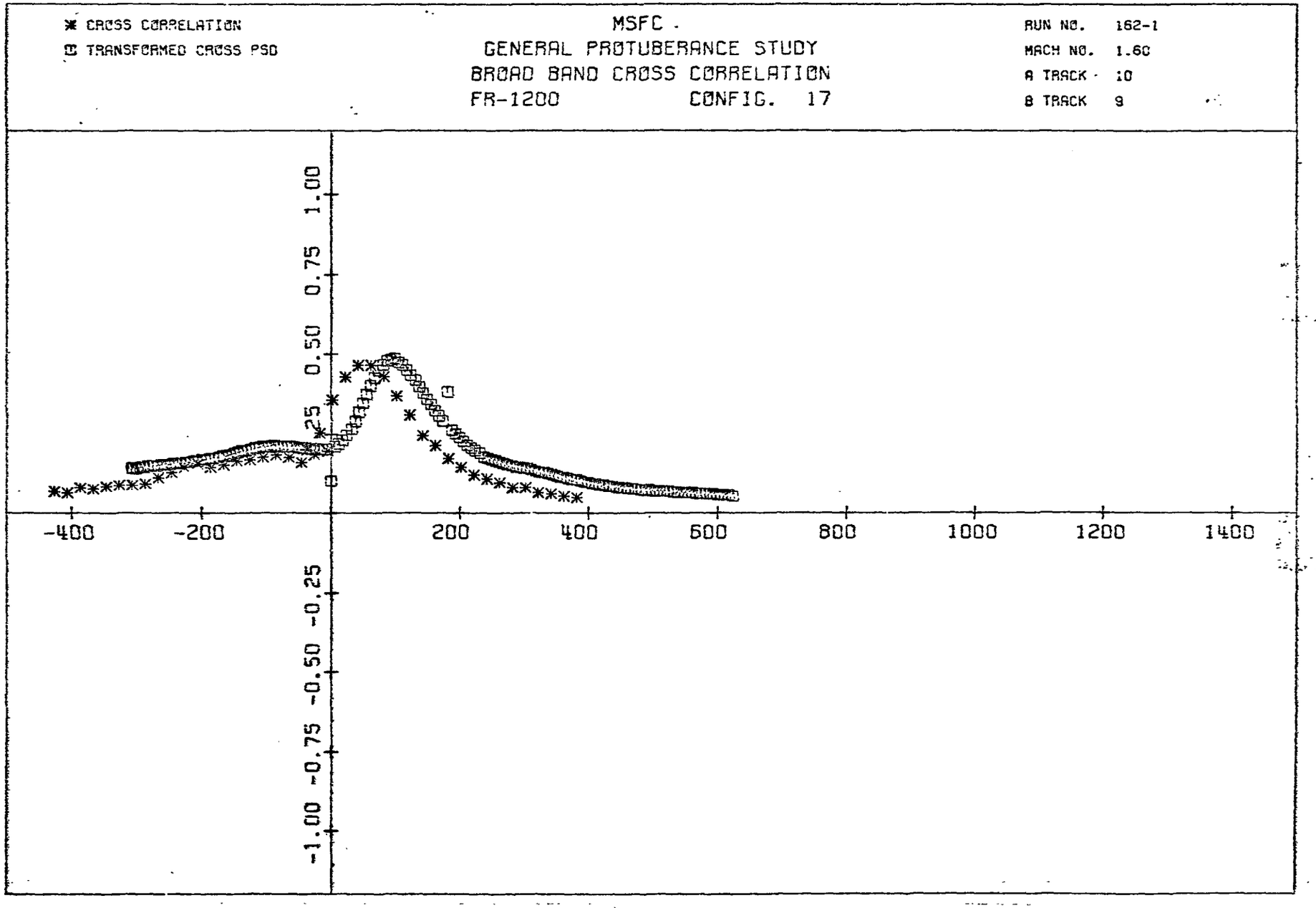

BAGANOFF ASSOCIATES

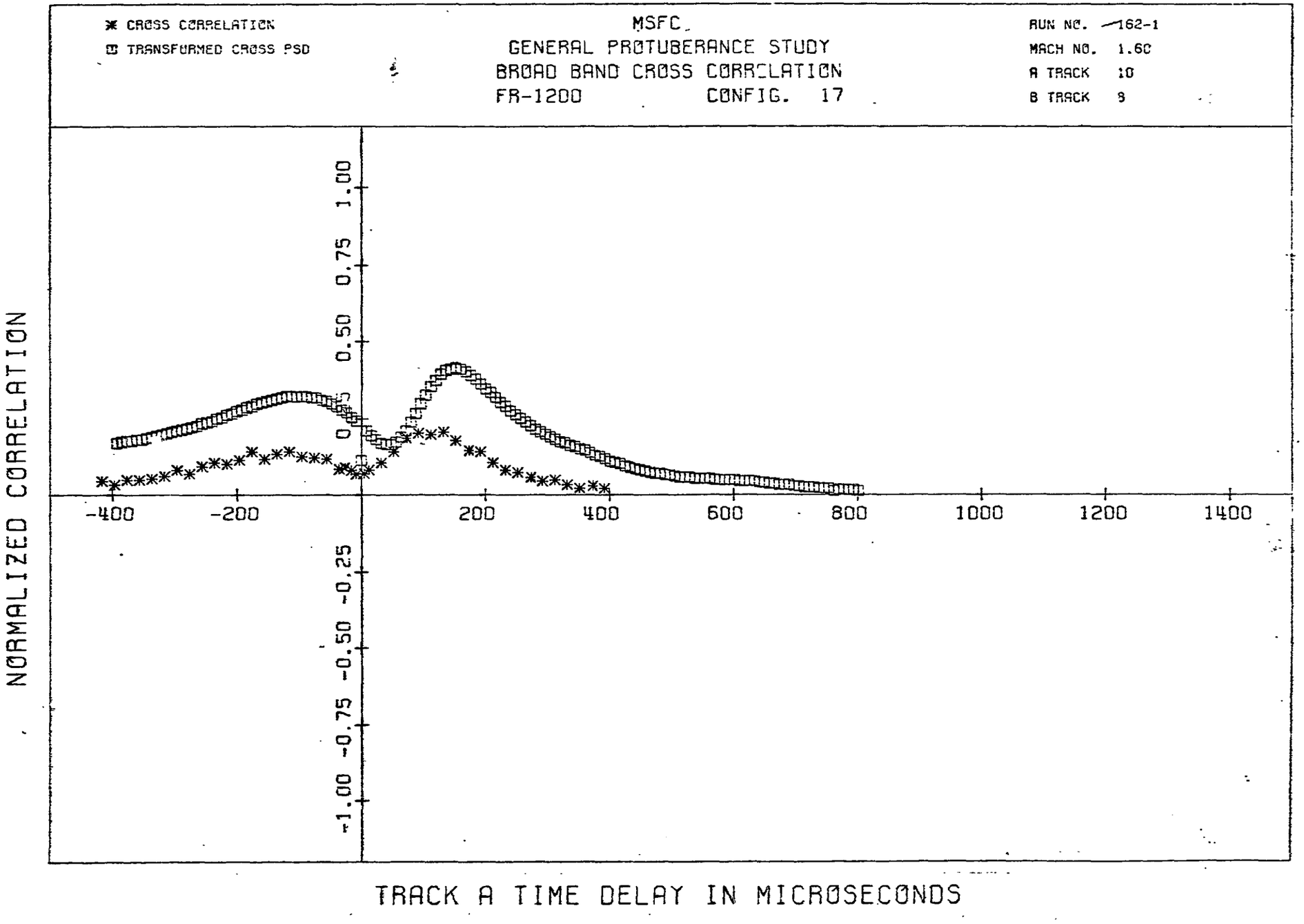

BAGANOFF ASSOCIATES

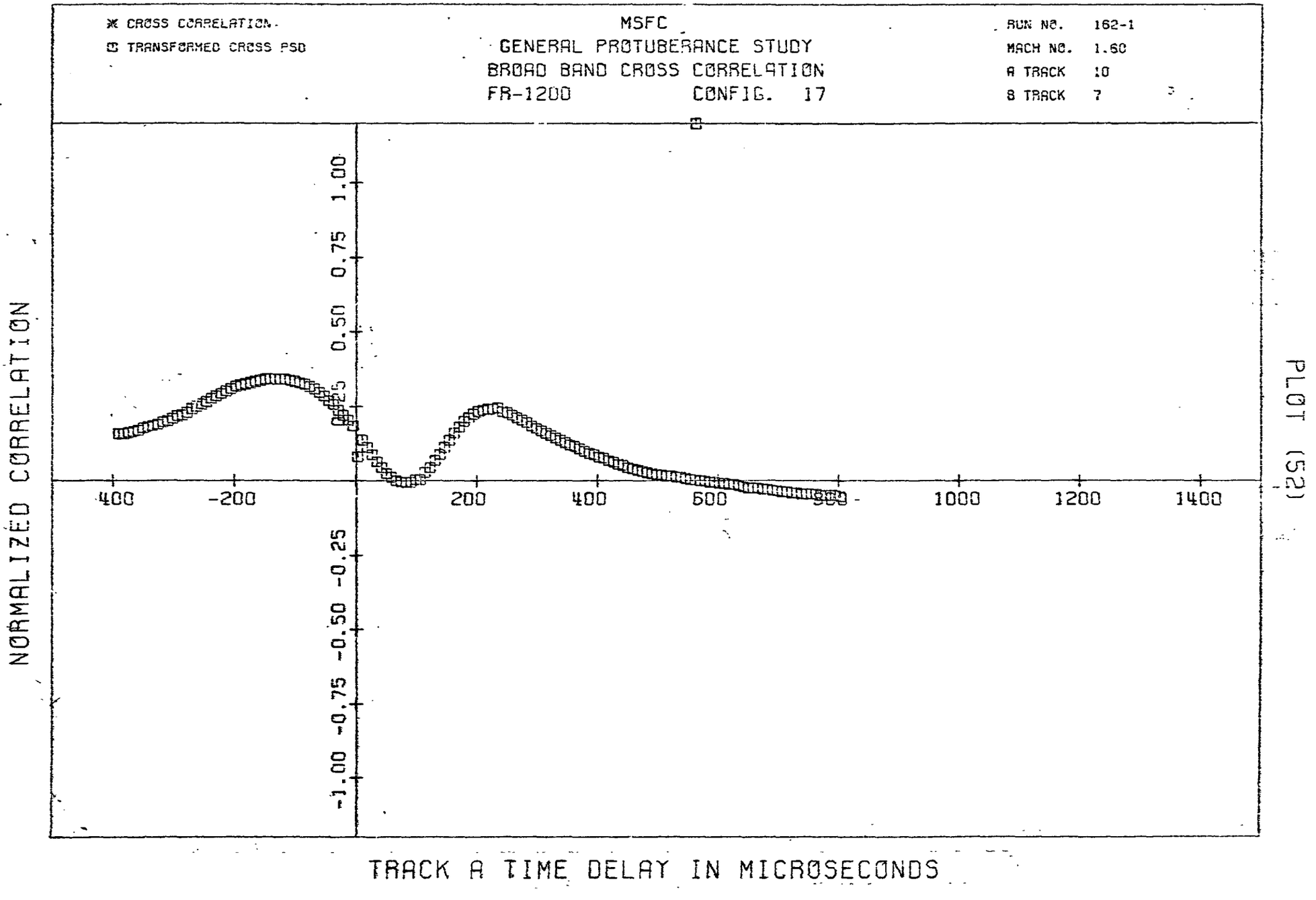

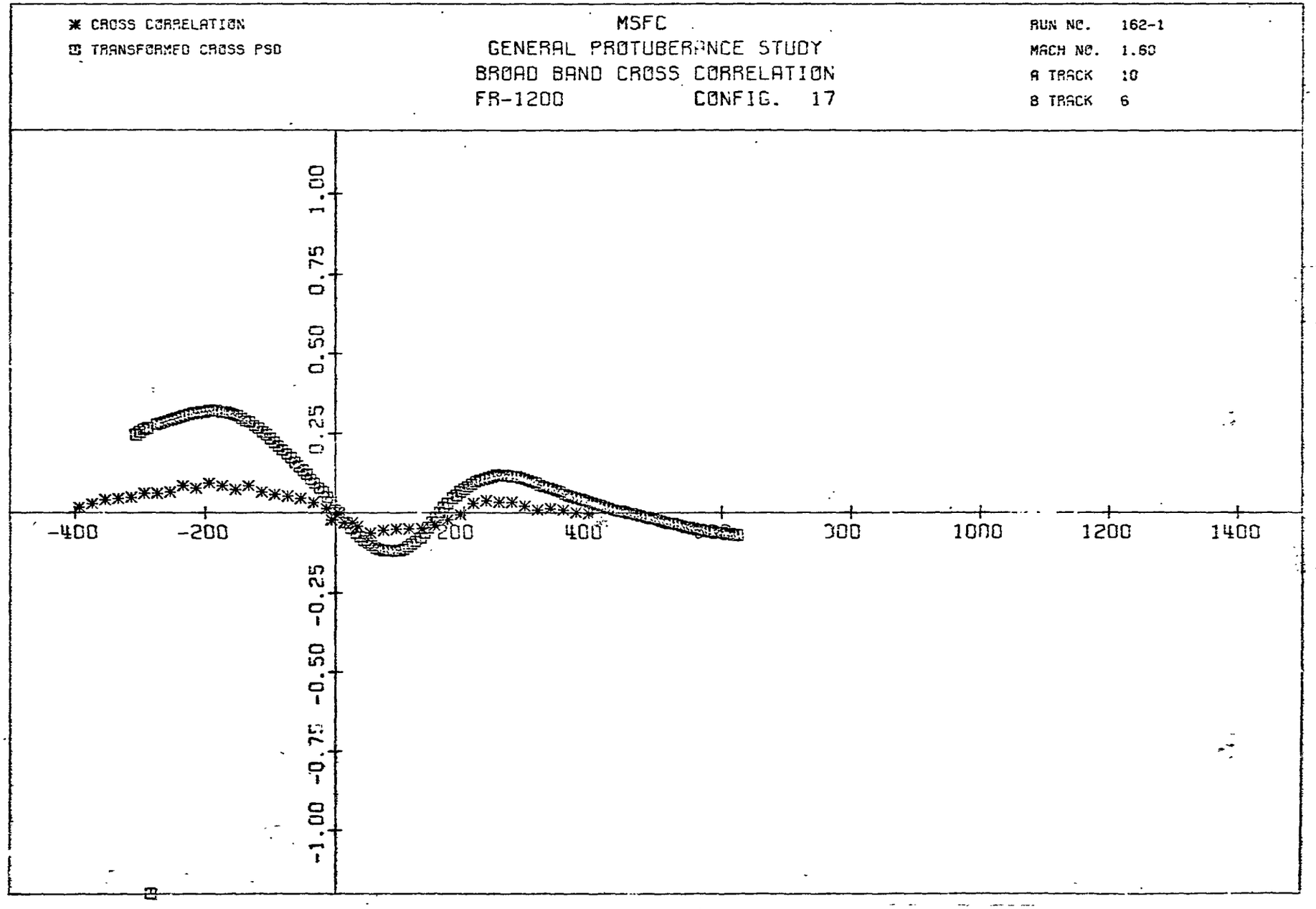
* CROSS CORRELATION
⊡ TRANSFORMED CROSS PSD
MSFC
GENERAL PROTUBERANCE STUDY
BROAD BAND CROSS CORRELATION
FR-1200 CONFIG. 17
RUN NO. 162-1
MACH NO. 1.60
A TRACK 10
B TRACK 6
NORMALIZED CORRELATION
1.00
0.75
0.50
0.25
-0.25
-0.50
-0.75
-1.00
-400
-200
200
400
1000
1200
1400
TRACK A TIME DELAY IN MICROSECONDS
PLOT (53)

BAGANOFF ASSOCIATES

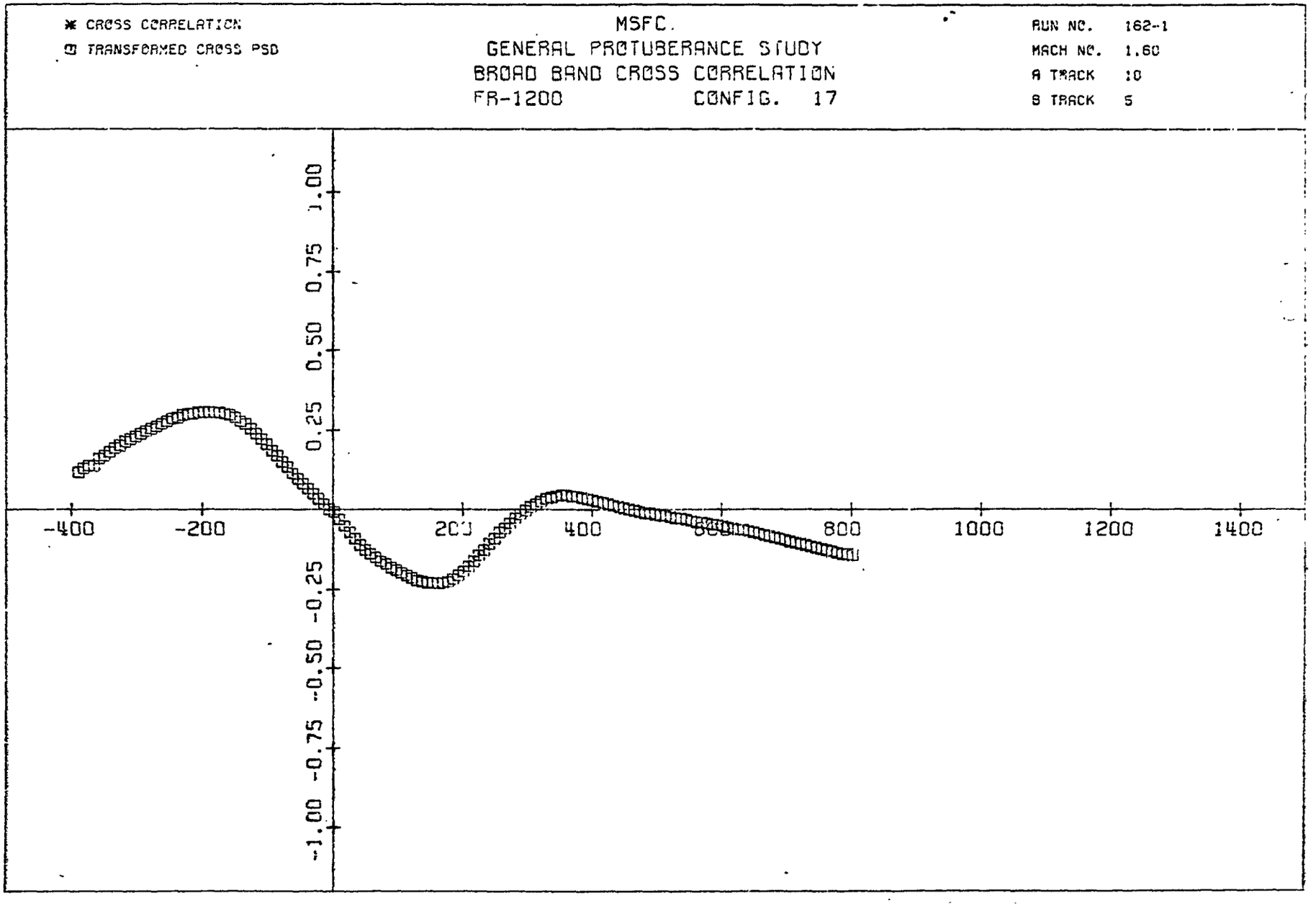

BAGANOFF ASSOCIATES

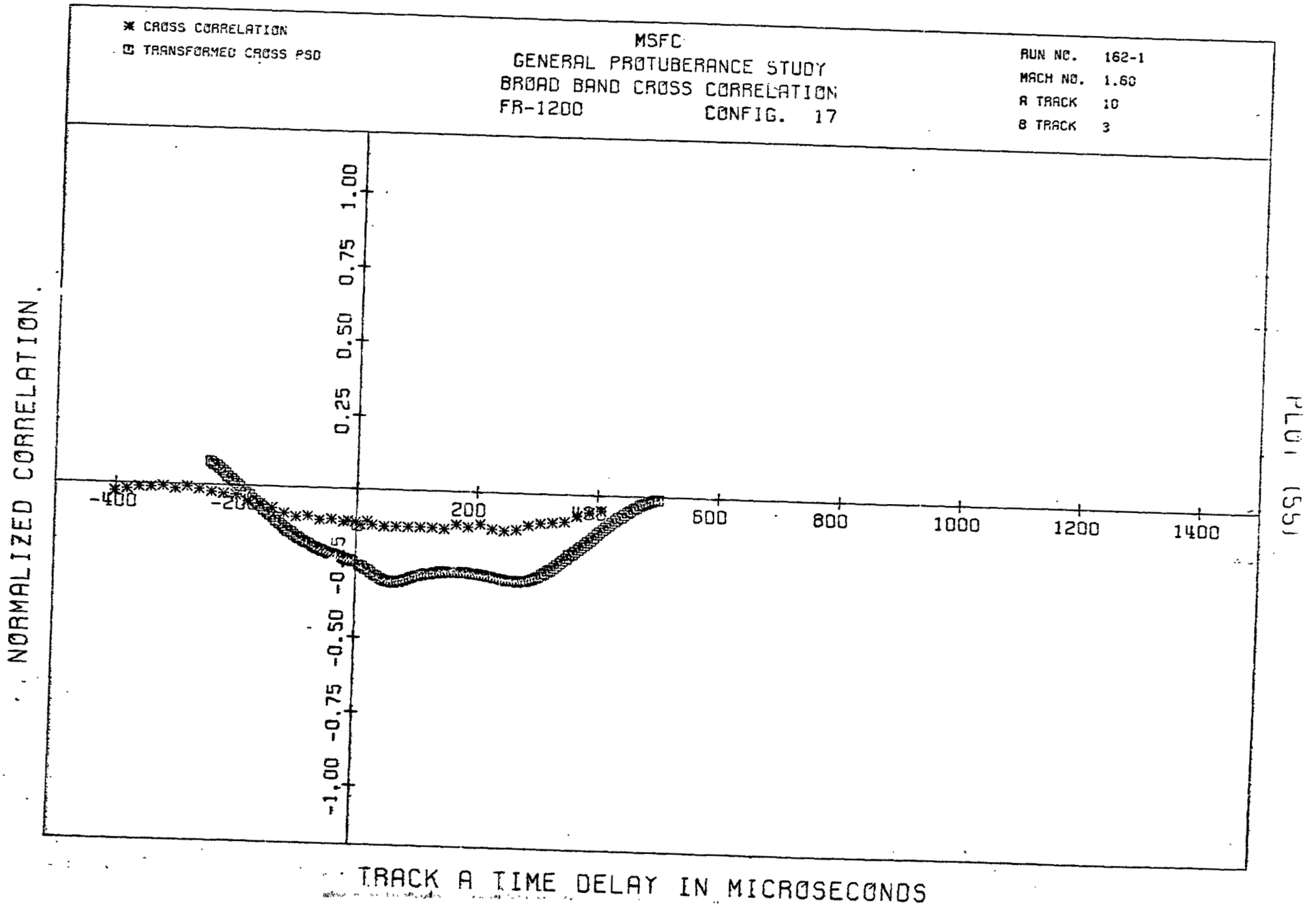

BAGANOFF ASSOCIATES

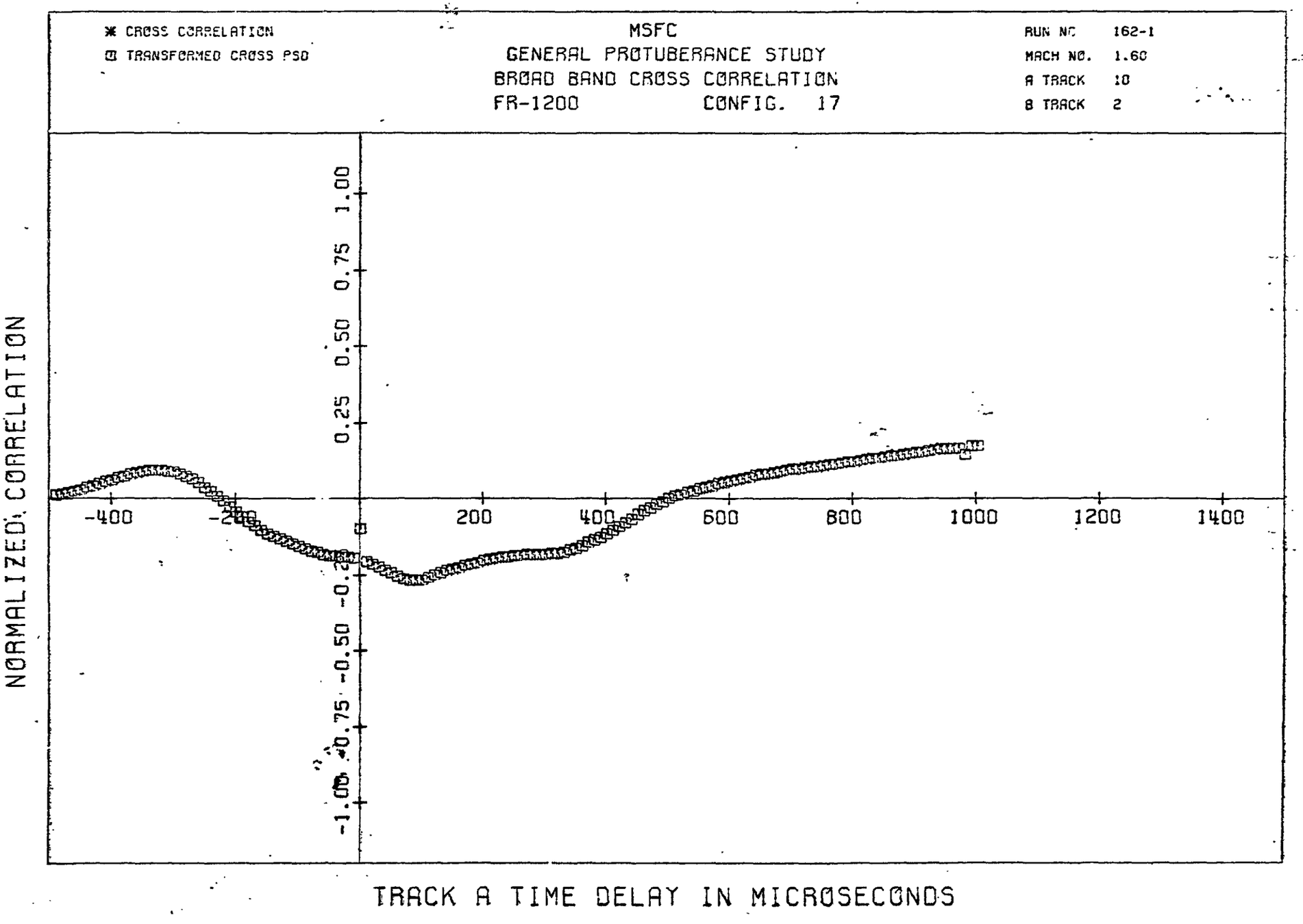

BAGANOFF ASSOCIATES

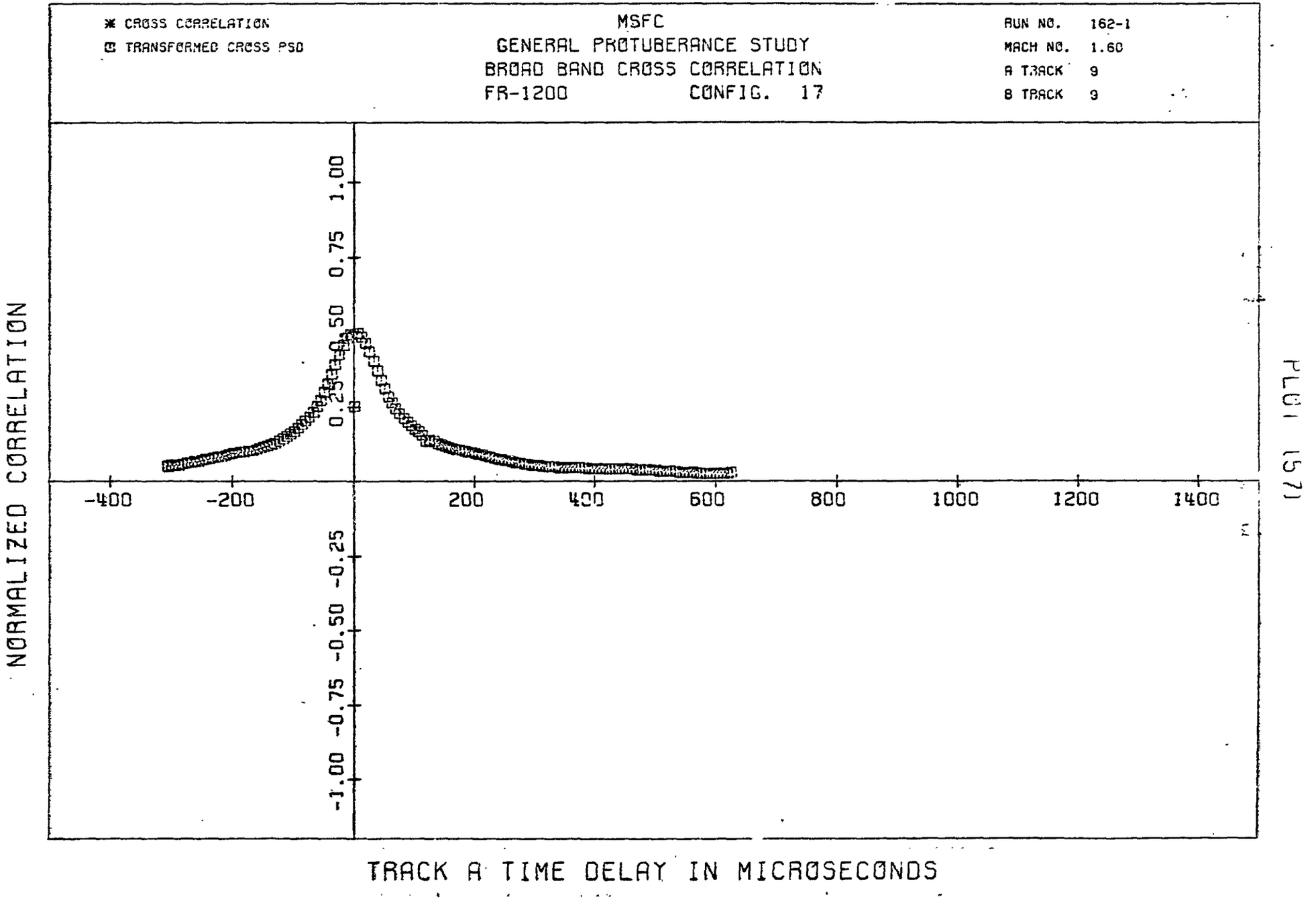

PLOT 1571

BAGANOFF ASSOCIATES

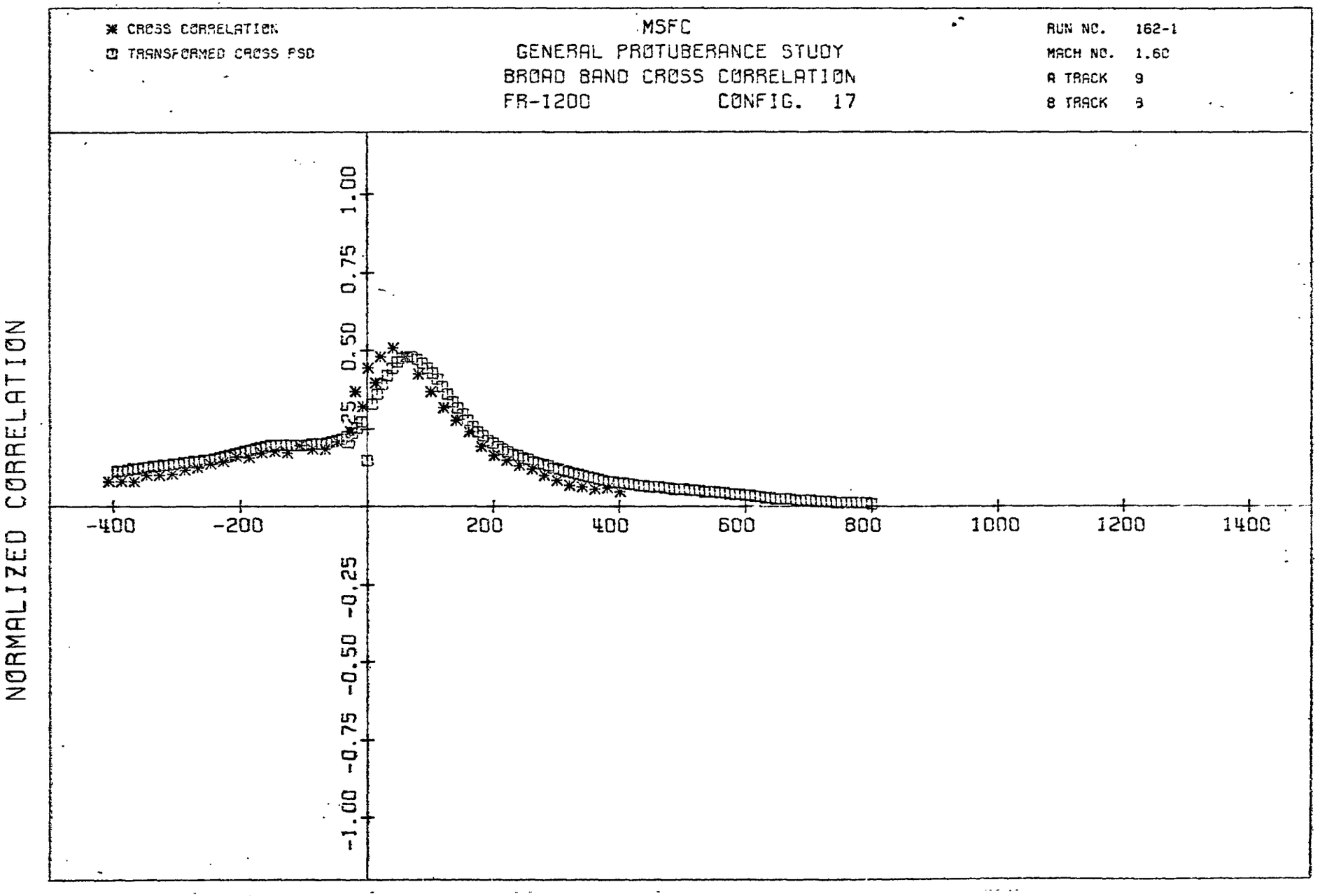

1581 1581

BAGANOFF ASSOCIATES

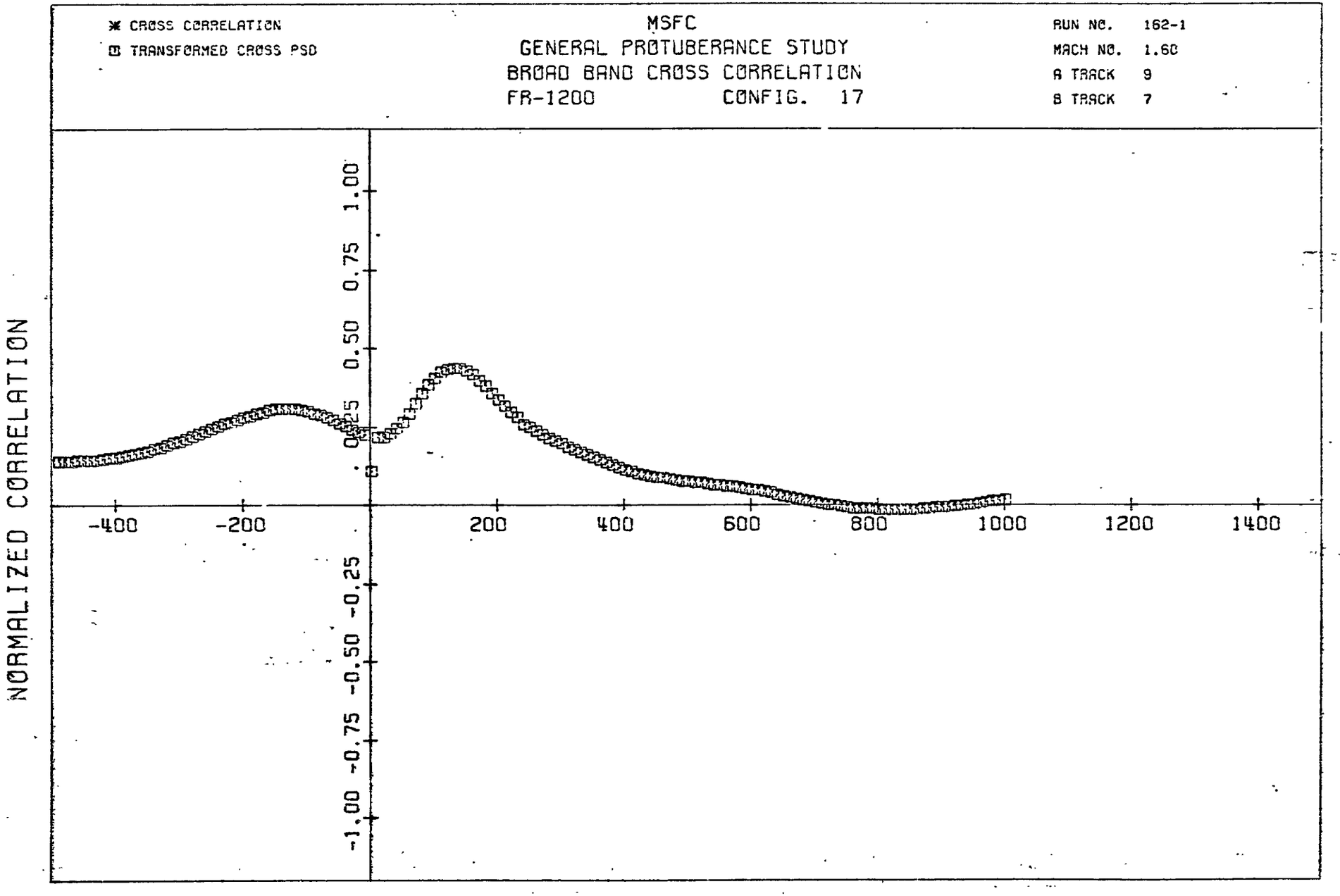

PLOT (59)

BAGANOFF ASSOCIATES

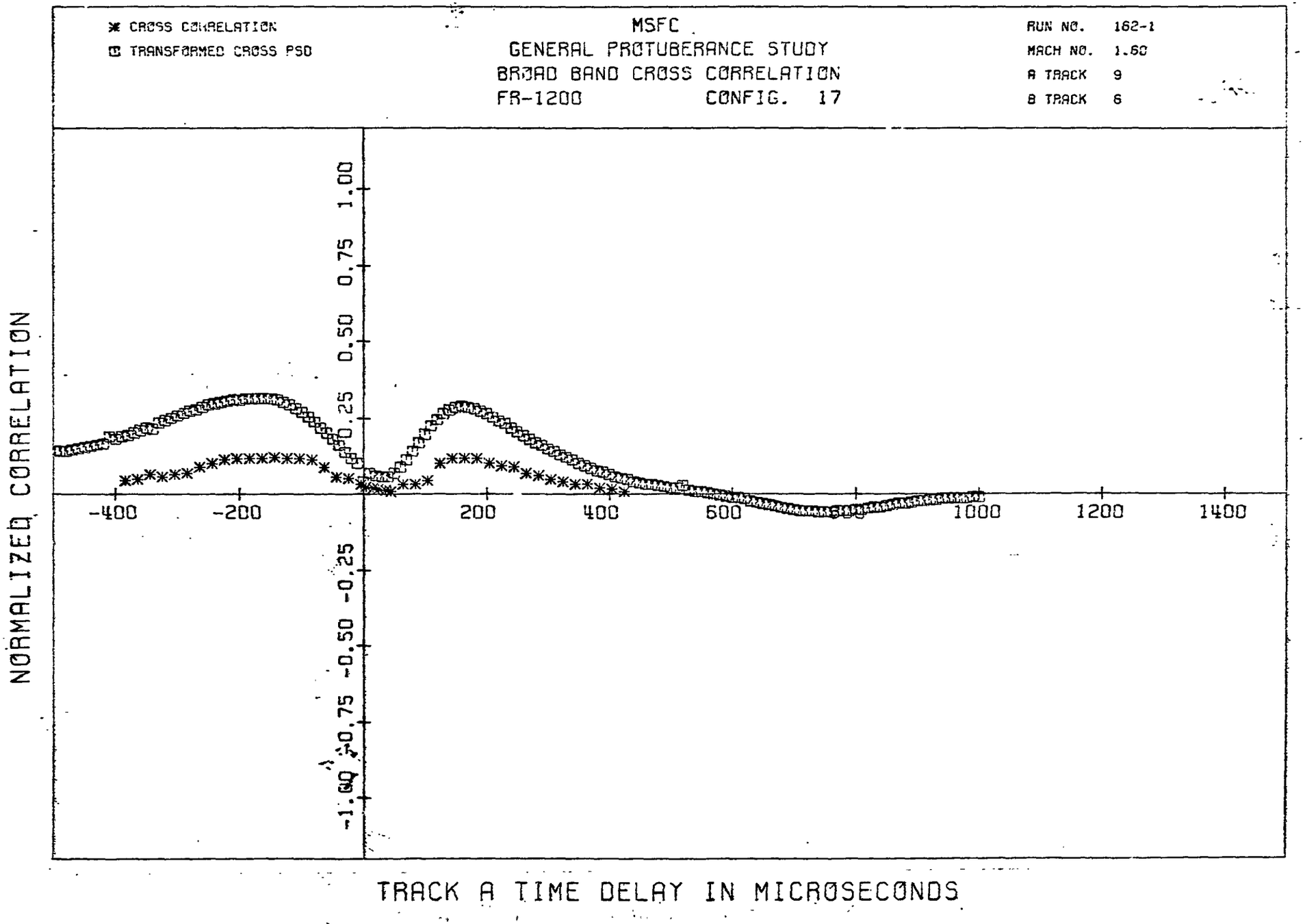

BAGANOFF ASSOCIATES

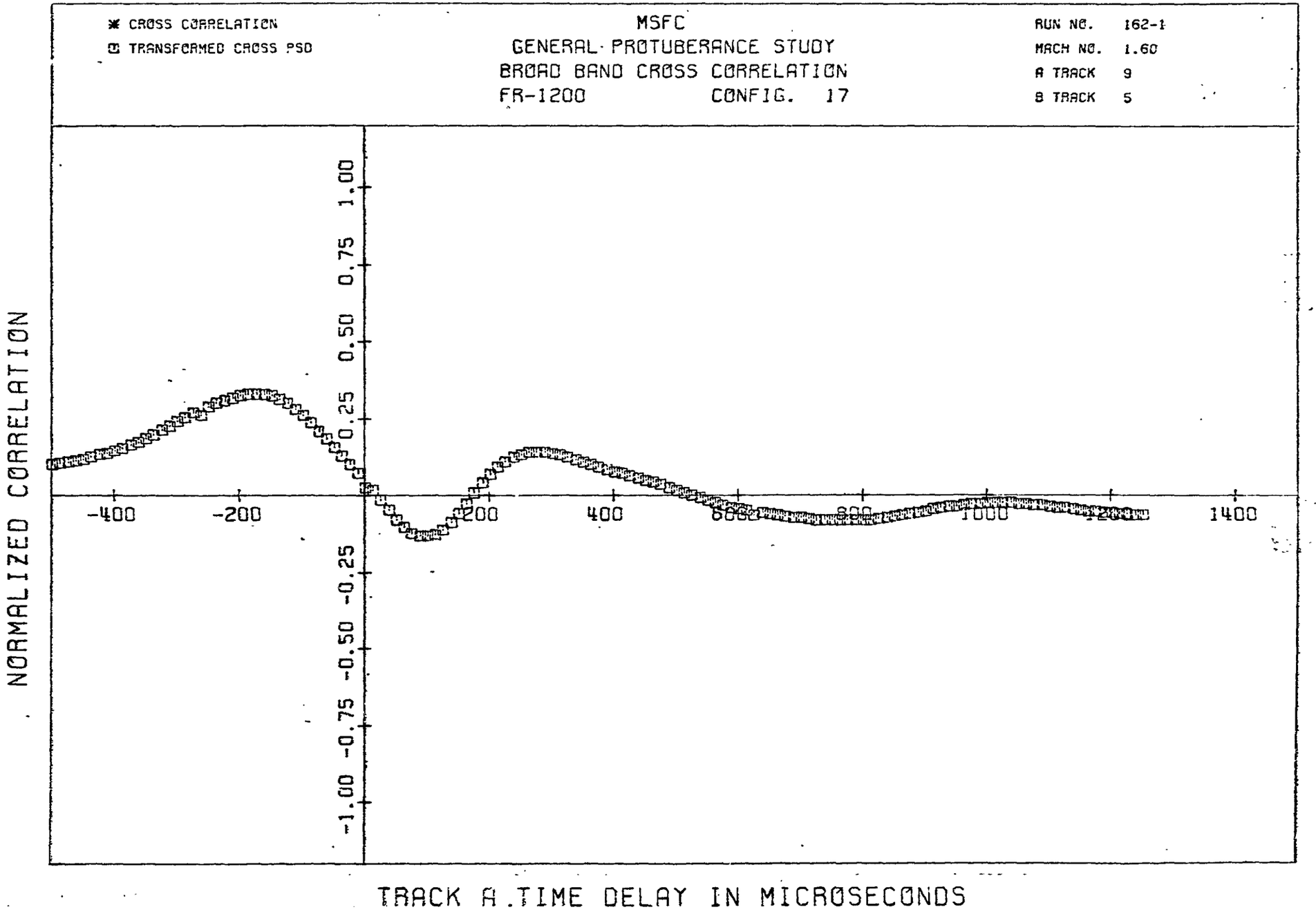

BAGANOFF ASSOCIATES

PLOT (62)

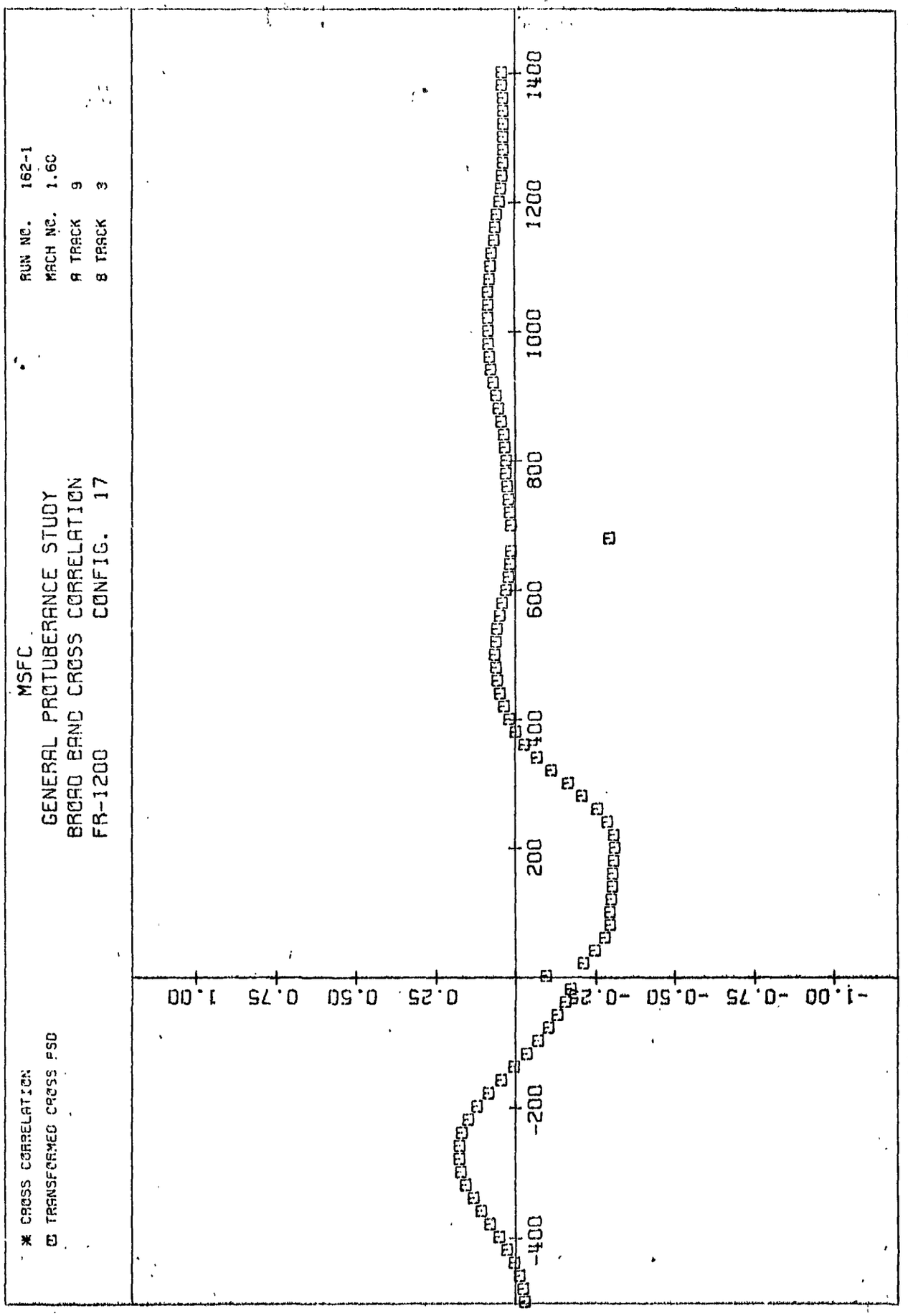

BAGANOFF ASSOCIATES

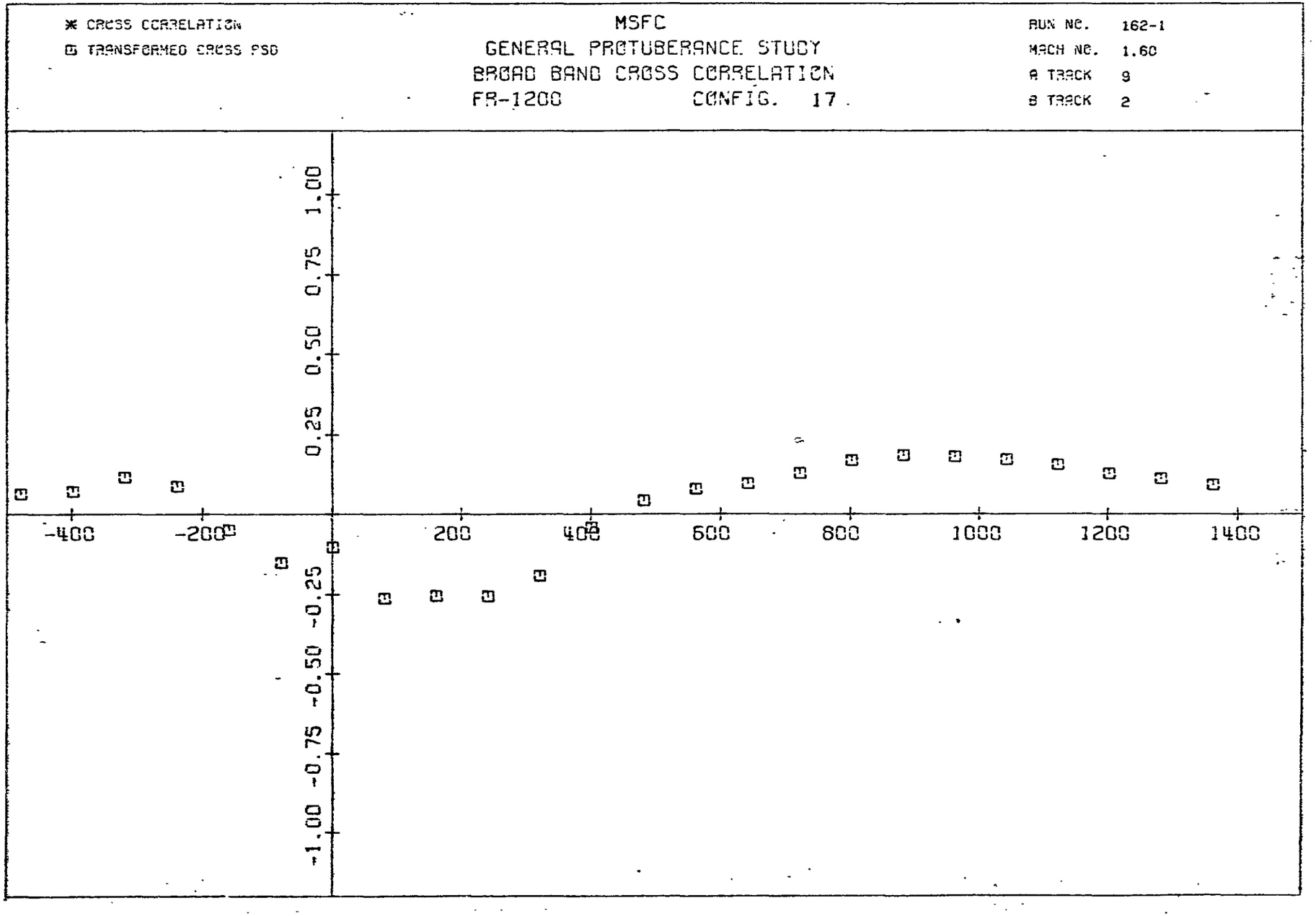

BAGANOFF ASSOCIATES

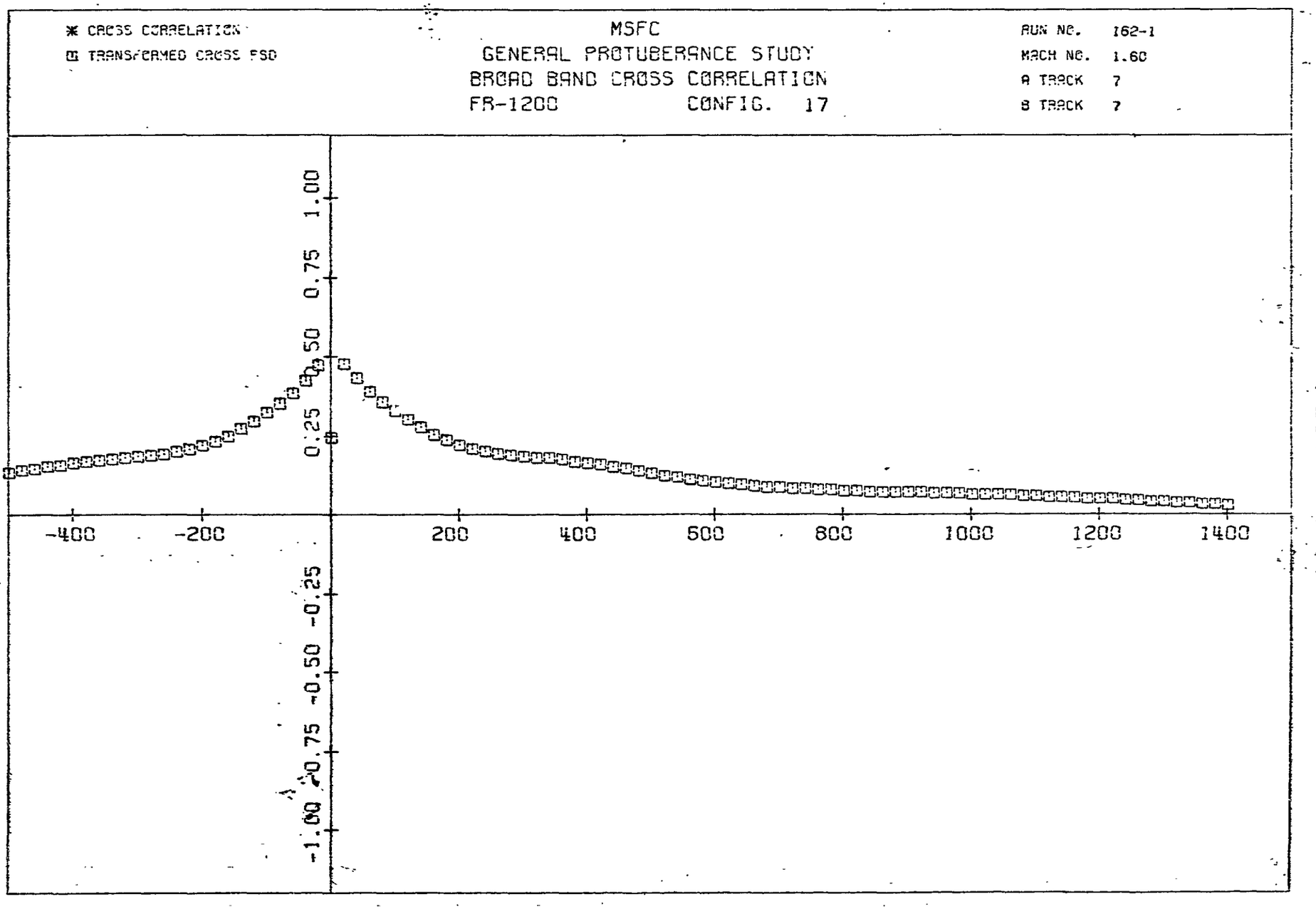

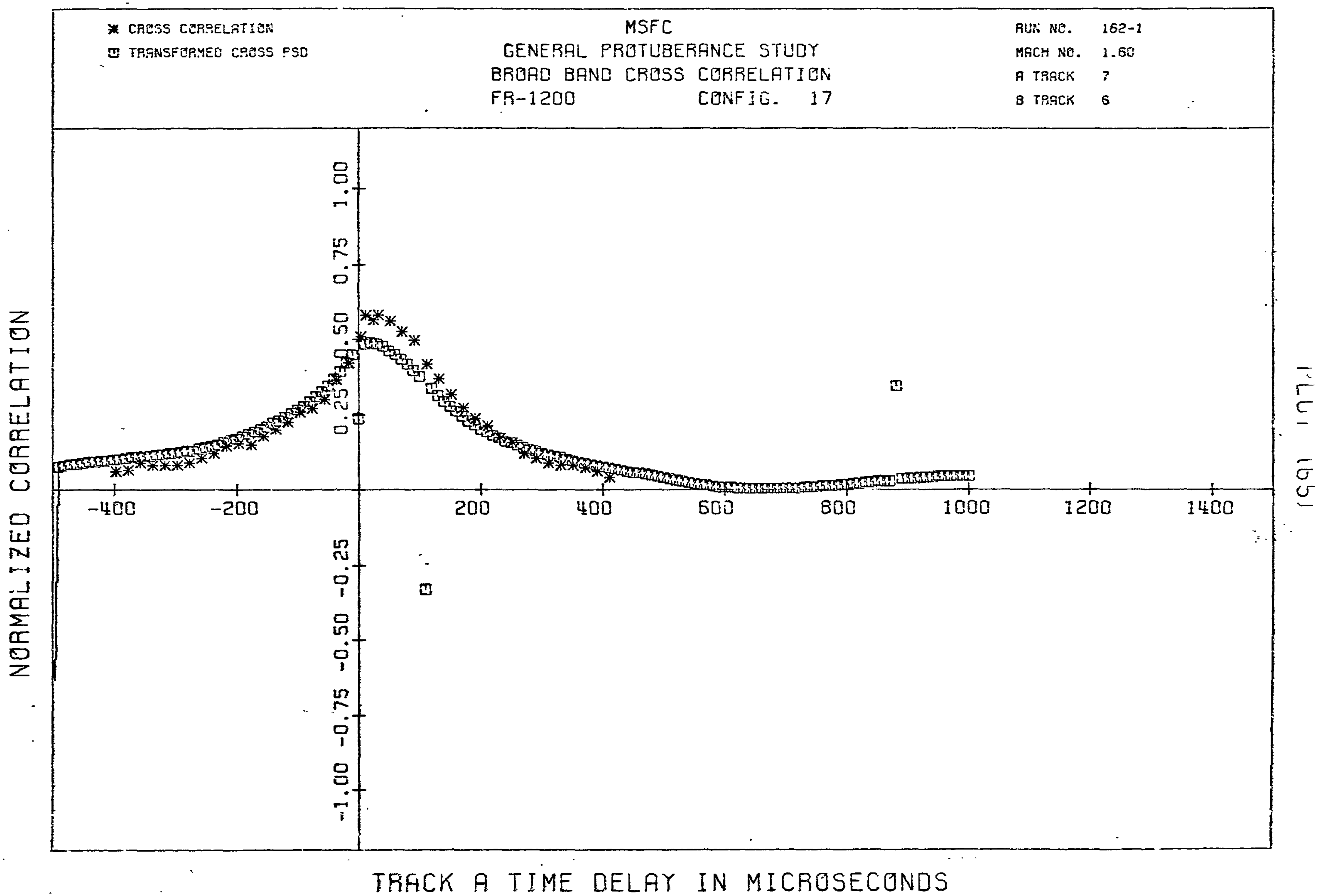

✱ CROSS CORRELATION
⊡ TRANSFORMED CROSS PSD
MSFC
GENERAL PROTUBERANCE STUDY
BROAD BAND CROSS CORRELATION
FR-1200 CONFIG. 17
RUN NO. 162-1
MACH NO. 1.60
A TRACK 7
B TRACK 6
1.00
0.75
0.50
0.25
0
-0.25
-0.50
-0.75
-1.00
-400
-200
200
400
600
800
1000
1200
1400
NORMALIZED CORRELATION
TRACK A TIME DELAY IN MICROSECONDS
PLOT (65)

BAGANOFF ASSOCIATES

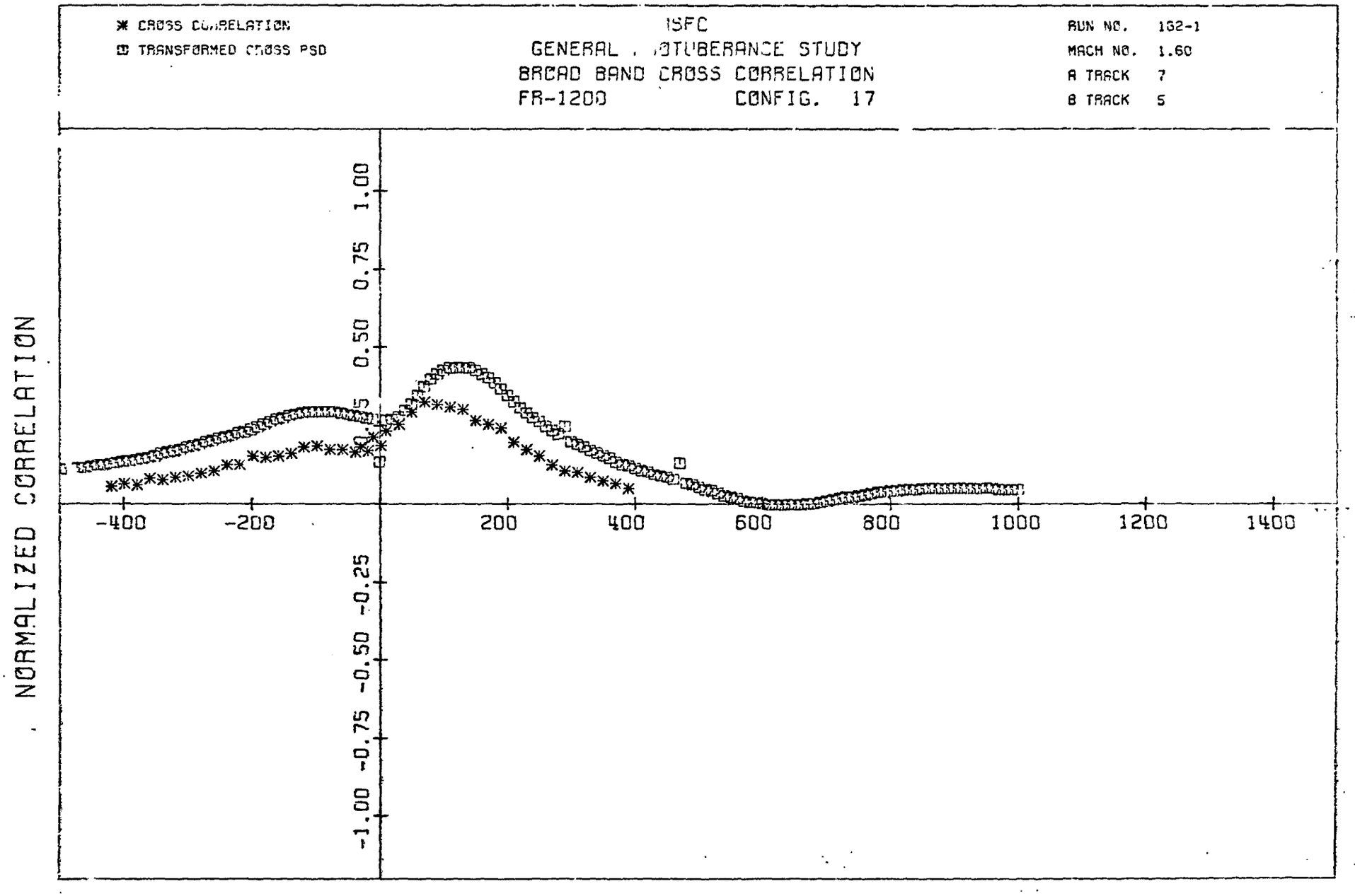

BAGANOFF ASSOCIATES

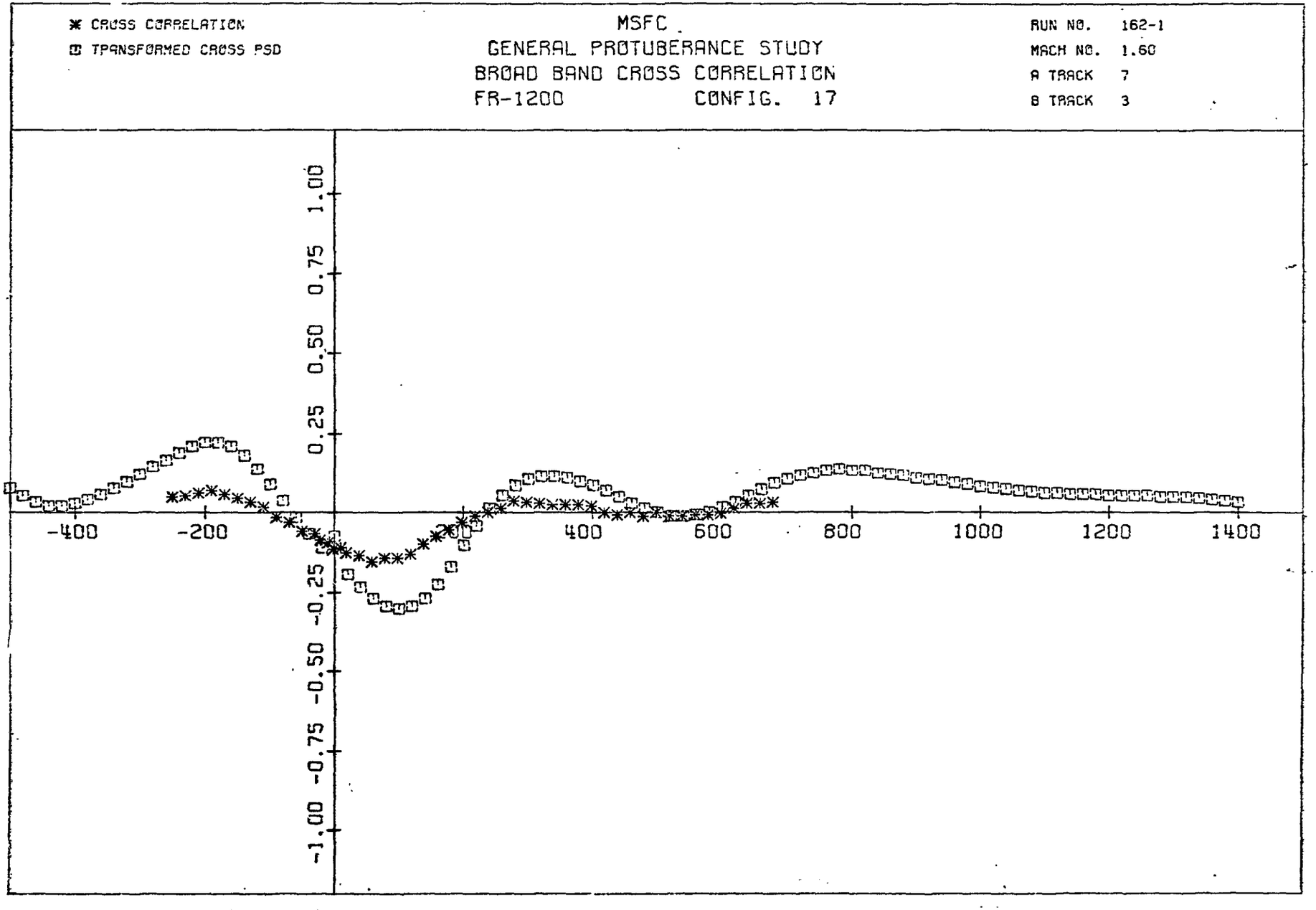

PLOT (67)

BAGANOFF ASSOCIATES

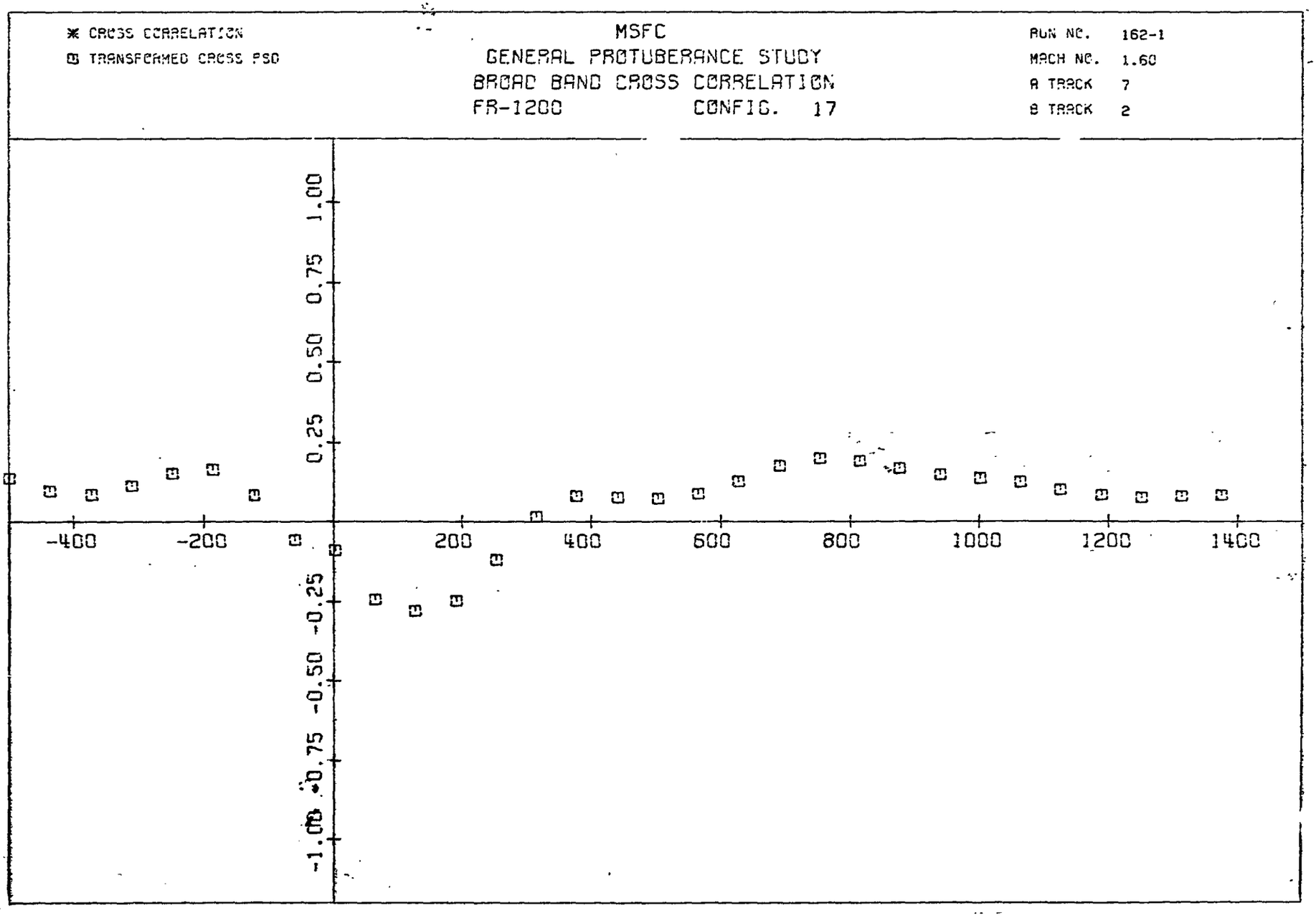

PLOT (68)

BAGANOFF ASSOCIATES

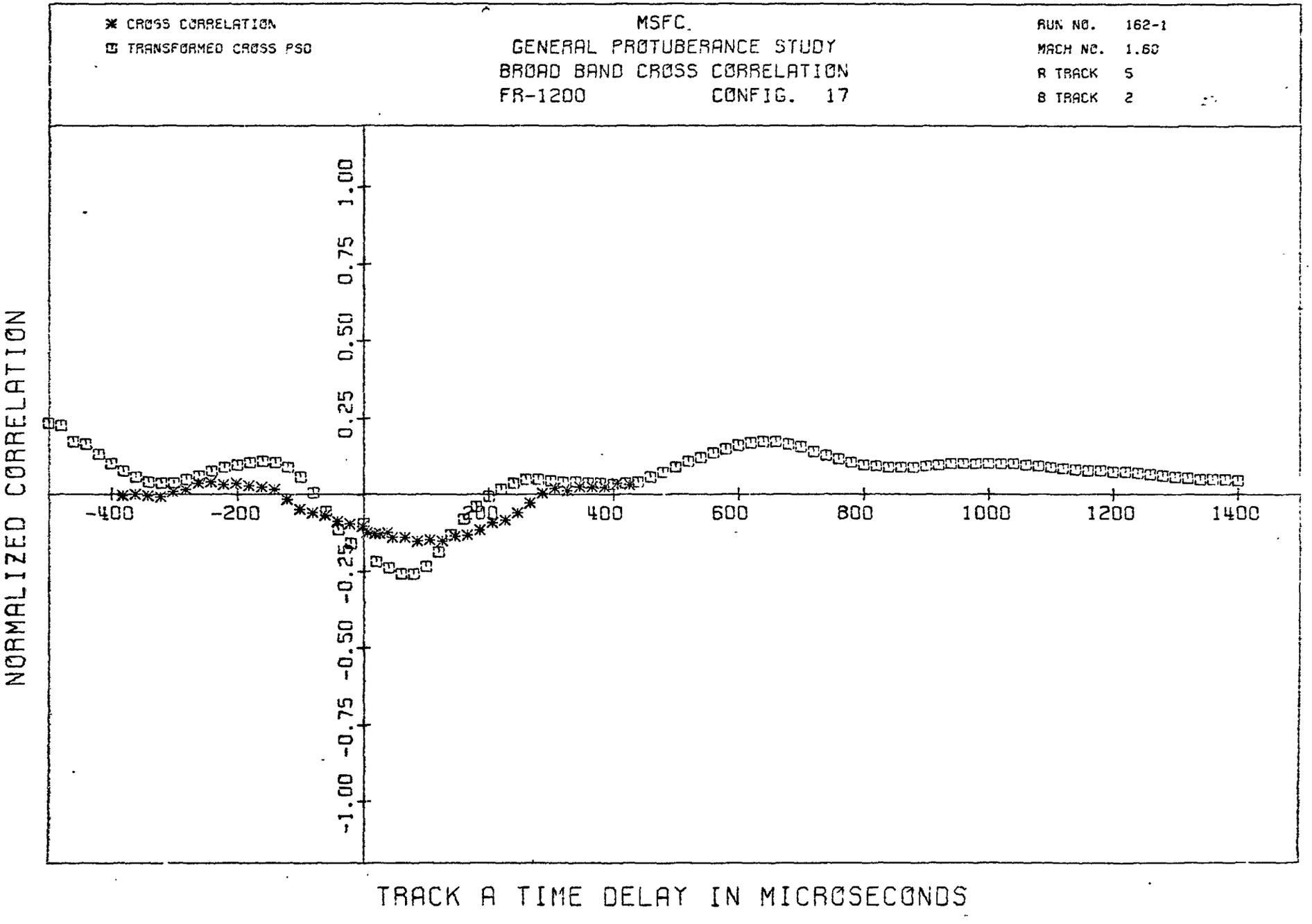

(691 197)

BAGANOFF ASSOCIATES

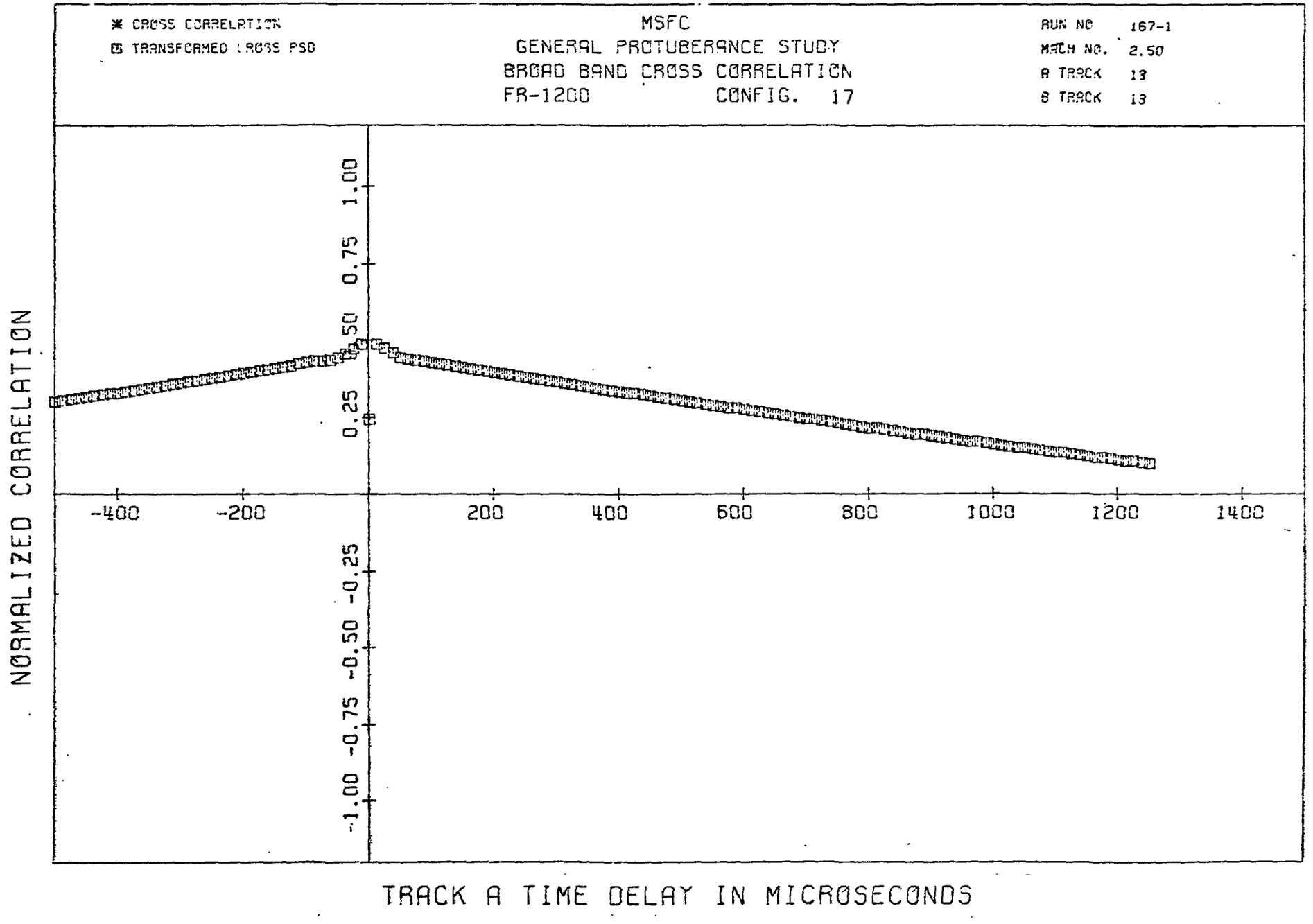

BAGANOFF ASSOCIATES

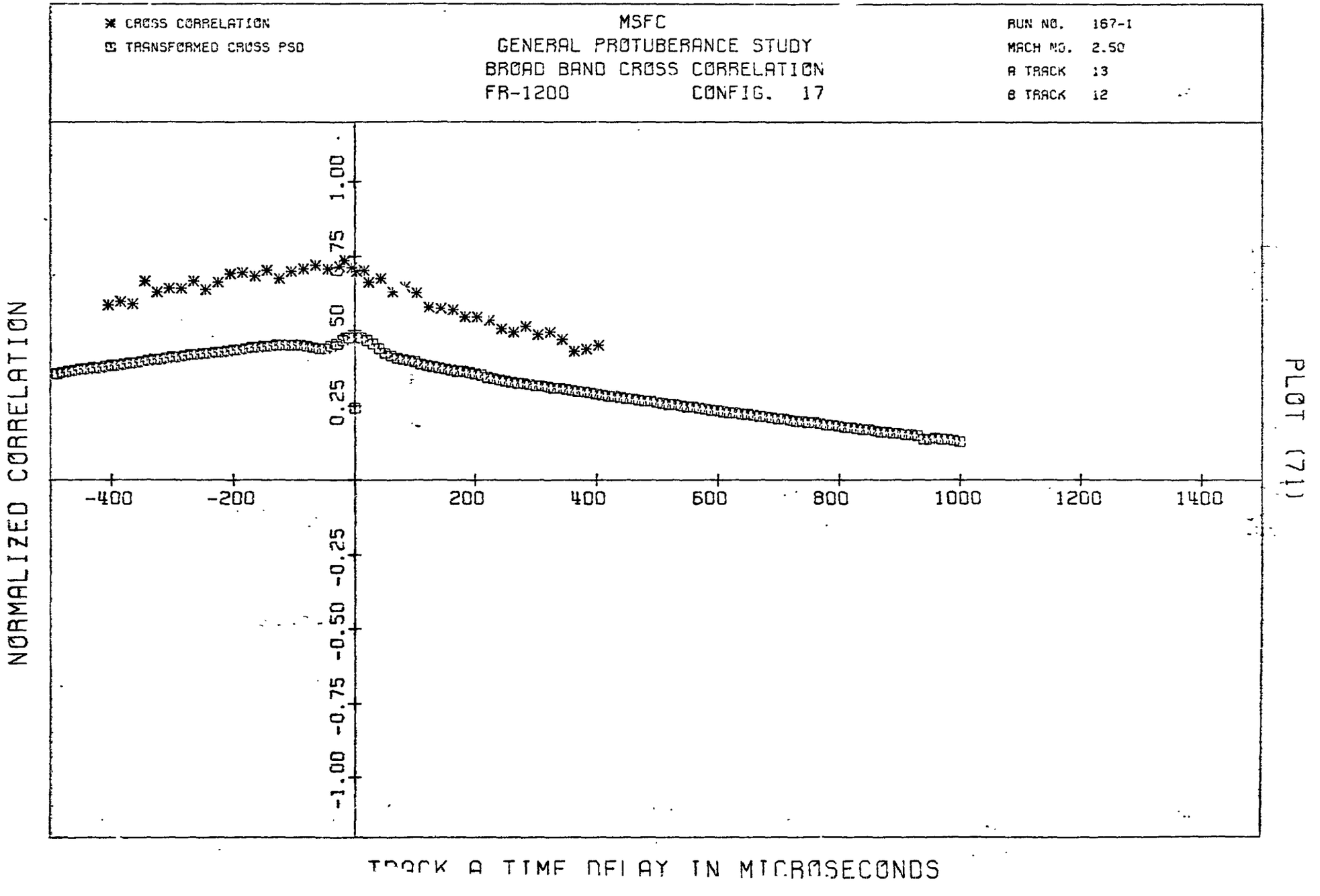

BAGANOFF ASSOCIATES

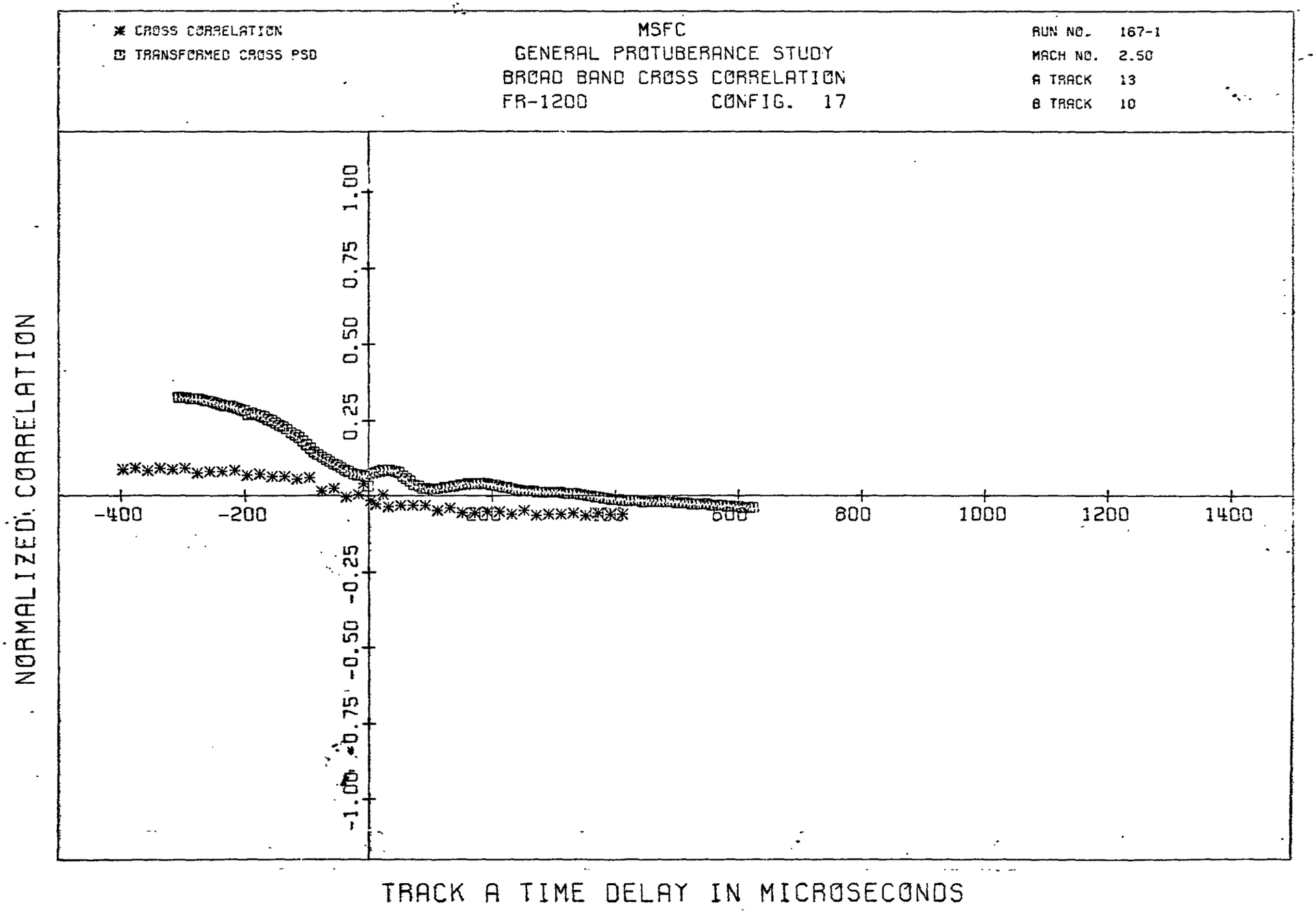

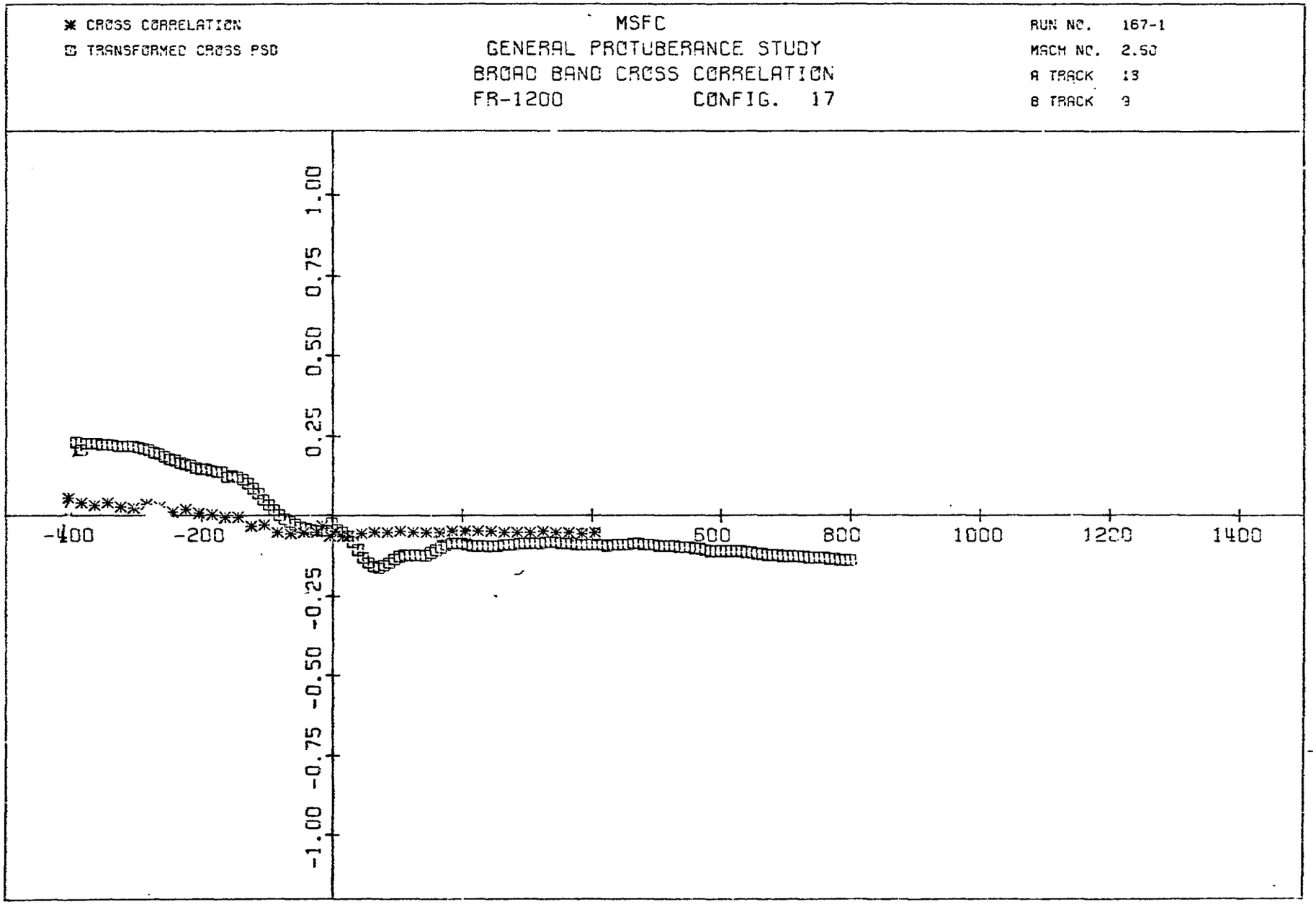
* CROSS CORRELATION
⊡ TRANSFORMED CROSS PSD
MSFC
GENERAL PROTUBERANCE STUDY
BROAD BAND CROSS CORRELATION
FR-1200 CONFIG. 17
RUN NO. 167-1
MACH NO. 2.50
A TRACK 13
B TRACK 9
NORMALIZED CORRELATION
1.00
0.75
0.50
0.25
-0.25
-0.50
-0.75
-1.00
-400
-200
500
800
1000
1200
1400
TRACK A TIME DELAY IN MICROSECONDS
PLOT (73)

PLOT (74)

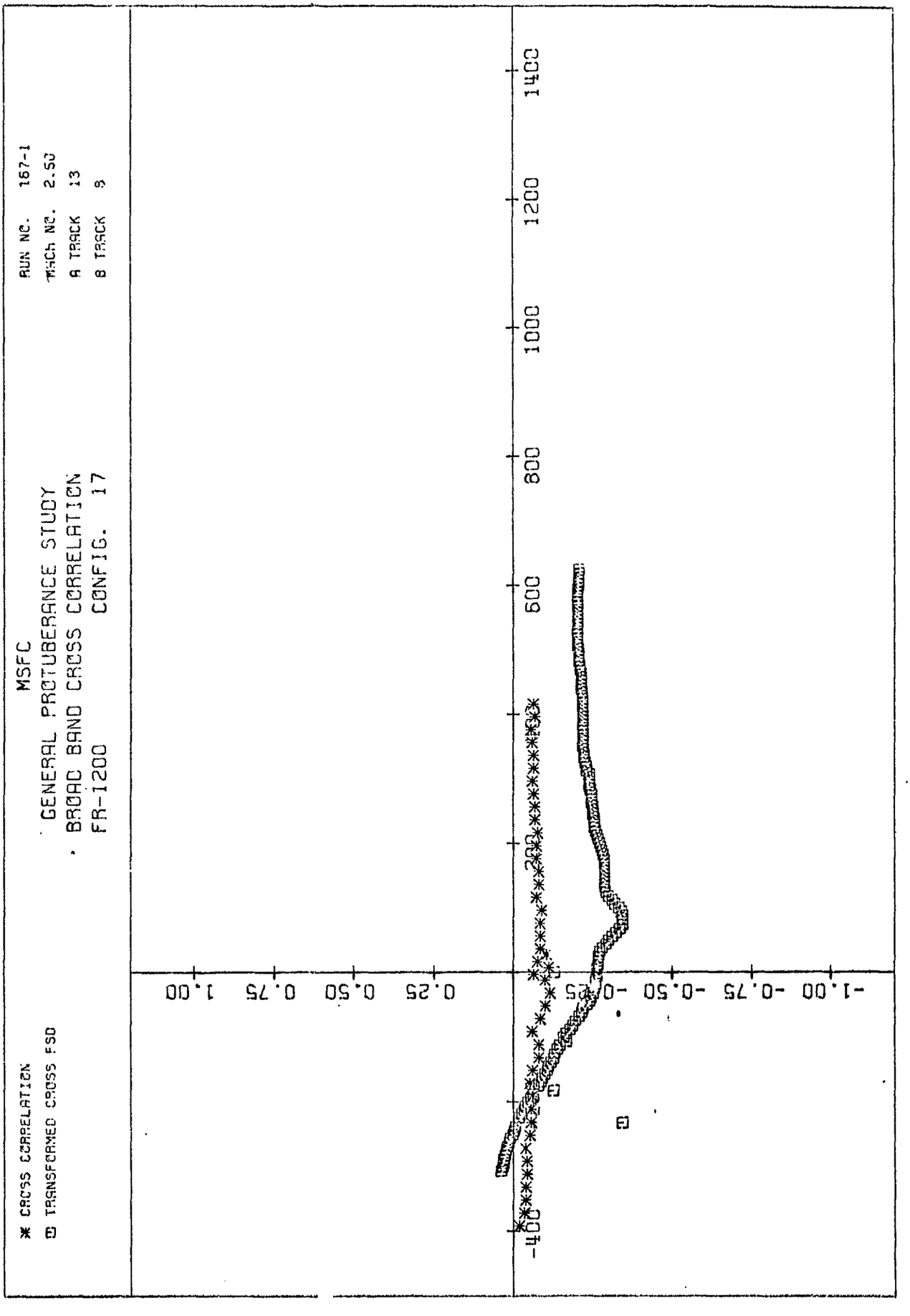
MSFC
GENERAL PROTUBERANCE STUDY
BROAD BAND CROSS CORRELATION
FR-1200 CONFIG. 17
RUN NO. 167-1
MACH NO. 2.50
A TRACK 13
B TRACK 8
* CROSS CORRELATION
B TRANSFORMED CROSS PSD
1.00
0.75
0.50
0.25
-1.00
-0.75
-0.50
-0.25
1400
1200
1000
800
600
200
-400
NORMALIZED CORRELATION
TRACK A TIME DELAY IN MICROSECONDS

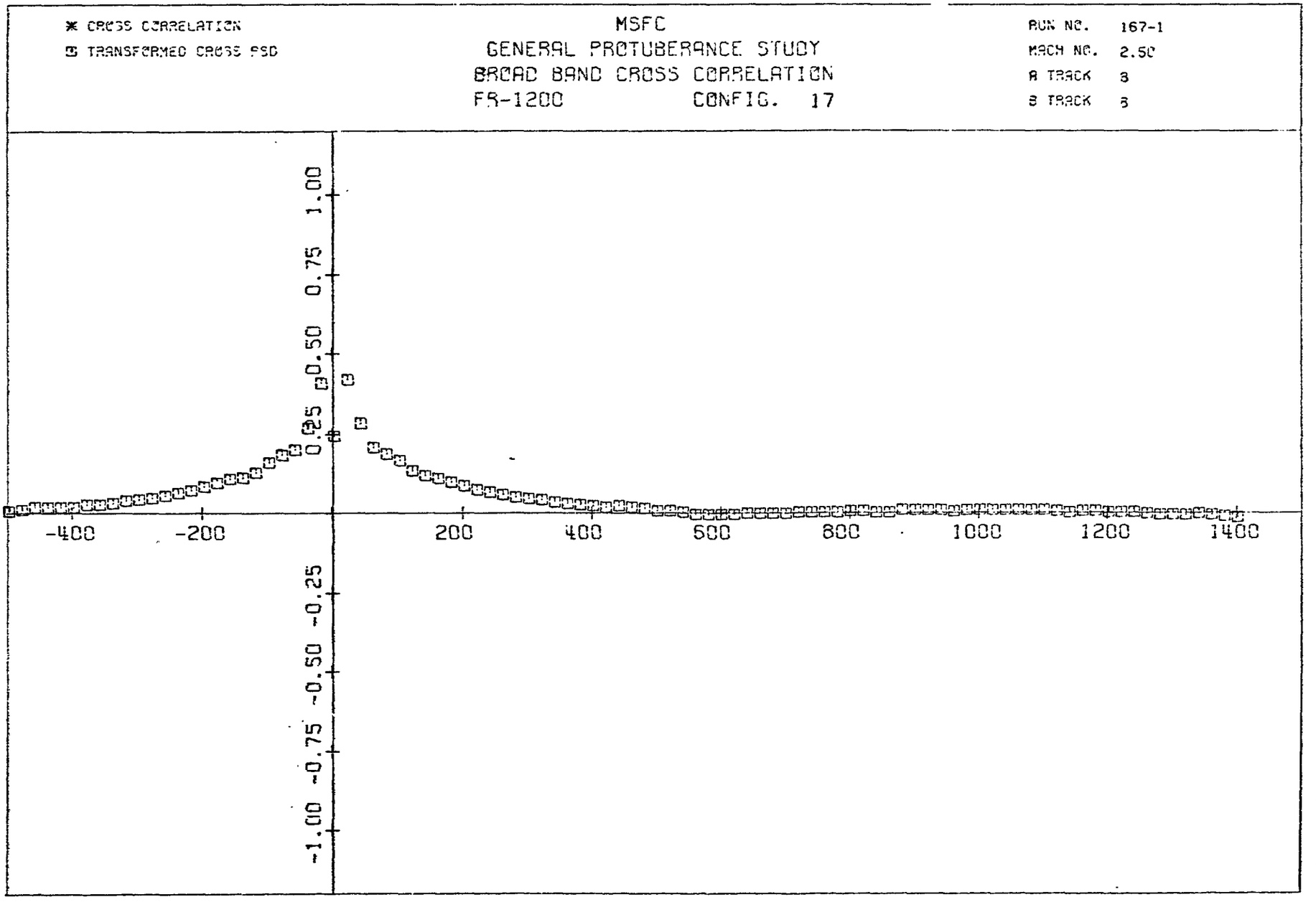
* CROSS CORRELATION
B TRANSFORMED CROSS PSD
MSFC
GENERAL PROTUBERANCE STUDY
BROAD BAND CROSS CORRELATION
FR-1200 CONFIG. 17
RUN NO. 167-1
MACH NO. 2.50
A TRACK B
B TRACK B
NORMALIZED CORRELATION
1.00
0.75
0.50
0.25
-0.25
-0.50
-0.75
-1.00
-400
-200
200
400
600
800
1000
1200
1400
TRACK A TIME DELAY IN MICROSECONDS

PLOT (75)

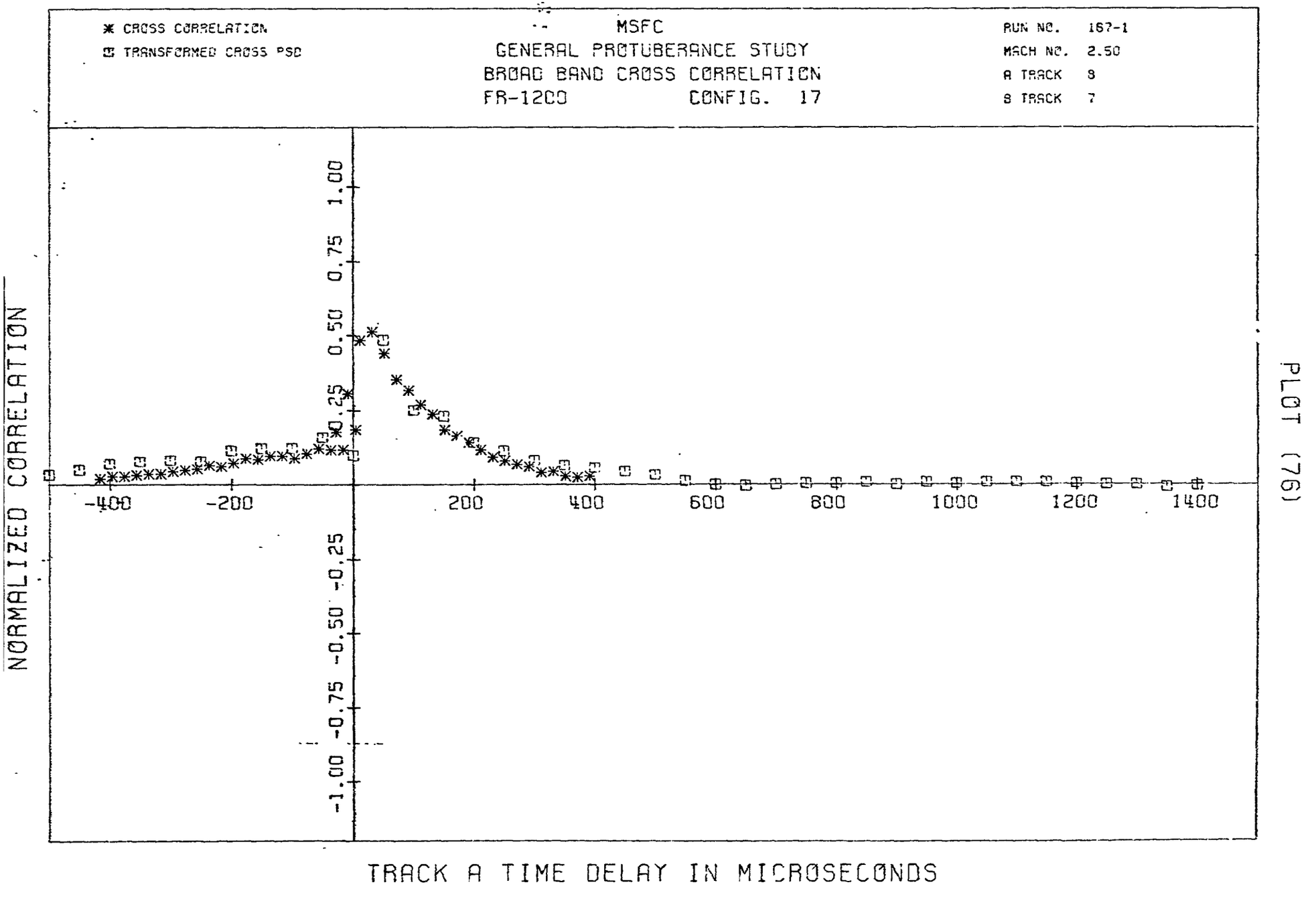
* CROSS CORRELATION
⊡ TRANSFORMED CROSS PSD
MSFC
GENERAL PROTUBERANCE STUDY
BROAD BAND CROSS CORRELATION
FR-1200 CONFIG. 17
RUN NO. 167-1
MACH NO. 2.50
A TRACK 8
B TRACK 7
NORMALIZED CORRELATION
1.00
0.75
0.50
0.25
-0.25
-0.50
-0.75
-1.00
-400
-200
200
400
600
800
1000
1200
1400
TRACK A TIME DELAY IN MICROSECONDS
PLOT (76)

PLOT (77)

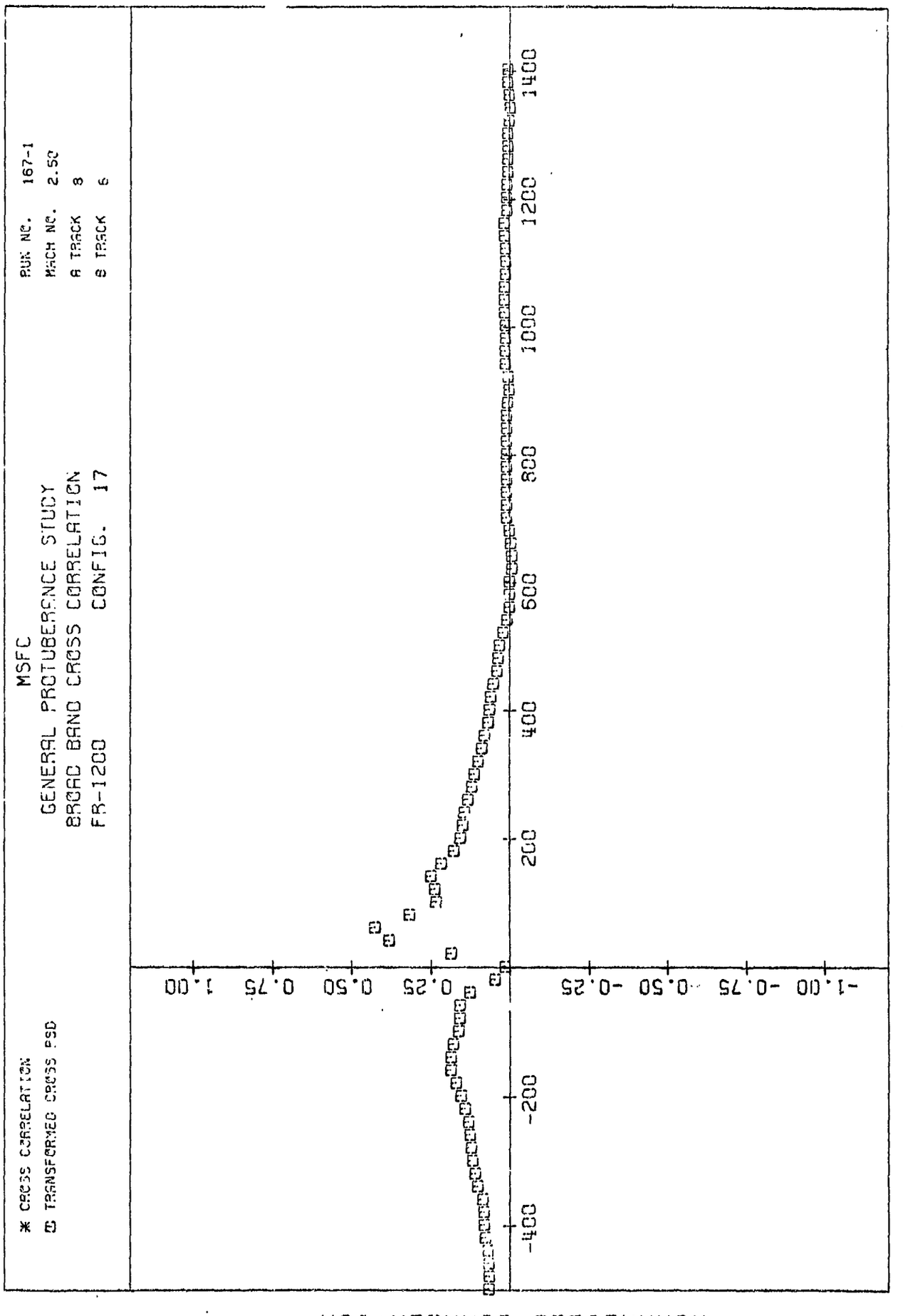
* CROSS CORRELATION
B TRANSFORMED CROSS PSD
MSFC
GENERAL PROTUBERANCE STUDY
BROAD BAND CROSS CORRELATION
FR-1200 CONFIG. 17
RUN NO. 167-1
MACH NO. 2.50
A TRACK 8
B TRACK 6
NORMALIZED CORRELATION
TRACK A TIME DELAY IN MICROSECONDS
1.00
0.75
0.50
0.25
-1.00
-0.75
-0.50
-0.25
-400
-200
200
400
600
800
1000
1200
1400

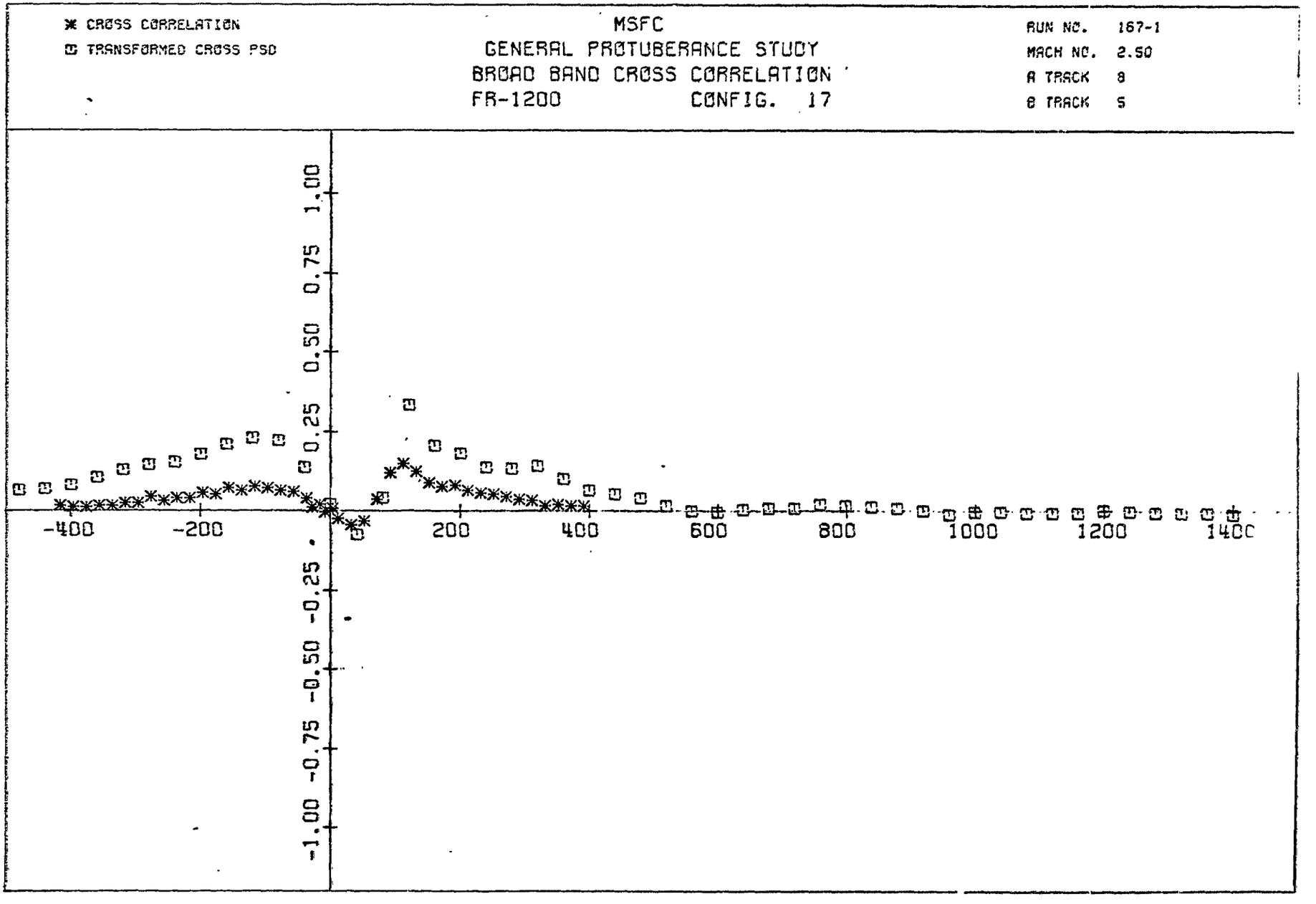
* CROSS CORRELATION
□ TRANSFORMED CROSS PSD
MSFC
GENERAL PROTUBERANCE STUDY
BROAD BAND CROSS CORRELATION
FR-1200 CONFIG. 17
RUN NO. 167-1
MACH NO. 2.50
A TRACK 8
B TRACK 5
NORMALIZED CORRELATION
1.00
0.75
0.50
0.25
-0.25
-0.50
-0.75
-1.00
-400
-200
200
400
600
800
1000
1200
1400
TRACK A TIME DELAY IN MICROSECONDS

PLOT (78)

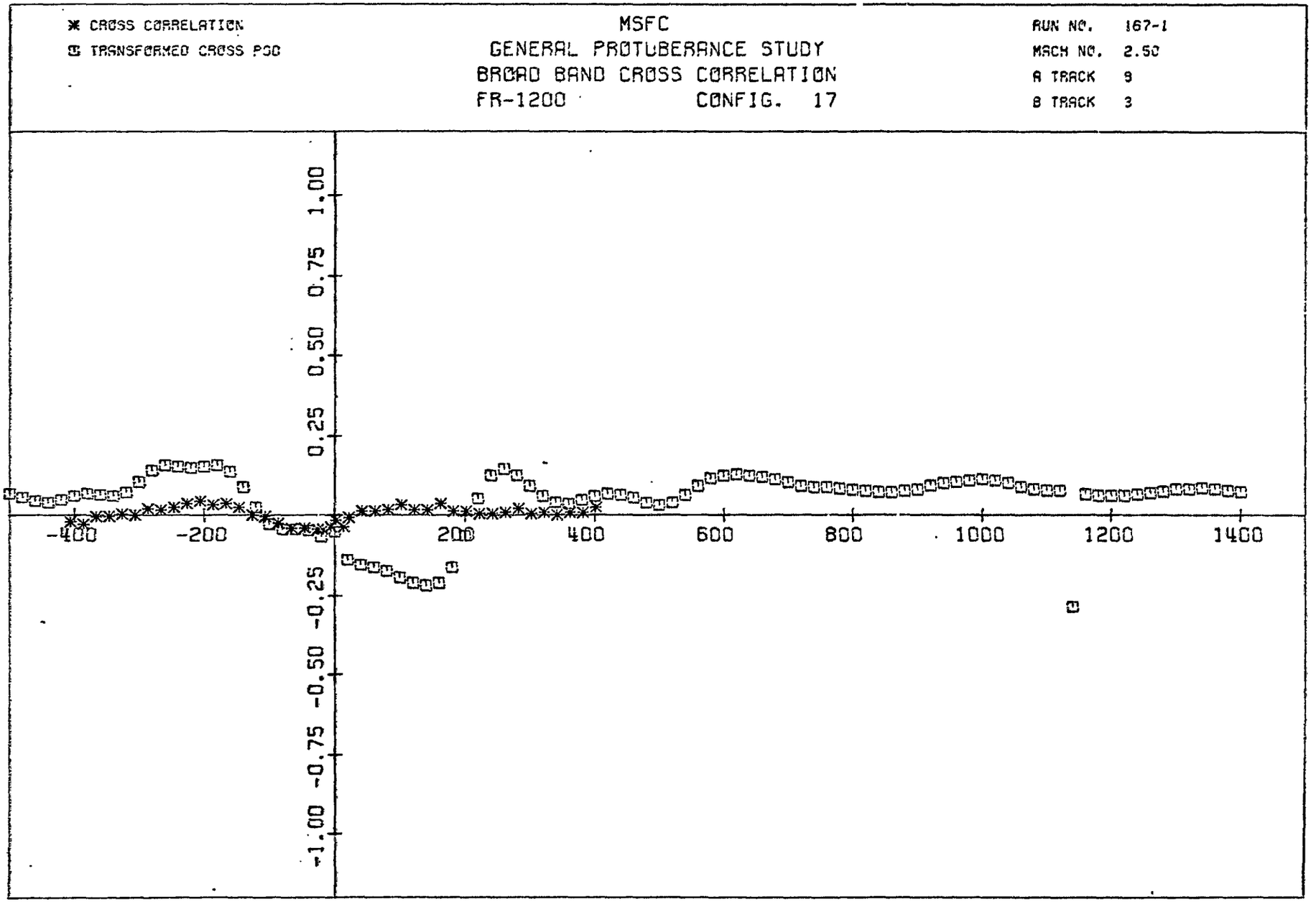
* CROSS CORRELATION
□ TRANSFORMED CROSS POC
MSFC
GENERAL PROTUBERANCE STUDY
BROAD BAND CROSS CORRELATION
FR-1200 CONFIG. 17
RUN NO. 167-1
MACH NO. 2.50
A TRACK 9
B TRACK 3
NORMALIZED CORRELATION
1.00
0.75
0.50
0.25
-0.25
-0.50
-0.75
-1.00
-400
-200
200
400
600
800
1000
1200
1400
TRACK A TIME DELAY IN MICROSECONDS
PLOT (79)

BAGHNOFF ASSOCIATES

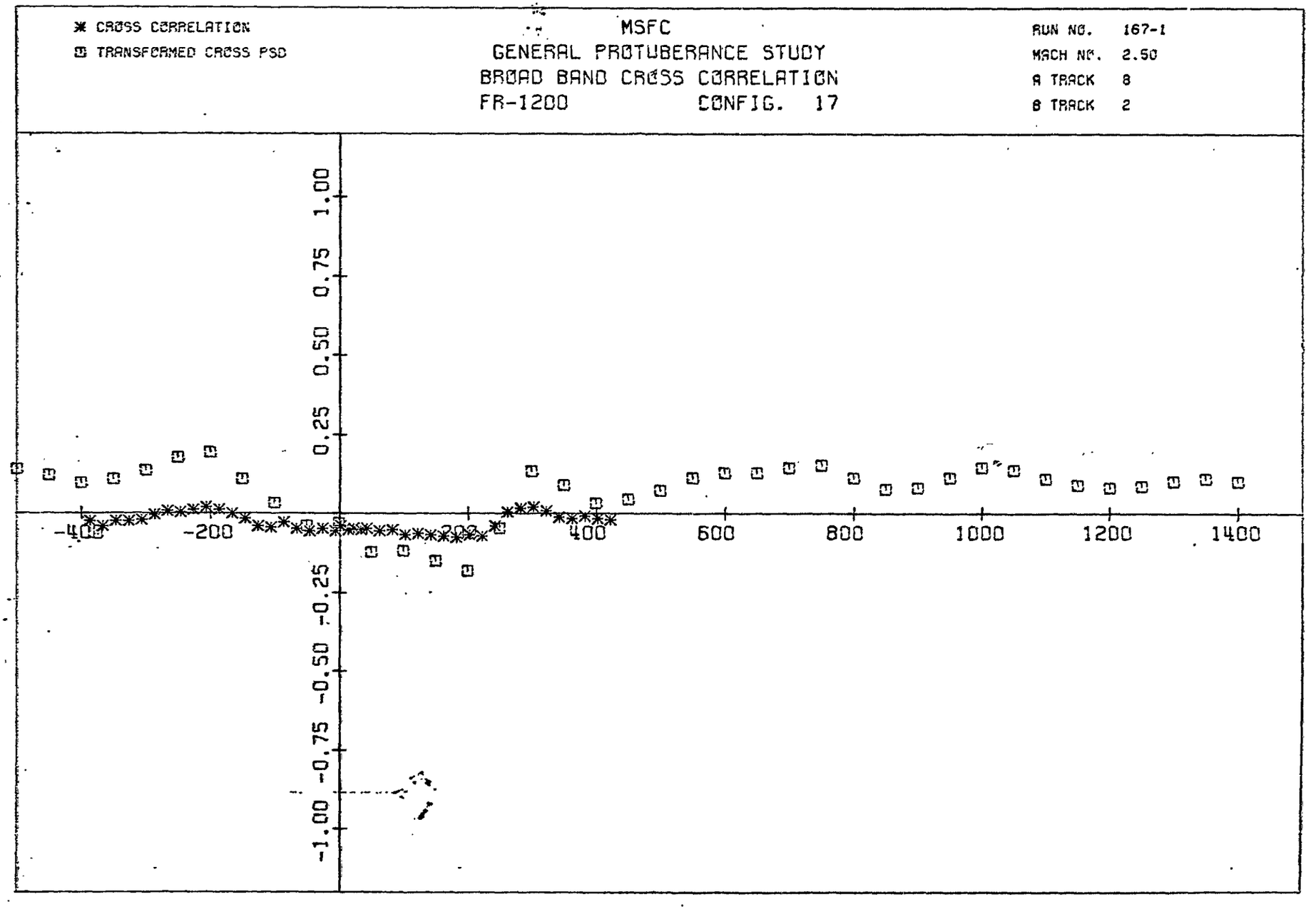

PLOT (80)

BAGANOFF ASSOCIATES

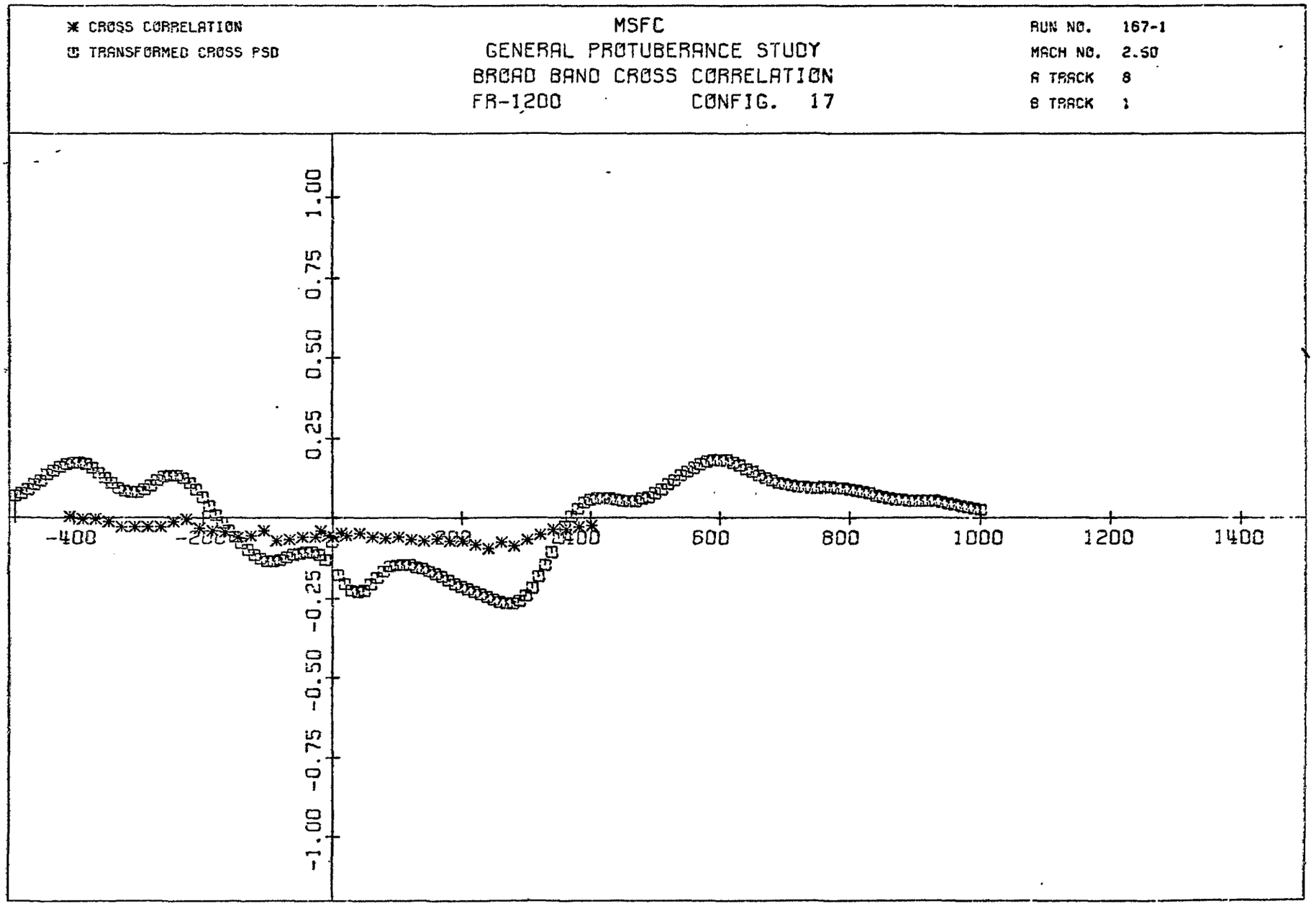

BAGANOFF ASSOCIATES

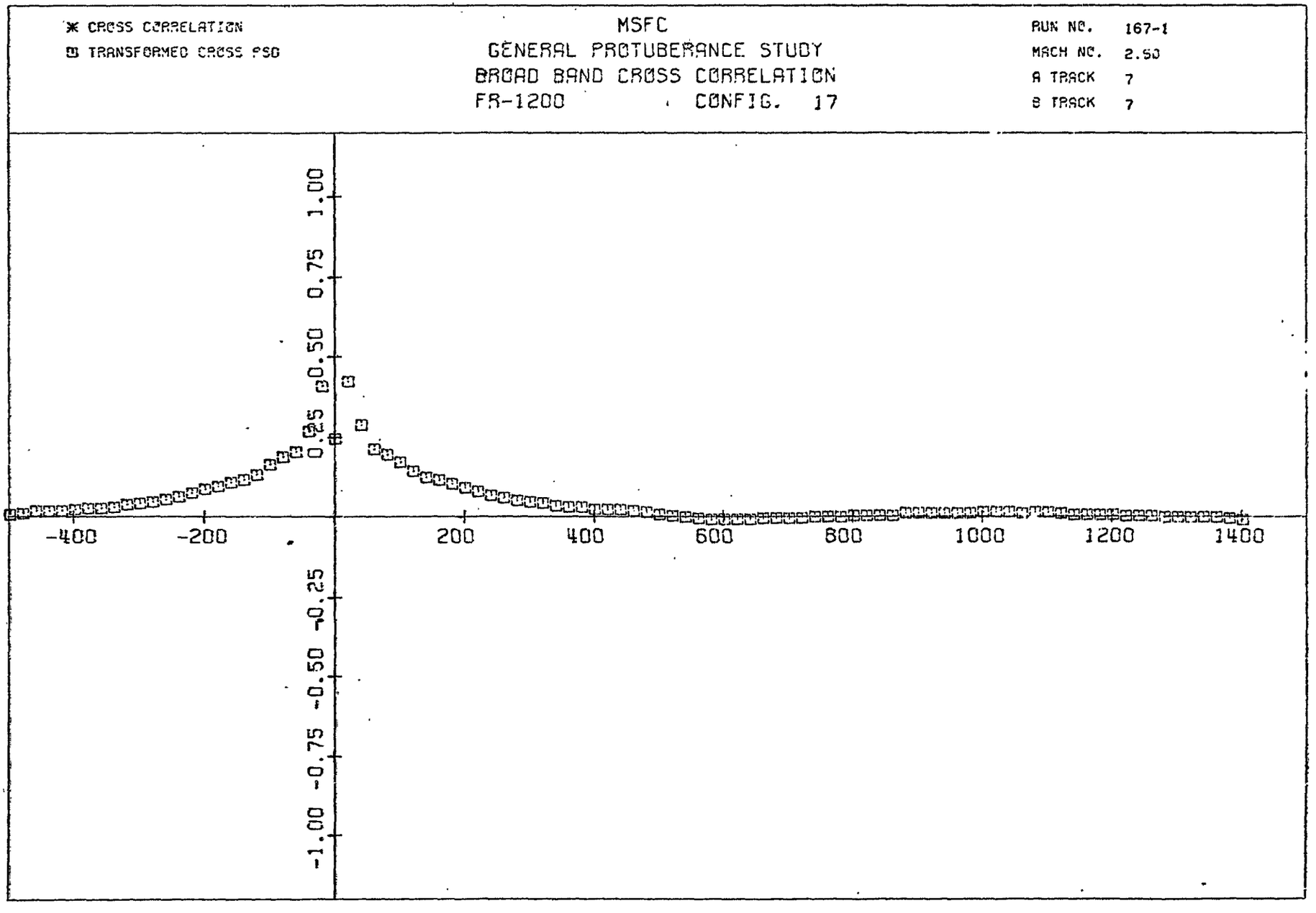

NORMALIZED CORRELATION

TRACK A TIME DELAY IN MICROSECONDS

PLOT (82)

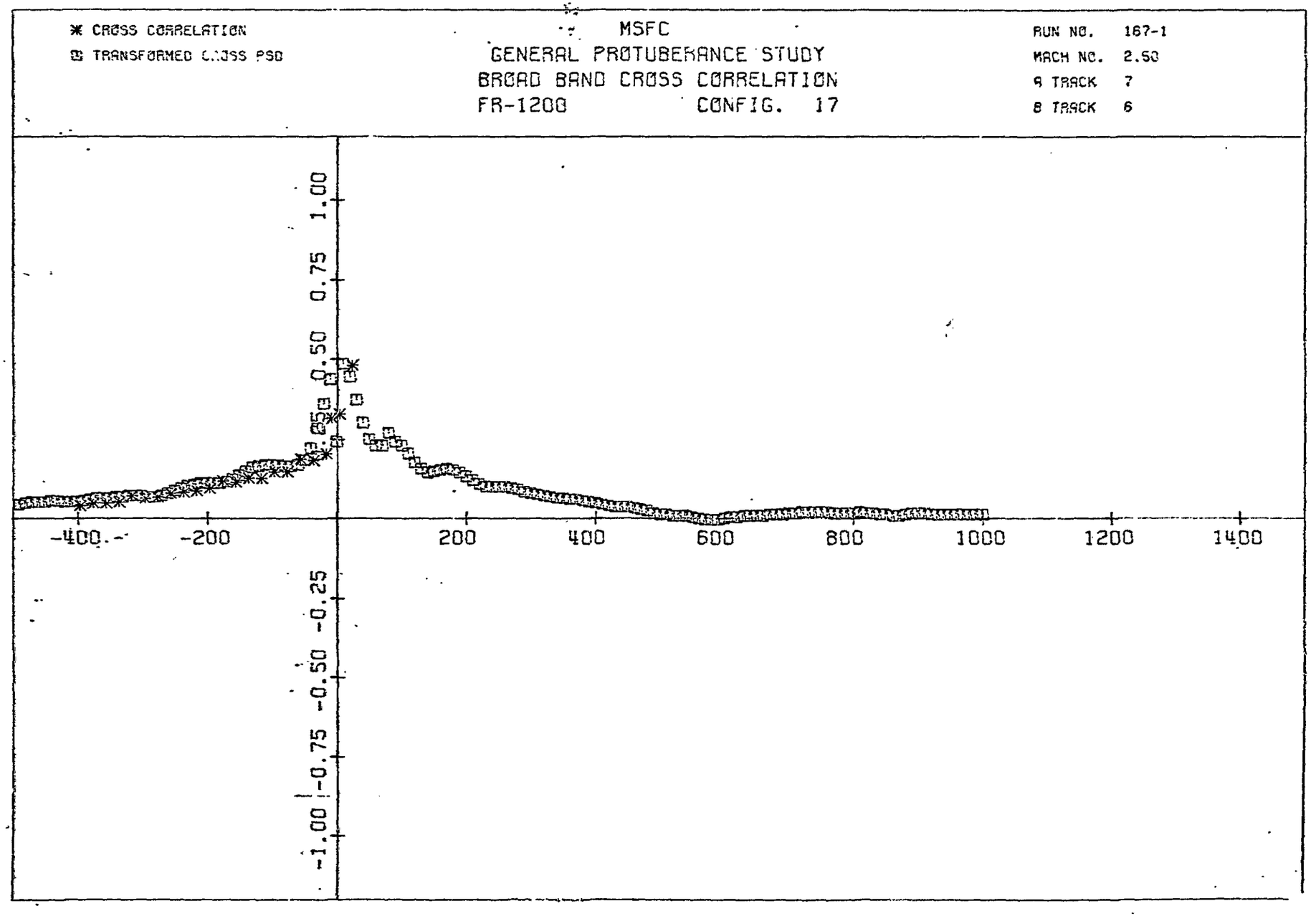
* CROSS CORRELATION
⊡ TRANSFORMED CROSS PSD
MSFC
GENERAL PROTUBERANCE STUDY
BROAD BAND CROSS CORRELATION
FR-1200 CONFIG. 17
RUN NO. 167-1
MACH NO. 2.50
9 TRACK 7
8 TRACK 6
NORMALIZED CORRELATION
1.00
0.75
0.50
0.25
-0.25
-0.50
-0.75
-1.00
-400
-200
200
400
600
800
1000
1200
1400
TRACK A TIME DELAY IN MICROSECONDS
PLOT (83)

BAGANOFF ASSOCIATES

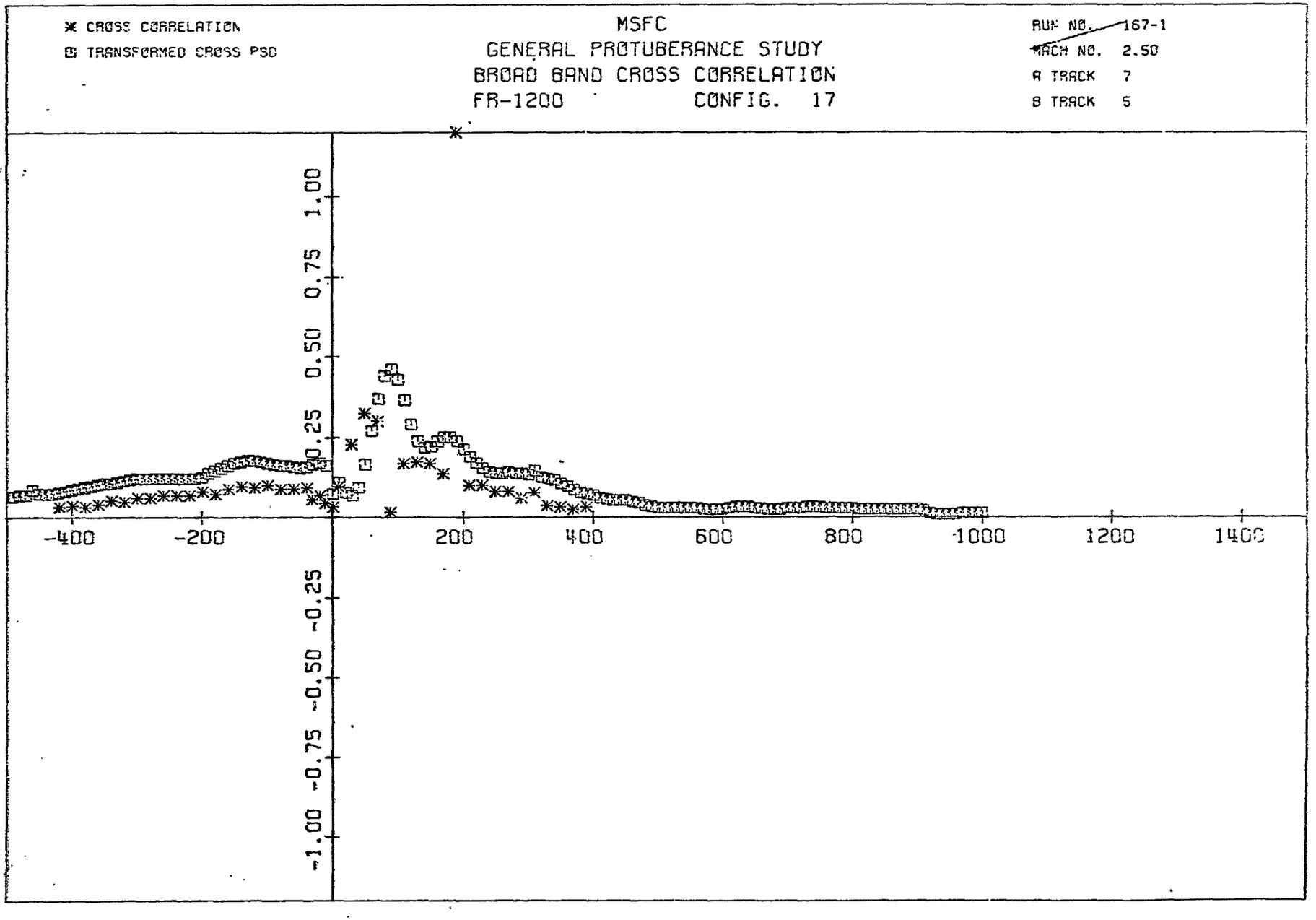

NORMALIZED CORRELATION

PLOT (84)

TRACK A TIME DELAY IN MICROSECONDS

BAGANOFF ASSOCIATES

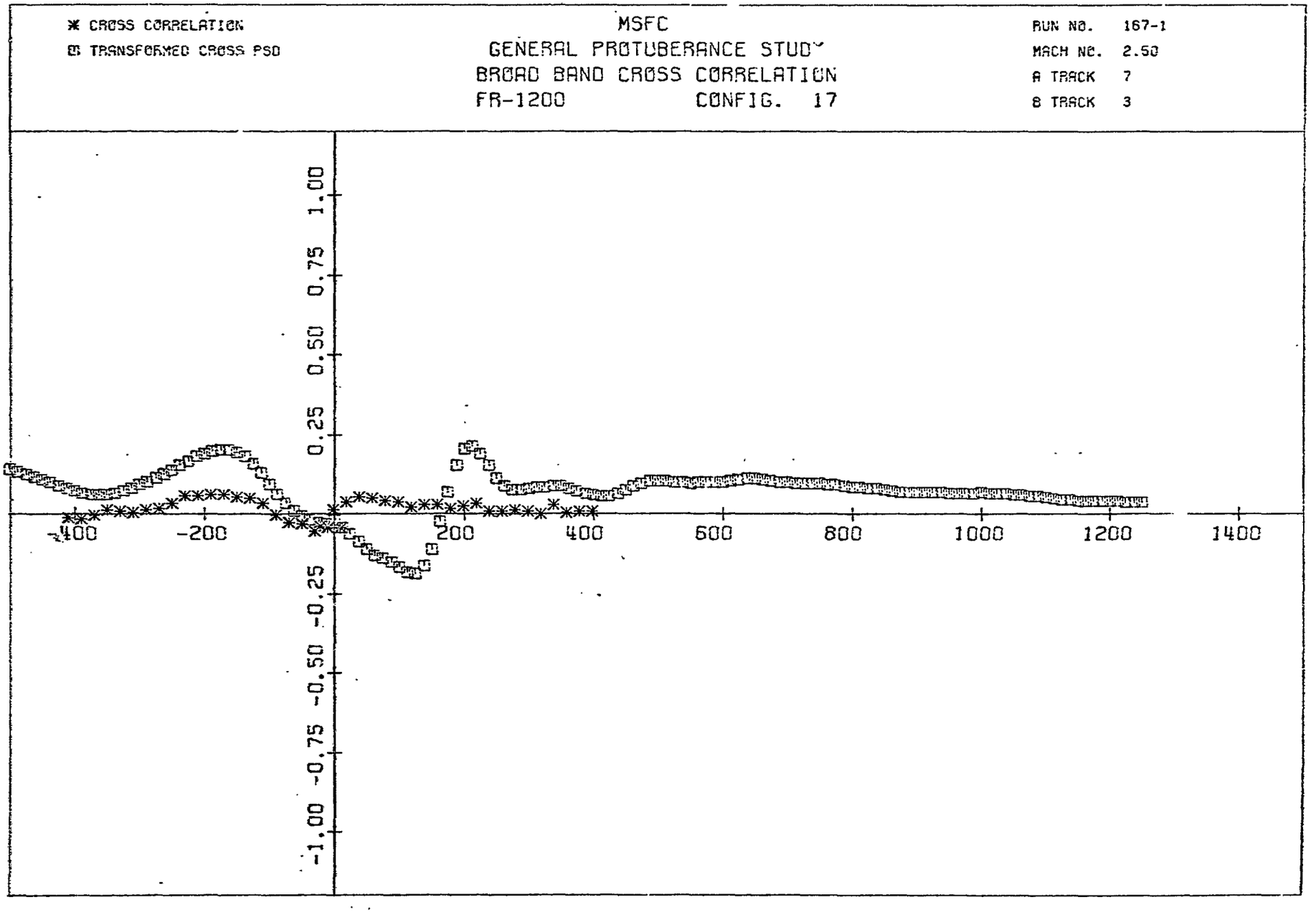

NORMALIZED CORRELATION

PLOT (85)

TRACK A TIME DELAY IN MICROSECONDS

BAGANOFF ASSOCIATES

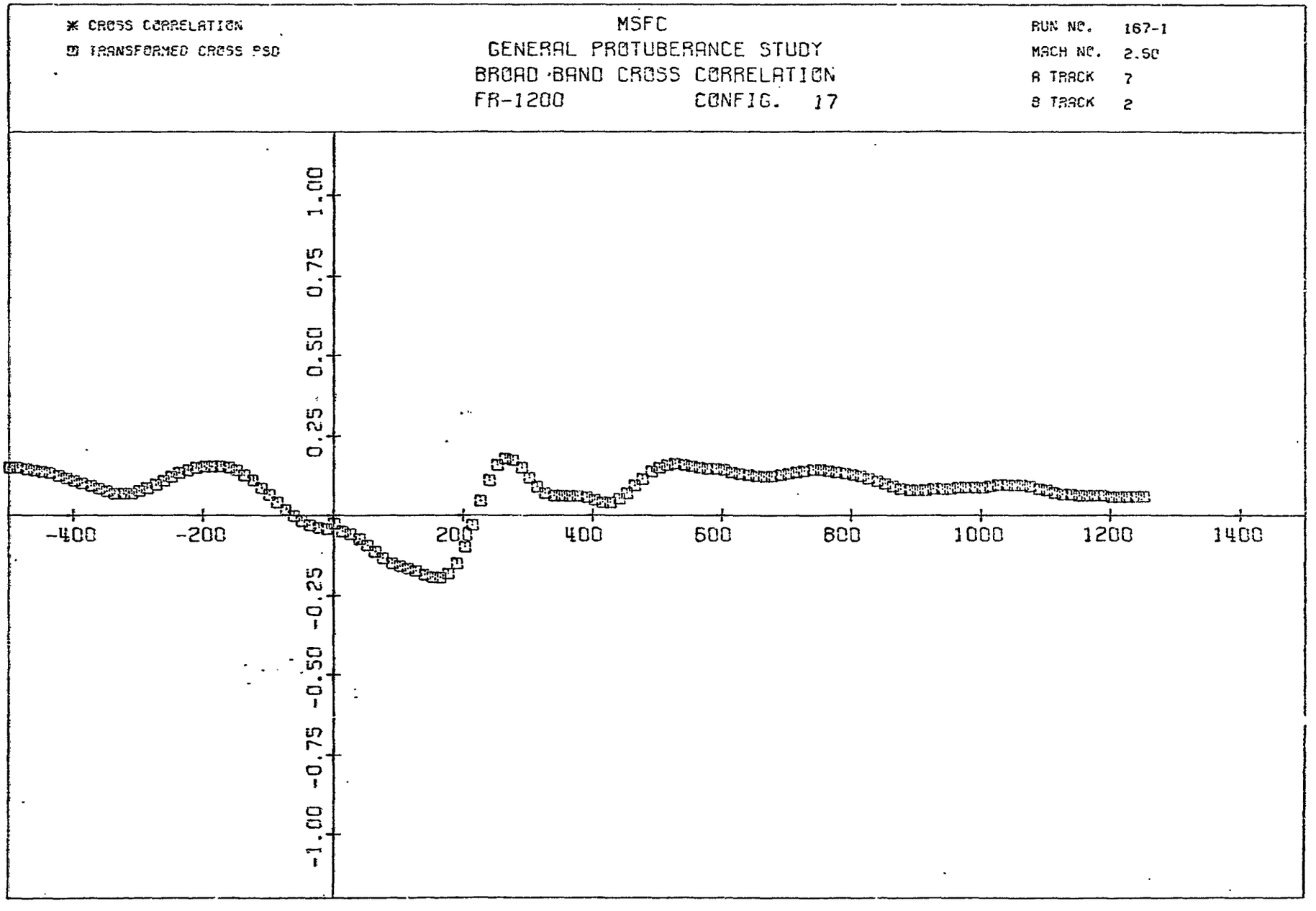

PLOT (86)

BAGANOFF ASSOCIATES

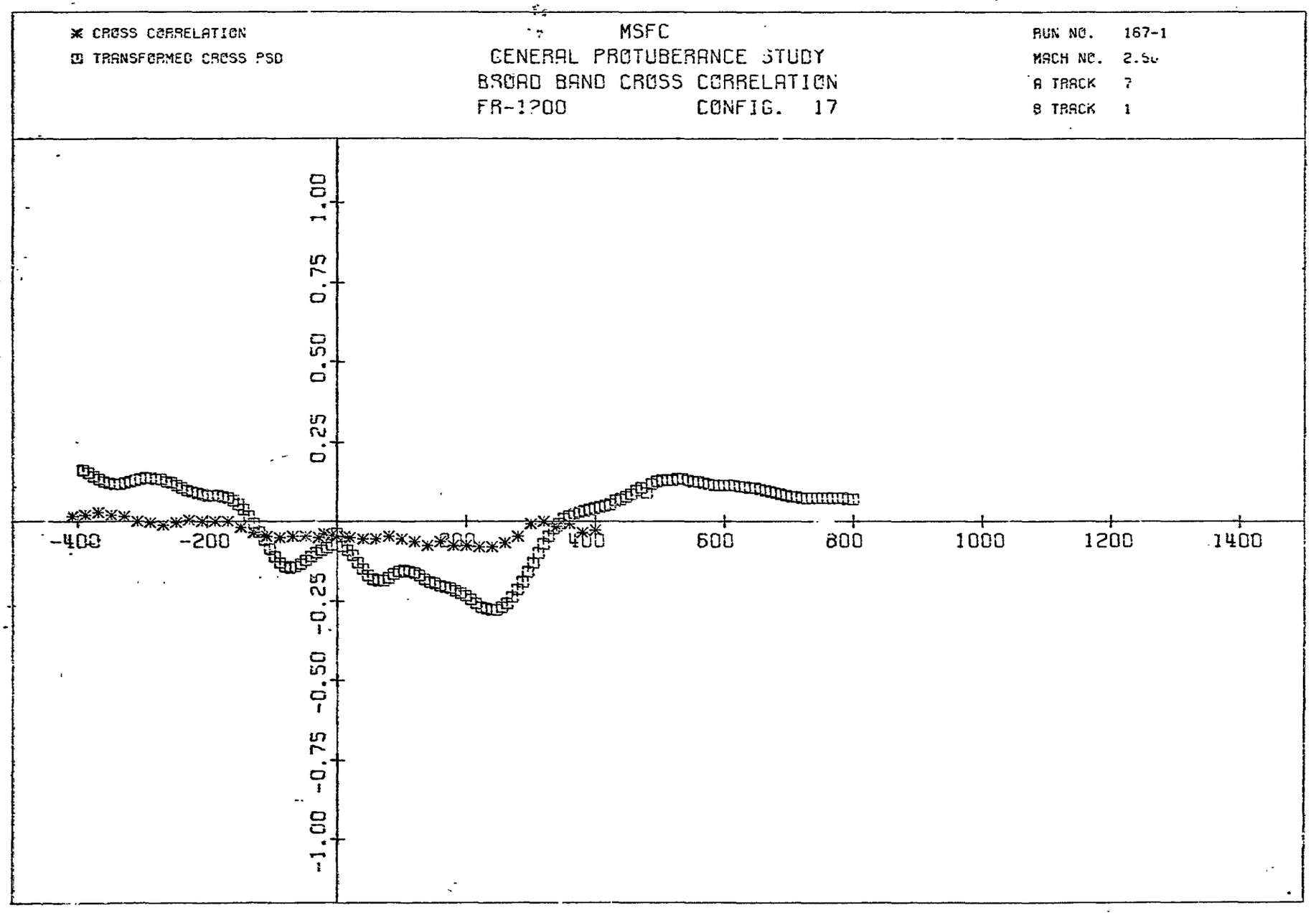

PLOT (87)

BAGANOFF ASSOCIATES

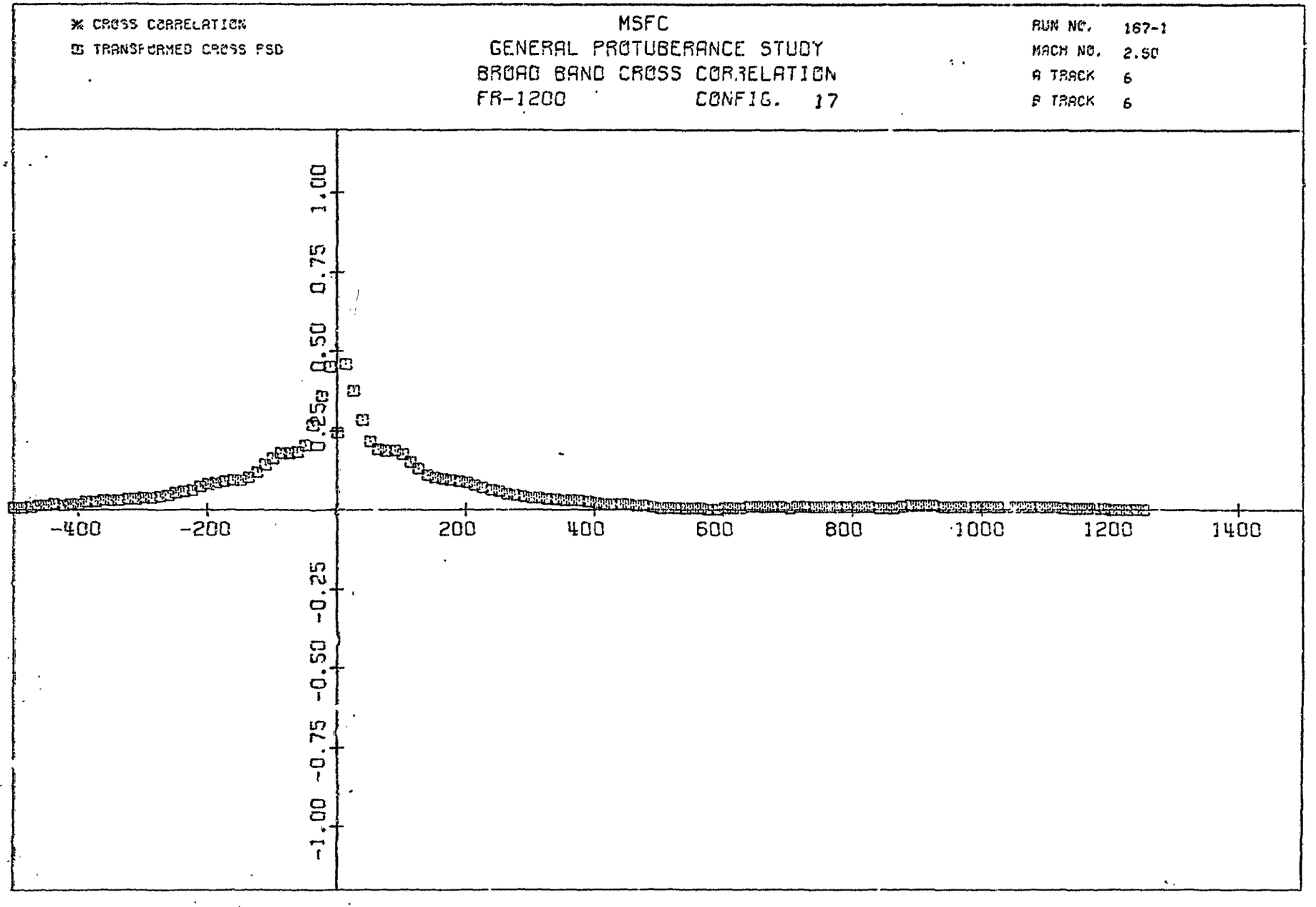

PLOT (88)

BAGANOFF ASSOCIATES

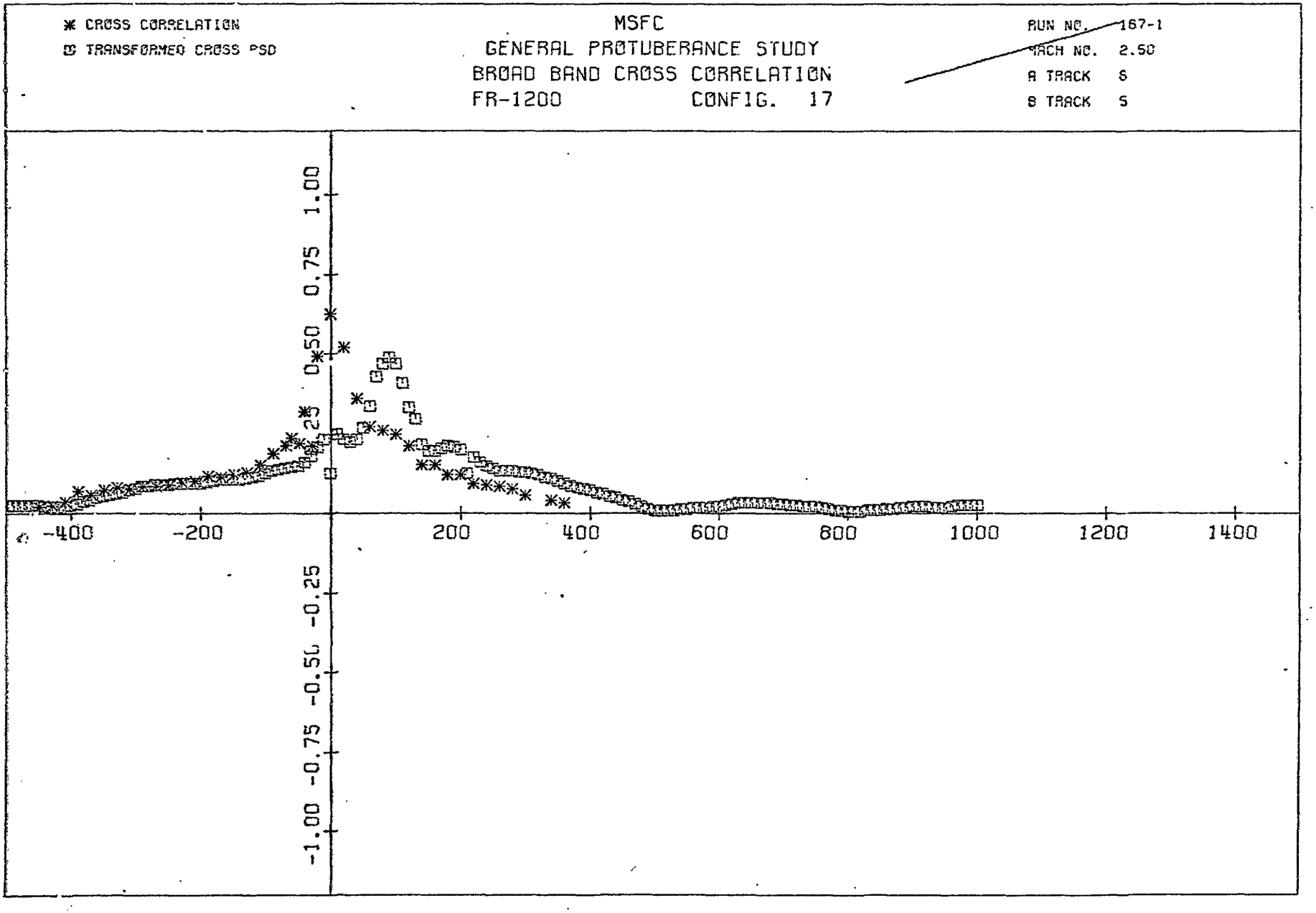

PLOT (89)

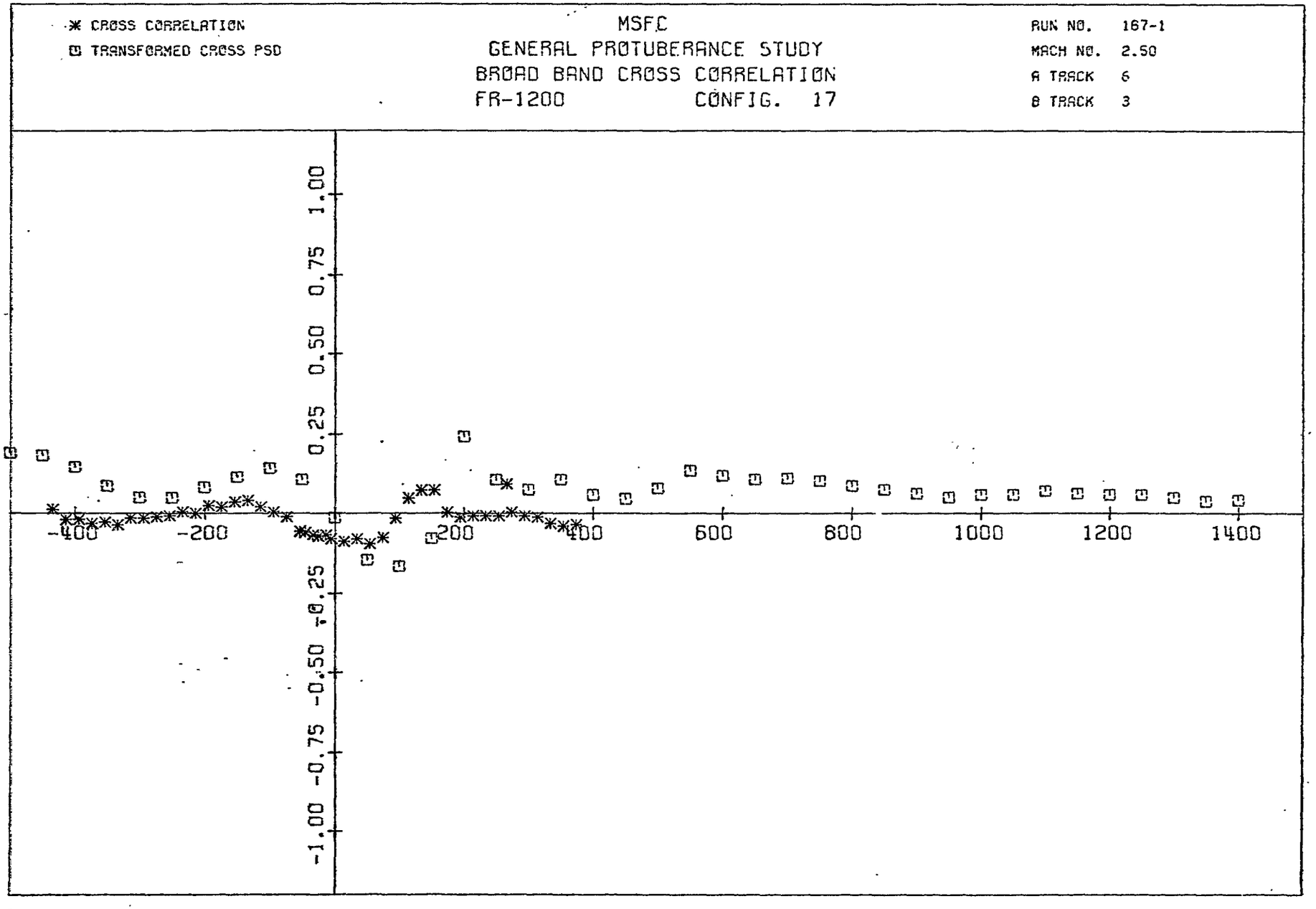
* CROSS CORRELATION
TRANSFORMED CROSS PSD
MSFC
GENERAL PROTUBERANCE STUDY
BROAD BAND CROSS CORRELATION
FR-1200 CONFIG. 17
RUN NO. 167-1
MACH NO. 2.50
A TRACK 6
B TRACK 3
1.00
0.75
0.50
0.25
-0.25
-0.50
-0.75
-1.00
-400
-200
200
400
600
800
1000
1200
1400
NORMALIZED CORRELATION
TRACK A TIME DELAY IN MICROSECONDS

PLOT (90)

BAGANOFF ASSOCIATES

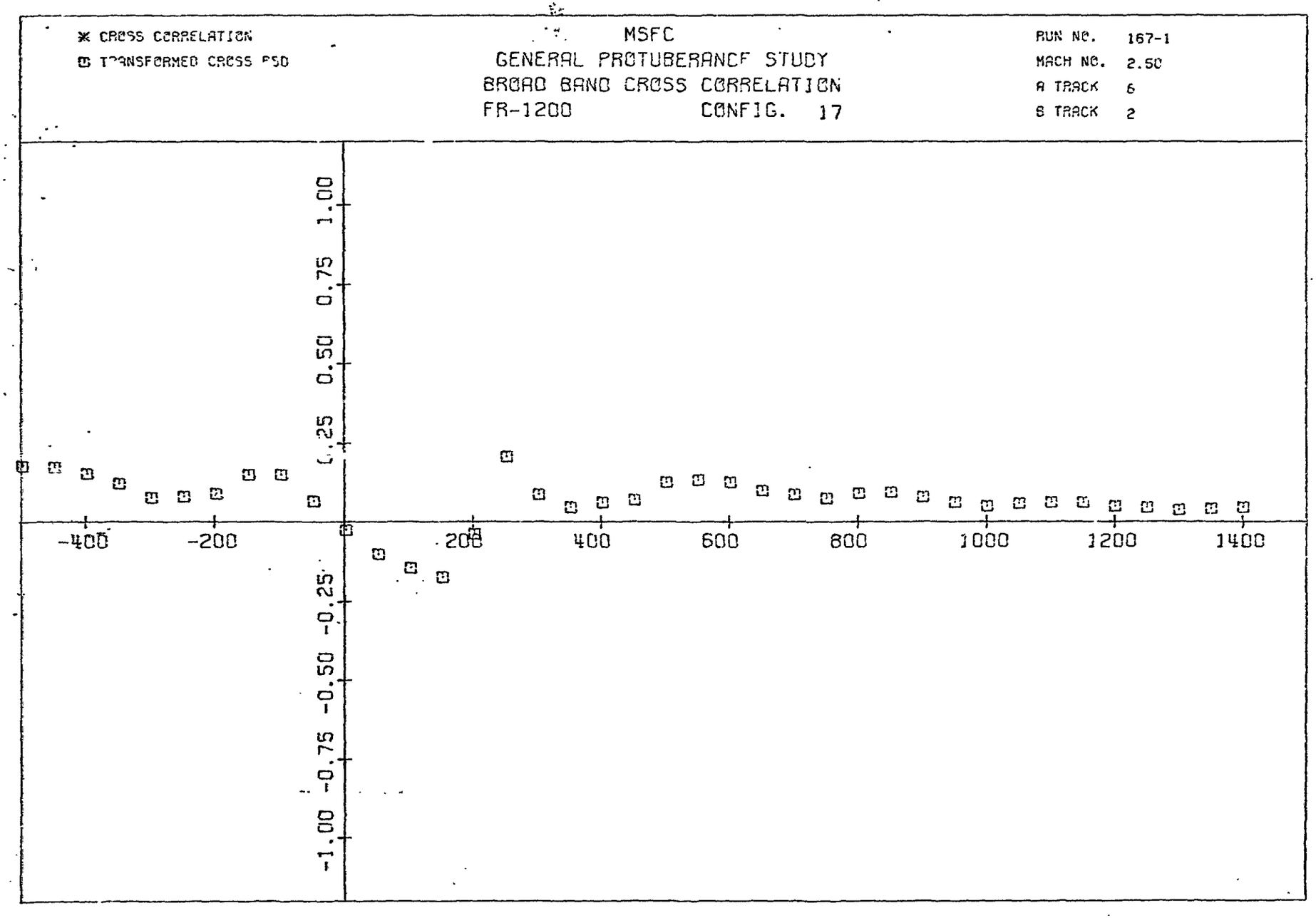

PLOT (91)

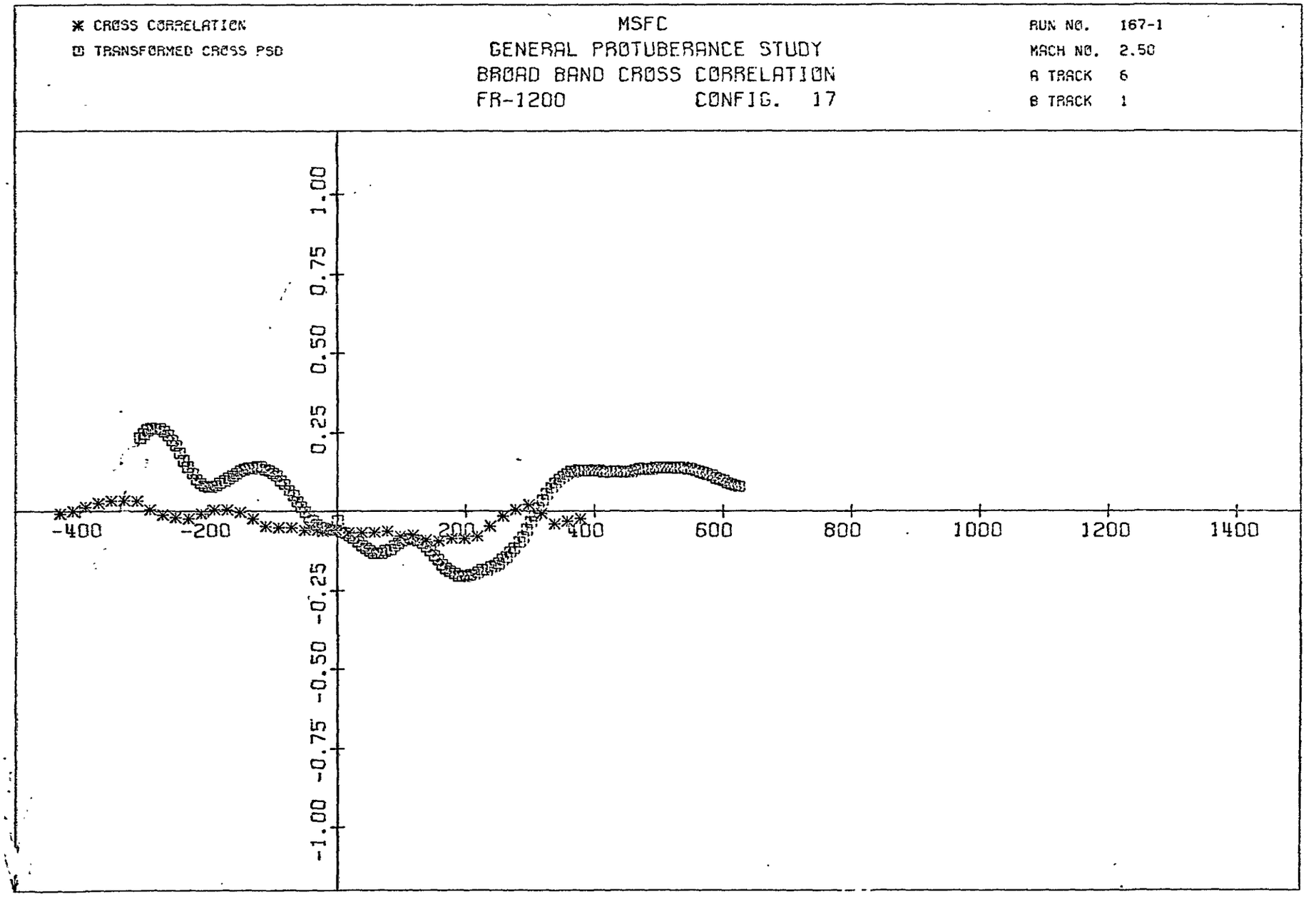

NORMALIZED CORRELATION

PLOT (92)

TRACK A TIME DELAY IN MICROSECONDS

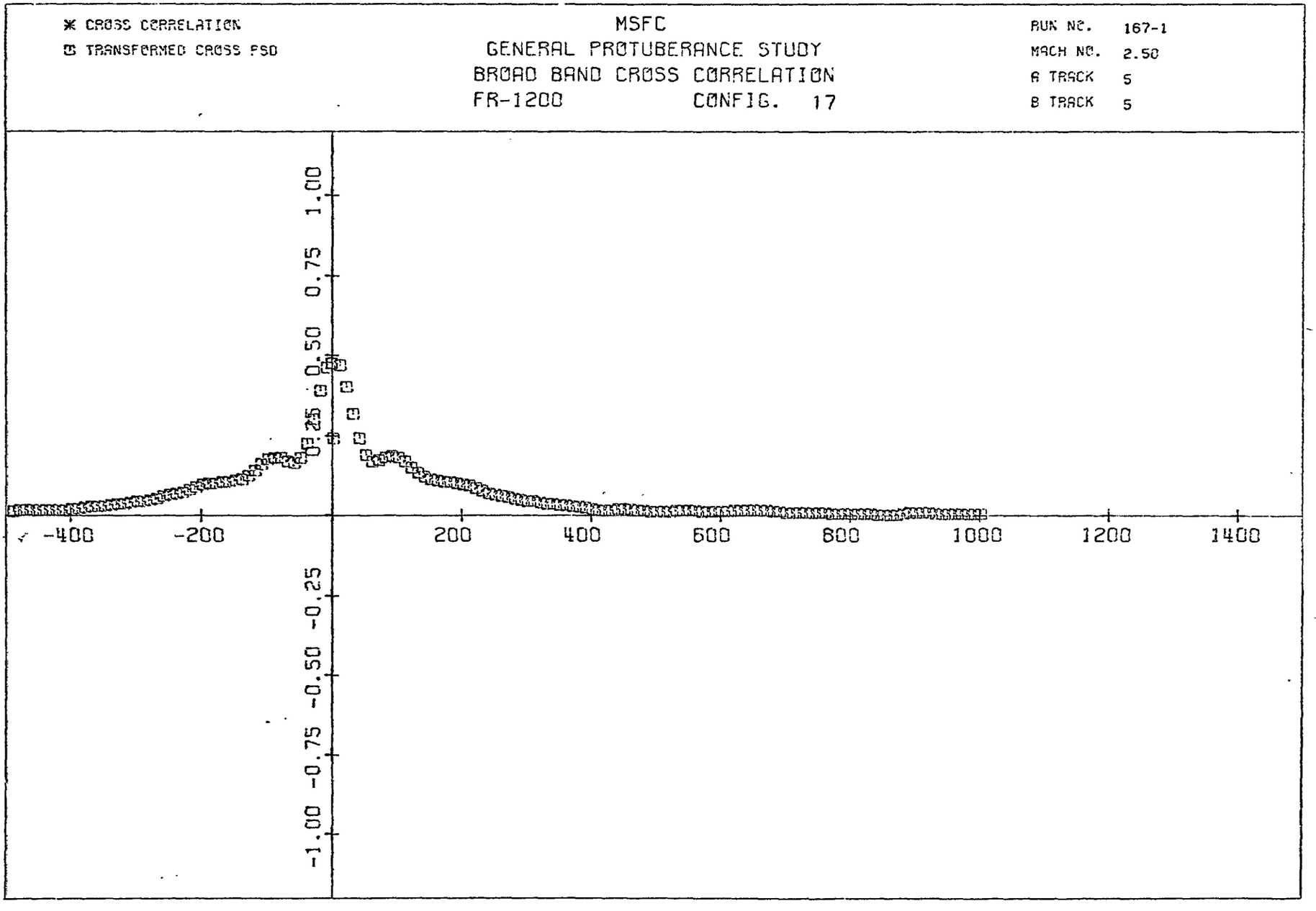
* CROSS CORRELATION
⊡ TRANSFORMED CROSS PSD
MSFC
GENERAL PROTUBERANCE STUDY
BROAD BAND CROSS CORRELATION
FR-1200 CONFIG. 17
RUN NO. 167-1
MACH NO. 2.50
A TRACK 5
B TRACK 5
1.00
0.75
0.50
0.25
-0.25
-0.50
-0.75
-1.00
-400
-200
200
400
600
800
1000
1200
1400
NORMALIZED CORRELATION
TRACK A TIME DELAY IN MICROSECONDS

PLOT (93)

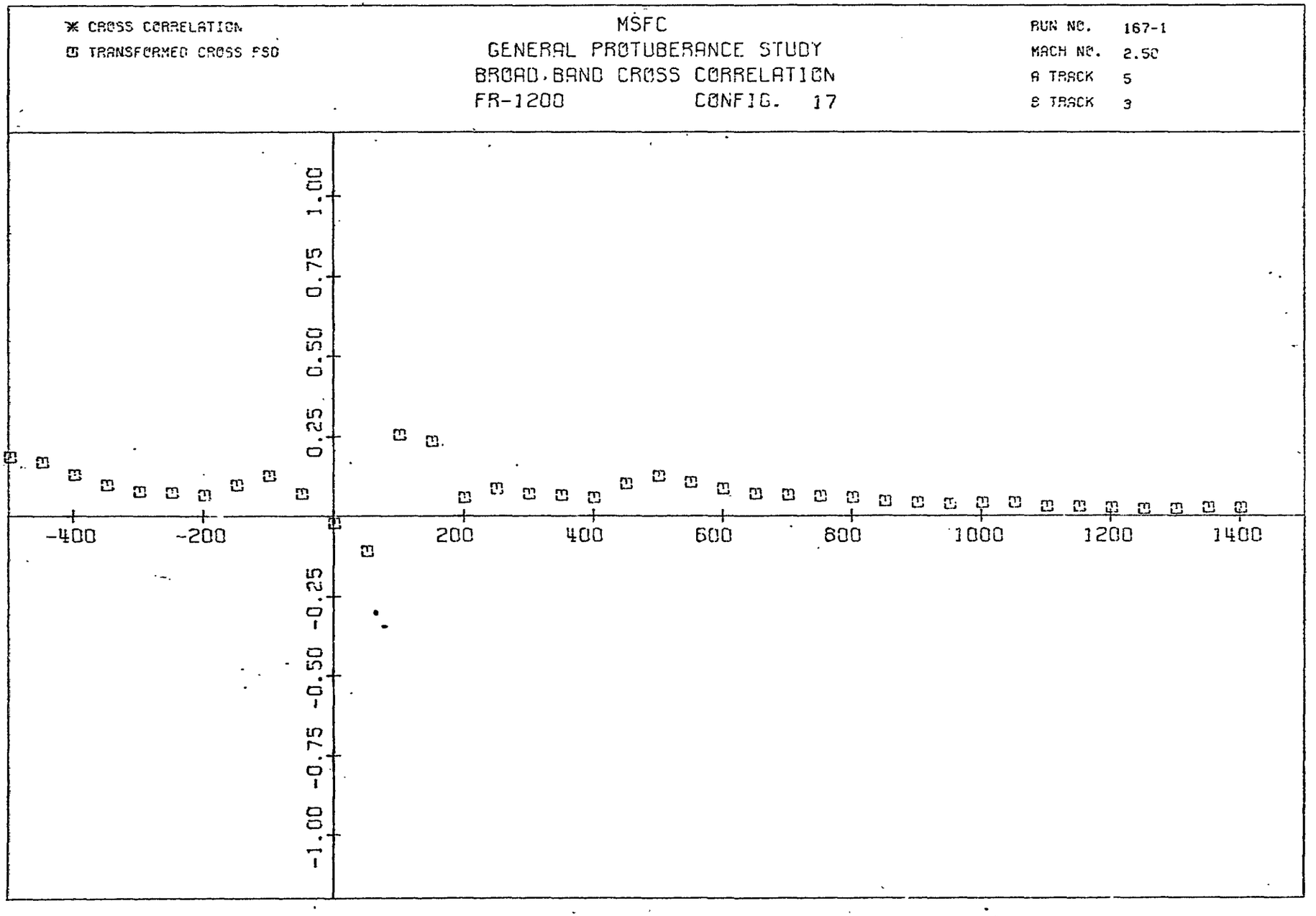
* CROSS CORRELATION
⊡ TRANSFORMED CROSS PSD
MSFC
GENERAL PROTUBERANCE STUDY
BROAD-BAND CROSS CORRELATION
FR-1200 CONFIG. 17
RUN NO. 167-1
MACH NO. 2.50
A TRACK 5
B TRACK 3
1.00
0.75
0.50
0.25
-0.25
-0.50
-0.75
-1.00
-400
-200
200
400
600
800
1000
1200
1400
NORMALIZED CORRELATION
TRACK A TIME DELAY IN MICROSECONDS
PLOT (9H)

BAGANOFF ASSOCIATES

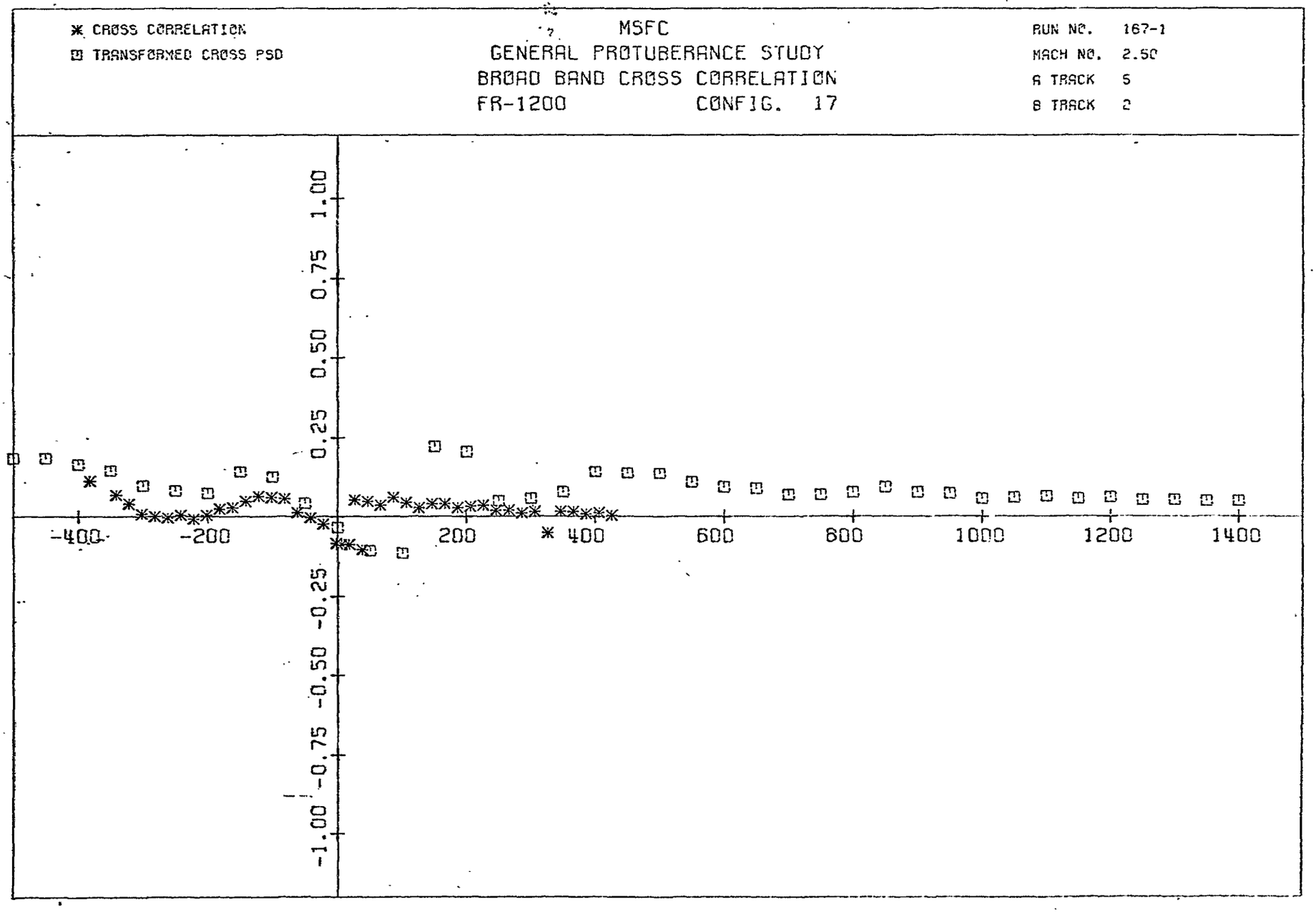

PLOT (95)

BAGANOFF ASSOCIATES

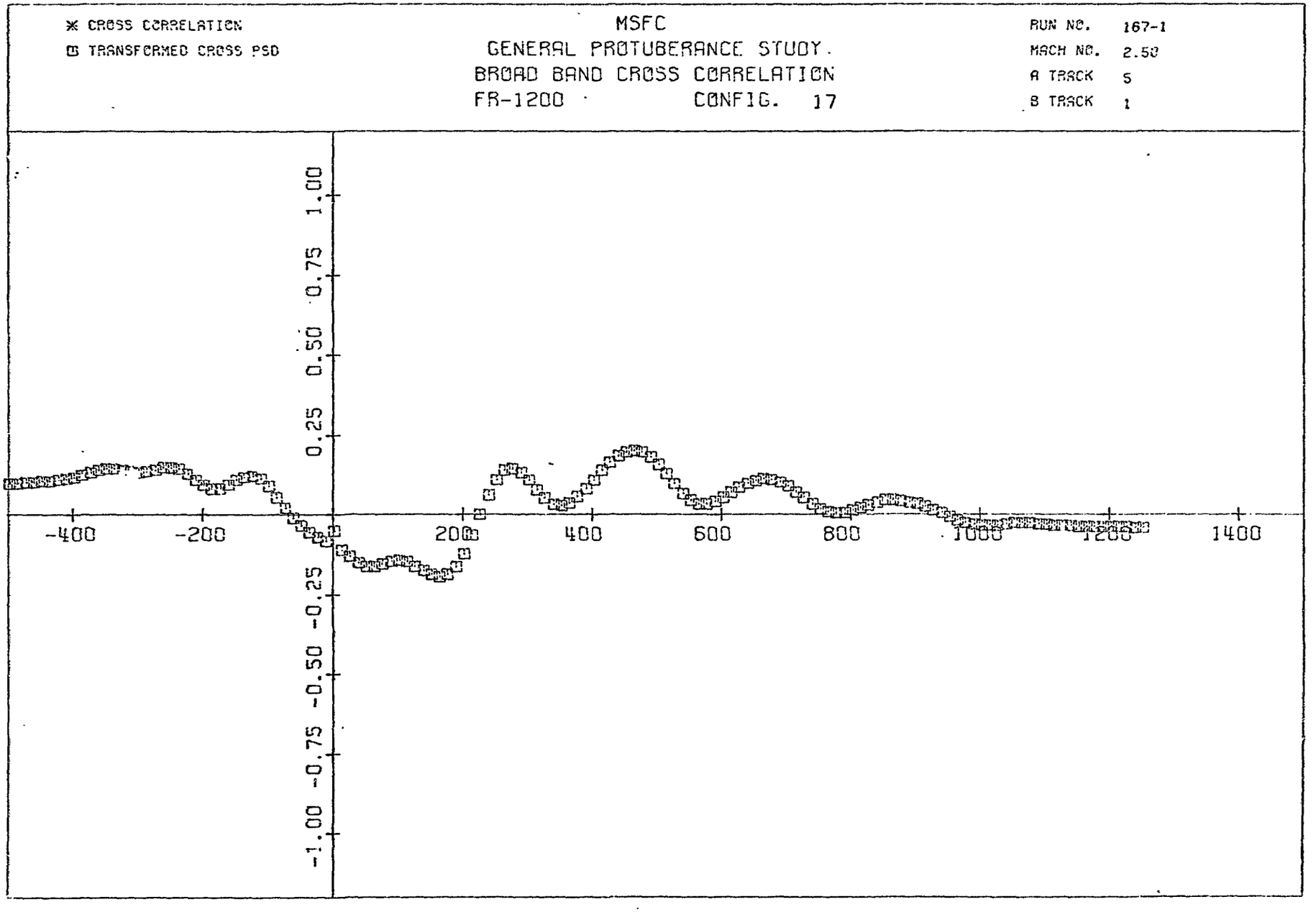

NORMALIZED CORRELATION

PLOT (96)

TRACK A TIME DELAY IN MICROSECONDS

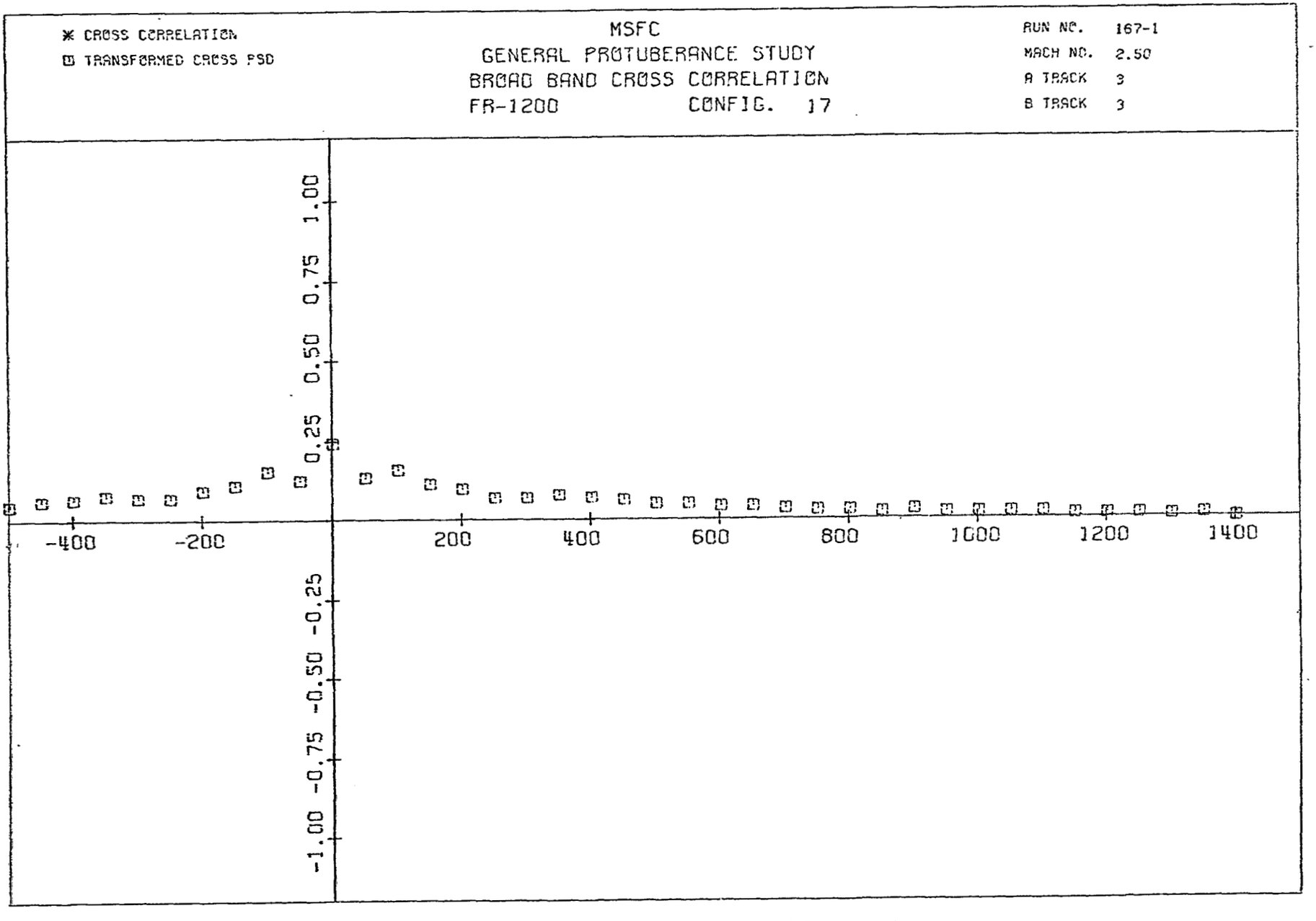
* CROSS CORRELATION
⊡ TRANSFORMED CROSS PSD
MSFC
GENERAL PROTUBERANCE STUDY
BROAD BAND CROSS CORRELATION
FR-1200 CONFIG. 17
RUN NO. 167-1
MACH NO. 2.50
A TRACK 3
B TRACK 3
NORMALIZED CORRELATION
1.00
0.75
0.50
0.25
-0.25
-0.50
-0.75
-1.00
-400
-200
200
400
600
800
1000
1200
1400
TRACK A TIME DELAY IN MICROSECONDS

PLOT (97)

BAGANOFF ASSOCIATES

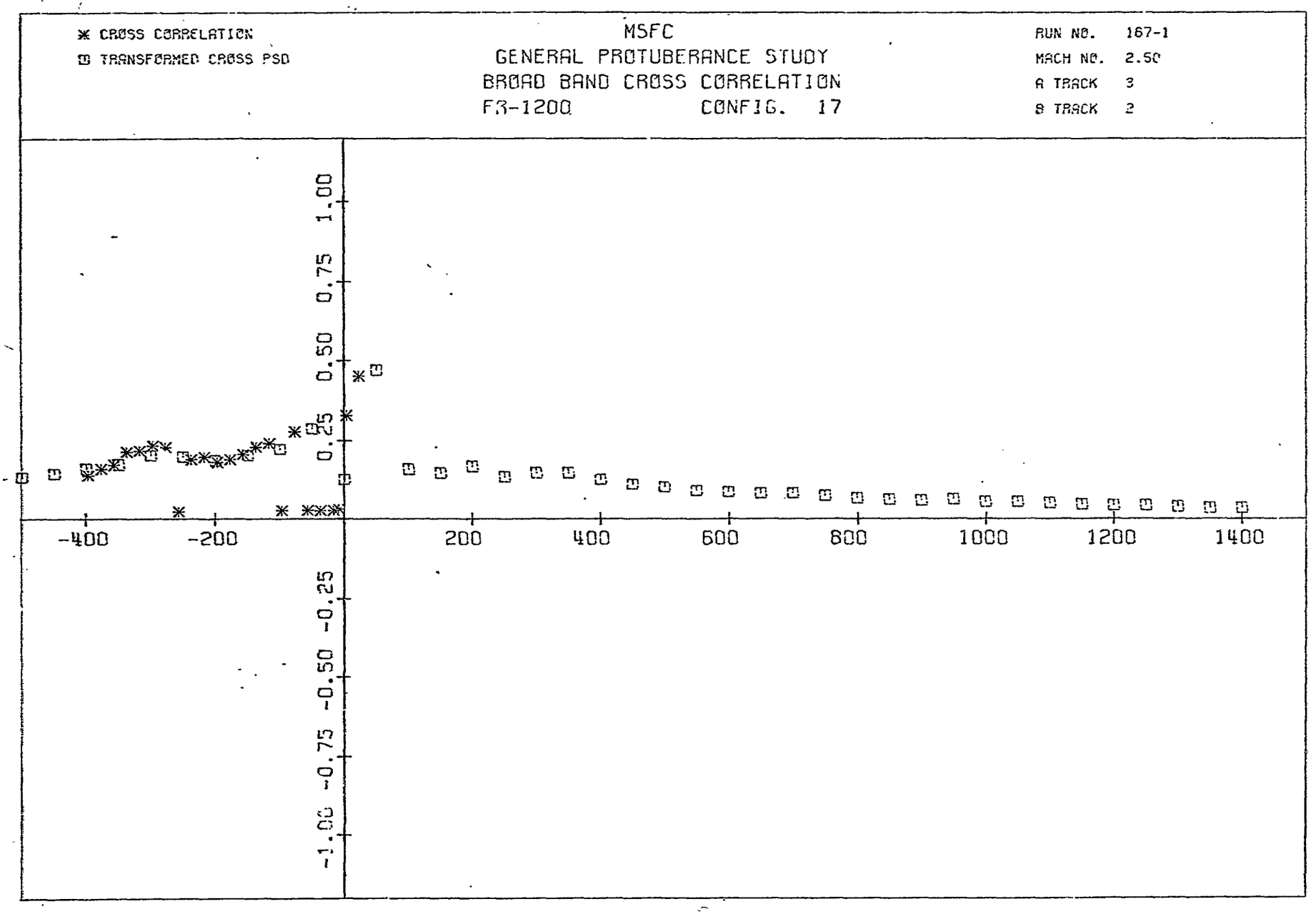

PLOT (98)

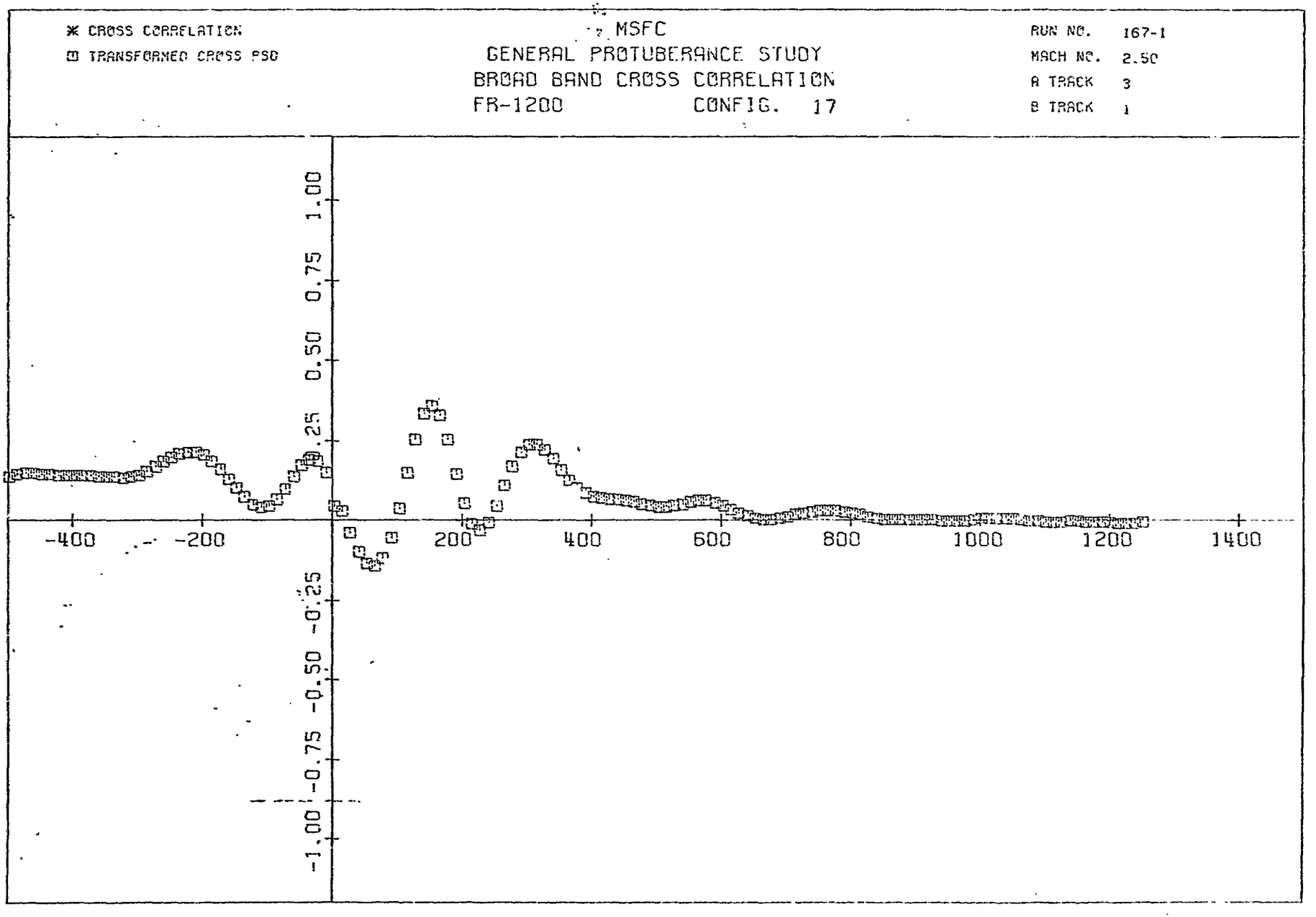
* CROSS CORRELATION
⊡ TRANSFORMED CROSS PSD
MSFC
GENERAL PROTUBERANCE STUDY
BROAD BAND CROSS CORRELATION
FR-1200 CONFIG. 17
RUN NO. 167-1
MACH NO. 2.50
A TRACK 3
B TRACK 1
NORMALIZED CORRELATION
1.00
0.75
0.50
0.25
-0.25
-0.50
-0.75
-1.00
-400
-200
200
400
600
800
1000
1200
1400
TRACK A TIME DELAY IN MICROSECONDS

PLOT (99)

BAGANOFF ASSOCIATES

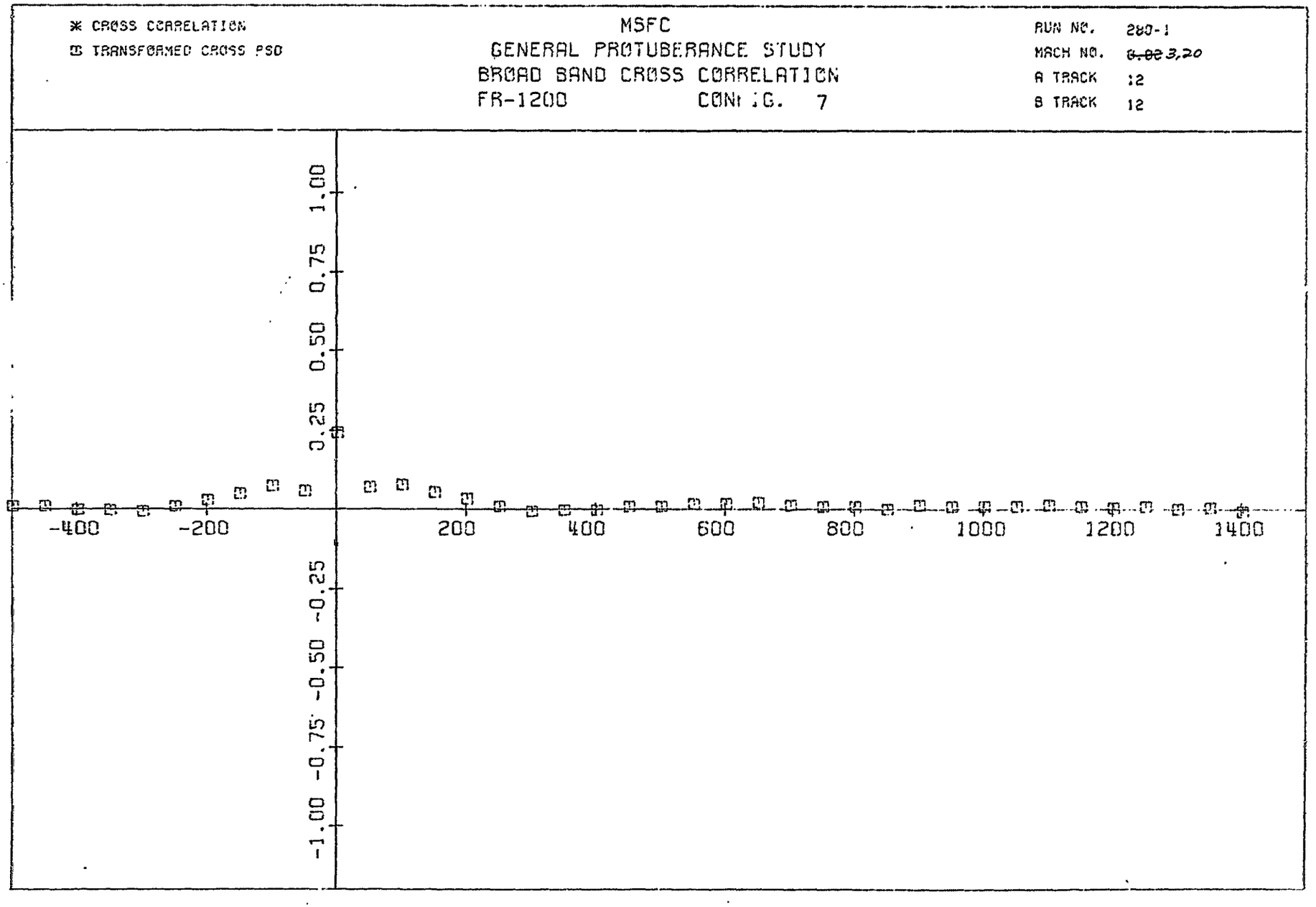

BAGANOFF ASSOCIATES

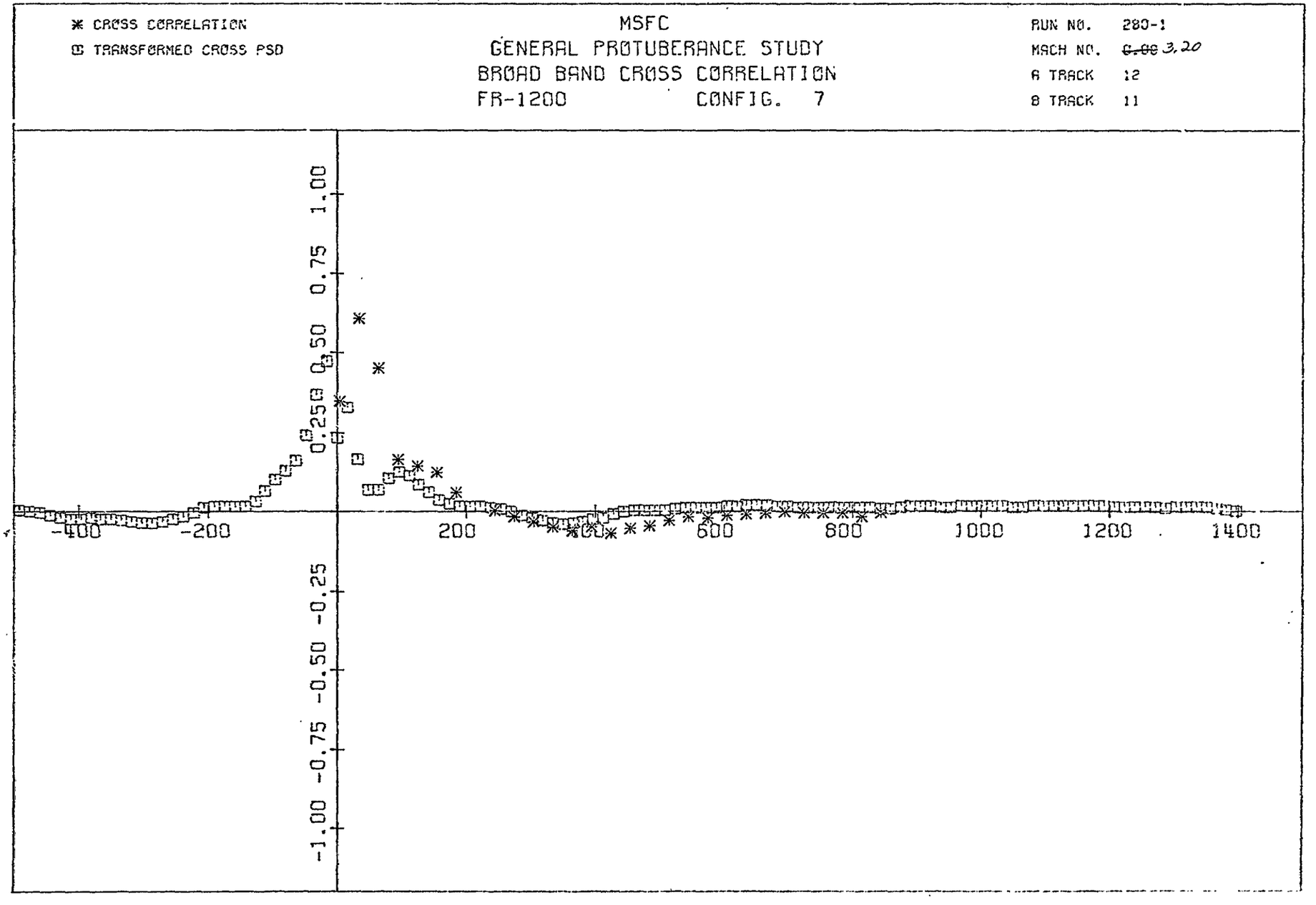

BAGANOFF ASSOCIATES

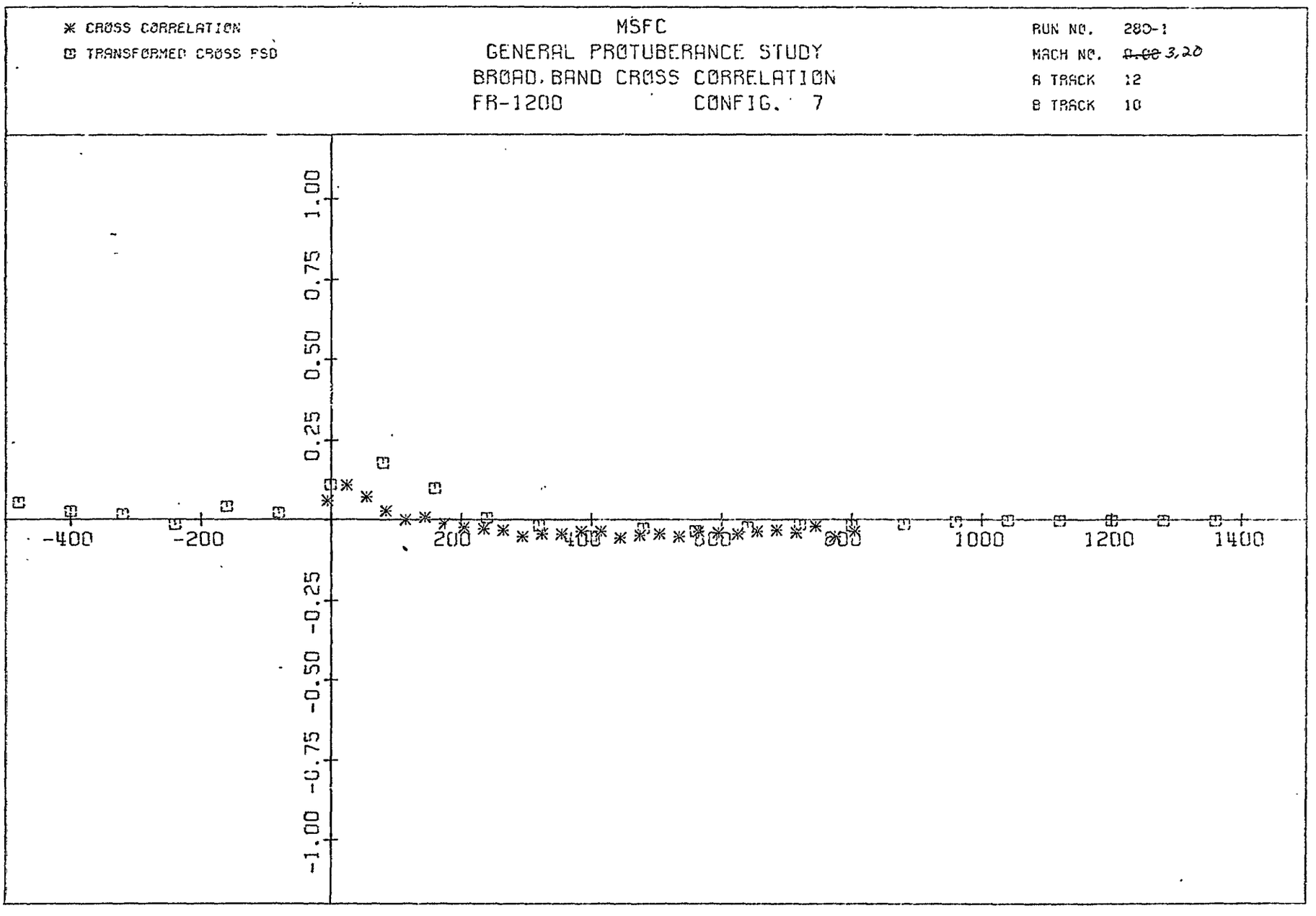

PLOT (102)

BAGANOFF ASSOCIATES

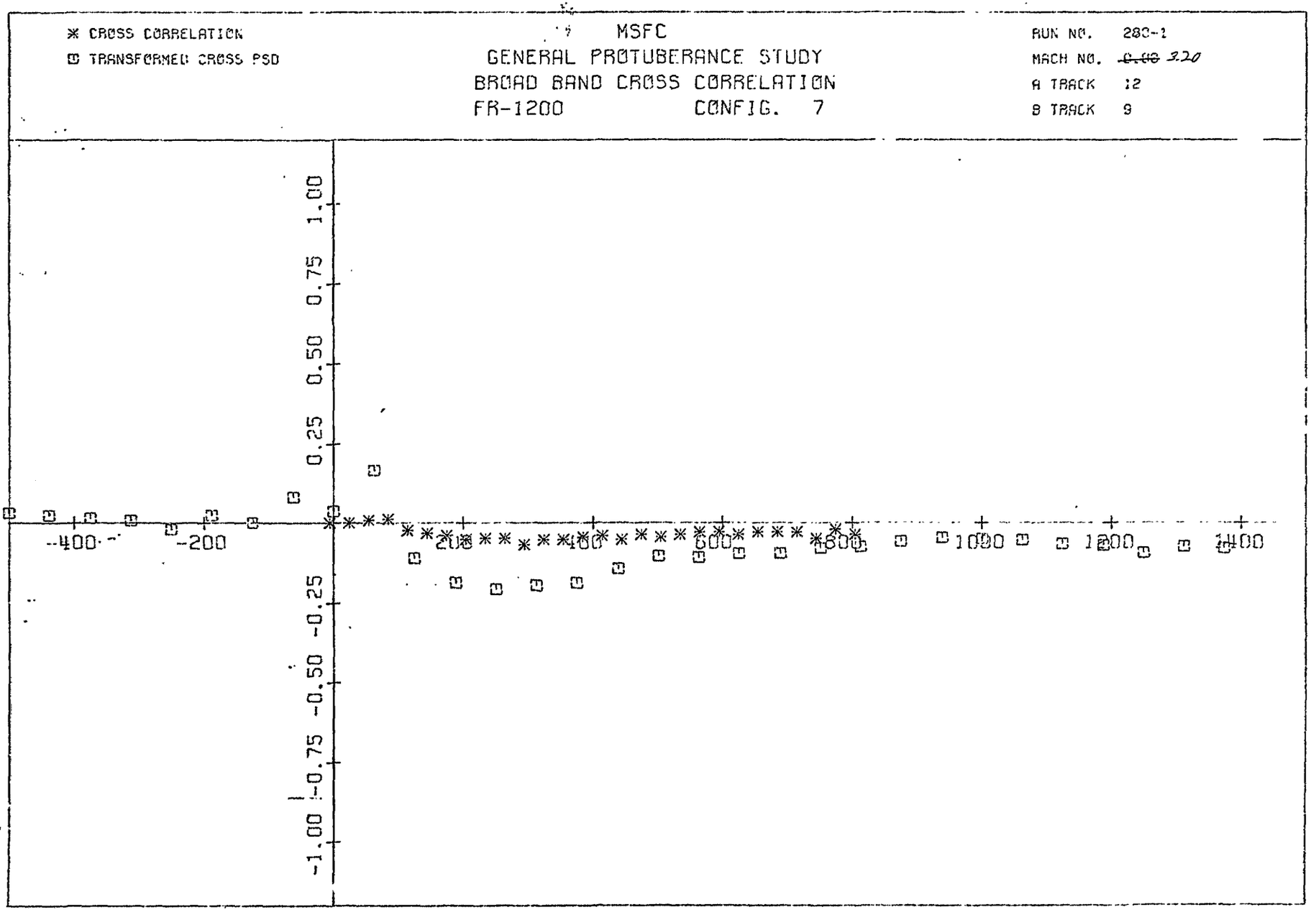

PLOT (103)

BAGANOFF ASSOCIATES

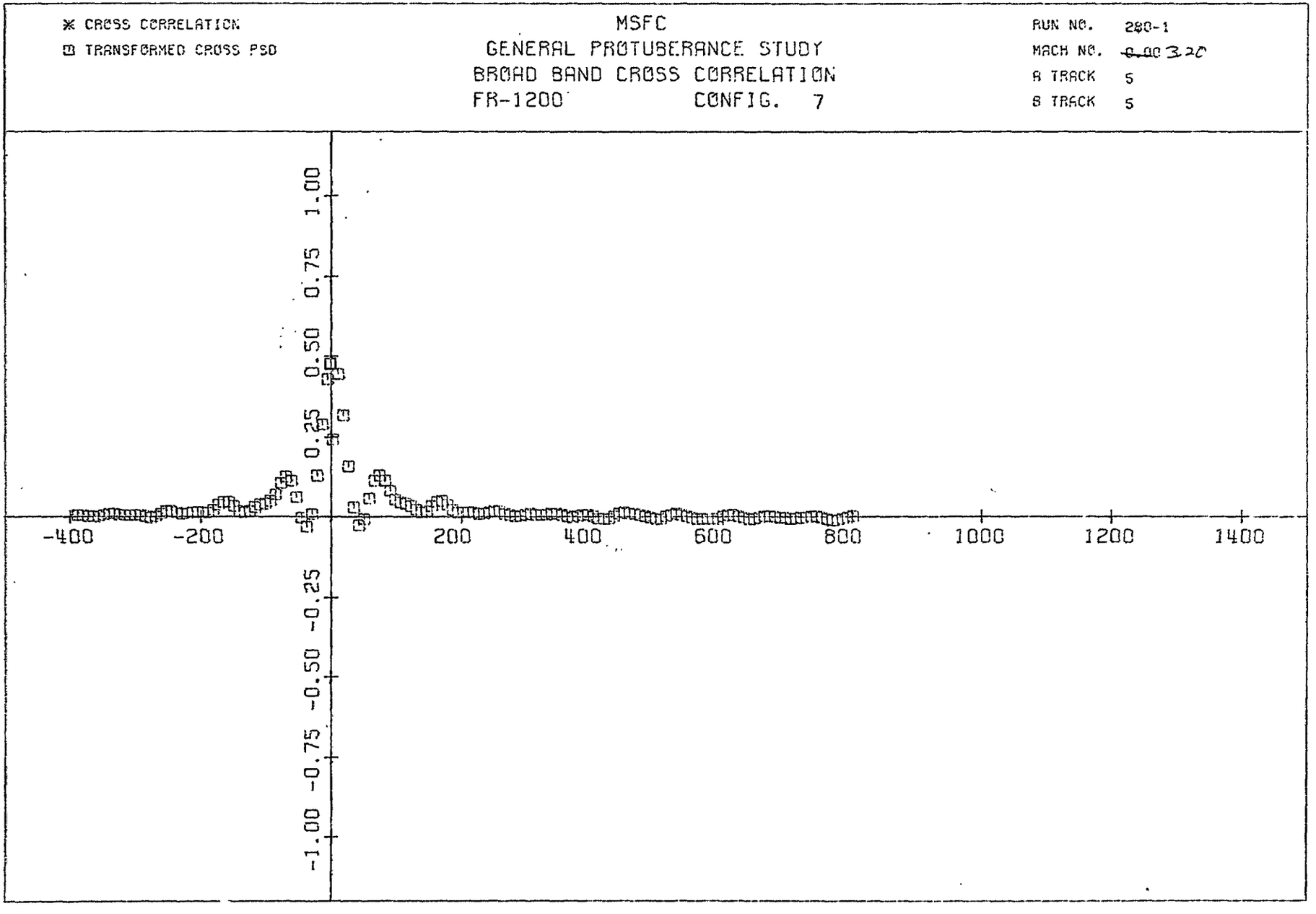

BAGANOFF ASSOCIATES

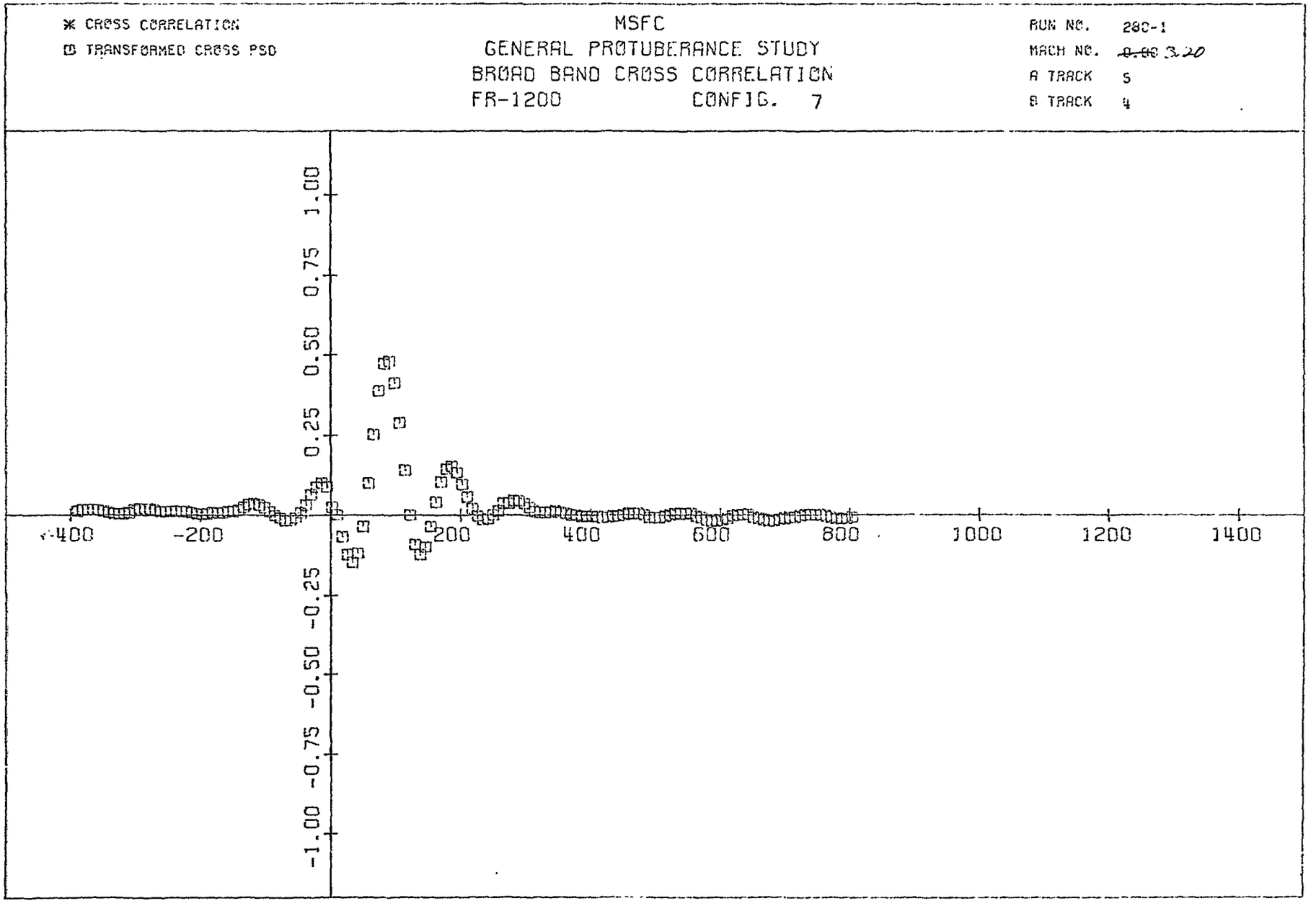

BAGANOFF ASSOCIATES

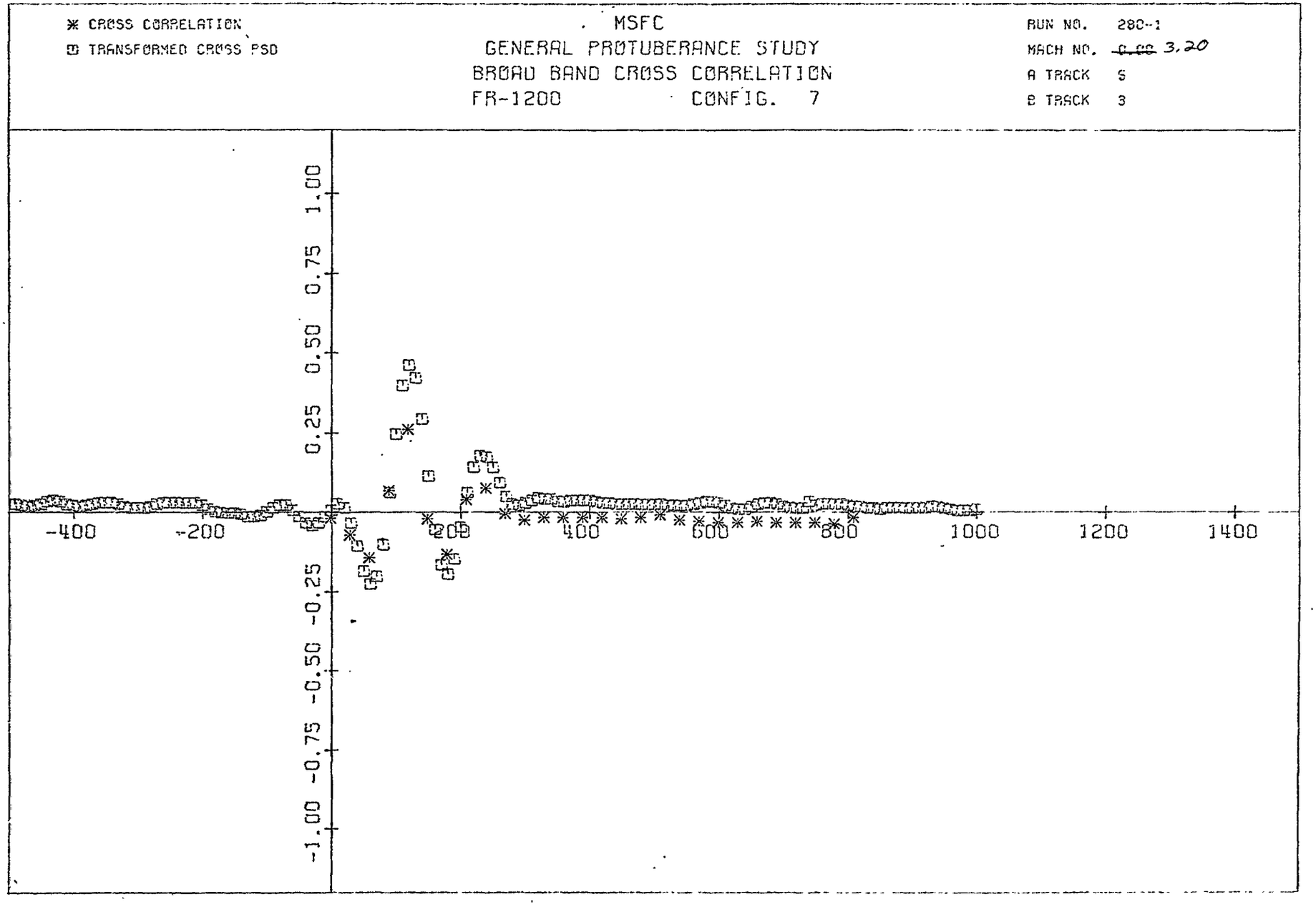

BAGANOFF ASSOCIATES

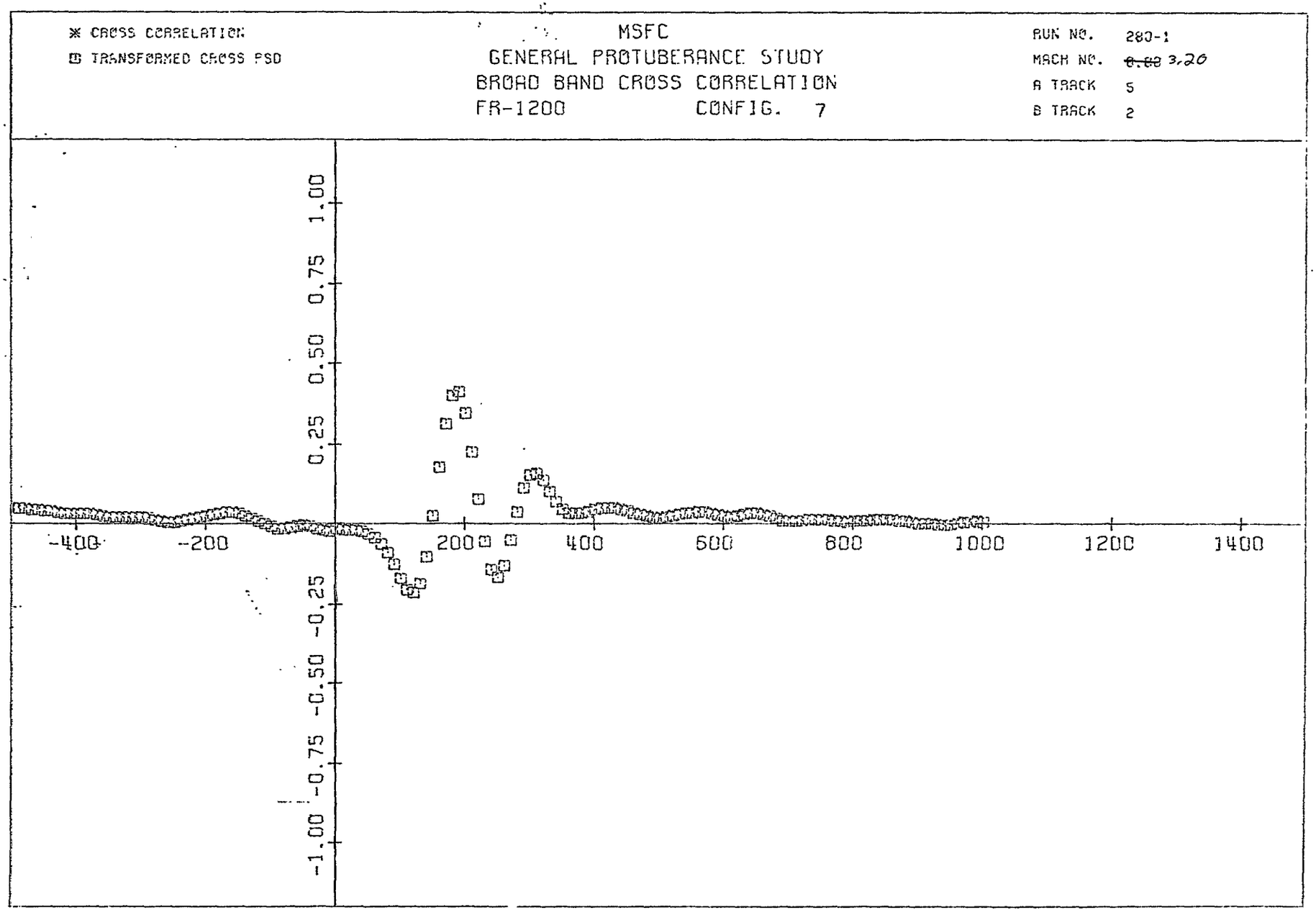

NORMALIZED CORRELATION

TRACK A TIME DELAY IN MICROSECONDS

PLOT (1071)

BAGANOFF ASSOCIATES

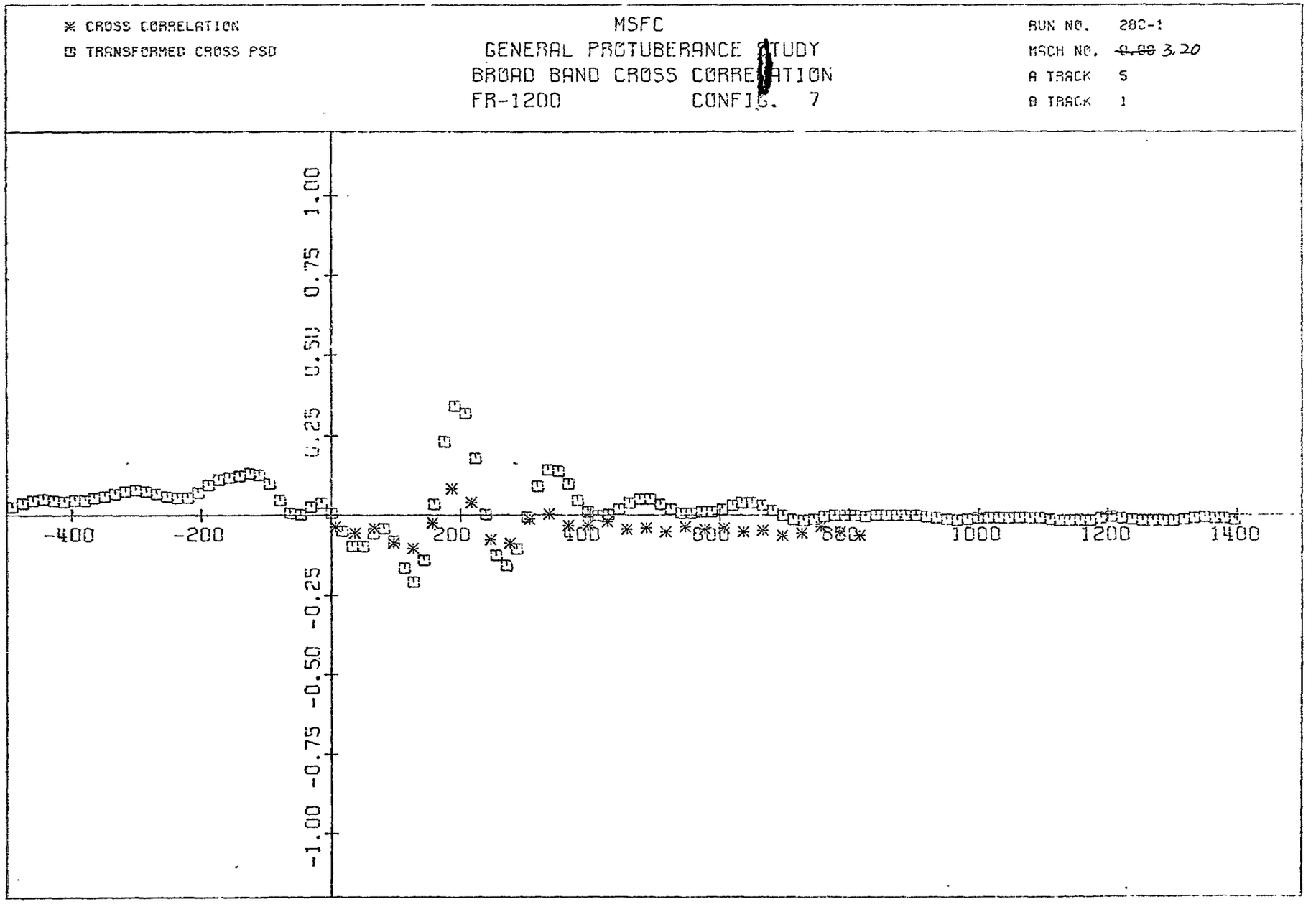

PLOT (108)

BAGANOFF ASSOCIATES

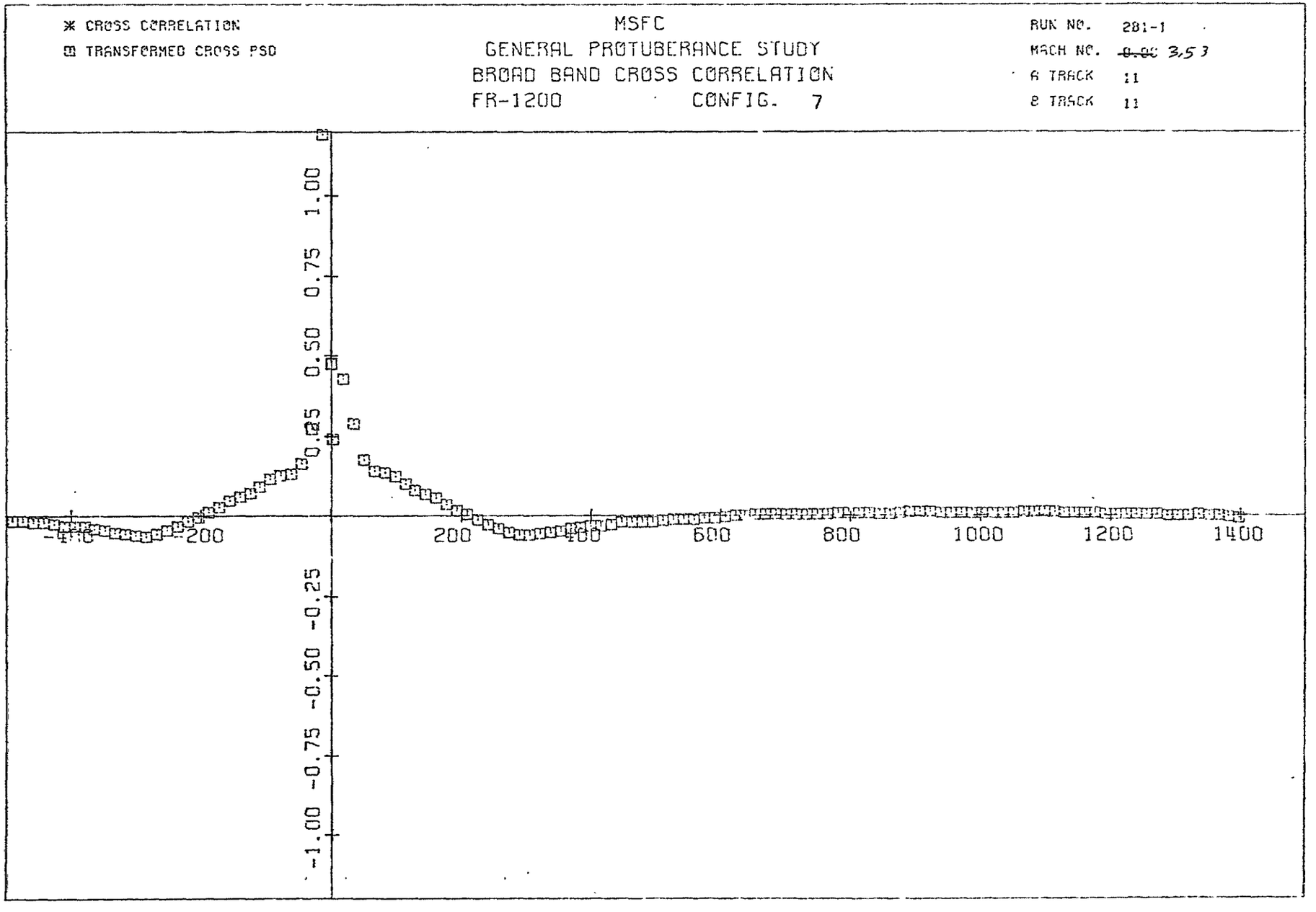

PLOT (109)

BAGANOFF ASSOCIATES

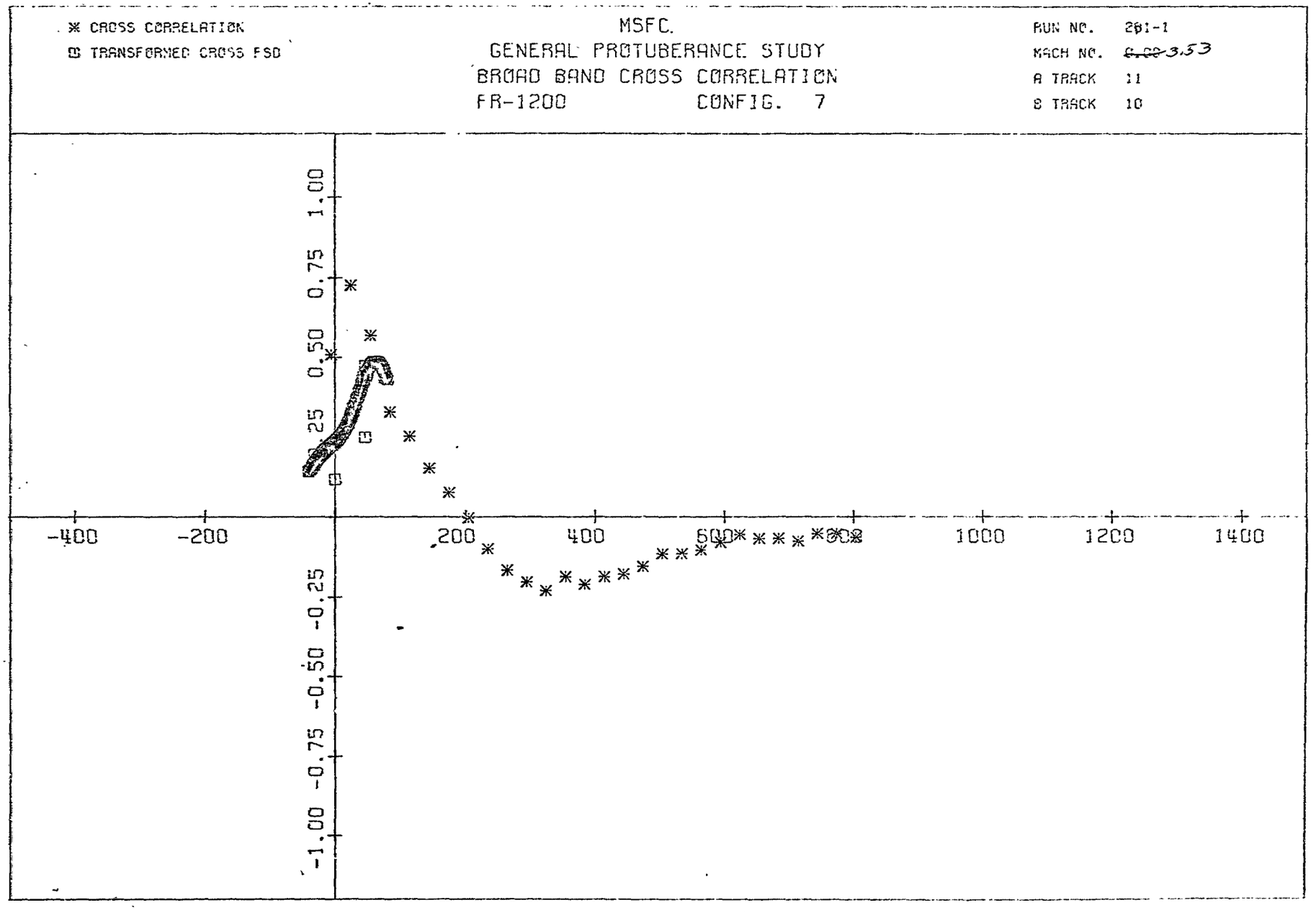

BAGANOFF ASSOCIATES

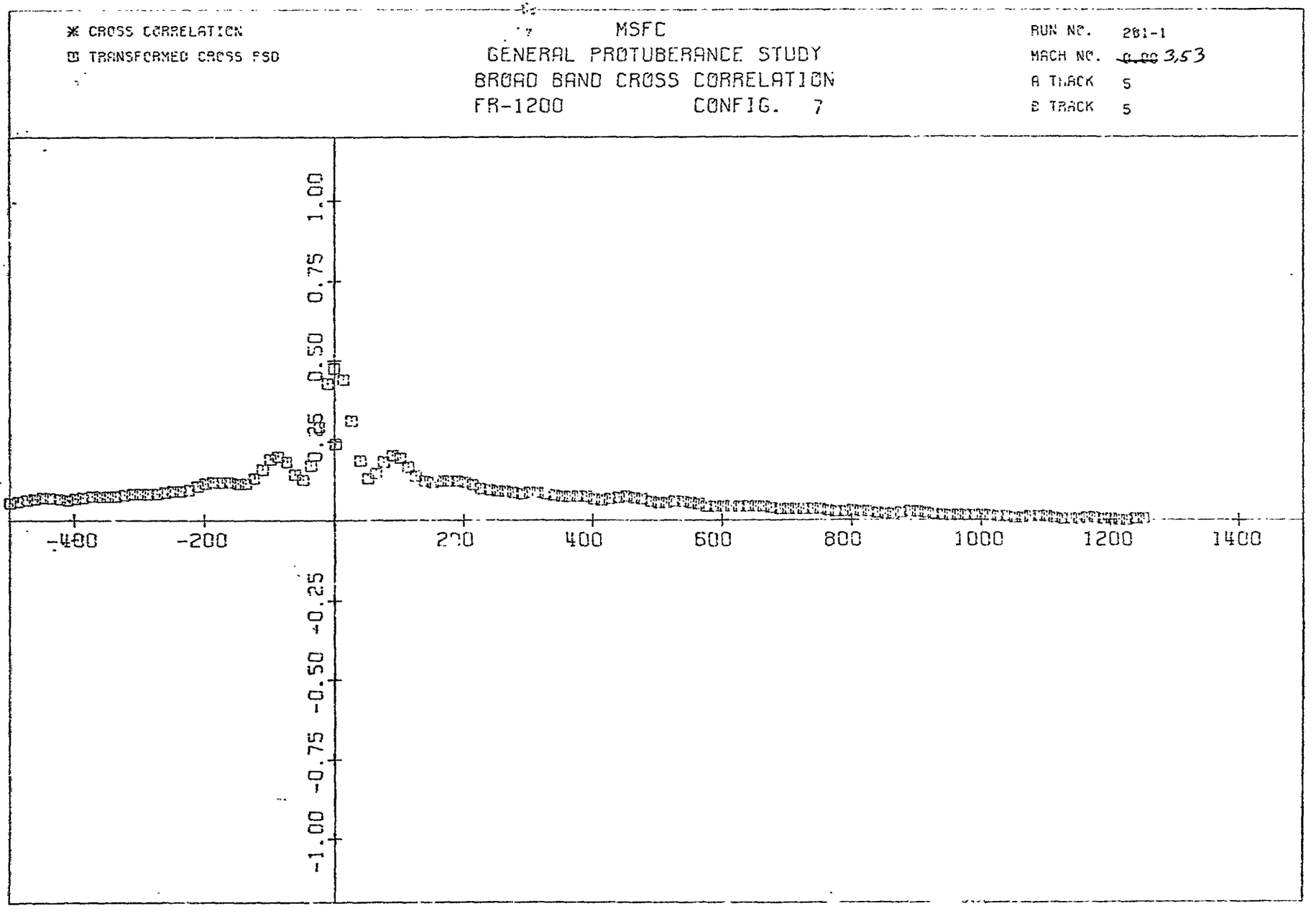

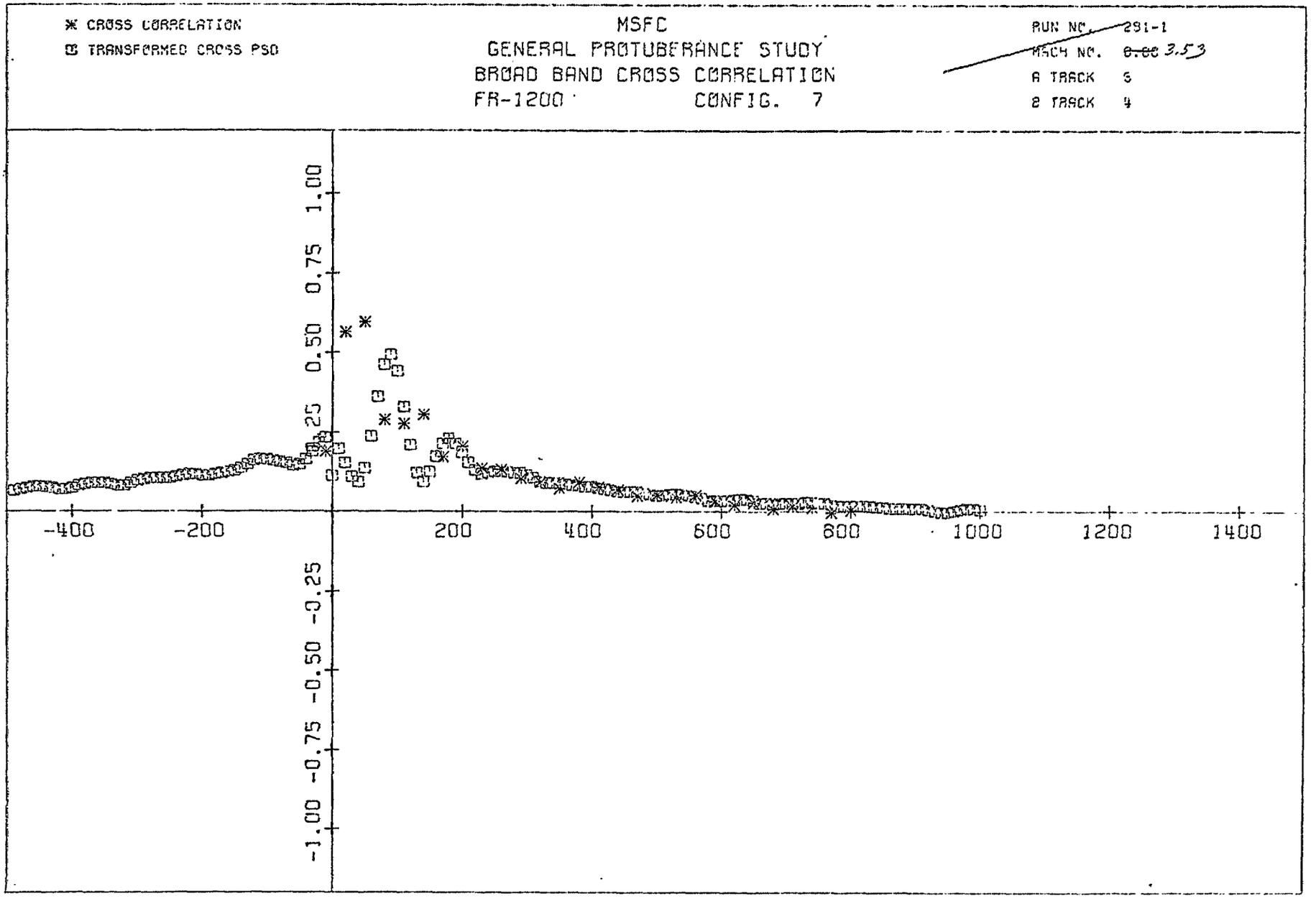
* CROSS CORRELATION
⊡ TRANSFORMED CROSS PSD
MSFC
GENERAL PROTUBERANCE STUDY
BROAD BAND CROSS CORRELATION
FR-1200 CONFIG. 7
RUN NO. 291-1
MACH NO. 3.53
A TRACK 6
B TRACK 4
NORMALIZED CORRELATION
1.00
0.75
0.50
0.25
-0.25
-0.50
-0.75
-1.00
-400
-200
200
400
600
800
1000
1200
1400
TRACK A TIME DELAY IN MICROSECONDS

PLOT (112)

PLOT (113)

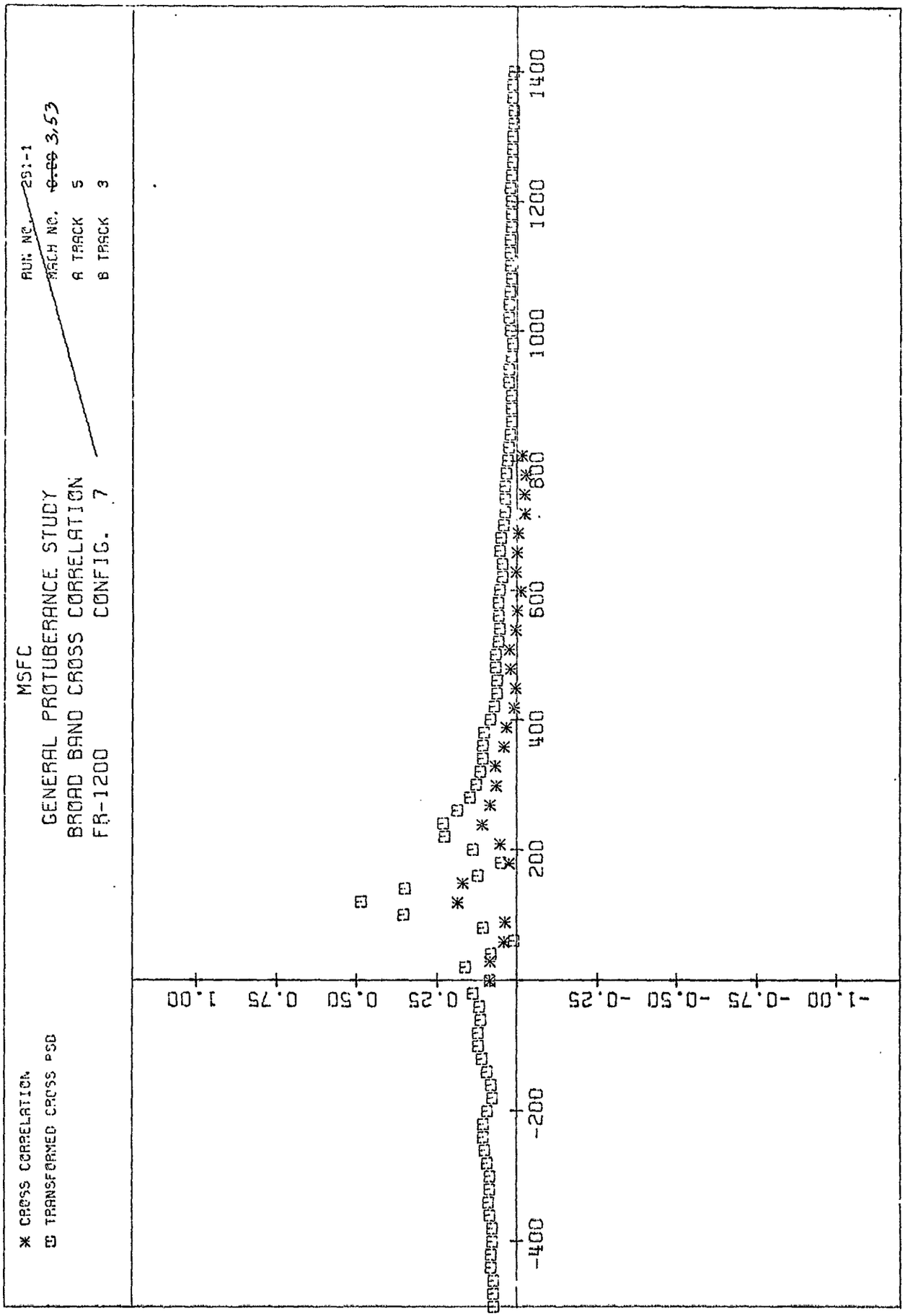

PLOT (114)

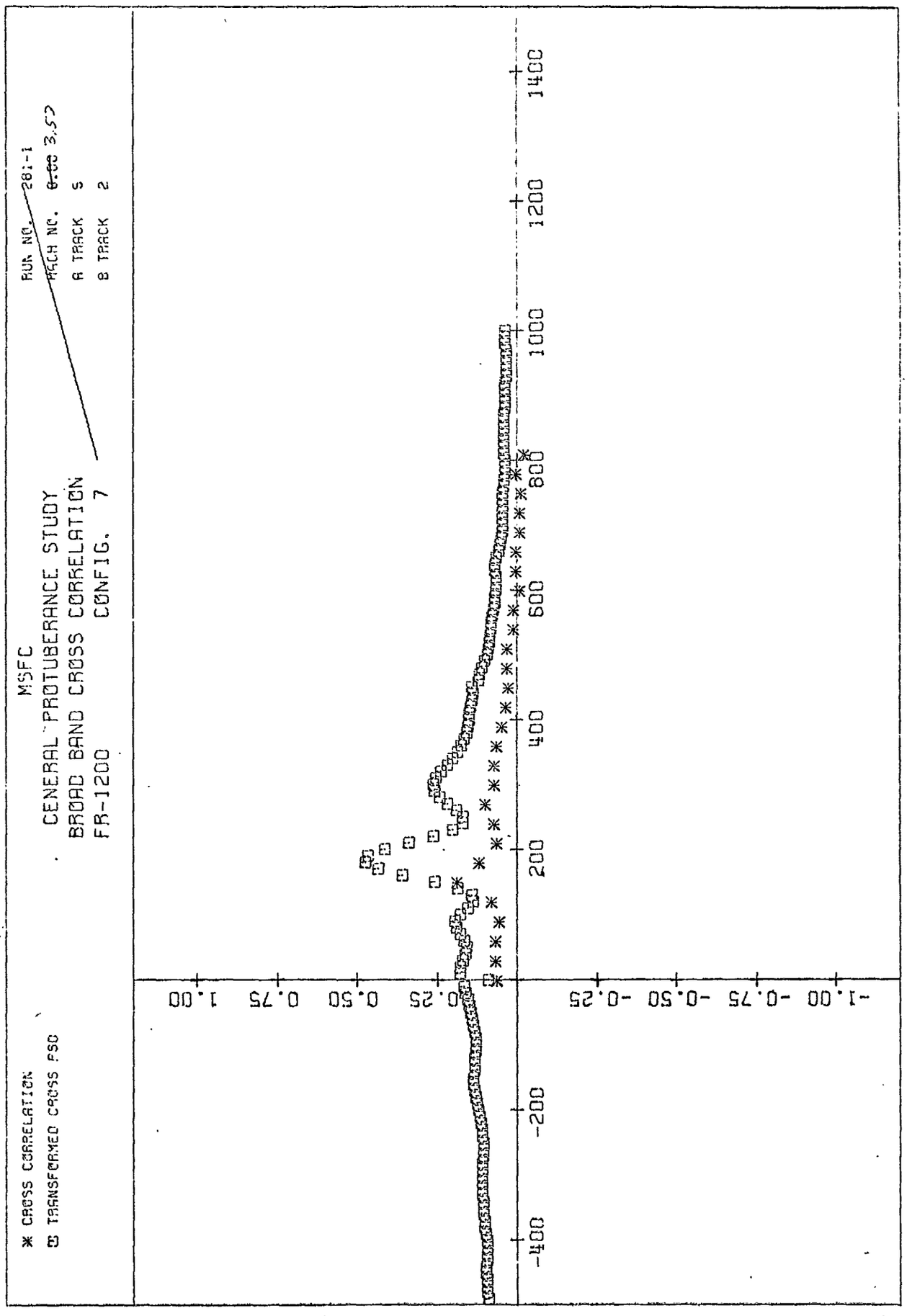

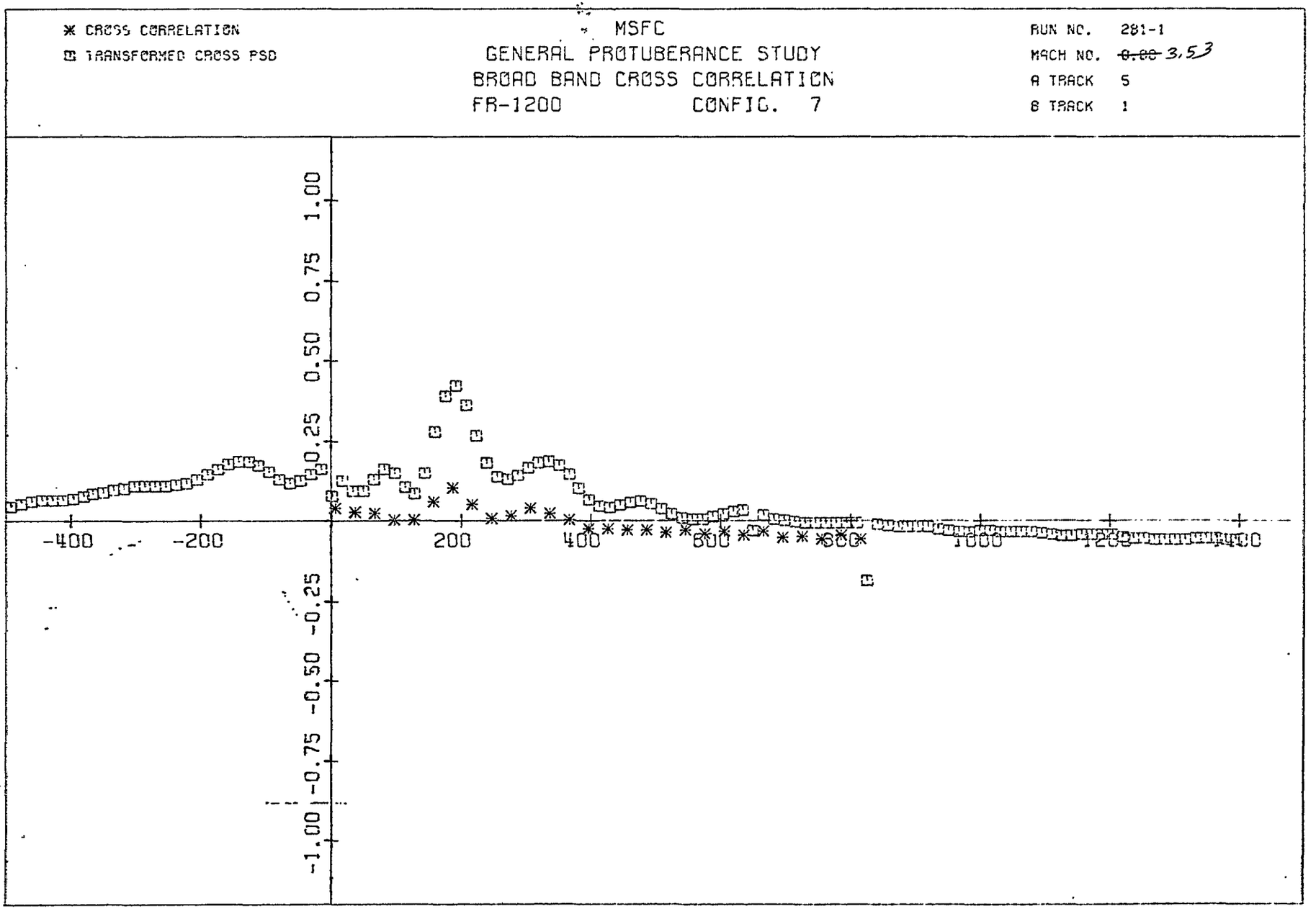
* CROSS CORRELATION
⊡ TRANSFORMED CROSS PSD
MSFC
GENERAL PROTUBERANCE STUDY
BROAD BAND CROSS CORRELATION
FR-1200 CONFIG. 7
RUN NO. 281-1
MACH NO. ~~0.60~~ 3.53
A TRACK 5
B TRACK 1
NORMALIZED CORRELATION
1.00
0.75
0.50
0.25
-0.25
-0.50
-0.75
-1.00
-400
-200
200
400
600
800
1000
1200
TRACK A TIME DELAY IN MICROSECONDS

PLOT (115)

PLOT (116)

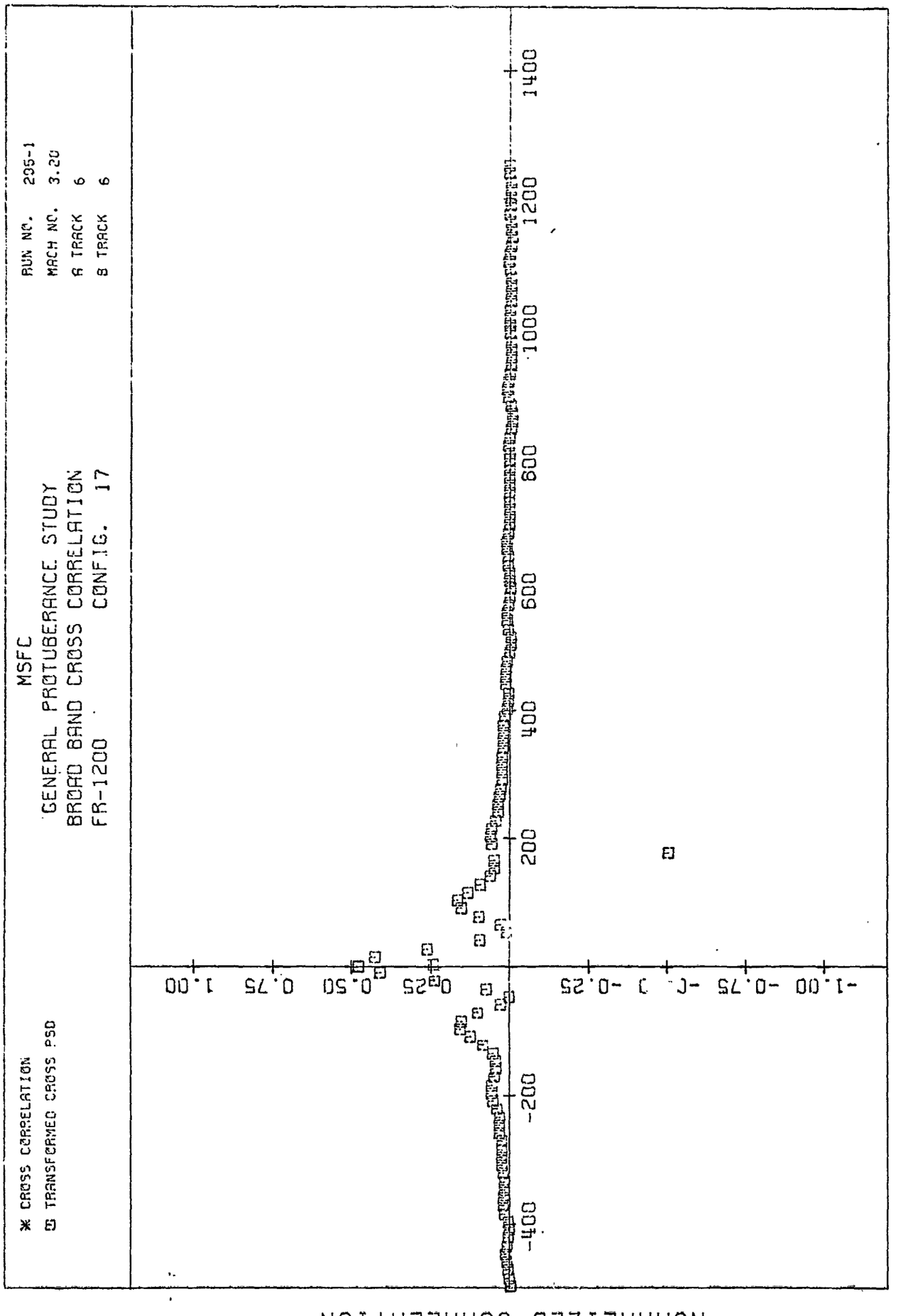

BAGHNUFF ASSOCIATES

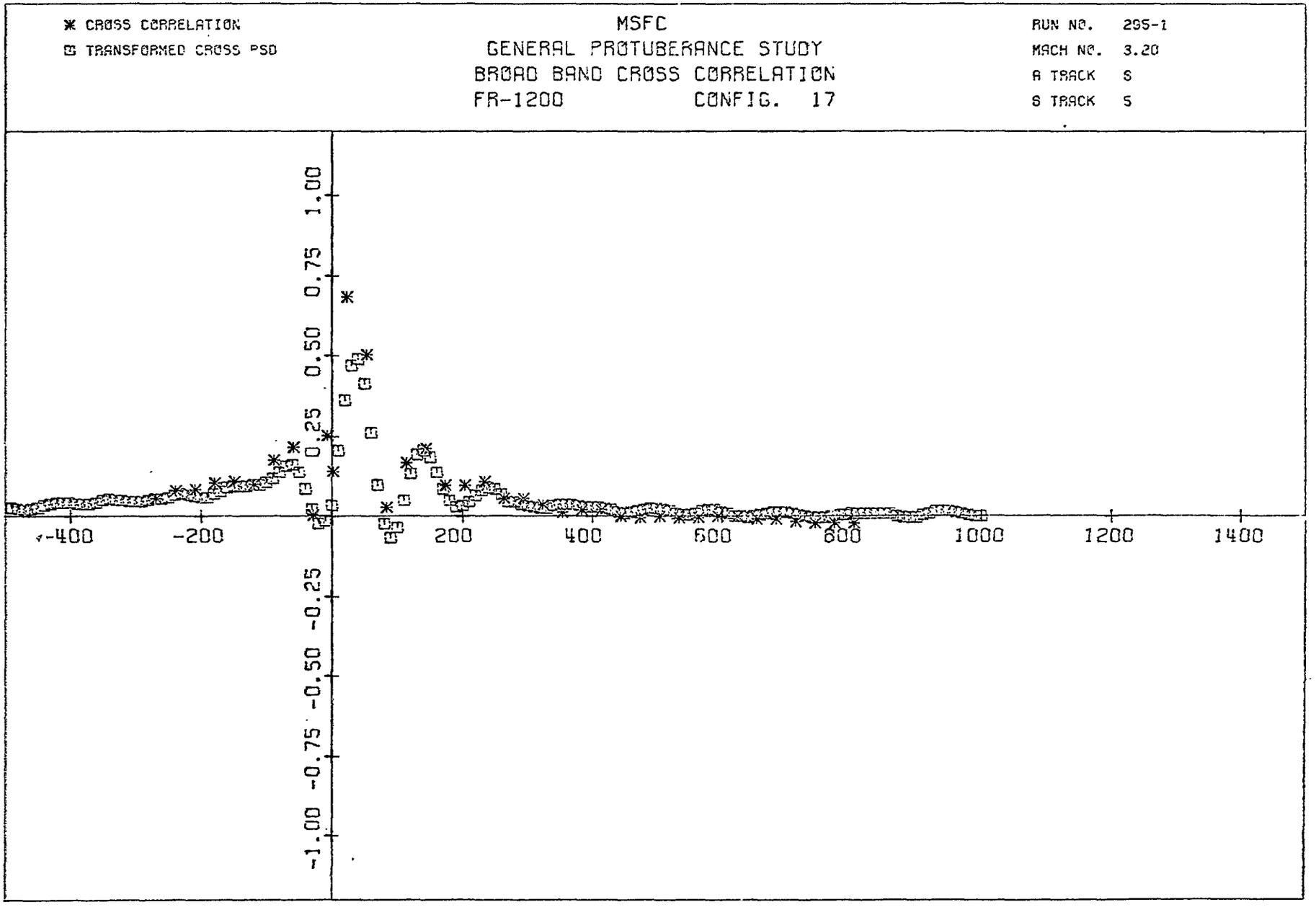

BAGANOFF ASSOCIATES

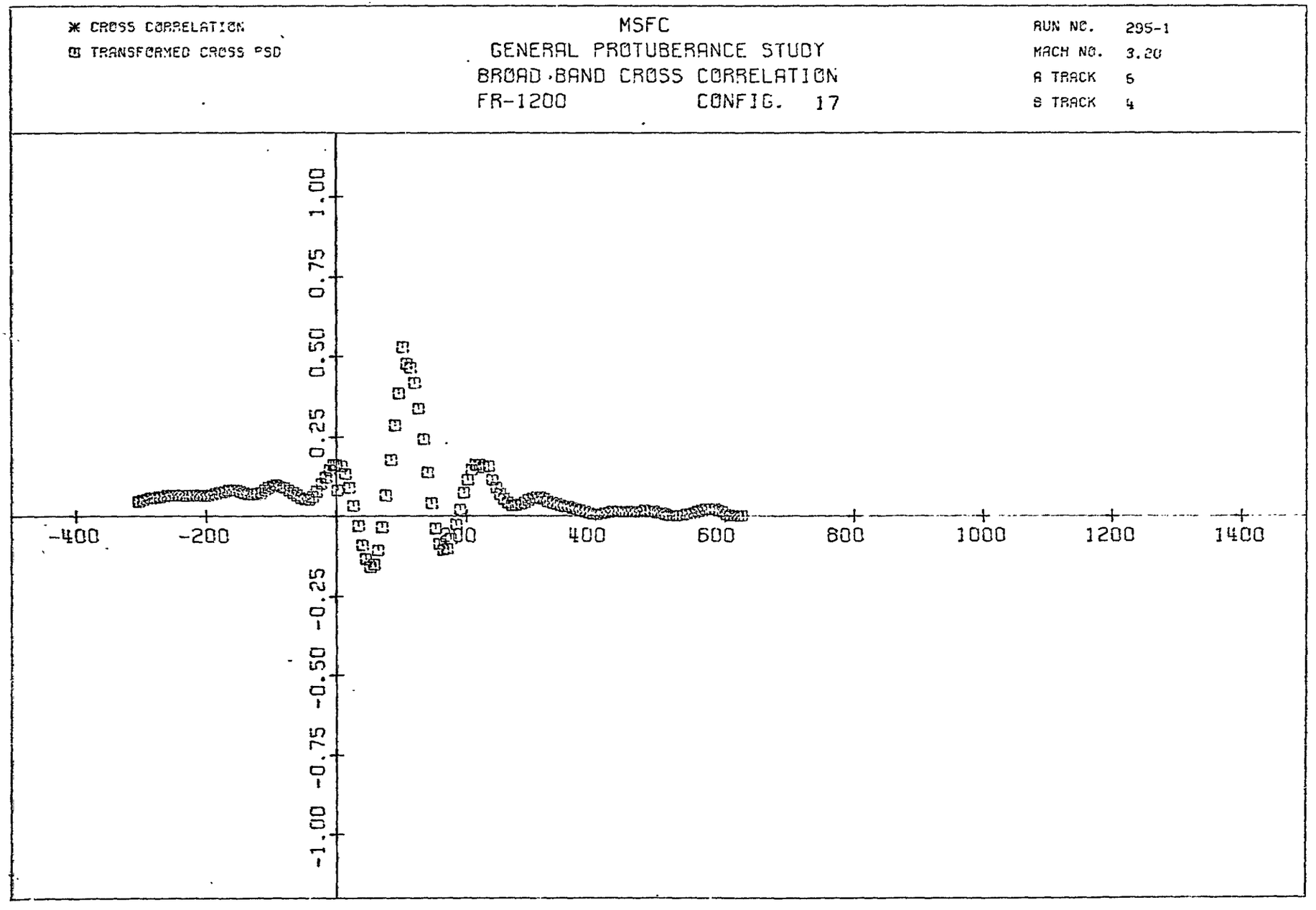

PLOT (118)

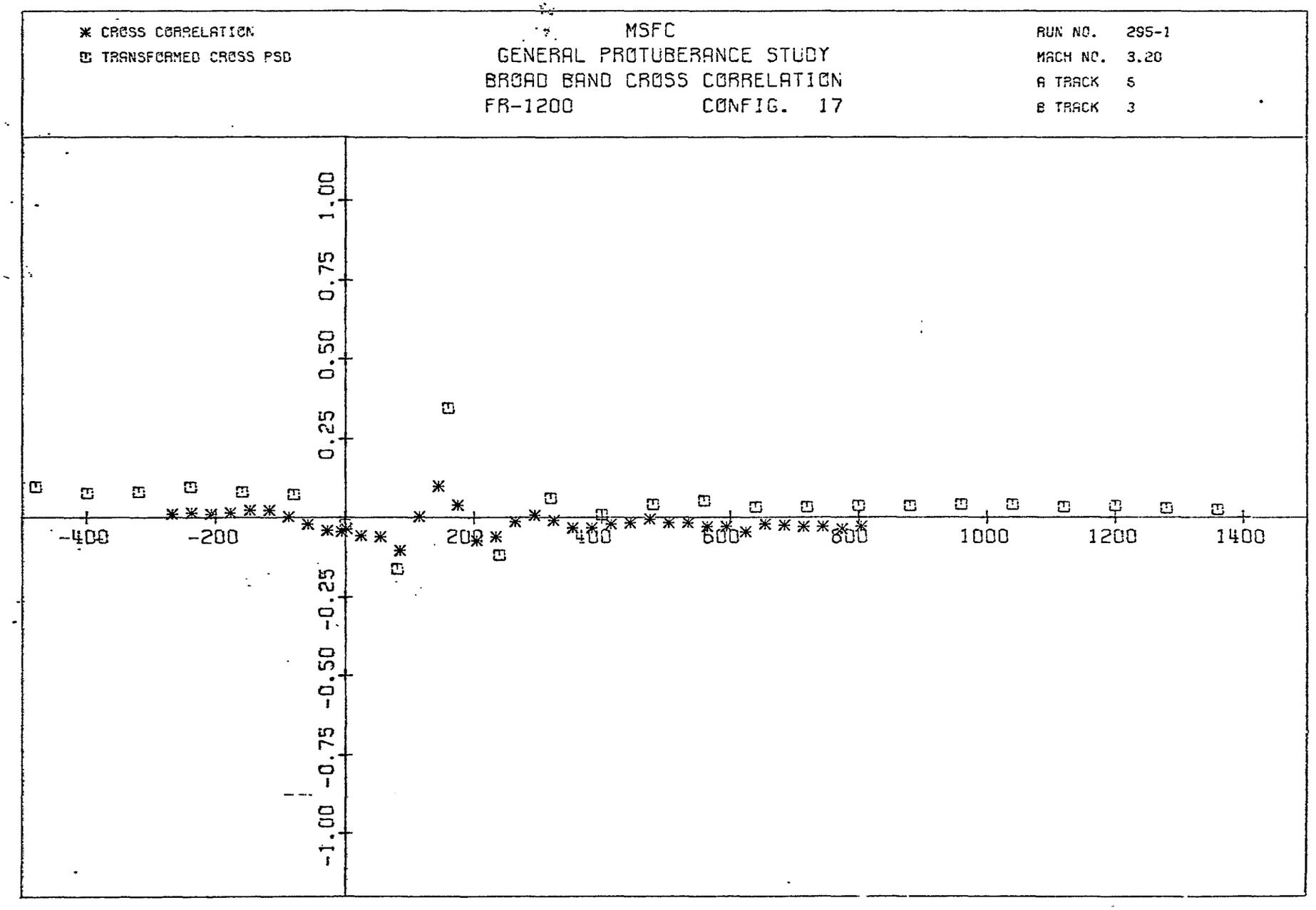
* CROSS CORRELATION
⊡ TRANSFORMED CROSS PSD
MSFC
GENERAL PROTUBERANCE STUDY
BROAD BAND CROSS CORRELATION
FR-1200 CONFIG. 17
RUN NO. 295-1
MACH NO. 3.20
A TRACK 5
B TRACK 3
NORMALIZED CORRELATION
1.00
0.75
0.50
0.25
-0.25
-0.50
-0.75
-1.00
-400
-200
200
400
600
800
1000
1200
1400
TRACK A TIME DELAY IN MICROSECONDS

PLOT (119)

BAGANOFF ASSOCIATES

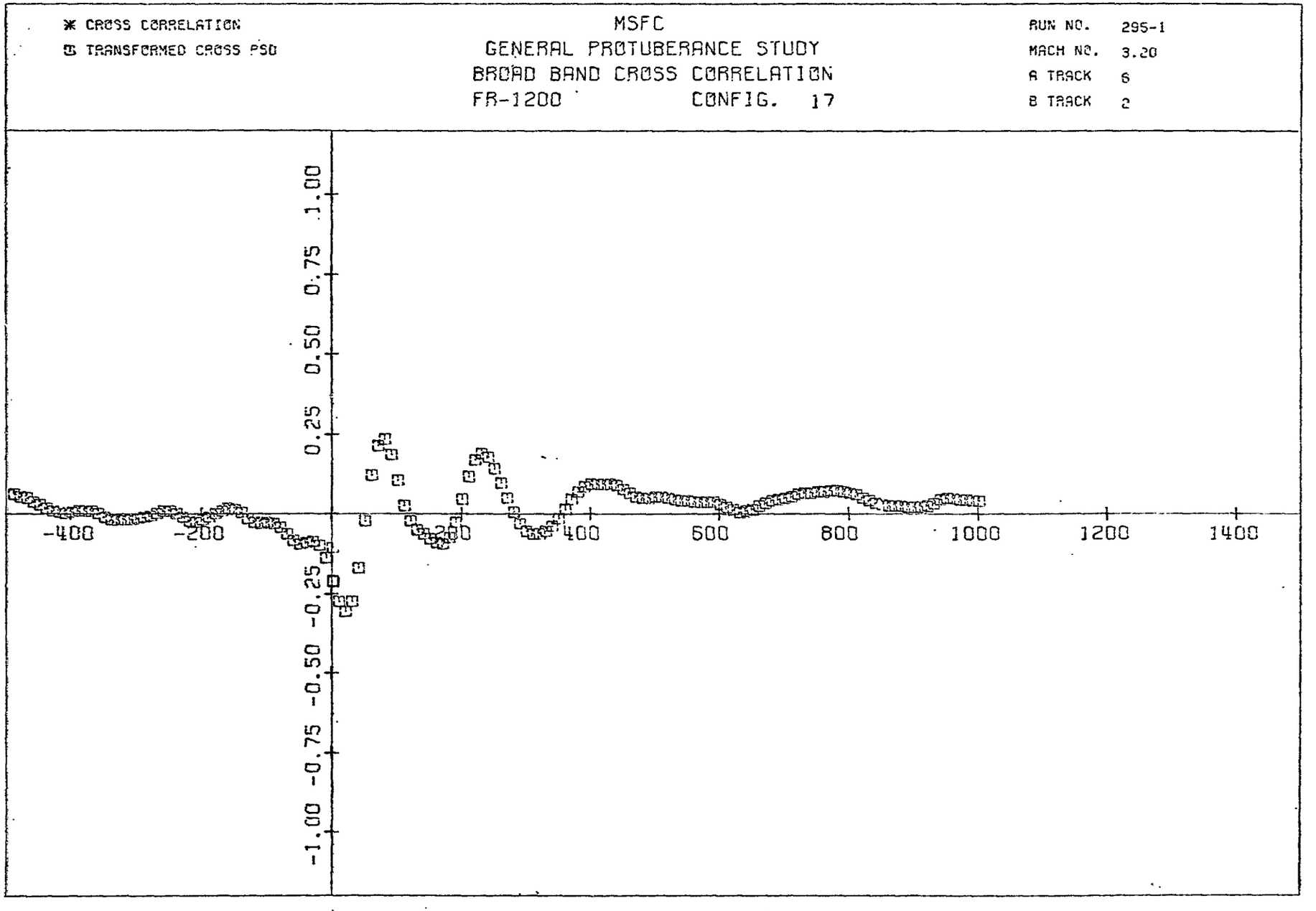

BAGANOFF ASSOCIATES

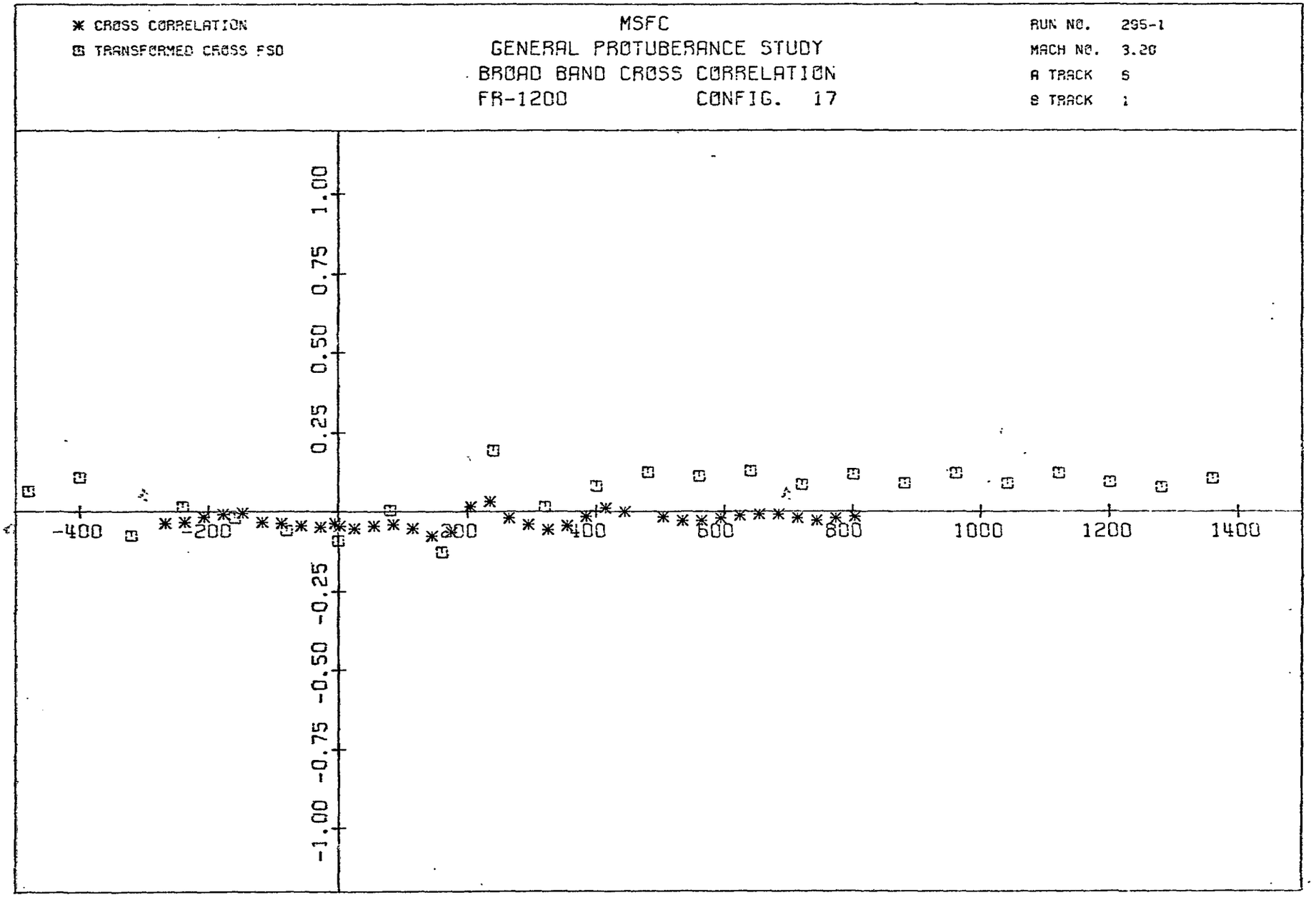

NORMALIZED CORRELATION

PLOT (121)

TRACK A TIME DELAY IN MICROSECONDS